

# **Skeletal muscle mTORC1 regulates whole-body metabolism**

**Inauguraldissertation**

zur

Erlangung der Würde eines Doktors der Philosophie

vorgelegt der

Philosophisch-Naturwissenschaftlichen Fakultät

der Universität Basel

von

**Maitea Guridi Ormazabal**

aus Spanien

Basel, 2016

Originaldokument gespeichert auf dem Dokumentenserver der Universität  
Basel

[edoc.unibas.ch](http://edoc.unibas.ch)

Genehmigt von der Philosophisch-Naturwissenschaftlichen Fakultät  
auf Antrag von

Prof. Dr. Markus A. Rüegg

Prof. Dr. Christoph Handschin

Basel, den 08.12.2015

Prof. Dr. Jörg Schibler

## Contents

1. ABSTRACT .....	4
2. INTRODUCTION.....	6
2.1. Skeletal muscle and metabolism.....	6
2.2. mTORC1 signaling .....	8
2.3. Endoplasmic reticulum stress.....	11
2.4. Fibroblast Growth Factor 21 .....	13
3. RESULTS .....	20
3.1. Manuscript 1.....	20
3.2. Manuscript 2.....	86
3.3. Creation and characterization of a new mouse model .....	132
4. CONCLUDING REMARKS.....	155
5. REFERENCES.....	163
6. APPENDIX.....	183
6.1. Publication 3 .....	183
6.2. Publication 4 .....	197
7. ACKNOWLEDGEMENTS .....	213
8. CURRICULUM VITAE.....	215

## 1. ABSTRACT

Skeletal muscle, which represents over 40% of the total body mass, is a dynamic tissue with a key role in the maintenance of metabolic homeostasis. Several lines of evidence indicate that alterations of the normal muscle function, as for example in muscular dystrophies, obesity or diabetes, can affect the metabolism at the whole-body level (DeFronzo & Tripathy, 2009; Llagostera et al, 2007). We focused on the mTORC1 signaling pathway in skeletal muscle, responsible for the transduction of insulin signaling and nutrient sensing from the cell surface to the increased protein synthesis and anabolic processes that allow cells to grow and proliferate (Laplante & Sabatini, 2012). We decided to characterize the metabolic phenotype of young and old RAmKO (Raptor muscle knock-out) and TSCmKO (TSC1 muscle knock-out) mice, where mTORC1 activity in skeletal muscle is inhibited or constitutively activated respectively. Young RAmKO mice were lean and dystrophic, insulin resistant, with increased energy expenditure and resistant to a HFD. This correlated with an increase in histone deacetylases (HDACs) and a down-regulation of genes involved in glucose and fatty acid metabolism. Young TSCmKO mice were lean, glucose intolerant with a decrease in Akt signaling pathway, resistant to a HFD and showed reduced accumulation of glycogen and lipids in the liver. Both mouse models developed a myopathy with age, with decreased fat and lean mass, and both RAmKO and TSCmKO mice developed metabolic acidosis with insulin resistance and increased intramyocellular lipid content.

While the effects of mTORC1 inhibition in skeletal muscle of young mice were limited to muscle, its sustained activation caused changes not only in skeletal muscle but also at the whole-body level. TSCmKO mice were lean, with increased insulin sensitivity and fatty acid oxidation, and showed changes in other metabolic organs. This indicated the possible influence of a muscle secreted myokine. Secretion of fibroblast growth factor 21 (FGF21) by skeletal muscle has been shown to protect from diet-induced obesity and insulin resistance (Kim et al, 2013c). We showed that most of the metabolic phenotype of TSCmKO mice was due to increased plasma concentrations of FGF21, a hormone that stimulates glucose uptake and fatty acid oxidation. FGF21 was released from skeletal muscle mainly because of mTORC1-triggered ER stress and activation of the PERK-eIF2 $\alpha$ -ATF4 pathway. Treatment of TSCmKO mice with a

chemical chaperone, which alleviates ER stress, reduced FGF21 production in muscle and increased body weight. Moreover, injection of function-blocking antibodies directed against FGF21 largely normalized the metabolic phenotype of the mice. We further confirmed the involvement of muscle FGF21 in the development of the TSCmKO mice phenotype by genetic knock-out of FGF21 specifically in skeletal muscle. DKO mice (muscle TSC1/FGF21 KO) showed normalized plasma glucose and ketone body levels, as well as an increase in body weight, growth and lean mass. This was a direct consequence of muscle secreted FGF21, as plasma FGF21 levels were normalized in DKO mice. Surprisingly, fat mass was still reduced in these mice. We observed increased expression of fatty acid oxidation markers in the muscle of DKO and a decrease in the lipid content, which could contribute to the ongoing wasting of the adipose tissue. Nevertheless, this could indicate either a compensatory mechanism that did not allow DKO mice to gain fat mass, or a FGF21-independent mechanism causing the increased lipolysis of white adipose tissue. Interestingly, when we knocked-out FGF21 specifically in skeletal muscle in a non-genetically altered mouse, we observed the development of obesity induced diabetes, as these mice became heavier, with increased fat mass, higher plasma glucose levels and glucose intolerance.

In conclusion, we have confirmed that alterations to mTORC1 signaling pathway in skeletal muscle directly affect whole body metabolism, which highlights the importance of this tissue in maintaining energy stability. Moreover, we show that proper balance in mTORC1 signaling is essential for muscle tissue integrity and metabolic homeostasis, since both long-term activation and inhibition originated a myopathy that mimicked the main metabolic complications of dystrophic patients. Furthermore, activation of mTORC1 in skeletal muscle, through induction of ER stress, increased the secretion of FGF21 into the circulation, which caused progressive metabolic adaptations to compensate for the altered muscle dynamics. Thus, muscle mTORC1 could serve as a potential target to treat metabolic complications of diseases like diabetes, obesity and muscle dystrophies.

## 2. INTRODUCTION

### 2.1. Skeletal muscle and metabolism

Skeletal muscle is a highly plastic organ, the largest of the body, which represents over 40% of the total body mass. It is a form of striated muscle responsible for voluntary movement as it is under the control of the somatic nervous system. Skeletal muscle is made up of myocytes or muscle fibers, which are long, cylindrical multinucleated cells. Muscle fibers are composed of myofibrils, which in turn are composed of repetitions of actin and myosin filaments that build up the basic functional unit of the muscle fiber, the sarcomere. The most notorious function of skeletal muscle is to generate the force needed to produce movement in the external environment. As a consequence, it accounts for much of the body's energy consumption. In addition to its mechanical function, skeletal muscle has a key role in the maintenance of metabolic homeostasis. It accounts for 70-80% of postprandial glucose uptake, serves as a glycogen storing tissue and a major protein source for other organs in the body (Meyer et al, 2002). In recent years skeletal muscle has gained relevance as a metabolic organ, as it has been reported that it can secrete myokines into the bloodstream that act upon other metabolic organs (Pedersen & Febbraio, 2012). These endocrine hormones include, among others: myostatin, a member of the Transforming growth factor-beta (TGF- $\beta$ ) family that modulates adipose tissue and skeletal muscle growth (Feldman et al, 2006; McPherron et al, 1997); Interleukin 6 (IL-6), a cytokine that is secreted in response to exercise and regulates glucose metabolism (Pedersen & Febbraio, 2008; Serrano et al, 2008); Interleukin 15 (IL-15), another cytokine with anabolic effects in muscle and a role in lipid metabolism (Nielsen et al, 2007); Insulin like growth factor 1 (IGF-1) and IGF-2, growth factors that might be involved in muscle-bone crosstalk and osteogenesis (Hamrick, 2010); Irisin, a peroxisome proliferator-activated receptor gamma coactivator 1-alpha (PGC1 $\alpha$ ) derived myokine that drives adipose tissue browning and thermogenesis (Bostrom et al, 2012) and Fibroblast growth factor 21 (FGF21), a newly discovered growth factor induced upon stress which can regulate glucose and fatty acid metabolism (Kim et al, 2013c). These myokines serve as a communication mechanism between skeletal muscle and other metabolic organs like liver, pancreas and adipose tissue, which altogether coordinate the metabolic balance of the body.

The term metabolism covers the set of life-sustaining chemical transformations within the cells of living organisms. These complex biochemical reactions produce the energy required for anabolic and biosynthetic processes. Muscle contraction depends on the chemical energy of adenosine triphosphate (ATP). The 3 major pathways that supply energy in the form of ATP to meet the energy demands of skeletal muscle are glycogen metabolism, lipid metabolism and the purine nucleotide pathway. There are a group of disorders called metabolic myopathies that refer to hereditary muscle disorders which are consequence of specific enzymatic defects caused by genetic mutations. They have common abnormalities in energy metabolism of the muscle that result in skeletal muscle dysfunction. They include glycogen storage diseases like McArdle's disease (caused by a myophosphorilase deficiency) or Pompe disease (result of acid maltase deficiency); lipid storage diseases like carnitine palmytoyltransferase (CPT) deficiency; or defects in purine nucleotide metabolism like in Limb-girdle muscular dystrophy (Cruz Guzman Odel et al, 2012; Lieberman et al, 2012; Santalla et al, 2014). Several of these skeletal muscle diseases end up being multi-systemic disorders involving also the heart, liver, brain, retina and kidneys. The pathophysiology of most metabolic myopathies is related to the impaired energy production or production of reactive oxygen species (ROS) and the abnormal function of mitochondria, peroxisomes and lysosomes (D'Amico & Bertini, 2013). Skeletal muscle is a key regulator of whole-body metabolic homeostasis, as evidenced by the fact that patients suffering from muscular dystrophies often develop complications like insulin resistance or glucose intolerance. People with myotonic dystrophy 1 (DM1) do not display clinical symptoms of diabetes, but show a 70% decrease in insulin sensitivity of the muscle (Moxley et al, 1978; Moxley et al, 1984), most likely caused by aberrant regulation of the insulin receptor (IR) (Savkur et al, 2001). Duchenne muscular dystrophy (DMD) patients also show reduced IR expression (DePirro et al, 1982) and alterations in glucose transporter 4 (GLUT4) in muscle fibers, which could be involved in the development of obesity, hyperinsulinemia and insulin resistance observed in these patients (Rodriguez-Cruz et al, 2015). Insulin resistance and glucose intolerance are also observed in patients with Amyotrophic Lateral Sclerosis (Reyes et al, 1984) and Friedreich's Ataxia (Khan et al, 1986). Insulin resistance is an important factor for the development of type II diabetes (Reaven et al, 1988) and a risk factor for cardiovascular

disease, dyslipidemia, hypertension and obesity (Kahn et al, 2006). Obesity and type II diabetes are growing health problems world-wide that have reached epidemic proportions, therefore understanding the pathophysiological mechanisms leading to the development of these diseases, and the involvement of skeletal muscle in this process is of great importance.

## **2.2. mTORC1 signaling**

The role of skeletal muscle as a metabolic organ is thus evident. However, the signaling pathways involved in regulating its metabolic functions need yet to be clearly identified. Several molecular pathways are important in governing muscle mass and metabolism: namely the growth induction by IGF-1/ Insulin activated phosphoinositide-3 kinase (PI3K)- Akt pathway; protein degradation regulated by Forkhead box O (Foxo) transcription factors and the autophagy-lysosomal and proteasomal degradation pathways; and protein translation and synthesis regulated by the mammalian target of rapamycin complex 1 (mTORC1) pathway.

Insulin and IGF-1 are known major regulators of muscle protein and glucose homeostasis. They bind to IR and IGF-1 receptor (IGF1R) on the surface of muscle cells to activate PI3K and downstream anabolic processes. PI3K catalyzes the synthesis of the lipid phosphatidylinositol 3,4,5-triphosphate (PIP3), which in turn interacts with different proteins via the pleckstrin homology (PH) domain to recruit them to the cell membrane (Maffucci & Falasca, 2001). Muscle-specific knockout of IGF1R and IR causes a 60% decrease in muscle mass with decreased fasting glycemia and increased basal glucose uptake (O'Neill et al, 2015). The link between surface insulin signaling and intracellular signaling cascades is the signal transducer Akt or protein kinase B (PKB). Akt is a family of serine/threonine-specific protein kinases, with Akt1 being ubiquitously expressed (Chen et al, 2001), Akt 3 expressed in brain, lung and kidneys (Brodbeck et al, 1999; Easton et al, 2005) while Akt2 is the predominant form expressed in insulin responsive tissues, such as adipose tissue, liver and skeletal muscle (Altomare et al, 1995). Skeletal muscle-specific transgenic mice expressing a constitutively active form of Akt showed muscle hypertrophy due to the growth of fast/glycolytic type II fibers and increased strength with resistance to obesity induced by a high-fat diet (HFD) (Izumiya et



al, 2008b). Akt phosphorylates many downstream targets to regulate growth, degradation and cell metabolism. Some of Akt targets involved in transducing the surface insulin signaling to the metabolism of the cell are Akt substrate of 160 KDa (AS160) or TBC1D4 and TBC1D1, two Rab GTPase-activating proteins. AS160 can regulate insulin- and contraction-stimulated glucose uptake into skeletal muscle by translocating GLUT4 to the plasma membrane (Kramer et al, 2006), while TBC1D1 is involved in basal glucose absorption into skeletal muscle by regulating GLUT1 expression (Zhou et al, 2008).

Both insulin and IGF-1 have been shown to stimulate muscle protein synthesis (Rommel et al, 2001) and inhibit protein degradation via the ubiquitin –proteasome and autophagy-lysosome pathways (Mammucari et al, 2007; Sandri et al, 2004). IGF-1 treatment is sufficient to cause muscle hypertrophy via Akt mediated activation of mTORC1 (Rommel et al, 2001). Skeletal muscle mass is ultimately determined by the net difference in the rates of protein degradation and protein synthesis (Goodman et al, 2011), of which mTORC1 is the key regulator. mTORC1 is a serine/threonine protein kinase evolutionarily conserved from yeast to humans, that is involved in nutrient sensing and the regulation of growth and metabolism (Sabatini et al, 1994). mTORC1 is rapamycin sensitive and is composed of mTOR, regulatory-associated protein of mTOR (raptor), mLST8 and the later identified partners PRAS40 and DEPTOR (Peterson et al, 2009; Thedieck et al, 2007). mTOR, part of the mTORC1, can also assemble into mTOR complex 2 (mTORC2), which is composed of rapamycin-insensitive companion of mTOR (riCTOR), mLST8, DEPTOR, mSIN1 and protor1/2 (Laplante & Sabatini, 2012). mTORC2 is only sensitive to long-term or chronic exposure to rapamycin (Sarbasov et al, 2006; Ye et al, 2012), and it is known to regulate cytoskeletal organization and cell survival (Laplante & Sabatini, 2012). mTORC1 is a known master regulator of cell growth and metabolism by controlling: 1) protein synthesis through the phosphorylation of eukaryotic initiation factor 4E (eIF4E)-binding protein 1 (4EBP1) and the p70 ribosomal S6 kinase 1 (S6K1); 2) protein degradation through nuclear factor erythroid–derived2-related factor 1 (NRF1) dependent increase in proteasomal degradation (Zhang et al, 2014); 3) by inhibiting autophagy, a catabolic recycling cellular process, through the phosphorylation of Unc 51-like kinase 1 (Ulk1) and inhibition of the formation of the autophagy initiation complex Ulk1/FIP200/ATG13; 4) by

regulating lipid synthesis through inhibition of Lipin1 and activation of sterol regulatory-element binding protein 1 (SREBP1) (Lamming & Sabatini, 2013); and 5) by promoting mitochondrial metabolism and biogenesis through binding and activation of the transcription factor ying-yang 1 (YY1) and its interaction with PGC1 $\alpha$  (Laplante & Sabatini, 2013).

Thus, mTORC1 is a very complex signaling network that has been widely studied in multiple tissues, with the results normally affecting life span, cell growth and whole-body metabolism. Although complete elimination of mTORC1 in mammals causes embryonic lethality (Guertin et al, 2006), animals lacking one of its substrates, S6K1, show increased lifespan and increased insulin sensitivity (Selman et al, 2009), owing to the loss of a negative feedback loop from S6K1 to insulin receptor substrate 1 (IRS1) and enhanced  $\beta$ -oxidation (Um et al, 2004). mTORC1 activation is sufficient to stimulate glycolysis, the oxidative arm of the pentose phosphate pathway and de novo lipid synthesis in cells (Duvel et al, 2010). Livers with constitutive mTORC1 activity by deletion of tuberous sclerosis complex 1 (TSC1) resist hepatic steatosis induced by a HFD, independent of Akt, due to an up-regulation of Cpt1a and the antioxidant protein Nrf2 (Kenerson et al, 2015). Adipose-specific knockout of raptor results in lean mice with enhanced mitochondrial respiration, due to mitochondrial uncoupling and increased energy expenditure (Polak et al, 2008a). In skeletal muscle, inactivation of mTORC1 causes impairment of oxidative metabolism, altered mitochondrial regulation and accumulation of glycogen associated with Akt hyperactivation, which leads to a severe myopathy (Bentzinger et al, 2008b; Risson et al, 2009b). Surprisingly, constitutive activation of mTORC1 in skeletal muscle also leads to the development of a progressive myopathy, due to the inhibition of the autophagy process (Castets et al, 2013) and the increased ubiquitination and degradation of proteins through the proteasome (Bentzinger et al, 2013). In addition, in mice deficient for *Lmna*, the gene that encodes A-type lamins, inhibition of mTORC1 signaling by rapamycin treatment rescues cardiac and skeletal muscle function by decreasing the accumulation of desmin in these tissues and by improving defective autophagy (Ramos et al, 2012). This shows that mTORC1 is a key player in regulating muscle health and metabolism, but there is still much to elucidate about the molecular mechanisms behind. Therefore, mTORC1 is a key target to

study the signaling pathways involved in muscle dystrophies and the effect of muscle on whole-body metabolism.

### **2.3. Endoplasmic reticulum stress**

Loss of TSC1 or TSC2 and the consequent hyperactivation of mTORC1 was shown to induce endoplasmic reticulum stress (ERS), a conserved cellular stress response, in cell lines (Young et al, 2013) and in mouse and human tumors (Ozcan et al, 2008). mTORC1 pathway, regulator of protein synthesis and translation, has a bidirectional crosstalk with the ERS pathway (Appenzeller-Herzog & Hall, 2012) and it can even selectively activate cell death (Kato et al, 2012). Folding and maturation of newly synthesized proteins take place in the endoplasmic reticulum (ER), and uncontrolled protein synthesis and dysfunctional nutrient sensing can overwhelm the folding capacity of the ER and challenge its integrity. The resulting ERS leads to the activation of a complex signaling network called the unfolded protein response (UPR) (Marciniak & Ron, 2006; Schroder & Kaufman, 2005). The ER homeostasis can be perturbed by physiological and pathological insults such as high protein demand, viral infections, environmental toxins, inflammatory cytokines, and increased protein translation resulting in an accumulation of misfolded and unfolded proteins in the ER lumen. There are several available chemicals to induce ERS and activate the UPR, like tunicamycin, thapsigargin, dithiothreitol (DTT) and MG132 (Osowski & Urano, 2011b), mainly used in a cell culture system. Physiological perturbants known to induce ERS include starvation, exercise and a HFD (Deldicque et al, 2012).

There are three effectors of the UPR localized at the ER membrane: inositol-requiring enzyme-1 (IRE1), PKR-like endoplasmic reticulum kinase (PERK) and activating transcription factor 6 (ATF6), each responsible for initiating a downstream cascade of distinct regulatory processes. Activated IRE1 $\alpha$  splices and activates XBP-1 mRNA transcription factor which induces transcription of endoplasmic reticulum associated protein degradation (ERAD) components such as EDEM and HRD1; ATF6 transits to the Golgi and is cleaved to be activated as a transcription factor to regulate ER chaperons such as Grp78 (Bip) and Grp94. When PERK is activated, it phosphorylates and inhibits eukaryotic translation initiation factor 2- $\alpha$  (eIF2 $\alpha$ )

to reduce mRNA translation, which selectively increases translation of ATF4. Downstream targets of ATF4 during activated UPR include CHOP, Tribble 3 and Gadd34. The process of the UPR is divided into two phases: in an initial physiological response, the UPR tries to overcome the ER overload by promoting a global translational attenuation through inhibition of eIF2 $\alpha$  to alleviate protein trafficking to the ER, and the activation of chaperons that aid in protein folding to relieve the ERS, like Hspa5, Ddit3, Xbp1 and Grp78. By contrast, upon chronic activation of the UPR the ER cannot overcome the stress stimuli and activates the apoptotic branch of the IRE1 $\alpha$ -ASK1-JNK signaling pathway, CHOP regulation of BCL2 protein family members and apoptotic genes, ER localized Bax and Bak, GSK3 $\beta$  and caspases that will promote cell death (Xu et al, 2005). Moreover, when ERS is unresolved it also promotes apoptosis by the activation of ATF4, a master regulator of the integrated stress response (ISR) known to be selectively translated by eIF2 $\alpha$  upon ERS (Appenzeller-Herzog & Hall, 2012; Harding et al, 2000), which activates its downstream targets CHOP and GADD34 (Osowski & Urano, 2011a) promoting cell death. It has been described that upon ERS the endoplasmic reticulum expands and suffers conformational changes characterized by swollen tubules and even aggregated clusters (Akiyama et al, 2009; Riggs et al, 2005; Varadarajan et al, 2012), which can be detected by electron microscopy.

ERS is known to be involved in the pathophysiological process of different diseases: neurodegenerative diseases associated with inclusion body formation and protein aggregation have been linked to ERS, including amyotrophic lateral sclerosis, Parkinson's disease, Huntington's disease and others (Xu et al, 2005). For example, autopsy studies suggest that the PERK-eIF2 $\alpha$  pathway is hyperactive in the brain of Alzheimer's disease, implying that ERS is activated (Unterberger et al, 2006). ERS is also associated to the development of metabolic complications like insulin resistance in diabetes, as it appears to act directly as a negative modulator of the insulin signaling pathway and by promoting lipid accumulation (Flamment et al, 2012; Salvado et al, 2015). Obesity can activate ERS in the liver by increasing the demand on the protein folding capacity of the ER, and this is linked to the activation of Kruppel-like factor 15 (KLF-15) and the development of hepatic insulin resistance (Jung et al, 2013). As a consequence, apoptosis of hepatic stellate cells can occur through JNK pathway activated

Calpain/Caspase-12 (Huang et al, 2014). Aberrant calcium regulation in the ER causes protein unfolding, because of the calcium dependent nature of ER chaperones (Ma & Hendershot, 2004). The strongest link between ER calcium regulation and the cell death machinery is found in the BCL-2 family of proteins, many of which reside in part in the ER membranes. Calcium homeostasis is especially important in the sarcoplasmic reticulum (SR), which functions as an intracellular calcium store in skeletal muscle. Dysregulation of sarcoplasmic reticulum calcium release and mutations in the ryanodine receptor have been associated with ERS and impaired muscle function (Bellinger et al, 2008). However, there is not much known about the cause or consequences of ERS activation in skeletal muscle (Deldicque et al, 2012). ERS was first observed in myotonic dystrophy type I and sporadic inclusion body myositis, which had higher expression of ER chaperons (Vitadello et al, 2010). HFD fed mice showed activated ERS in skeletal muscle, and ultra-endurance exercise also activated the UPR in human skeletal muscle (Deldicque et al, 2012; Kim et al, 2011). It was recently reported that activation of ATF4 can promote muscle atrophy during fasting or immobilization by promoting the activation of Gadd45 and p21 (Ebert et al, 2012; Ebert et al, 2010; Fox et al, 2014). Specific evidence linking ERS to muscle dystrophies was recently shown by De Palma *et al.*, who demonstrated increased activation of the UPR in skeletal muscle of myopathies caused by mutations of the collagen VI genes (De Palma et al, 2014). In addition, deletion of hexose-6-phosphate dehydrogenase (H6PD), the enzyme that catalyzes the pentose phosphate pathway inside the ER, activates the UPR and induces a myopathy with fasting hypoglycemia and increased insulin sensitivity (Lavery et al, 2008). Interestingly, ERS was shown to contribute to the pathophysiology of DMD because Caspase-12 ablation, an apoptosis initiator specifically activated by ERS, preserved mdx mice muscle function and recovered 75% of muscle force (Moorwood & Barton, 2014). Therefore, ERS is an interesting pathway to study in skeletal muscle as it could be involved in the pathophysiology of myopathies and the regulation of metabolic homeostasis.

#### **2.4. Fibroblast Growth Factor 21**

Fibroblast growth factors (FGF) are a family of 22 proteins involved in the regulation of mitosis, development, transformation, angiogenesis and survival in mammal cells (Beenken &

Mohammadi, 2009). They are heparin-binding secreted proteins that interact with cell-surface-associated FGF receptors (FGFR) for signal transduction. Recently FGF19, FGF21 and FGF23 were described to form part of an endocrine sub-group, because they lack a conventional heparin-binding domain and can reach circulation to act as endocrine hormones (Kharitononkov, 2009). Instead of heparin, FGF19, FGF21 and FGF23 use Klotho co-factor proteins to allow binding and activation of FGFR (Kurosu & Kuro, 2009). FGF19 is most highly expressed in gut, requires  $\beta$ -Klotho (KLB) or Klotho to bind to FGFR4 and is essential to regulate bile-acid metabolism and also has a role in promoting glucose and fatty acid metabolism. FGF23 primarily originates from bone, requires  $\alpha$ -Klotho to bind to FGFR1c and is essential in the control of phosphate and vitamin D metabolism (Adams et al, 2012b; Angelin et al, 2012; Kharitononkov, 2009).

The endocrine FGF that has attracted more attention due to its potential as an anti-obesity and anti-diabetic drug is FGF21, which is currently being tested in clinical trials (Gaich et al, 2013; Gimeno & Moller, 2014; Kharitononkov et al, 2013). FGF21 was first discovered in an in-vitro glucose uptake assay looking for novel proteins with therapeutic potential to treat diabetes mellitus (Nishimura et al, 2000). FGF21 was shown to increase insulin activity and induce glucose uptake in 3T3-L1 and human primary adipocytes. The insulin and FGF21 pathways appeared to be interdependent, and the interest grew to find if FGF21 could be used to treat diabetes without the side effects of insulin therapy, such as hypoglycemia and weight gain. The first evidence of FGF21's in-vivo bioactivity was shown with FGF21 administration to obese (ob/ob) and diabetic (db/db) mice, which led to a profound weight loss and plasma glucose lowering with no hypoglycemia (Kharitononkov et al, 2005; Kim et al, 2013a). FGF21 over-expressing transgenic mice showed decreased body weight, lower glycemia and resistance to diet-induced obesity (Berglund et al, 2009; Fisher et al, 2010; Kharitononkov et al, 2005). Importantly, it was established that FGF21 had no mitotic effect and transgenic animals were partially protected from chemically-induced malignancies (Huang et al, 2006), while interestingly showing extended lifespan (Zhang et al, 2012).

FGF21 selectively requires  $\beta$ -Klotho (Adams et al, 2012a; Ding et al, 2012; Ogawa et al, 2007) to act through FGFR1 and FGFR2 to induce an improved metabolic profile: it reduces serum insulin, cholesterol, triglycerides, leptin and glucose levels, while improving glucose control, uptake and insulin sensitivity to confer resistance to diet and age-induced weight gain and fat accumulation (Inagaki et al, 2007; Kharitononkov et al, 2005). In contrast, FGF21 deficiency leads to an increase in body weight, development of a fatty liver, glucose intolerance and increased serum insulin and triglycerides, which is exacerbated when placing the mice on a HFD or ketogenic diet (Badman et al, 2007; Kharitononkov, 2009). Potential target tissues of FGF21, due to a selective KLB expression in metabolically active tissues, include liver, white and brown adipose tissues, pancreas and the brain (Angelin et al, 2012; Kharitononkov, 2009). FGF21 was first shown to be secreted by liver upon fasting and starvation through Peroxisome proliferator-activated receptor  $\alpha$  (PPAR $\alpha$ ), which is known to regulate fat utilization during starvation (Inagaki et al, 2007). The effects of FGF21 during starvation include increased ketogenesis in the liver, lipolysis in white adipose tissue and reduced physical activity and hypothermia due to a hibernation-like state to preserve energy (Inagaki et al, 2007). FGF21 increases fatty acid oxidation, tricarboxylic acid cycle (TCA) flux and gluconeogenesis in the liver by inducing PGC1 $\alpha$  during the progression from fasting to starvation (Cornu et al, 2014; Potthoff et al, 2009). In addition, a HFD or ketotic diet can also induce FGF21 in the liver downstream of PPAR $\alpha$  (Badman et al, 2007), which identifies FGF21 as a critical regulator of lipid homeostasis, besides its role in glucose metabolism and insulin sensitization. However, there is some contradiction in current literature as to whether FGF21 induces or inhibits gluconeogenesis in the liver, which could be due to the differences in the feeding status and the animal models used: while some studies show FGF21 increasing gluconeogenesis in the liver in response to fasting through PGC1 $\alpha$  activation (Cornu et al, 2014; Potthoff et al, 2009), other recent studies have shown that it actually inhibits gluconeogenesis by regulating STAT3-SOCS signaling pathway (Berglund et al, 2009; Wang et al, 2014). Nevertheless, the action of FGF21 on liver has been shown to be critical to regulate glycemia independently of insulin, by increasing energy metabolism via the activation of brown fat and browning of white fat (Emanuelli et al, 2014). An unexpected outcome of increased FGF21 is growth impairment due

to FGF21 blocking growth hormone (GH) signaling in the liver by inhibition of STAT5 and subsequent decrease in IGF-1 production (Inagaki et al, 2008; Kubicky et al, 2012) and by preventing the effects of the GH on chondrocytes through increased leptin receptor overlapping transcript expression (LEPROT and LEPROT1) (Wu et al, 2013). These studies show that FGF21 is a key controller of metabolism through the regulation of the body's starvation response by activating critical pathways of energy conservation and re-distribution.

Adipose tissue is one of the main target tissues of FGF21 action, and it is also able to secrete FGF21. The main effect of FGF21 on whole-body metabolism is the increase in energy expenditure and thermogenesis, which was shown to be induced through activation of white adipose tissue browning (Fisher et al, 2012). Adipose-derived FGF21 acts in an autocrine/paracrine manner to increase expression of UCP1, PGC1 $\alpha$  and other thermogenic genes in fat tissues (Fisher et al, 2012; Sammons & Price, 2014). This is achieved by the activation of AMPK and sirtuin 1 in adipocytes resulting in enhanced mitochondrial oxidative function (Chau et al, 2010) to regulate energy metabolism. Adipose tissue FGF21 can also be induced by fasting, HFD feeding and PPAR $\gamma$  agonists, which shows another mechanism by which adipose tissue can influence and correct hyperglycemia and whole-body insulin sensitivity (Muisse et al, 2008). The main molecular mechanism unraveled to be activated by FGF21 in adipose tissue is phosphorylation of FRS2 and subsequent activation of the MAPK signaling cascade. FGF21 also induces GLUT1 expression and glucose uptake through sequential activation of ERK1/2 and SRF/Elk-1 transcription factors (Ge et al, 2011). In addition, it was shown that the action of FGF21 on energy expenditure, insulin action and glucose homeostasis was mediated through the secretion of adiponectin by adipose tissue, which is considered a downstream effector of FGF21 responsible of its systemic effects (Holland et al, 2013; Lin et al, 2013). Interestingly, while FGF21 can act directly on white adipose tissue to modulate the expression of metabolic genes, its effect on energy expenditure, body weight and insulin levels is mediated through its action on the central nervous system. FGF21 can cross the blood-brain barrier, and act on the suprachiasmatic nucleus in the hypothalamus and in the hindbrain to increase corticosterone levels, which in turn modulates circadian behavior (Bookout et al, 2013; Owen et al, 2014). FGF21 can also contribute to the neuroendocrine control of female



reproduction during nutritional deprivation by inhibiting the vasopressin-kisspeptin signaling cascade (Owen et al, 2013). These studies show the broad range of action of FGF21 as a metabolic hormone in different tissues to modulate whole-body metabolism.

Initially it was thought that FGF21 could only be secreted by the liver, which was shown to be the main organ involved in the fasting and starvation response regulated by FGF21 (Markan et al, 2014). Nevertheless, in recent years several studies have shown that brain, pancreas, adipose tissue and muscle are also capable of secreting FGF21 (Kharitononkov, 2009). The first study reporting that FGF21 could be a muscle secreted myokine showed that it was under the control of Akt and the insulin signaling pathway, as skeletal muscle-specific Akt1 transgenic mice had increased expression of FGF21 in muscle and increased FGF21 concentration in serum (Izumiya et al, 2008a). However, research on FGF21 as a myokine was scarce until 2012, when Kim *et al.* reported that autophagy deficiency and mitochondrial function impairment could induce a strong up-regulation of FGF21 in skeletal muscle, which in turn caused a strong phenotype in these mice conferring them lean and resistance to a HFD, with an improved metabolic profile (Kim et al, 2013c). Another recent study showed that skeletal muscle mitochondrial uncoupling can also induce FGF21 and cause metabolic changes at the whole-body level (Keipert et al, 2014), which helped establish mitochondrial dysfunction and oxidative stress as the main inducers of FGF21 in skeletal muscle through the activation of ATF4. The metabolic profile of these two transgenic mouse models, with over-expression of skeletal muscle Atg7 and Ucp1 respectively, was very similar as both were lean, with increased browning of white adipose tissue, fatty acid oxidation and improved insulin sensitivity. Interestingly, as this profile is also similar to FGF21 over-expressing transgenic mice, it was finally accepted that skeletal muscle can be an important source of FGF21 which can influence whole-body metabolism. A few following studies showed that this was also the case in humans, as it was reported that patients of muscle-manifesting mitochondrial disorders and HIV had increased expression of FGF21 in muscle and increased plasma FGF21 (Lindegard et al, 2013; Suomalainen, 2013) which correlated with the lipodystrophy and lipid disturbances observed in these patients (Lindegard et al, 2013). Yet, muscle is still not considered a target for FGF21 action. This is somehow counter-intuitive, as one of the main actions of FGF21 is the regulation

of glucose metabolism, and skeletal muscle is the main organ for glucose disposal and storage. Moreover, Keipert et al. reported that skeletal muscle expressed KLB (Keipert et al, 2014), which would make muscle a target for FGF21 action. In addition, FGF21 can increase basal and insulin stimulated glucose uptake in human myotubes through induction of GLUT1 (Mashili et al, 2011). Thus, skeletal muscle not only is a source of FGF21, but seems to also be a potential target to its action.

But, can circulating FGF21 be an indicator of metabolic imbalance? Based on the therapeutic effect of FGF21 for obese and diabetic animals, it was assumed that high circulating FGF21 would be beneficial. However, many studies demonstrated that FGF21 levels were increased in subjects with obesity, type 2 diabetes, insulin resistance or fatty liver disease (Chavez et al, 2009; Dushay et al, 2010; Zhang et al, 2008), which were then termed as states of resistance to FGF21. In some cases elevated FGF21 levels correlated with the degree of metabolic disturbance, thus this pointed towards a possible involvement of FGF21 in disease, and its induction as a “stress” hormone. This correlates with FGF21 being induced in patients with mitochondrial disease and muscle manifestations (Suomalainen et al, 2011). In skeletal muscle, FGF21 is induced upon mitochondrial impairment and oxidative stress, through the activation of ATF4, a key component of the integrated stress response (Keipert et al, 2014; Kim et al, 2013b; Kim et al, 2013c; Touvier et al, 2015). In the liver, FGF21 is induced by fasting and starvation, which constitute metabolic stresses. A growing number of studies with animals and patients indicate that FGF21 can also be induced by pathogenic conditions, such as liver injury, viral infection and cancer (Dasarathy et al, 2011; Domingo et al, 2010; Yang et al, 2013; Yilmaz et al, 2010). Endoplasmic reticulum stress was reported to induce FGF21 through the PERK/eIF2 $\alpha$ /ATF4 pathway in hepatocytes (Schaap et al, 2013) dependent on ATF4 and CHOP (Wan et al, 2014). Two in vivo studies showed that FGF21 could be induced in the liver through ERS: one reporting PERK/eIF2 $\alpha$ /ATF4 being the activating pathway (Kim et al, 2015), while the other argued that FGF21 is regulated through the IRE1 $\alpha$ -Xbp1 branch of the UPR (Jiang et al, 2014). Thus, FGF21 is attracting more attention, not only because of its potential beneficial effects, but for its role as a stress induced hormone both in the liver and in the muscle (Kim &

Lee, 2014; Luo & McKeehan, 2013). Nevertheless, the molecular pathways that induce FGF21, as well as the mechanisms activated by FGF21 in different tissues still need further studying.

## 3. RESULTS

### 3.1. Manuscript 1

#### **Activation of mTORC1 in skeletal muscle regulates whole-body metabolism through FGF21**

Maitea Guridi<sup>1</sup>, Lionel A. Tintignac<sup>1, 2</sup>, Shuo Lin<sup>1</sup>, Barbara Kupr<sup>1</sup>, Perrine Castets<sup>1, 3</sup>, Markus A. Rüegg<sup>1\*</sup>

<sup>1</sup>Biozentrum, University of Basel, CH-4056 Basel, Switzerland; <sup>2</sup>INRA, UMR866, Université Montpellier 1, Université Montpellier 2, 34090 Montpellier, France; <sup>3</sup>Neuromuscular Research Center, Departments of Neurology and Biomedicine, Pharmazentrum, Basel University Hospital, 4056 Basel, Switzerland

**\*Corresponding author:**

markus-a.ruegg@unibas.ch, Tel: +41 61 267 22 23, Fax: +41 61 267 22 08

## ABSTRACT

Skeletal muscle is the largest organ, comprising 40% of the total body lean mass, and affects whole-body metabolism in multiple ways. We investigated the signaling pathways involved in this process using TSCmKO mice, which have a skeletal muscle-specific depletion of TSC1 (tuberous sclerosis complex 1). This deficiency results in the constitutive activation of mTORC1, which enhances cell growth by promoting protein synthesis. TSCmKO mice were lean, with increased insulin sensitivity, as well as changes in white and brown adipose tissue and liver indicative of increased fatty acid oxidation. These differences were due to increased plasma concentrations of FGF21, a hormone that stimulates glucose uptake and fatty acid oxidation. Skeletal muscle of TSCmKO mice released FGF21 because of mTORC1-triggered endoplasmic reticulum (ER) stress and activation of a pathway involving PERK (protein **kinase** RNA-like ER **kinase**), eIF2 $\alpha$  (eukaryotic translation initiation factor 2 $\alpha$ ), and ATF4 (activating transcription factor 4). Treatment of TSCmKO mice with a chemical chaperone that alleviates ER stress reduced FGF21 production in muscle and increased body weight. Moreover, injection of function-blocking antibodies directed against FGF21 largely normalized the metabolic phenotype of the mice. Thus, sustained activation of mTORC1 signaling in skeletal muscle regulated whole-body metabolism through the induction of FGF21, which over the long-term caused severe lipodystrophy.

## INTRODUCTION

Skeletal muscle is a dynamic tissue with a key role in the maintenance of metabolic homeostasis. Several lines of evidence indicate that alterations of the normal muscle function, as for example in muscular dystrophies, obesity or diabetes, can affect the metabolism at the whole-body level (DeFronzo & Tripathy, 2009; Llagostera et al, 2007). The effect of muscle on the global metabolism has been linked to the discovery of specific cytokines secreted by the muscle, called myokines, which exert effects on angiogenesis, myogenesis and energy metabolism (Pedersen & Febbraio, 2012). Specifically, fibroblast growth factor 21 (FGF21) is secreted by skeletal muscle and protects from diet-induced obesity and insulin resistance (Kim et al, 2013c). FGF21 is a member of an atypical subfamily of FGFs that is released into the circulation because of the lack of a heparin-binding domain and thus acts as an endocrine factor (Angelin et al, 2012). FGF21 is at the center of extensive research as a target molecule to treat metabolic disorders, such as diabetes and obesity (Gaich et al, 2013). FGF21 promotes weight loss through an increase in fatty acid oxidation and lowers triglyceridemia and decreases glycemia by improving insulin sensitivity (Inagaki et al, 2007). Transgenic mice overexpressing FGF21 in the liver are protected against diet-induced obesity (Kharitonov et al, 2005) and FGF21 pharmacotherapy in diabetic and obese mice rapidly improves metabolic abnormalities (Holland et al, 2013; Xu et al, 2009). FGF21 is primarily synthesized in liver upon starvation or a high fat diet (HFD), and can also be induced in adipose tissue (Badman et al, 2007; Wang et al, 2008). In skeletal muscle, FGF21 is secreted in response to the activation of cellular stress pathways, such as autophagy impairment and/or mitochondrial dysfunction (Keipert et al, 2014; Kim et al, 2013c).

The mammalian target of rapamycin (mTOR) is a master regulator of metabolic homeostasis and its deregulation is associated with metabolic disorders, such as obesity and diabetes. mTOR is an atypical serine/threonine protein kinase that senses nutrient availability and cellular energy status to promote anabolic processes (Laplante & Sabatini, 2012). mTOR assembles into two distinct multi-protein complexes: mTORC1, which promotes cell growth through the regulation of protein synthesis, and mTORC2, which regulates cytoskeleton organization. Development of transgenic mouse models deficient for components of mTORC1 or mTORC2 in metabolic organs, such as adipose tissue or liver, have shown that these complexes play essential roles in glucose and lipid homeostasis (Hagiwara et al, 2012; Polak et al, 2008a). We have previously shown that mice with muscle-specific depletion of raptor (RAmKO mice), an essential component of mTORC1, develop a progressive myopathy (Bentzinger et al, 2008b). Surprisingly, mice with muscle-specific depletion of the mTORC1 inhibitor TSC1 (TSCmKO mice), characterized by sustained mTORC1 activation and increased protein synthesis, also develop a late-onset myopathy (Castets et al, 2013) with a marked atrophy of most muscles (Bentzinger et al, 2013). These alterations in TSCmKO muscle are related to increased proteasome activity and to the blockade of autophagy induction (Bentzinger et al, 2013; Castets et al, 2013). Concomitant with the myopathy, TSCmKO mice show decreased fat mass (Castets et al, 2013), suggesting that constitutive mTORC1 activation in skeletal muscle may exert endocrine effects on non-muscle tissues. In addition, RAmKO mice and mice deficient for mTOR in skeletal muscle have altered glucose metabolism (Bentzinger et al, 2008b; Risson et al, 2009b), pointing to a possible role of muscle mTORC1 signaling in the regulation of whole-body metabolism.

In this study, we examined the global metabolic changes in TSCmKO mice starting at a young age and show that they were resistant to obesity and developed a severe lipodystrophy with age. The constitutive activation of mTORC1 in muscle led to an increased FGF21 synthesis and higher concentration of FGF21 in plasma. This was largely due to the endoplasmic reticulum (ER) stress-activated PERK-eIF2 $\alpha$ -ATF4 pathway. Thus we showed that specific perturbation of mTORC1 signaling in muscle modified whole-body homeostasis by inducing release of FGF21 as a myokine.



## RESULTS

### **mTORC1 activation in skeletal muscle promotes a lean phenotype**

In TSCmKO mice, mTORC1 is constitutively activated in skeletal muscle and they develop a late-onset myopathy in conjunction with a reduced body weight resulting from the loss of both fat and lean mass (Castets et al, 2013). To determine if these differences in body mass were a consequence of the myopathy, we analyzed the progression of the metabolic phenotype of TSCmKO mice, starting at the age of 10 weeks when the mice are healthy with no signs of a myopathy (Fig S1A). At this young age, TSCmKO mice were 15% lighter than control mice, and this difference increased to 31% at 40 weeks of age (Fig 1A; Table S1). We also noticed that the tibia length was slightly but significantly reduced in TSCmKO mice compared to age-matched control mice (Table S1), suggesting a difference in overall growth. Analysis of plasma revealed no changes in growth hormone (GH) concentrations (Fig S1B) but a significant decrease in insulin-like growth factor (IGF-1) (Fig 1B), which could correlate with the reduced growth (LeRoith & Yakar, 2007). While the difference in tibia length between TSCmKO and control mice remained constant between 10 and 40 weeks of age, the weight difference was progressive and increased with age (Table S1).

The activity and the feeding behavior of the mutant and control mice were similar (Fig S1C-1F). Lean mass was reduced in TSCmKO mice but followed the same pattern with age as in control mice (Fig 1C). In contrast, the loss in fat mass in TSCmKO mice increased with age (Fig 1D, 1E). The difference in fat mass between control and TSCmKO mice was exaggerated by placing the mice on a 14-week-long high fat diet (HFD), starting at the age of 10 weeks. As expected, the body weight of the control mice progressively increased (Fig 1F), which was

largely due to a gain in fat mass (Fig 1D), and these mice developed hepatic steatosis (Fig 1G). In contrast, TSCmKO mice were resistant to these changes (Fig 1D, 1F, 1G). Compared to controls, TSCmKO mice ate more and were more active during the HFD (Fig S1G, S1H). Together, these results emphasized the inability of mutant mice to gain weight, which was mainly due to a change in fat mass, and they pointed toward a major perturbation of the global metabolism in TSCmKO mice.

### **TSCmKO mice show an increase in fatty acid oxidation**

To further examine the resistance of TSCmKO mice to HFD, we measured energy expenditure. While it was similar between 10-week-old control and mutant mice, energy expenditure was increased in 40-week-old TSCmKO mice and in mutant mice on the HFD (Fig 2A). The enhanced energy expenditure correlated with increased transcription of *Ucp2* (which encodes uncoupling protein 2) in skeletal muscle (Fig 2B). Since UCPs uncouple energy production from oxidative phosphorylation, we also measured ATP concentrations and found a significant reduction in TSCmKO skeletal muscle (Fig 2C). Consistently, in TSCmKO muscle, the phosphorylation (Ser<sup>173</sup>) and thus activation of the AMP-activated protein kinase (AMPK) was increased (Fig 2D). Furthermore, the abundance of pyruvate dehydrogenase kinase (PDK4) was increased (Fig 2D), suggesting that TSCmKO muscle fibers switched to fatty acids as energy substrate. Expression of *Pdk4*, as well as other genes associated with fatty acid oxidation, such as *peroxisome proliferator activated receptor-γ coactivator 1-beta* (*Ppargc1b*) and *fatty acid binding protein 3* (*Fabp3*) were increased in TSCmKO muscle (Fig 2B). The expression of all the genes measured in TSCmKO liver was unchanged (Fig S2A), except for that of *acetyl-CoA carboxylase 1* (*Acac1*),

which encodes an enzyme involved in fatty acid synthesis, and *peroxisome proliferator activated receptor-γ coactivator 1-alpha (Ppargc1a)*, which encodes the transcriptional coactivator PGC1α which is involved in the control of fatty acid oxidation (Puigserver, 2005) (Fig 2E). These results suggest that fatty acid oxidation could also be increased in the liver of mutant mice (Wu et al, 1999).

Increased fatty acid oxidation, as observed for example during fasting, induces ketone body synthesis in the liver as an alternative source of energy (Newman & Verdin, 2014). The concentration of β-hydroxybutyrate, which indicates ketone body production, was increased in the plasma of TSCmKO mice compared to controls (Fig 2F). Moreover, we found increased expression of mRNAs encoding the main enzymes involved in ketone body catabolism, such as *D-β-hydroxybutyrate dehydrogenase 1 (Bdh1)* and *3-oxoacid-CoA transferase 1 (Oxct1)*, in TSCmKO skeletal muscle, while the expression of ketogenic genes *3-hydroxy 3-methylglutaryl-CoA synthase 2 (Hmgcs2)* and *Acetyl-CoA acyltransferase 1 (Acat1)*, was significantly decreased (Fig 2B). Likewise, OXCT1 protein abundance was significantly increased in mutant muscle (Fig 2D). These results support the notion that the enhanced fatty acid oxidation caused increased ketogenesis in the liver of TSCmKO mice, which in turn, led to a higher utilization of ketone bodies in mutant muscle.

As a global change in fatty acid metabolism would also have an impact on the white adipose tissue (WAT), we analyzed the histology of the subcutaneous-inguinal WAT in 12-week-old control and TSCmKO mice. Mutant mice had smaller multilocular adipocytes (Fig 2G), also called brite or beige adipocytes, a phenotype suggestive of the “browning” of WAT, a process characterized by increased number of mitochondria and thermogenic capacity (Bartelt &

Heeren, 2014). Furthermore, there were smaller and fewer lipid droplets in the adipocytes of brown adipose tissue (BAT) of the mutant mice (Fig 2G), indicative of increased fatty acid oxidation. Accordingly, the mRNA and/or protein abundance of PGC1 $\alpha$ , carnitine palmitoyltransferase 1 (CPT-I), *Ucp1*, *PR domain containing 16 (Prdm16)* and *cell death-inducing DFF $\alpha$ -like effector  $\alpha$  (Cidea)*, which are markers for WAT browning and fatty acid oxidation (Puigserver, 2005; Seale et al, 2011), were increased in the WAT of TSCmKO mice (Fig 2H, 2I). Moreover, the phosphorylated, active form of the hormone-sensitive lipase (HSL) was increased in WAT from TSCmKO mice (Fig 2I). Consistent with increased triglyceride breakdown and enhanced fatty acid oxidation, free fatty acid concentration was increased in plasma from starved TSCmKO mice compared to control mice (Fig S2B). However, plasma triglyceride and cholesterol concentrations were unchanged in TSCmKO mice (Table S2). We therefore concluded that the increased fatty acid oxidation in WAT, BAT, liver and muscle, combined with increased ketogenesis in liver, resulted in the progressive loss of fat mass and adipose depots in TSCmKO mice.

### **TSCmKO mice have increased glucose absorption and improved insulin sensitivity**

Next we examined glucose homeostasis in the mice. Glucose blood concentrations were significantly reduced in TSCmKO mice at 10 and 40 weeks of age and remained significantly lower on the HFD (Fig 3A). Similarly, plasma insulin concentration was decreased and remained low on the HFD (Fig 3B). The low concentrations of insulin were unlikely due to a deficiency of the pancreas because its histology (general tissue integrity and presence of Langerhans islets) was similar to that of controls (Fig S3A). Moreover, although insulin concentrations were low in

TSCmKO mice in both starved and fed conditions, they were efficiently increased upon glucose administration (Fig 3C). Additionally, during an insulin tolerance test while on HFD, TSCmKO mice showed improved insulin sensitivity compared to the control mice (Fig 3D). Another mechanism that regulates plasma glucose concentrations is liver gluconeogenesis. While we did not detect gluconeogenesis defects in 10-week-old TSCmKO mice when compared to control animals (Fig S3B), gluconeogenesis became impaired in 24-week-old TSCmKO mice as shown by decreased glucose production in a pyruvate tolerance test (Fig 3E). Hence, these results indicated a general change in glucose metabolism in TSCmKO mice.

We next analyzed the expression of glucose metabolism genes in skeletal muscle. While the expression of most of the genes measured was unchanged (Fig S3C), that of *Slc2a1*, which encodes the glucose transporter GLUT1, was significantly increased in TSCmKO mice (Fig 3F). Likewise, GLUT1 protein abundance was increased while the amount of GLUT4 remained unchanged in TSCmKO muscle (Fig 3G). Although TSCmKO muscle did not show changes in the expression of genes encoding enzymes involved in glycolysis (Fig S3C), it contained more glycogen than control muscle (Fig 3H). As expected, reduced Akt activity in TSCmKO muscle (Bentzinger et al, 2013) led to a significant decrease in the inhibitory phosphorylation (Ser<sup>9</sup>) of glycogen synthase kinase 3- $\beta$  (GSK3 $\beta$ ) (Fig 3G). However, despite GSK3 $\beta$  being more active, phosphorylation of its target, glycogen synthase (GS), was unchanged in mutant muscle (Fig 3G), because increased availability of its substrate glucose might counteract the inhibitory activity of GSK3 $\beta$ . Hence, the increase in glucose uptake through GLUT1 under basal condition, rather than changes in glycolysis, might be responsible for the increase in glycogen in TSCmKO muscle.

Transcript and protein abundance of GLUT1 and GLUT4 was increased in WAT of TSCmKO mice (Fig 3I, 3J), suggesting higher glucose uptake in this non-muscle tissue. The phosphorylation (and activation) of Akt substrate of 160 kDa (AS160) was also increased in the WAT of mutant mice (Fig 3J); activated AS160 favors glucose absorption upon insulin signaling (Sano et al, 2003; Tan et al, 2012). An *in vivo* 2-deoxyglucose uptake test confirmed increased glucose absorption in muscle and WAT of mutant mice (Fig 3K). In contrast, expression of genes involved in glucose metabolism and transport were unchanged in the liver of TSCmKO mice (Fig S3D). These results indicated that sustained mTORC1 activity in skeletal muscle reduced glycemia, because of the enhanced insulin sensitivity and increased glucose absorption in muscle and WAT.

To determine if these changes in glucose metabolism were a direct consequence of mTORC1 activity in muscle, we also examined glucose metabolism in RAMKO mice, which lack mTORC1 signaling in skeletal muscle (Bentzinger et al, 2008b). While plasma glucose and insulin concentrations were unchanged in 10-week-old RAMKO mice (Fig S3E, S3F), the mice were insulin resistant when compared to control littermates (Fig 3L). Together, these results point to a major role for mTORC1 signaling in muscle in regulating whole-body glucose metabolism.

### **TSCmKO muscle secretes FGF21**

Changes in whole-body metabolism in the TSCmKO mice suggested the action of a secreted myokine (Pedersen & Febbraio, 2012). One candidate is FGF21, a starvation-induced hormone that can decrease glycemia and promote fatty acid oxidation (Angelin et al, 2012). At the age of 10 weeks, plasma concentrations of FGF21 were not detectable by ELISA in fed mice. As

reported by others, 24-hour starvation increased FGF21 concentration (Fig 4A). Plasma FGF21 concentrations were significantly higher in starved TSCmKO mice, and were also higher in 24-week-old fed mutant mice compared to control littermates (Fig 4A). These results were confirmed by Western blot analysis of plasma FGF21 (Fig S4A). Besides the liver, which is the main FGF21 secretory organ (Badman et al, 2007), FGF21 can also be secreted by WAT (Wang et al, 2008), BAT (Hondares et al, 2010), pancreas (Johnson et al, 2009) and skeletal muscle (Izumiya et al, 2008a; Keipert et al, 2014). Thus, to determine the origin of the increased plasma concentrations of FGF21 in mutant mice, we compared transcript and protein abundance of FGF21 in these tissues between control and TSCmKO mice. While *Fgf21* expression was significantly reduced in liver from TSCmKO mice, it was significantly increased in *tibialis anterior* (TA) muscle from mutant mice (Fig 4B). *β-Klotho* encodes the essential co-receptor of FGF21 (Ding et al, 2012), and its expression was unaltered, except in WAT where it was significantly increased (Fig 4B). FGF21 protein abundance was unchanged in all organs, but was increased in TSCmKO muscle (Fig 4C). Moreover, HFD treatment increased expression of *Fgf21* in the liver of control mice as previously reported (Badman et al, 2007), while *Fgf21* expression was unchanged in the liver of TSCmKO mice but significantly increased in the muscle of mutant mice (Figure S4B). This increase in FGF21 abundance was a direct consequence of mTORC1 signaling because three-day treatment with the mTORC1 inhibitor rapamycin normalized *Fgf21* expression in TSCmKO muscle (Fig 4D). Furthermore, while FGF21 plasma concentrations were unchanged in 20-week-old RAmKO mice (Fig 4E), FGF21 protein abundance was significantly reduced in the targeted muscle (Fig 4F). Together, these results indicate that the increased

plasma FGF21 concentrations in TSCmKO mice originated from skeletal muscle and they shed light on a role of mTORC1 signaling in regulating FGF21 in skeletal muscle.

### **mTORC1-activated ER stress induces FGF21 in skeletal muscle**

*Fgf21* expression in muscle correlates with increased abundance of activating transcription factor 4 (ATF4) (Keipert et al, 2014; Kim et al, 2013c). ATF4 is a critical regulator of the integrated stress response, which is induced by various cellular stresses including amino acid depletion, endoplasmic reticulum (ER) or oxidative stress (Harding et al, 2000). In 10-week-old TSCmKO mice, the protein abundance of ATF4 was increased (Fig 5A) whereas *Atf4* expression was not altered (Fig S5A). In contrast, skeletal muscle from 12-week-old RAmKO mice contained lower amounts of ATF4 (Fig 4F).

Two pathways have previously been implicated in the ATF4-mediated increase in FGF21 abundance in muscle: impaired autophagy and mitochondrial dysfunction (Keipert et al, 2014; Kim et al, 2013c). Autophagy induction is inhibited in the TSCmKO mice by phosphorylation of Unc-51 like autophagy activating kinase 1 (Ulk1) (Castets et al, 2013). Ulk1 is part of the autophagy initiation complex and mutation of Ser<sup>757</sup> in Ulk1 to Ala restores autophagy induction in TSCmKO mice (Castets et al, 2013). To examine the effect of autophagy on FGF21 abundance in TSCmKO muscle, we electroporated mutant Ulk1 into TA muscle. Despite partial restoration of autophagy in the electroporated muscle, we did not observe a decrease in FGF21 mRNA or protein abundance in TSCmKO mice (Fig S5B, S5C). The electroporation *per se* did not affect FGF21 abundance (Fig S5D, S5E). In contrast, autophagy restoration in control mice was sufficient to decrease FGF21 mRNA and protein abundance (Fig S5B, S5C). TSCmKO mice at the



age of 10 to 12-weeks did not show changes in mitochondrial DNA (Bentzinger et al, 2013) or expression of genes involved in the mitochondrial respiratory chain or ROS production (Fig S5F). Moreover, the oxidative capacity of TSCmKO muscle is enhanced (Bentzinger et al, 2013) and the overall oxidation status of muscle proteins was not changed in mutant muscle (Fig S5G). These results indicated the existence of another pathway that mediated the increase in ATF4 and FGF21 abundance in the TSCmKO mice.

Indeed, examination of TSCmKO muscle by electron microscopy revealed the presence of irregularly shaped ER clusters (Fig 5B) suggestive of dysfunctional ER and ER stress (Varadarajan et al, 2012). The ER stress pathway that leads to an increase in ATF4 abundance acts through PKR-like endoplasmic reticulum kinase (PERK), which in turn inhibits its downstream target eukaryotic translation initiation factor 2-alpha (eIF2 $\alpha$ ) (Kim et al, 2008). Indeed, like ATF4 abundance, the phosphorylation of PERK and eIF2 $\alpha$  were increased in TSCmKO muscle (Fig 5A). In addition, the abundance of the ER stress marker binding immunoglobulin protein (BiP) was significantly increased (Fig 5A). Upon activation of ER stress, the unfolded protein response (UPR) is initiated to re-establish normal ER function (Kim et al, 2008). TSCmKO muscle had increased expression of genes involved in the UPR – such as *DNA-damage-inducible transcript 3 (Ddit3)*, which encodes CHOP, a pro-apoptotic transcription factor; *heat shock 70kDa protein 5 (Hspa5)*, which encodes the ER chaperone BiP; *X-box binding protein 1 (Xbp1)*, which encodes a transcription factor that controls genes involved in protein folding, and *Tribbles homolog 3 (Trib3)*, which is induced by CHOP and is involved in cell death (Hetz, 2012; Ohoka et al, 2005) (Fig 5C). Increased mTORC1 activity has been proposed to induce ER stress by increasing protein translation (Appenzeller-Herzog & Hall, 2012). Accordingly, protein synthesis (Bentzinger et al,

2013) and protein translation (Fig S5H) were increased in TSCmKO muscle. Moreover, rapamycin treatment significantly decreased the expression of *Hspa5* and *Ddit3* in TSCmKO and control mice (Fig S5I), demonstrating a role for mTORC1 in ER stress induction. To confirm that changes in mTORC1 signaling can directly modulate FGF21 abundance in muscle fibers, we studied the regulation of FGF21 *in vitro*. Acute mTORC1 activation in C2C12 myotubes by insulin induced FGF21 at the mRNA and protein levels, an effect that was abolished by pre-treatment of the cells with rapamycin (Fig 5D and 5E). Similarly, the ER stress inducer thapsigargin also promoted the accumulation of FGF21 at the mRNA and protein levels (Fig 5D, 5E). These results provide independent evidence suggesting that mTORC1 activation and ER stress induce FGF21 in muscle cells.

Lastly, to test directly whether alleviation of ER stress would normalize FGF21 *in vivo*, we treated control and TSCmKO mice with 4-phenylbutyric acid (4-PBA), a chemical chaperone that assists in protein folding (Ozcan et al, 2006). Four-week treatment decreased the abundance of ATF4 and the phosphorylation of PERK and eIF2 $\alpha$  (Fig 5F). Moreover, expression of the ER stress markers *Ddit3*, *Hspa5*, *Xbp1* and *Trib3* was reduced in TSCmKO muscle treated with 4-PBA (Fig 5G). In addition, the treatment and ER stress alleviation also decreased FGF21 mRNA expression and protein abundance (Fig 5F, 5G). Together, these results suggest that ER stress caused by sustained mTORC1 activation is the main cause for the induction of FGF21 in TSCmKO muscle.

### **Blocking of FGF21 normalizes the metabolism of TSCmKO mice**

Because 4-PBA treatment decreased FGF21 abundance in the muscle of TSCmKO mice, we also tested whether this treatment would normalize the metabolism of these mice. The 4-week treatment prompted a significant, progressive weight gain in TSCmKO mice (Fig 6A) that was likely due to an increase in lean mass (Fig 6B). Body temperature, which is decreased in FGF21 transgenic mice (Inagaki et al, 2007), and was significantly lower in TSCmKO mice (Fig 6C), was also normalized by 4-PBA treatment (Fig 6C). Blood glucose concentrations were the same in control and mutant mice after the treatment (Fig S6A), while insulin concentration remained low (Fig S6B).

To directly test whether blocking FGF21 would affect metabolism, we next injected a FGF21-neutralizing antibody (Omar et al, 2014) into 12- and 24-week-old TSCmKO mice. As expected, plasma concentrations of FGF21 were significantly decreased after anti-FGF21 antibody administration (Fig S6C). Injection of the antibody also normalized blood  $\beta$ -ketone (Fig 6D) and blood glucose concentrations (Fig 6E). Similar to the 4-PBA treatment, plasma insulin concentrations were not affected (Fig S6D). Inhibition of plasma FGF21 also improved liver gluconeogenesis in 24-week-old TSCmKO mice, as reflected by an increase in the rate of glucose production when compared to IgG-injected TSCmKO mice (Fig 6F). On the contrary, treatment of control mice with the FGF21-neutralizing antibody did not change plasma glucose, insulin and ketone body concentrations or pyruvate tolerance (Figure S6F-6I). Finally, FGF21 neutralization significantly reduced the expression of *Slc2a1*, *Slc2a4*, *Ppargc1a* (Fisher et al, 2012) and *Prdm16* in the WAT of TSCmKO mice without changing that of *Ucp1* and *Cpt1b* (Fig 6G). These results are consistent with FGF21 promoting glucose absorption and fatty acid

oxidation in the WAT of TSCmKO mice through transcriptional regulation. In addition, FGF21 neutralization decreased the expression of *Fabp3*, *Bdh1* and *Oxct1* in skeletal muscle without changing that of *Slc2a1* and *Pdk4* (Fig 6H), which correlates with a decrease in fatty acid oxidation and ketone body utilization. Control mice treated with the FGF21-neutralizing antibody showed increased expression of *Slc2a1*, *Slc2a4* and *Fgf21* in WAT, with no changes in gene expression in muscle or liver (Figure S6J). In contrast, the overnight treatment with the anti-FGF21 antibody was not sufficient to normalize the expression of *Ppargc1a* in liver from TSCmKO mice (Fig S6E). Together, these results suggest that FGF21 secreted by TSCmKO muscle is responsible for the overall metabolic changes in these mice, and that it acts directly on non-muscle tissues, such as WAT, to modify glucose and fatty acid metabolism.

## DISCUSSION

Skeletal muscle represents roughly 40% of the whole-body mass and thereby is the major supplier of amino acids for other metabolic organs like liver, in addition to being involved in the maintenance of metabolic homeostasis. We have previously shown that sustained mTORC1 activation in skeletal muscle blocks autophagy induction and causes a late-onset myopathy (Castets et al, 2013). In this study, we described how the metabolic phenotype of TSCmKO mice changed with age. We then characterized the underlying molecular pathways in young, healthy mice to ensure that metabolic changes were not secondary to the late-onset myopathy (Castets et al, 2013). TSCmKO mice were lean, which correlated with improved insulin sensitivity and increased fatty acid oxidation. The leanness was likely caused by mTORC1 inducing FGF21 as a myokine through the ER stress-induced activation of ATF4. Consistent with this interpretation, attenuation of ER stress by 4-PBA decreased FGF21 mRNA and protein abundance and alleviated several of the disease symptoms in TSCmKO mice. In addition, direct inhibition of circulating FGF21 with a neutralizing antibody also normalized most of the TSCmKO metabolic phenotype. Thus, in TSCmKO mice, the mTORC1 pathway in skeletal muscle regulates body-wide energy metabolism through FGF21.

Perturbations of mTORC1 in other tissues, such as WAT or liver, can affect leanness in mice (Peterson et al, 2011; Polak et al, 2008a; Yecies et al, 2011). Surprisingly, both activation and inhibition of mTORC1 result in resistance to diet-induced obesity, although specific consequences in other, non-targeted metabolic organs and the potential contribution of circulating factors have not been investigated and leanness has been attributed to different molecular mechanisms in the targeted tissues. In our study, we also identified molecular

changes in the targeted muscle tissue that might contribute to the metabolic phenotype of TSCmKO mice, such as modifications in *Ucp2*, *Ppargcb* and GLUT1 mRNA and protein abundance. In addition, we identified mTORC1-triggered ER stress in skeletal muscle as the main driver of the metabolic changes observed on the whole-body level. We have previously reported that overall protein synthesis in TSCmKO muscle is increased (Bentzinger et al, 2013), and here we showed an increase in translation initiation. Uncontrolled protein synthesis can result in ER stress and activate the UPR, by overwhelming the folding capacity of the ER (Appenzeller-Herzog & Hall, 2012; Xu et al, 2005). In an initial physiological response, induction of UPR effectors, such as PERK, leads to a global translational attenuation through inhibition of eIF2 $\alpha$  and to the activation of chaperones to relieve the ER stress. In contrast, unresolved ER stress and chronic activation of the UPR promote apoptosis by the activation of ATF4 downstream targets, such as CHOP and GADD34 (Kim et al, 2008). In TSCmKO muscle, the PERK-eIF2 $\alpha$ -ATF4 pathway was activated and chaperones and ER stress markers were increased. Decreased Akt activity in TSCmKO muscle (Bentzinger et al, 2013) may also contribute to the increased activity of PERK and the activation of the eIF2 $\alpha$ -ATF4 pathway, because PERK is inhibited by Akt-dependent phosphorylation (Mounir et al, 2011). Furthermore, consistent with the previously described ER conformational changes upon ER stress (Riggs et al, 2005; Varadarajan et al, 2012), muscle fibers of TSCmKO mice contained swollen tubules and aggregated clusters. We conclude that ER stress in muscle of TSCmKO mice is driven by the increase in protein synthesis and translation initiation caused by activated mTORC1.

We found that ER stress induced changes in whole-body metabolism through activation of ATF4, which in turn induces FGF21 (Kim et al, 2013c). We described the broad metabolic effects of FGF21 as a myokine, including changes in energy expenditure, ketogenesis, gluconeogenesis, fat mass, body temperature and growth. These metabolic perturbations were consistent with the phenotype of FGF21-overexpressing transgenic mice (Inagaki et al, 2007; Kharitononkov et al, 2005) and some of these effects have been attributed to FGF21 secreted from skeletal muscle (Keipert et al, 2014; Kim et al, 2013c). Although these studies have linked increased FGF21 abundance in skeletal muscle to disturbances of mitochondrial integrity or autophagy impairment, we did not observe changes in the expression of mitochondrial genes or oxidative stress in skeletal muscle of young TSCmKO mice. In addition, partial restoration of autophagy did not normalize FGF21 abundance in TSCmKO muscle. The induction of FGF21 in skeletal muscle has been linked to activation of the PI3K/Akt pathway (Izumiya et al, 2008a), which we showed was due to mTORC1 activation and its effect on ER stress, because Akt activity was attenuated in TSCmKO muscle, presumably due to the negative feedback loop of S6K on IRS-1, which in turn dampens PI3K-Akt signaling (Bentzinger et al, 2013). In support of this notion, activated mTORC1 in liver-specific TSC1 knockout mice also leads to FGF21 secretion (Cornu et al, 2014) and both ATF4 and FGF21 abundance were reduced in RAmKO muscle.

We showed that the main molecular mechanism driving FGF21 synthesis relied on mTORC1-induced ER stress. Increased mTORC1 activity or ER stress induced the accumulation of FGF21 in C2C12 myotubes. We further confirmed this molecular pathway by treating TSCmKO mice with 4-PBA, an FDA-approved chemical chaperone that is a candidate drug to treat diabetes, cancer and protein misfolding diseases (Iannitti & Palmieri, 2011; Ozcan et al,

2006). In TSCmKO muscle, 4-PBA treatment attenuated ER stress by reducing PERK-eIF2 $\alpha$ -ATF4 signaling, decreased the expression of UPR markers and reduced FGF21 mRNA and protein abundance without affecting mTORC1 activity. Long-term treatment with 4-PBA also increased the weight of the TSCmKO mice and normalized their body temperature.

The metabolic phenotype of TSCmKO mice is reminiscent of the action of FGF21 on metabolic organs. WAT is the main target tissue of FGF21 (Bookout et al, 2013; Ding et al, 2012; Kharitonov et al, 2005), and TSCmKO WAT showed increased mRNA and protein abundance of many regulators of browning, fatty acid oxidation and glucose metabolism, which were associated with increased glucose uptake and lipolysis. In addition, WAT was the only tissue in TSCmKO mice that showed significantly increased expression the gene encoding the  $\beta$ -Klotho receptor, an effect that is also seen in mice with increased plasma FGF21 concentration (Keipert et al, 2014) or in cultured adipocytes treated with FGF21 (Wei et al, 2012). The liver of TSCmKO mice showed increased expression of *Ppargc1a*, which correlates with increased fatty acid oxidation induced by FGF21 (Badman et al, 2007; Potthoff et al, 2009). FGF21 also induces ketogenesis in the liver (Inagaki et al, 2007) and TSCmKO mice had higher plasma  $\beta$ -ketone concentration and increased expression of genes involved in ketone body breakdown in muscle. TSCmKO mice also had reduced liver gluconeogenesis, which is consistent with the suppression of hepatic gluconeogenesis by FGF21 (Berglund et al, 2009; Wang et al, 2014).

We showed that acute inhibition of FGF21 in the blood with an FGF21-blocking antibody normalized several of the metabolic traits of TSCmKO mice, such as plasma  $\beta$ -ketone and glucose concentrations, thus confirming the functional role of FGF21 as a hormone in the mutant mice. The decreased plasma concentration of  $\beta$ -ketones was associated with reduced



expression of genes involved in ketone body breakdown in skeletal muscle. Similarly, normalization of plasma glucose concentration after blocking of FGF21 could be the result of improved liver gluconeogenesis and lower glucose uptake by WAT, which could be due to normalized expression of glucose transporter-encoding genes. Likewise, markers of fatty acid oxidation and browning were also normalized in WAT. In skeletal muscle, however, the increased expression of several metabolic genes in TSCmKO mice was not affected by inhibition of plasma FGF21, suggesting that those genes were induced by the autocrine action of FGF21 or directly by mTORC1 activation.

The phenotype of TSCmKO mice resembles the metabolism characteristic of starvation in several aspects. The “starvation” signal in TSCmKO mice could reflect the mTORC1-dependent increase in anabolic processes, which results in substantial energy depletion and exhaustion of ATP stores, as has been described in other TSC-deficient cell types (Inoki et al, 2003; Young et al, 2013). As in starvation, where liver is the main source for the increase in plasma FGF21 concentrations (Markan et al, 2014), the increase of FGF21 in the plasma of TSCmKO mice could constitute a stress signal to other metabolic organs to deliver fatty acids to muscle and might be the cause of the progressive loss of fat mass. Constitutive mTORC1 activity also renders hypoxic cells critically dependent on exogenous unsaturated lipids for survival, due to the induction of the UPR by deregulated lipid and protein synthesis in tumor cells (Young et al, 2013). In addition, many highly aggressive human cancers trigger increased release of fatty acids from lipid stores, contributing to the cachexia observed in patients. Furthermore, plasma FGF21 concentration is increased in HIV patients, and increased skeletal muscle FGF21 abundance has been specifically linked with lipodystrophy and lipid disturbances in these

patients (Domingo et al, 2010; Lindegaard et al, 2013). While FGF21 over-expressing transgenic mice are lighter and resistant to obesity, they do not develop lipodystrophy (Kharitononkov et al, 2005; Zhang et al, 2012), which suggests that stress-induced FGF21 could have disease-specific effects. In this context, solving the mechanisms of mTORC1-induced FGF21 secretion adds valuable knowledge in understanding disease-related metabolic changes that occur in pathologies, such as diabetes, cancer or HIV.

In addition to its positive effects on obesity and diabetes (Gaich et al, 2013), FGF21 can have detrimental consequences, including growth retardation (Inagaki et al, 2008; Wu et al, 2013), lower body temperature and decreased activity (Inagaki et al, 2007). Moreover, FGF21 decreases female fertility (Owen et al, 2013) and causes bone loss (Wei et al, 2012). Some of these aspects, such as lower body temperature and impaired growth, were also observed in the TSCmKO mice. The body temperature in the TSCmKO mice was reduced in the evening upon fasting, which is likely a direct effect of FGF21 causing torpor to conserve energy (Cornu et al, 2014; Inagaki et al, 2007). On the other hand, impaired growth in TSCmKO mice might be a consequence of decreased IGF-1 plasma concentration due to FGF21 action in the liver, as observed in other mouse models with increased plasma FGF21 (Inagaki et al, 2007; Keipert et al, 2014). Because changes in mTORC1 activity cause the perturbations observed in TSCmKO mice, it would also be interesting to investigate FGF21 signaling in other muscle pathologies in which mTORC1 signaling is deregulated (Ramos et al, 2012; Spitali et al, 2013). Nevertheless, our results suggest that alterations in mTORC1 signaling in skeletal muscle can directly affect whole-body metabolism, and they define broad effects for muscle-secreted FGF21. Moreover,

our study may bring new insights into the mechanisms responsible for metabolic changes that arise from altered muscle integrity and health.

## **MATERIAL AND METHODS**

**Mice.** Generation of TSCmKO and RAmKO transgenic mice and their genotyping have been previously described (Bentzinger et al, 2008b; Castets et al, 2013; Kwiatkowski et al, 2002). Control mice were littermates floxed for *Rptor* (gene encoding raptor) or *Tsc1* but not expressing Cre-recombinase. Mice were maintained in a conventional facility with a fixed light cycle (23°C – 12 hr dark-light cycle) and were fed standard chow (KLIVA NAFAG, 1304811) or a HFD containing 60% fat (KLIBA NAFAG, 2127.PH.A05) *ad libitum*. HFD was started at 10 weeks of age, and continued for 14 weeks. 10-week-old CLAMS (Comprehensive Lab Animal Monitoring System) and HFD analysis were performed only in male mice, while other experiments were performed both in male and female mice. In some experiments, mice were intraperitoneally injected with rapamycin (LC Laboratories, 2 mg/kg) for 3 days, as described previously (Bodine et al, 2001). Euthanasia was performed at 10 am after food removal at 6 am the same morning, except for the anti-FGF21 antibody injected mice which were euthanized at 2 pm, with food removal at 9 am. All procedures were performed in accordance with Swiss regulations for animal experimentation and approved by the veterinary commission of the Canton Basel-Stadt.

**Body composition analysis.** Magnetic resonance analysis of body composition (fat, lean and water measurements) was performed in conscious immobilized mice using the EchoMRI-100H body composition analyzer (EchoMRI, TM).

**Animal monitoring.** Analysis of global metabolic parameters and behavior of mice was performed by the use of CLAMS. Mice were individually caged and adapted to their new environment for 1 day before starting the measurements, which were done for the following 3 or 4 days. Food and water intake, as well as activity, oxygen consumption, CO<sub>2</sub> consumption, heat and activity were determined with the Oxymax software (Columbus Instruments).

**Blood analyses.** Blood was obtained from the tail veins of living mice. For glucose measurement, food was removed at 9 am and glucose was measured at 2 pm with the One Touch Ultra Easy glucose meter (LifeScan, Inc.). Plasma  $\beta$ -ketone and FGF21 measurements were performed at 9 am in the morning in mice fed *ad libitum*, using the Freestyle Precision  $\beta$ -ketone meter (Abbott Diabetes Care Ltd.) and the Mouse and Rat FGF-21 ELISA kit (BioVendor), respectively. FGF21 and FFA analysis in starved mice was conducted at 9 am, with food deprivation at 6 pm. Plasma FFA concentrations were measured using HR Series NEFA-HR kit (Wako). Plasma IGF-1, GH and insulin concentrations were measured at 9 am in the morning, after food removal at 6 am, using Mouse/Rat IGF-I Quantikine ELISA kit (R&D Systems), Mouse growth hormone ELISA kit (Crystal Chem, Inc.) and Ultra-Sensitive Mouse Insulin ELISA kit (Crystal Chem, Inc.), respectively. Triglyceride and cholesterol concentrations were measured with a Cobas C111 machine (Roche), from the same plasma obtained at 9 am after food removal at 6 am.

**Glucose, Insulin and Pyruvate tolerance tests.** Glucose and pyruvate tolerance tests were performed in overnight (16 hr) fasted mice by intraperitoneal injection of 1.5 g/kg glucose (Merck) and pyruvate (SIGMA-ALDRICH), respectively. Insulin tolerance test was performed in 5

hr fasted mice at 2 pm, after 0.75 U/kg insulin (Humalog, Eli Lilly) intraperitoneal injection. The guidelines from the Vanderbilt MMPC program were followed for glucose homeostasis experiments (McGuinness et al, 2009).

**4-PBA Treatment.** Mice were treated with 4-phenylbutyric acid (SIGMA) at 1 g/kg/day, starting at the age of 10 weeks. 4-PBA was diluted in drinking water at 10 mg/ml; pH was adjusted to 7.34; and the solution was filtered through 0.22  $\mu$ m filter and kept at 4°C. Mice were given free access to the drinking solution, which was changed every 3 days and the remaining volume was measured to calculate the intake of each mouse. Mice were weighed every 3 days during the 4 weeks of the treatment.

**FGF21-neutralizing antibody.** Mice were intraperitoneally injected with 250  $\mu$ g/kg of anti-Fgf21 monoclonal antibody (AIS, The University of Hong Kong) diluted in 0.9% NaCl solution at 6 pm. Control groups were intraperitoneally injected with 250  $\mu$ g/kg of purified rabbit IgG (ChromPure Rabbit IgG, Jackson ImmunoResearch Laboratories, Inc) diluted in 0.9% NaCl (Joseph et al, 2012; Omar et al, 2014).

**Body temperature measurement.** Body temperature was measured using a rectal thermometer (Physitemp BAT-12, Physitemp Instruments, Inc.) at 5 pm in 8 hour-fasted conscious mice.

**Muscle ATP measurement.** To determine ATP content in skeletal muscle, a luminescence assay was used (CellTiter-Glo Luminescent Cell Viability Assay, Promega). Frozen *extensor digitorum*

*longus* (EDL) muscle was homogenized in 0.2 ml lysis buffer (0.2% Triton X-100, 4 mM EDTA in water), and the homogenate was cleared by centrifugation at 14000 rpm, 4°C, 15 min. The supernatant was diluted in PBS and the reaction mix, containing luciferase and substrate, was added. Luminosity was measured using a Tecan Infinite F500 luminometer (Tecan), and quantified according to an ATP standard curve (SIGMA-ALDRICH).

**Muscle glycogen measurement.** For the analysis of muscle glycogen content, a glycogen assay kit was used (SIGMA-ALDRICH). Frozen quadriceps was homogenized, half in 2 M HCl solution and the other half in 2 M NaOH solution. Samples were boiled at 95°C for 1 hr, centrifuged at 14000 rpm for 10 min and the supernatant was then mixed with glucose and the assay reagent as determined by the manufacturer. Glycogen was determined by absorbance using a spectrophotometer (Ultrospec II, LKB Biochrom).

**In vivo 2-deoxyglucose uptake measurement.** To measure glucose uptake into TA muscle and WAT, a 2-deoxyglucose (2-DG) uptake measurement kit was used (Cosmo Bio, Co.). After food removal at 9 am, mice were intraperitoneally injected with insulin at 0.75 U/kg (Humalog, Eli Lilly). Ten minutes later mice were intraperitoneally injected with 5 µg of 2-deoxyglucose (Sigma). Mice were sacrificed 45 minutes after 2-DG injection, and tissues were dissected for further analysis. 50 mg of WAT and 10 mg of TA muscle were homogenized in 500 µl of 10mM Tris-HCl (pH 8.1), and then incubated at 95°C for 15 minutes. Samples were centrifuged for 15 min at 17,800 g (4°C), and the supernatant was diluted in 10 mM Tris-HCl (Saito et al, 2011). 20 µl of the diluted samples were used for further analysis according to the manufacturer's

instructions (Cosmo Bio, Co.) for a final absorbance measurement according to a 2DG6P standard curve.

**In vivo muscle electroporation.** Electroporation into muscle fibers and Ulk1 plasmid generation were performed as previously described (Castets et al, 2013; Kong et al, 2004).

**Cell culture.** Mouse C2C12 myoblasts were maintained at 37°C and 5% CO<sub>2</sub> in Dulbecco's modified Eagle's medium (DMEM) containing antibiotics (100 units/ml of penicillin, 100 µg/ml of streptomycin sulfate), L-Glutamine, sodium pyruvate and 20% fetal bovine serum (FBS). Myoblasts were set up for experiments on day 0 in 6-well plates at a density of 7,500 cells/cm<sup>2</sup>. On day 2, differentiation was induced by replacing 20% FBS with 2% FBS and media was changed every 2 days afterwards. On day 6, cells were treated with DMEM containing 10 nmol/l of insulin (Sigma) or 500 nM of thapsigargin (Tocris Bioscience). For the inhibition group, cells were pre-treated with 100 nM rapamycin (LC laboratories) for 15 minutes before addition of insulin. For the control group, cells were treated with the vehicle, containing DMSO and ethanol in DMEM media. One hour after the treatment, wells were washed once with warm PBS and cells were collected for RNA and protein extraction.

**Transcript Expression Analyses.** Total RNA were extracted from frozen muscle using the SV Total RNA Isolation System (Promega). DNase-treated RNA were reverse transcribed using the iScript cDNA synthesis kit (BioRad) and amplified with the Applied Biosystem Power Sybr Green



Master Mix. Data were analyzed using the StepOne software, normalized to *β-actin* expression and relative to expression in control mice. Primers are listed in Table S3.

**Protein translation analysis.** EDL muscles were powdered on dry ice before lysis in cold pull-down buffer (20 mM HEPES pH 7.4, 50 mM KCl, 0.2 mM EDTA, 25 mM  $\beta$ -glycerophosphate, 0.5 mM Na-orthovanadate, 1 mM DTT, 0.5% Triton X-100 and 50 mM NaF) supplemented with complete protease inhibitor cocktail (Roche). Cells were disrupted by additional homogenization in a Potter-homogenizer and 10 min incubation on ice before centrifugation for 10 min at 10000 rpm at 4°C. Total protein concentration was determined (BCA Protein Assay, Pierce) and 200  $\mu$ g of total lysate were used for m7GTP pull down assay. After pre-clearing of the samples with Glutathion-sepharose beads (GE Healthcare, Amersham Biosciences) for 30 min at 4°C, 15  $\mu$ l of a 50% slurry of m7GTP-Sepharose CL-4B (GE Healthcare, Amersham Biosciences) were incubated with the pre-cleared supernatant for 4 hr at 4°C on a rotating wheel. After 4 washes, the samples were denaturized 10 min at 95°C before separation on a gradient (3-12%) polyacrylamide SDS gel (Novex). Eif4E and 4EBP1 abundance on the m7GTP mimicking cap were quantified by chemiluminescence detection on a nitrocellulose membrane.

**Protein oxidation measurement.** The extent of oxidation of residues in protein lysates were determined with the Oxyblot detection kit according to the manufacturer's protocol (Millipore). Total protein extract were used in duplicate and subjected to derivatization of protein carbonyl groups in the presence of 2,4-Dinitrophenylhydrazine (DNPH) or not (control) for 15 min at

room temperature. After neutralization of the reaction, the samples were reduced by addition of 2-mercaptoethanol and boiled 10 min at 95°C before separation on a gradient (3-12%) polyacrylamide SDS gels (Novex). Upon transfer on nitrocellulose membranes, the detection of modified proteins was achieved with a rabbit anti-DNP antibody (Millipore) and secondary anti-Rabbit HRP antibody. Signal intensity was quantified and normalized to total protein amount after Ponceau staining of the nitrocellulose membrane.

**Western Blotting.** TA muscles, WAT, BAT, liver and pancreas were frozen in liquid nitrogen and pulverized on dry ice. They were lysed in cold RIPA buffer (50 mM Tris HCl pH 8, 150 mM NaCl, 1% NP-40, 0.5% sodium deoxycholate, 0.1% SDS) supplemented with protease inhibitor and phosphatase inhibitor cocktail tablets (Roche). Cell lysates were incubated on ice for 2 hr, sonicated two times for 15 sec and centrifuged at 13600 g for 20 min at 4°C. Cleared lysates were used to determine total protein amount (BCA Protein Assay, Pierce). Proteins were separated in 7 to 15% polyacrylamide SDS gels and transferred to nitrocellulose membranes. Blood FGF21 analysis was performed on immunodepleted plasma using the ProteoPrep 20 Immunodepletion Kit (SIGMA-ALDRICH). HRP-conjugated secondary antibodies were used and chemiluminescence was detected with LumiGLO chemiluminiscent substrate system (KPL). Signal was captured on a Fusion Fx machine (Vilber Lourmat) and analyzed with the FUSION Capt FX software. The following antibodies were used for immunoblotting or immunohistochemistry: Phospho-AMPK Ser<sup>173</sup> (#2535), AMPK (#2532), PGC1 $\alpha$  (#2178), Phospho-HSL Ser<sup>660</sup> (#4126),  $\beta$ -actin (#4970), Phospho-GSK3 $\beta$  Ser<sup>9</sup> (#9322), GSK3 $\beta$  (#9315), Phospho-GS Ser<sup>641</sup> (#3891), GS (#3886), Phospho-Akt Ser<sup>473</sup> (#4058), Phospho-AS160 Thr<sup>642</sup>

(#8881), AS160 (#2670), eEF2 (#2232), Ulk1 (#8054), Phospho-PERK Thr<sup>980</sup> (#3179), PERK (#3192), Phospho-eIF2 $\alpha$  Ser<sup>51</sup> (#9721), eIF2 $\alpha$  (#9722), S6 (#2217), Phospho-eIF4E Ser<sup>209</sup> (#9741), 4E-BP1 (#9452) from Cell Signaling; PDK4 (sc-130841), CPT1 (sc-20670), GLUT4 (sc-7938), GLUT1 (sc-7903), ATF4 (sc-200) from Santa Cruz;  $\alpha$ -actinin (7732) from Sigma; FGF21 (#Q9JJN1) from R&D Systems, p62 (GP62-C) from Progen and DNP (MAB2223) from Millipore.

**Histology and electron microscopy.** Muscle, liver and pancreas were dissected and frozen in nitrogen-cooled isopentane. 10  $\mu$ m sections were cut using a Cryostat (Leica CM1950). Inguinal-subcutaneous WAT and BAT were dissected and fixed overnight in 4% paraformaldehyde. Samples were embedded in paraffin (Thermo Electron Corporation) and 4- $\mu$ m-thick sections were cut using a microtome (Microm HM 360). Sections were stained with Hematoxylin/Eosin (H&E) according to classical methods. Light microscopy observations were performed using an upright microscope (DMR, Leica) and pictures were captured using a monochrome camera (DS-Ri1, Nikon). Transmission electron microscopy was performed as described elsewhere (Moll et al, 2001).

**Statistical analyses.** Results are expressed as mean  $\pm$  SEM of independent animals, with  $n$  (number of individual experiments)  $\geq 3$ . Statistical comparison of two conditions was performed using the Student's  $t$ -test, comparison of 3 or more groups was performed using the One-way or Two-way ANOVA test with Tukey correction for multiple comparisons and analysis of normalized data or data sets where time is a variable was done using the linear regression model (GraphPad Prism Software). A 0.05 level of confidence was accepted for statistical significance.

## REFERENCES AND NOTES

1. R. A. DeFronzo, D. Tripathy, Skeletal muscle insulin resistance is the primary defect in type 2 diabetes. *Diabetes Care* **32 Suppl 2**, S157 (Nov, 2009).
2. E. Llagostera, D. Catalucci, L. Marti, M. Liesa, M. Camps, T. P. Ciaraldi, R. Kondo, S. Reddy, W. H. Dillmann, M. Palacin, A. Zorzano, P. Ruiz-Lozano, R. Gomis, P. Kaliman, Role of myotonic dystrophy protein kinase (DMPK) in glucose homeostasis and muscle insulin action. *PLoS One* **2**, e1134 (2007).
3. B. K. Pedersen, M. A. Febbraio, Muscles, exercise and obesity: skeletal muscle as a secretory organ. *Nat Rev Endocrinol* **8**, 457 (2012).
4. K. H. Kim, Y. T. Jeong, H. Oh, S. H. Kim, J. M. Cho, Y. N. Kim, S. S. Kim, H. Kim do, K. Y. Hur, H. K. Kim, T. Ko, J. Han, H. L. Kim, J. Kim, S. H. Back, M. Komatsu, H. Chen, D. C. Chan, M. Konishi, N. Itoh, C. S. Choi, M. S. Lee, Autophagy deficiency leads to protection from obesity and insulin resistance by inducing Fgf21 as a mitokine. *Nat Med* **19**, 83 (Jan, 2013).
5. B. Angelin, T. E. Larsson, M. Rudling, Circulating fibroblast growth factors as metabolic regulators--a critical appraisal. *Cell Metab* **16**, 693 (Dec 5, 2012).
6. G. Gaich, J. Y. Chien, H. Fu, L. C. Glass, M. A. Deeg, W. L. Holland, A. Kharitonov, T. Bumol, H. K. Schilske, D. E. Moller, The effects of LY2405319, an FGF21 analog, in obese human subjects with type 2 diabetes. *Cell Metab* **18**, 333 (Sep 3, 2013).
7. T. Inagaki, P. Dutchak, G. Zhao, X. Ding, L. Gautron, V. Parameswara, Y. Li, R. Goetz, M. Mohammadi, V. Esser, J. K. Elmquist, R. D. Gerard, S. C. Burgess, R. E. Hammer, D. J. Mangelsdorf, S. A. Kliewer, Endocrine regulation of the fasting response by PPARalpha-mediated induction of fibroblast growth factor 21. *Cell Metab* **5**, 415 (Jun, 2007).
8. A. Kharitonov, T. L. Shiyanova, A. Koester, A. M. Ford, R. Micanovic, E. J. Galbreath, G. E. Sandusky, L. J. Hammond, J. S. Moyers, R. A. Owens, J. Gromada, J. T. Brozinick, E. D. Hawkins, V. J. Wroblewski, D. S. Li, F. Mehrbod, S. R. Jaskunas, A. B. Shanafelt, FGF-21 as a novel metabolic regulator. *J Clin Invest* **115**, 1627 (Jun, 2005).
9. J. Xu, D. J. Lloyd, C. Hale, S. Stanislaus, M. Chen, G. Sivits, S. Vonderfecht, R. Hecht, Y. S. Li, R. A. Lindberg, J. L. Chen, D. Y. Jung, Z. Zhang, H. J. Ko, J. K. Kim, M. M. Veniant, Fibroblast growth factor 21 reverses hepatic steatosis, increases energy expenditure, and improves insulin sensitivity in diet-induced obese mice. *Diabetes* **58**, 250 (Jan, 2009).
10. W. L. Holland, A. C. Adams, J. T. Brozinick, H. H. Bui, Y. Miyauchi, C. M. Kusminski, S. M. Bauer, M. Wade, E. Singhal, C. C. Cheng, K. Volk, M. S. Kuo, R. Gordillo, A. Kharitonov, P. E. Scherer, An FGF21-adiponectin-ceramide axis controls energy expenditure and insulin action in mice. *Cell Metab* **17**, 790 (May 7, 2013).
11. M. K. Badman, P. Pissios, A. R. Kennedy, G. Koukos, J. S. Flier, E. Maratos-Flier, Hepatic fibroblast growth factor 21 is regulated by PPARalpha and is a key mediator of hepatic lipid metabolism in ketotic states. *Cell Metab* **5**, 426 (Jun, 2007).
12. H. Wang, L. Qiang, S. R. Farmer, Identification of a domain within peroxisome proliferator-activated receptor gamma regulating expression of a group of genes containing fibroblast growth factor 21 that are selectively repressed by SIRT1 in adipocytes. *Mol Cell Biol* **28**, 188 (Jan, 2008).
13. S. Keipert, M. Ost, K. Johann, F. Imber, M. Jastroch, E. M. van Schothorst, J. Keijer, S. Klaus, Skeletal muscle mitochondrial uncoupling drives endocrine cross-talk through the induction of FGF21 as a myokine. *Am J Physiol Endocrinol Metab* **306**, E469 (Mar 1, 2014).
14. M. Laplante, D. M. Sabatini, mTOR signaling in growth control and disease. *Cell* **149**, 274 (Apr 13, 2012).

15. P. Polak, N. Cybulski, J. N. Feige, J. Auwerx, M. A. Ruegg, M. N. Hall, Adipose-specific knockout of raptor results in lean mice with enhanced mitochondrial respiration. *Cell Metab* **8**, 399 (Nov, 2008).
16. A. Hagiwara, M. Cornu, N. Cybulski, P. Polak, C. Betz, F. Trapani, L. Terracciano, M. H. Heim, M. A. Ruegg, M. N. Hall, Hepatic mTORC2 activates glycolysis and lipogenesis through Akt, glucokinase, and SREBP1c. *Cell Metab* **15**, 725 (May 2, 2012).
17. C. F. Bentzinger, K. Romanino, D. Cloetta, S. Lin, J. B. Mascarenhas, F. Oliveri, J. Xia, E. Casanova, C. F. Costa, M. Brink, F. Zorzato, M. N. Hall, M. A. Ruegg, Skeletal muscle-specific ablation of raptor, but not of rictor, causes metabolic changes and results in muscle dystrophy. *Cell Metab* **8**, 411 (Nov, 2008).
18. P. Castets, S. Lin, N. Rion, S. Di Fulvio, K. Romanino, M. Guridi, S. Frank, L. A. Tintignac, M. Sinnreich, M. A. Ruegg, Sustained activation of mTORC1 in skeletal muscle inhibits constitutive and starvation-induced autophagy and causes a severe, late-onset myopathy. *Cell Metab* **17**, 731 (May 7, 2013).
19. C. F. Bentzinger, S. Lin, K. Romanino, P. Castets, M. Guridi, S. Summermatter, C. Handschin, L. A. Tintignac, M. N. Hall, M. A. Ruegg, Differential response of skeletal muscles to mTORC1 signaling during atrophy and hypertrophy. *Skelet Muscle* **3**, 6 (2013).
20. V. Risson, L. Mazelin, M. Roceri, H. Sanchez, V. Moncollin, C. Corneloup, H. Richard-Bulteau, A. Vignaud, D. Baas, A. Defour, D. Freyssenet, J. F. Tanti, Y. Le-Marchand-Brustel, B. Ferrier, A. Conjard-Duplany, K. Romanino, S. Bauche, D. Hantai, M. Mueller, S. C. Kozma, G. Thomas, M. A. Ruegg, A. Ferry, M. Pende, X. Bigard, N. Koulmann, L. Schaeffer, Y. G. Gangloff, Muscle inactivation of mTOR causes metabolic and dystrophin defects leading to severe myopathy. *J Cell Biol* **187**, 859 (Dec 14, 2009).
21. D. LeRoith, S. Yakar, Mechanisms of Disease: metabolic effects of growth hormone and insulin-like growth factor 1. *Nat Clin Pract End Met* **3**, 302 (2007).
22. P. Puigserver, Tissue-specific regulation of metabolic pathways through the transcriptional coactivator PGC1-alpha. *Int J Obes (Lond)* **29 Suppl 1**, S5 (Mar, 2005).
23. Z. Wu, P. Puigserver, U. Andersson, C. Zhang, G. Adelmant, V. Mootha, A. Troy, S. Cinti, B. Lowell, R. C. Scarpulla, B. M. Spiegelman, Mechanisms controlling mitochondrial biogenesis and respiration through the thermogenic coactivator PGC-1. *Cell* **98**, 115 (Jul 9, 1999).
24. J. C. Newman, E. Verdin, Ketone bodies as signaling metabolites. *Trends Endocrinol Metab* **25**, 42 (Jan, 2014).
25. A. Bartelt, J. Heeren, Adipose tissue browning and metabolic health. *Nature reviews. Endocrinology* **10**, 24 (Jan, 2014).
26. P. Seale, H. M. Conroe, J. Estall, S. Kajimura, A. Frontini, J. Ishibashi, P. Cohen, S. Cinti, B. M. Spiegelman, Prdm16 determines the thermogenic program of subcutaneous white adipose tissue in mice. *J Clin Invest* **121**, 96 (Jan, 2011).
27. H. Sano, S. Kane, E. Sano, C. P. Miinea, J. M. Asara, W. S. Lane, C. W. Garner, G. E. Lienhard, Insulin-stimulated phosphorylation of a Rab GTPase-activating protein regulates GLUT4 translocation. *J Biol Chem* **278**, 14599 (Apr 25, 2003).
28. S. X. Tan, Y. Ng, J. G. Burchfield, G. Ramm, D. G. Lambright, J. Stockli, D. E. James, The Rab GTPase-activating protein TBC1D4/AS160 contains an atypical phosphotyrosine-binding domain that interacts with plasma membrane phospholipids to facilitate GLUT4 trafficking in adipocytes. *Mol Cell Biol* **32**, 4946 (Dec, 2012).
29. E. Hondares, M. Rosell, F. J. Gonzalez, M. Giralt, R. Iglesias, F. Villarroya, Hepatic FGF21 expression is induced at birth via PPARalpha in response to milk intake and contributes to thermogenic activation of neonatal brown fat. *Cell Metab* **11**, 206 (Mar 3, 2010).

30. C. L. Johnson, J. Y. Weston, S. A. Chadi, E. N. Fazio, M. W. Huff, A. Kharitononkov, A. Koester, C. L. Pin, Fibroblast growth factor 21 reduces the severity of cerulein-induced pancreatitis in mice. *Gastroenterology* **137**, 1795 (Nov, 2009).
31. Y. Izumiya, H. A. Bina, N. Ouchi, Y. Akasaki, A. Kharitononkov, K. Walsh, FGF21 is an Akt-regulated myokine. *FEBS Lett* **582**, 3805 (Nov 12, 2008).
32. X. Ding, J. Boney-Montoya, B. M. Owen, A. L. Bookout, K. C. Coate, D. J. Mangelsdorf, S. A. Kliewer, betaKlotho is required for fibroblast growth factor 21 effects on growth and metabolism. *Cell Metab* **16**, 387 (Sep 5, 2012).
33. H. P. Harding, I. Novoa, Y. Zhang, H. Zeng, R. Wek, M. Schapira, D. Ron, Regulated translation initiation controls stress-induced gene expression in mammalian cells. *Mol Cell* **6**, 1099 (Nov, 2000).
34. S. Varadarajan, E. T. Bampton, J. L. Smalley, K. Tanaka, R. E. Caves, M. Butterworth, J. Wei, M. Pellicchia, J. Mitcheson, T. W. Gant, D. Dinsdale, G. M. Cohen, A novel cellular stress response characterised by a rapid reorganisation of membranes of the endoplasmic reticulum. *Cell Death Differ* **19**, 1896 (Dec, 2012).
35. I. Kim, W. Xu, J. C. Reed, Cell death and endoplasmic reticulum stress: disease relevance and therapeutic opportunities. *Nat Rev Drug Discov* **7**, 1013 (Dec, 2008).
36. C. Hetz, The unfolded protein response: controlling cell fate decisions under ER stress and beyond. *Nat Rev Mol Cell Biol* **13**, 89 (Feb, 2012).
37. N. Ohoka, S. Yoshii, T. Hattori, K. Onozaki, H. Hayashi, TRB3, a novel ER stress-inducible gene, is induced via ATF4-CHOP pathway and is involved in cell death. *Embo J* **24**, 1243 (Mar 23, 2005).
38. C. Appenzeller-Herzog, M. N. Hall, Bidirectional crosstalk between endoplasmic reticulum stress and mTOR signaling. *Trends Cell Biol* **22**, 274 (May, 2012).
39. U. Ozcan, E. Yilmaz, L. Ozcan, M. Furuhashi, E. Vaillancourt, R. O. Smith, C. Z. Gorgun, G. S. Hotamisligil, Chemical chaperones reduce ER stress and restore glucose homeostasis in a mouse model of type 2 diabetes. *Science* **313**, 1137 (Aug 25, 2006).
40. B. A. Omar, B. Andersen, J. Hald, K. Raun, E. Nishimura, B. Ahren, Fibroblast growth factor 21 (FGF21) and glucagon-like peptide 1 contribute to diabetes resistance in glucagon receptor-deficient mice. *Diabetes* **63**, 101 (Jan, 2014).
41. F. M. Fisher, S. Kleiner, N. Douris, E. C. Fox, R. J. Mepani, F. Verdeguer, J. Wu, A. Kharitononkov, J. S. Flier, E. Maratos-Flier, B. M. Spiegelman, FGF21 regulates PGC-1alpha and browning of white adipose tissues in adaptive thermogenesis. *Genes Dev* **26**, 271 (Feb 1, 2012).
42. J. L. Yecies, H. H. Zhang, S. Menon, S. Liu, D. Yecies, A. I. Lipovsky, C. Gorgun, D. J. Kwiatkowski, G. S. Hotamisligil, C. H. Lee, B. D. Manning, Akt stimulates hepatic SREBP1c and lipogenesis through parallel mTORC1-dependent and independent pathways. *Cell Metab* **14**, 21 (Jul 6, 2011).
43. T. R. Peterson, S. S. Sengupta, T. E. Harris, A. E. Carmack, S. A. Kang, E. Balderas, D. A. Guertin, K. L. Madden, A. E. Carpenter, B. N. Finck, D. M. Sabatini, mTOR complex 1 regulates lipin 1 localization to control the SREBP pathway. *Cell* **146**, 408 (Aug 5, 2011).
44. C. Xu, B. Bailly-Maitre, J. C. Reed, Endoplasmic reticulum stress: cell life and death decisions. *J Clin Invest* **115**, 2656 (Oct, 2005).
45. Z. Mounir, J. L. Krishnamoorthy, S. Wang, B. Papadopoulou, S. Campbell, W. J. Muller, M. Hatzoglou, A. E. Koromilas, Akt determines cell fate through inhibition of the PERK-eIF2alpha phosphorylation pathway. *Sci Signal* **4**, ra62 (Sep 27, 2011).
46. A. C. Riggs, E. Bernal-Mizrachi, M. Ohsugi, J. Wasson, S. Fatrai, C. Welling, J. Murray, R. E. Schmidt, P. L. Herrera, M. A. Permutt, Mice conditionally lacking the Wolfram gene in pancreatic islet beta cells exhibit diabetes as a result of enhanced endoplasmic reticulum stress and apoptosis. *Diabetologia* **48**, 2313 (Nov, 2005).

47. M. Cornu, W. Oppliger, V. Albert, A. M. Robitaille, F. Trapani, L. Quagliata, T. Fuhrer, U. Sauer, L. Terracciano, M. N. Hall, Hepatic mTORC1 controls locomotor activity, body temperature, and lipid metabolism through FGF21. *Proc Natl Acad Sci U S A* **111**, 11592 (Aug 12, 2014).
48. T. Iannitti, B. Palmieri, Clinical and experimental applications of sodium phenylbutyrate. *Drugs R D* **11**, 227 (Sep 1, 2011).
49. A. L. Bookout, M. H. de Groot, B. M. Owen, S. Lee, L. Gautron, H. L. Lawrence, X. Ding, J. K. Elmquist, J. S. Takahashi, D. J. Mangelsdorf, S. A. Kliewer, FGF21 regulates metabolism and circadian behavior by acting on the nervous system. *Nat Med* **19**, 1147 (Sep, 2013).
50. W. Wei, P. A. Dutchak, X. Wang, X. Ding, A. L. Bookout, R. Goetz, M. Mohammadi, R. D. Gerard, P. C. Dechow, D. J. Mangelsdorf, S. A. Kliewer, Y. Wan, Fibroblast growth factor 21 promotes bone loss by potentiating the effects of peroxisome proliferator-activated receptor gamma. *Proc Natl Acad Sci U S A* **109**, 3143 (Feb 21, 2012).
51. M. J. Potthoff, T. Inagaki, S. Satapati, X. Ding, T. He, R. Goetz, M. Mohammadi, B. N. Finck, D. J. Mangelsdorf, S. A. Kliewer, S. C. Burgess, FGF21 induces PGC-1alpha and regulates carbohydrate and fatty acid metabolism during the adaptive starvation response. *Proc Natl Acad Sci U S A* **106**, 10853 (Jun 30, 2009).
52. C. Wang, J. Dai, M. Yang, G. Deng, S. Xu, Y. Jia, G. Boden, Z. A. Ma, G. Yang, L. Li, Silencing of FGF-21 expression promotes hepatic gluconeogenesis and glycogenolysis by regulation of the STAT3-SOCS3 signal. *Febs J* **281**, 2136 (May, 2014).
53. E. D. Berglund, C. Y. Li, H. A. Bina, S. E. Lynes, M. D. Michael, A. B. Shanafelt, A. Kharitononkov, D. H. Wasserman, Fibroblast growth factor 21 controls glycemia via regulation of hepatic glucose flux and insulin sensitivity. *Endocrinology* **150**, 4084 (Sep, 2009).
54. K. Inoki, T. Zhu, K. L. Guan, TSC2 mediates cellular energy response to control cell growth and survival. *Cell* **115**, 577 (Nov 26, 2003).
55. R. M. Young, D. Ackerman, Z. L. Quinn, A. Mancuso, M. Gruber, L. Liu, D. N. Giannoukos, E. Bobrovnikova-Marjon, J. A. Diehl, B. Keith, M. C. Simon, Dysregulated mTORC1 renders cells critically dependent on desaturated lipids for survival under tumor-like stress. *Genes Dev* **27**, 1115 (May 15, 2013).
56. K. R. Markan, M. C. Naber, M. K. Ameka, M. D. Anderegg, D. J. Mangelsdorf, S. A. Kliewer, M. Mohammadi, M. J. Potthoff, Circulating FGF21 is liver derived and enhances glucose uptake during refeeding and overfeeding. *Diabetes* **63**, 4057 (Dec, 2014).
57. P. Domingo, J. M. Gallego-Escuredo, J. C. Domingo, M. Gutierrez Mdel, M. G. Mateo, I. Fernandez, F. Vidal, M. Giralt, F. Villarroya, Serum FGF21 levels are elevated in association with lipodystrophy, insulin resistance and biomarkers of liver injury in HIV-1-infected patients. *Aids* **24**, 2629 (Nov 13, 2010).
58. B. Lindegaard, T. Hvid, T. Grondahl, C. Frosig, J. Gerstoft, P. Hojman, B. K. Pedersen, Expression of fibroblast growth factor-21 in muscle is associated with lipodystrophy, insulin resistance and lipid disturbances in patients with HIV. *PLoS One* **8**, e55632 (2013).
59. Y. Zhang, Y. Xie, E. D. Berglund, K. C. Coate, T. T. He, T. Katafuchi, G. Xiao, M. J. Potthoff, W. Wei, Y. Wan, R. T. Yu, R. M. Evans, S. A. Kliewer, D. J. Mangelsdorf, The starvation hormone, fibroblast growth factor-21, extends lifespan in mice. *Elife* **1**, e00065 (2012).
60. T. Inagaki, V. Y. Lin, R. Goetz, M. Mohammadi, D. J. Mangelsdorf, S. A. Kliewer, Inhibition of growth hormone signaling by the fasting-induced hormone FGF21. *Cell Metab* **8**, 77 (Jul, 2008).
61. S. Wu, T. Grunwald, A. Kharitononkov, J. Dam, R. Jockers, F. De Luca, Increased expression of fibroblast growth factor 21 (FGF21) during chronic undernutrition causes growth hormone insensitivity in chondrocytes by inducing leptin receptor overlapping transcript (LEPROT) and leptin receptor overlapping transcript-like 1 (LEPROTL1) expression. *J Biol Chem* **288**, 27375 (Sep 20, 2013).

62. B. M. Owen, A. L. Bookout, X. Ding, V. Y. Lin, S. D. Atkin, L. Gautron, S. A. Kliewer, D. J. Mangelsdorf, FGF21 contributes to neuroendocrine control of female reproduction. *Nat Med* **19**, 1153 (Sep, 2013).
63. F. J. Ramos, S. C. Chen, M. G. Garelick, D. F. Dai, C. Y. Liao, K. H. Schreiber, V. L. MacKay, E. H. An, R. Strong, W. C. Ladiges, P. S. Rabinovitch, M. Kaeberlein, B. K. Kennedy, Rapamycin reverses elevated mTORC1 signaling in lamin A/C-deficient mice, rescues cardiac and skeletal muscle function, and extends survival. *Sci Transl Med* **4**, 144ra103 (Jul 25, 2012).
64. P. Spitali, P. Grumati, M. Hiller, M. Chrisam, A. Aartsma-Rus, P. Bonaldo, Autophagy is Impaired in the Tibialis Anterior of Dystrophin Null Mice. *PLoS Curr* **5**, (2013).
65. D. J. Kwiatkowski, H. Zhang, J. L. Bandura, K. M. Heiberger, M. Glogauer, N. el-Hashemite, H. Onda, A mouse model of TSC1 reveals sex-dependent lethality from liver hemangiomas, and up-regulation of p70S6 kinase activity in Tsc1 null cells. *Hum Mol Genet* **11**, 525 (Mar 1, 2002).
66. S. C. Bodine, T. N. Stitt, M. Gonzalez, W. O. Kline, G. L. Stover, R. Bauerlein, E. Zlotchenko, A. Scrimgeour, J. C. Lawrence, D. J. Glass, G. D. Yancopoulos, Akt/mTOR pathway is a crucial regulator of skeletal muscle hypertrophy and can prevent muscle atrophy in vivo. *Nat Cell Biol* **3**, 1014 (Nov, 2001).
67. O. P. McGuinness, J. E. Ayala, M. R. Laughlin, D. H. Wasserman, NIH experiment in centralized mouse phenotyping: the Vanderbilt experience and recommendations for evaluating glucose homeostasis in the mouse. *Am J Physiol Endocrinol Metab* **297**, E849 (Oct, 2009).
68. A. Joseph, K. Neff, J. Richard, L. Gao, D. Bangari, M. Joly, K. Culm-Merdek, R. Garman, J. Williams, S. Richards, M. Ruzek, Transient low-dose methotrexate induces tolerance to murine anti-thymocyte globulin and together they promote long-term allograft survival. *J Immunol* **189**, 732 (Jul 15, 2012).
69. K. Saito, S. Lee, T. Shiuchi, C. Toda, M. Kamijo, K. Inagaki-Ohara, S. Okamoto, Y. Minokoshi, An enzymatic photometric assay for 2-deoxyglucose uptake in insulin-responsive tissues and 3T3-L1 adipocytes. *Anal Biochem* **412**, 9 (May 1, 2011).
70. X. C. Kong, P. Barzagli, M. A. Ruegg, Inhibition of synapse assembly in mammalian muscle in vivo by RNA interference. *EMBO Rep* **5**, 183 (Feb, 2004).
71. J. Moll, P. Barzagli, S. Lin, G. Bezakova, H. Lochmuller, E. Engvall, U. Muller, M. A. Ruegg, An agrin minigene rescues dystrophic symptoms in a mouse model for congenital muscular dystrophy. *Nature* **413**, 302 (Sep 20, 2001).



**ACKNOWLEDGMENTS:** We thank Dr. C. Handschin for his remarks on the manuscript and Dr. K. Romanino, M. Kaiser, F. Olivieri, M. Cornu, V. Albert, M. Beer and K. Svensson for technical assistance. **FUNDING:** This work was supported by the Cantons of Basel-Stadt and Basel-Land, grants from the Swiss National Science Foundation and the Swiss Foundation for Research on Muscle Disease. **AUTHOR CONTRIBUTIONS:** M.G. designed and performed most of the experiments, analyzed the data and wrote the paper; L.A.T collaborated on the experimental design, performed protein oxidation and translation experiments, supervised the project and wrote the paper; S.L. collaborated on the electroporation experiments and tissue dissection; B.K. collaborated on the glucose homeostasis experiments and the CLAMS experiments; P.C. collaborated on the autophagy-related Western blot analysis and wrote the paper; M.A.R. designed the experiments, supervised the entire project and wrote the paper. All authors contributed and commented on the manuscript. **COMPETING INTERESTS:** The authors declare that they have no competing interests.

**FIGURE 1**

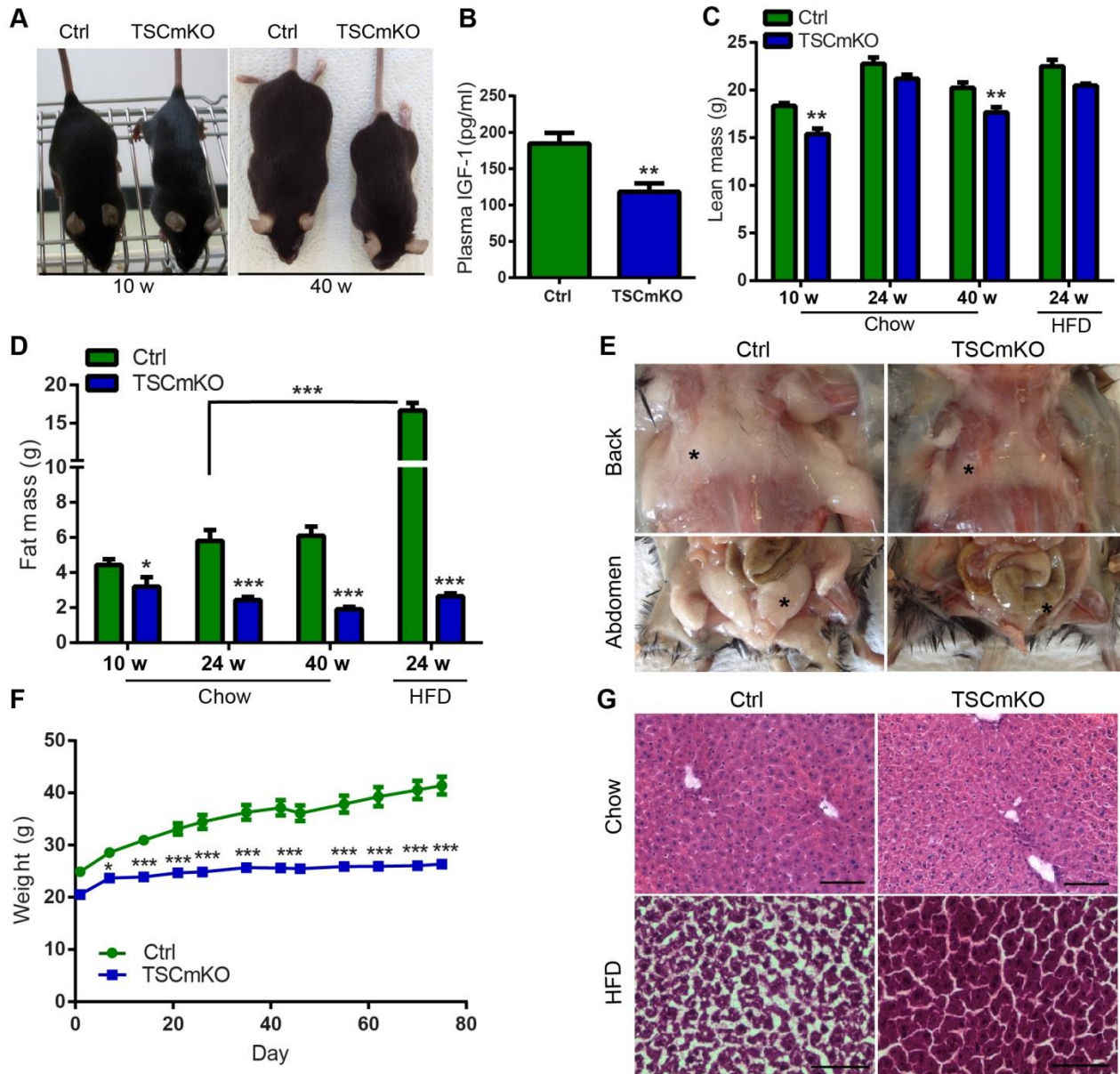


**Figure 1. TSCmKO mice show a decreased body mass and are resistant to HFD**

A. Pictures of 10- and 40-week-old TSCmKO and control (Ctrl) littermates.

B. Plasma IGF-1 concentrations were decreased in 12-week-old TSCmKO mice, compared to control littermates (n= 7 mice per genotype).

C, D. Echo-MRI analysis revealed decreased lean mass (C) and fat mass (D) in TSCmKO mice at 10 (n= 8 mice per genotype), 24 (n= 7 mice per genotype) and 40 (n= 8 mice per genotype) weeks of age under chow diet, and at 24 weeks of age with HFD (n= 6 mice per genotype).

E. Subscapular-subcutaneous (Back) and inguinal-perigonadal (Abdomen) fat deposits from 40-week-old control (Ctrl) and TSCmKO mice. Asterisks point at fat depots. Images are representative of 9 mice per genotype.

F. Weekly weight measurement during 14 week HFD showed the inability of TSCmKO mice to gain weight (n= 6 mice per genotype). Linear regression analysis showed that the two groups differ significantly ( $p < 0.001$ ).

G. H&E staining showed normal liver histology in 10-week-old TSCmKO and control (Ctrl) mice on a chow diet. After 14 week HFD, control mice, but not TSCmKO mice, showed hepatic steatosis. Images are representative of 4 sections from 3 mice per genotype and condition.

Scale bar, 100  $\mu\text{m}$ .

Data represent mean  $\pm$  SEM, \* $p < 0.05$ , \*\* $p < 0.01$ , \*\*\* $p < 0.001$ . w: weeks.

**FIGURE 2**

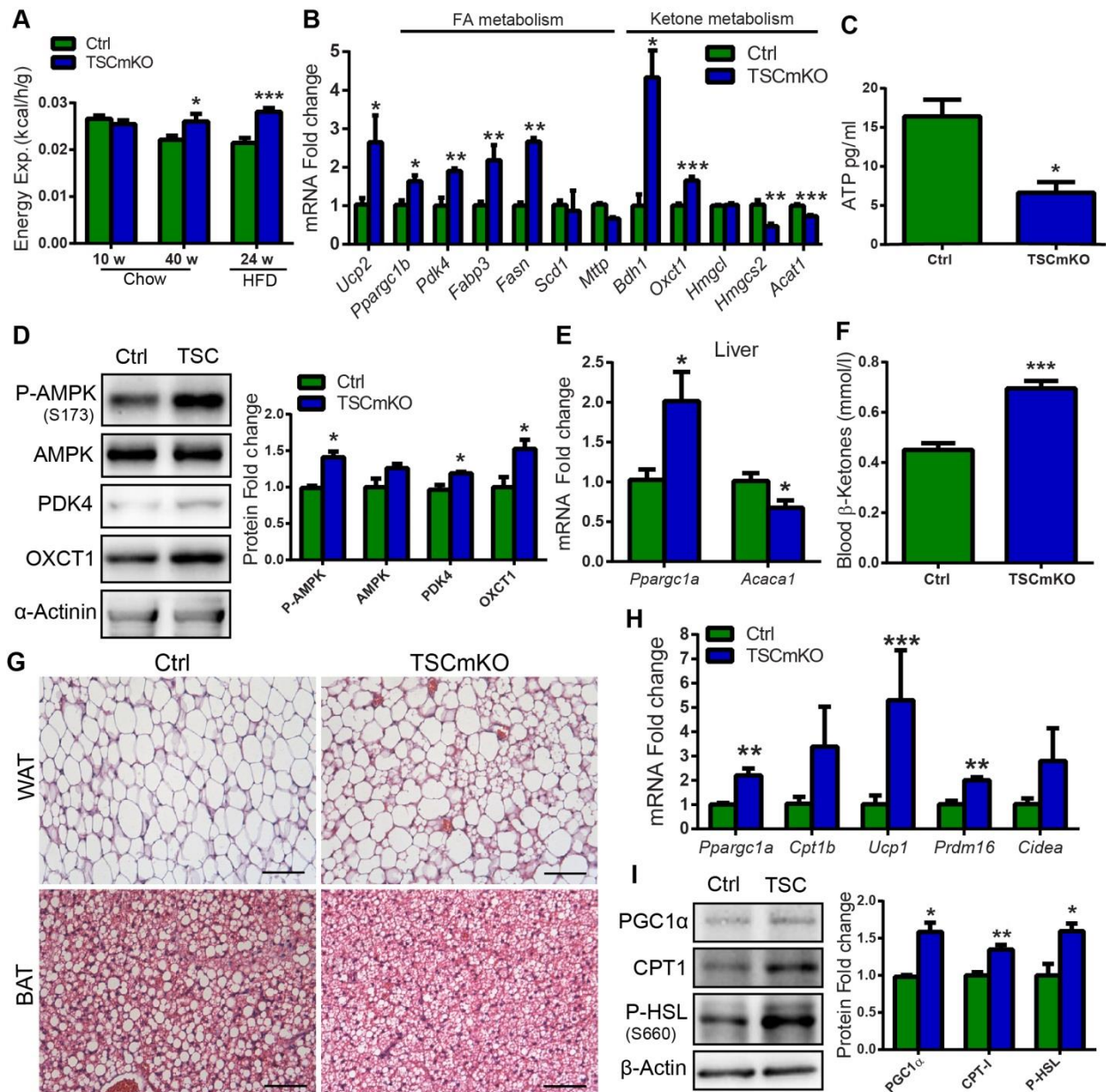


**Figure 2. TSCmKO mice show increased ketogenesis and fatty acid oxidation**

A. CLAMS analysis revealed normal energy expenditure in 10-week-old TSCmKO mice fed chow diet (n= 5 mice per genotype), but a significant increase in 40-week-old mutant mice fed a chow diet (n= 5 mice per genotype) and in 24-week-old TSCmKO mice fed a HFD (n= 6 mice per genotype).

B. TSCmKO mice showed increased expression of genes involved in fatty acid oxidation (*Ucp2*; *Ppargc1b*; *Pdk4*; *Fabp3*) and ketone catabolism (*Bdh1*; *Oxct1*), and reduced expression of ketogenesis genes (*Hmgcs2*; *Acat1*) in TA muscle at 10 weeks of age (n= 5 mice per genotype).

C. TSCmKO mice showed decreased ATP concentrations in EDL muscle at 10 weeks of age (n= 5 mice per genotype).

D. Immunoblots of TA muscle from 10-week-old TSCmKO (TSC) and control littermates (Ctrl) are shown for the indicated phospho (P)- and total proteins (n= 8 mice per genotype). Protein abundance was normalized to  $\alpha$ -actinin.

E. Lower *Acac1* and higher *Ppargc1a* expression in liver of 10-week-old TSCmKO mice (n= 5 mice per genotype).

F. Increased plasma  $\beta$ -ketone concentrations in 11-week-old TSCmKO mice revealed an increase in ketogenesis (n= 10 mice per genotype).

G. H&E staining of WAT and BAT from 12-week-old mice revealed increased browning of WAT and reduced lipid content in BAT of TSCmKO mice. Images are representative of 4 sections from 3 mice per genotype. Scale bar, 100  $\mu$ m.

H. TSCmKO mice showed increased expression of genes involved in fatty acid oxidation (*Ppargc1a*; *Cpt1b*) and markers for browning (*Ucp1*; *Prdm16*; *Cidea*) in inguinal-subcutaneous WAT at 12 weeks of age (n= 5 mice per genotype).

I. Immunoblots of WAT from 10-week-old TSCmKO (TSC) and control (Ctrl) littermates are shown for the indicated phospho (P)- and total proteins (n= 4 mice per genotype). Protein abundance is normalized to  $\beta$ -actin.

Data represent mean  $\pm$  SEM, \*p<0.05, \*\*p<0.01, \*\*\*p<0.001.

**FIGURE 3**

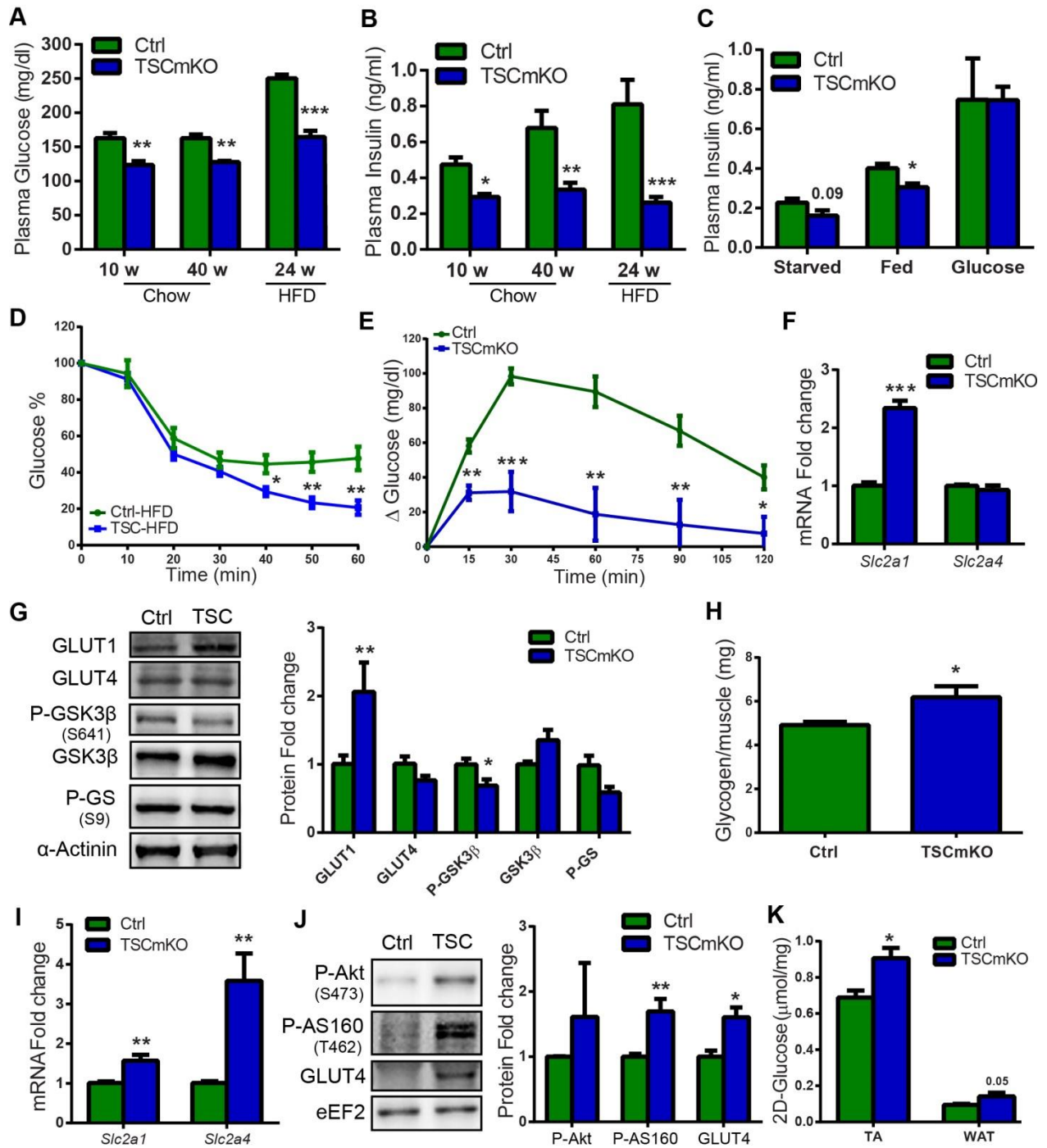


### Figure 3. TSCmKO mice show changes in glucose metabolism

A, B. Decreased blood glucose (A) and plasma insulin (B) concentrations in 10- and 40-week-old TSCmKO mice fed a chow diet (n= 8 mice per genotype), and in 24-week-old mutant mice under HFD (n= 6 mice per genotype). *w*: weeks.

C. Determination of plasma insulin concentration under starved or basal conditions, and 20 min after glucose injection, revealed normal glucose-stimulated insulin secretion in 10-week-old TSCmKO mice (n= 5 mice per genotype).

D. Insulin tolerance test performed on 24-week-old mice after 14 weeks of HFD (n= 6 mice per genotype) revealed increased insulin sensitivity in TSCmKO mice. Linear regression analysis shows that the two groups differed significantly (p=0.01).

E. Pyruvate tolerance test performed on 24-week-old mice revealed impaired liver gluconeogenesis in TSCmKO animals (n= 4 mice per genotype). Linear regression analysis shows that the two groups differed significantly (p<0.001).

F. Ten week-old TSCmKO mice showed increased expression of *Slc2a1* (which encodes GLUT1) and normal expression of *Slc2a4* (which encodes GLUT4) in TA muscle (n= 4 mice per genotype).

G. Immunoblots of TA muscle from 10-week-old TSCmKO (TSC) and control (Ctrl) mice are shown for the indicated phospho (P)- and total proteins (n= 4 mice per genotype). Protein abundance was normalized to  $\alpha$ -actinin.

H. Glycogen amount was increased in quadriceps muscle from 10-week-old TSCmKO mice (n= 5 mice per genotype).

I. TSCmKO mice showed increased expression of *Slc2a1* and *Slc2a4* (which encode GLUT1 and GLUT4) in inguinal-subcutaneous WAT at 12 weeks of age (n= 6 mice per genotype).

J. Immunoblots of WAT from 10-week-old TSCmKO (TSC) and control (Ctrl) mice are shown for the indicated phospho (P)- and total proteins (n= 4 mice per genotype). Protein abundance was normalized to eEF2.

K. Increased glucose absorption in TA muscle and WAT of 10-week-old TSCmKO mice is shown by a higher accumulation of 2-deoxyglucose (n= 3 mice per genotype).

L. Insulin tolerance test performed on 10-week-old mice revealed insulin resistance in RAmKO mice (n= 6 mice per genotype). Linear regression analysis shows that the two groups differ significantly (p=0.04).

Data represent mean  $\pm$  SEM, \*p<0.05, \*\*p<0.01, \*\*\*p<0.001.



**FIGURE 4**

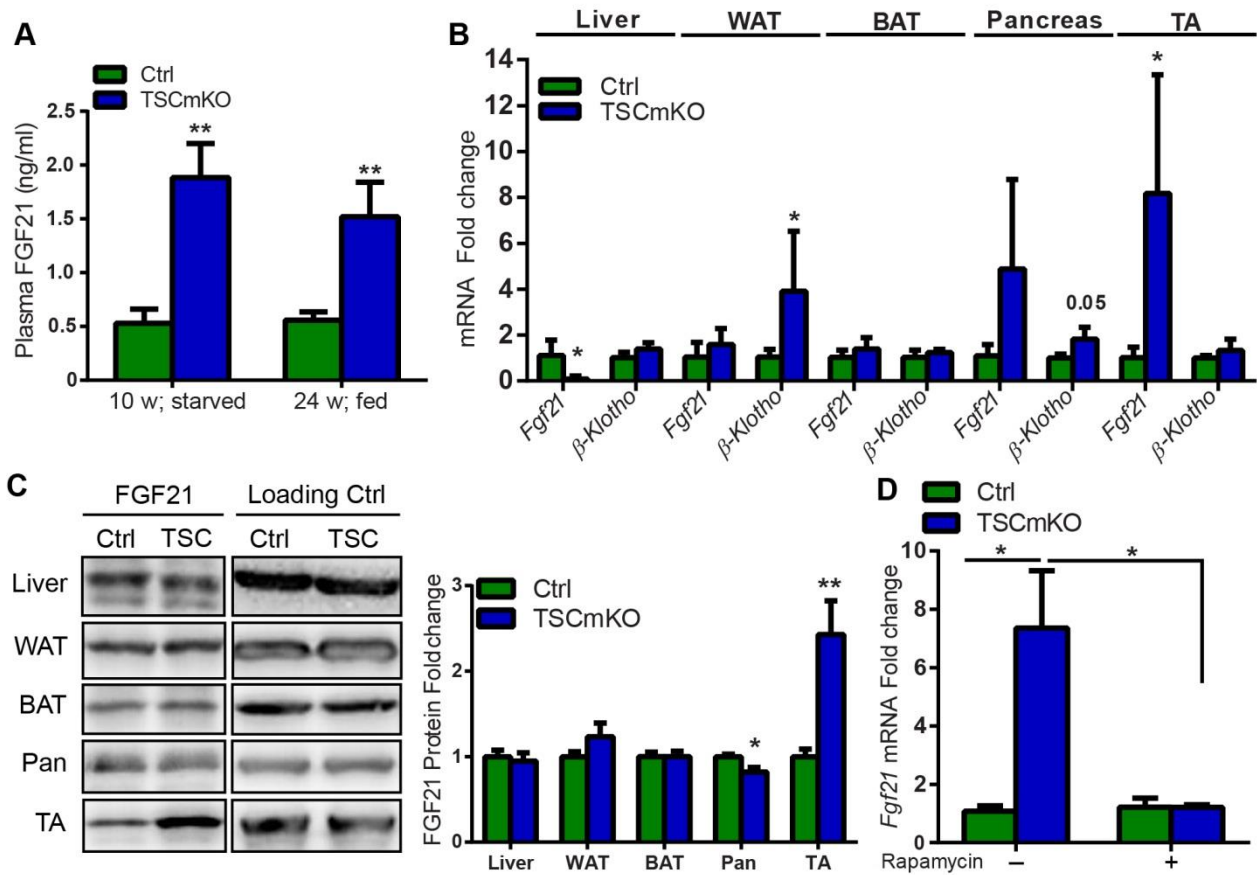


**Figure 4. FGF21 concentrations increase in TSCmKO mice**

A. Plasma concentration of FGF21 was increased in 10-week-old, starved (n= 3 mice per genotype) and 24-week-old, fed (n= 6 mice per genotype) TSCmKO mice.

B. Expression of *Fgf21* and  $\beta$ -*Klotho* genes in liver, WAT, BAT, pancreas and TA muscle from 10-week-old TSCmKO and control mice (n= 4 mice per genotype) revealed higher *Fgf21* expression in the skeletal muscle of mutant mice.

C. Immunoblot analysis of FGF21 is shown for liver, WAT, BAT, pancreas (Pan) and TA muscle from 10-week-old TSCmKO (TSC) and control (Ctrl) mice (n= 4 mice per genotype). Protein abundance was normalized to  $\beta$ -actin for liver, WAT and BAT; eEF2 for pancreas; and  $\alpha$ -actinin for TA (loading control).

D. Increased *Fgf21* expression in TA muscle of TSCmKO mice (n= 3 mice per genotype) was normalized after 3-day rapamycin treatment (n= 4 mice per genotype).

E. Plasma FGF21 concentration was not changed in 20-week-old RAmKO mice (n= 4 mice per genotype).

F. Immunoblot analysis of FGF21 and ATF4 is shown for TA muscle of 10-week-old RAmKO mice (n= 4 mice per genotype). Protein abundance was normalized to  $\alpha$ -actinin.

Data represent mean  $\pm$  SEM, \*p<0.05, \*\*p<0.01.

**FIGURE 5**

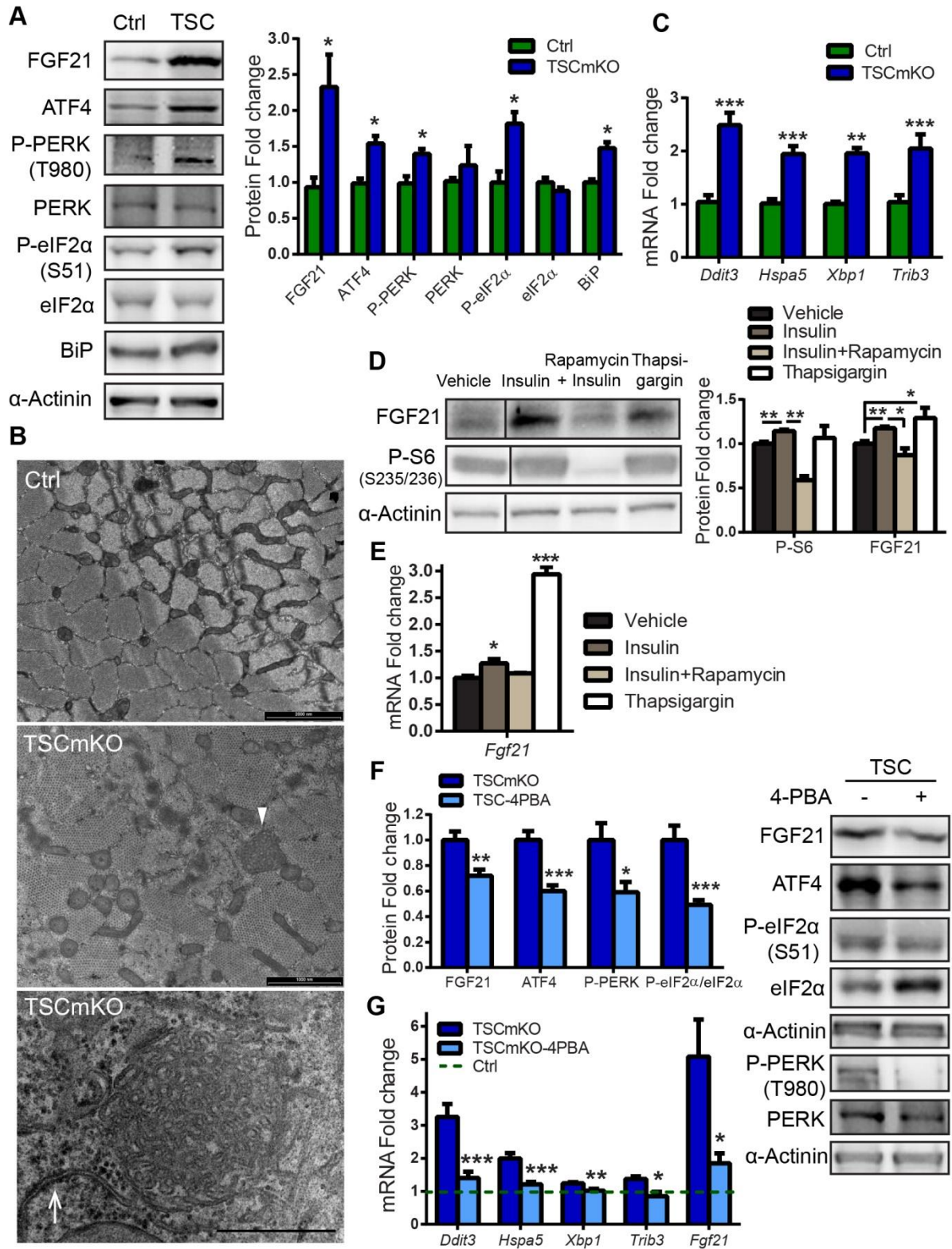


**Figure 5. Activation of mTORC1 increases FGF21 abundance in skeletal muscle through ER stress-mediated induction of the PERK-eIF2 $\alpha$ -ATF4 pathway**

A. Immunoblots of TA muscle from 10-week-old TSCmKO (TSC) and control (Ctrl) mice are shown for the indicated phospho (P)- and total proteins (n= 5 mice per genotype), which indicated an activation of ER stress. Protein abundance is normalized to  $\alpha$ -actinin.

B. Electron microscopic images of EDL muscle from 40-week-old control (Ctrl) and TSCmKO mice revealed ER aggregates in mutant muscle. Arrowhead and arrow point to ER cluster and rough ER detail, respectively. Scale bar, 2000 nm (top), 1000 nm (middle), 500 nm (bottom). Images are representative of 3 mice per genotype.

C. TSCmKO mice showed increased expression of ER stress and UPR markers in TA muscle at 10 weeks of age (n= 5 mice per genotype).

D. Immunoblots from C2C12 myotubes treated with insulin and thapsigargin showed accumulation of FGF21 upon mTORC1 activation and ER stress induction, which was abolished with rapamycin treatment (n= 4 sets of cells per condition). Protein abundance was normalized to  $\alpha$ -actinin.

E. C2C12 myotubes treated with insulin and thapsigargin showed increased transcriptional expression of *Fgf21*, which was blunted by rapamycin treatment (n= 4 sets of cells per condition).

F. Immunoblots of TA muscle are shown for the indicated phospho (P)- and total proteins in 4-PBA treated TSCmKO (TSC) mice (+) compared to untreated (-) mice (n= 7 mice per genotype and treatment). Protein abundance was normalized to  $\alpha$ -actinin.

G. 4-PBA treatment normalized the expression of UPR markers and *Fgf21* in gastrocnemius and TA muscle from 14-week-old TSCmKO mice (n= 7 mice per genotype and treatment).

Data represent mean  $\pm$  SEM, \*p<0.05, \*\*p<0.01, \*\*\*p<0.001.

**FIGURE 6**

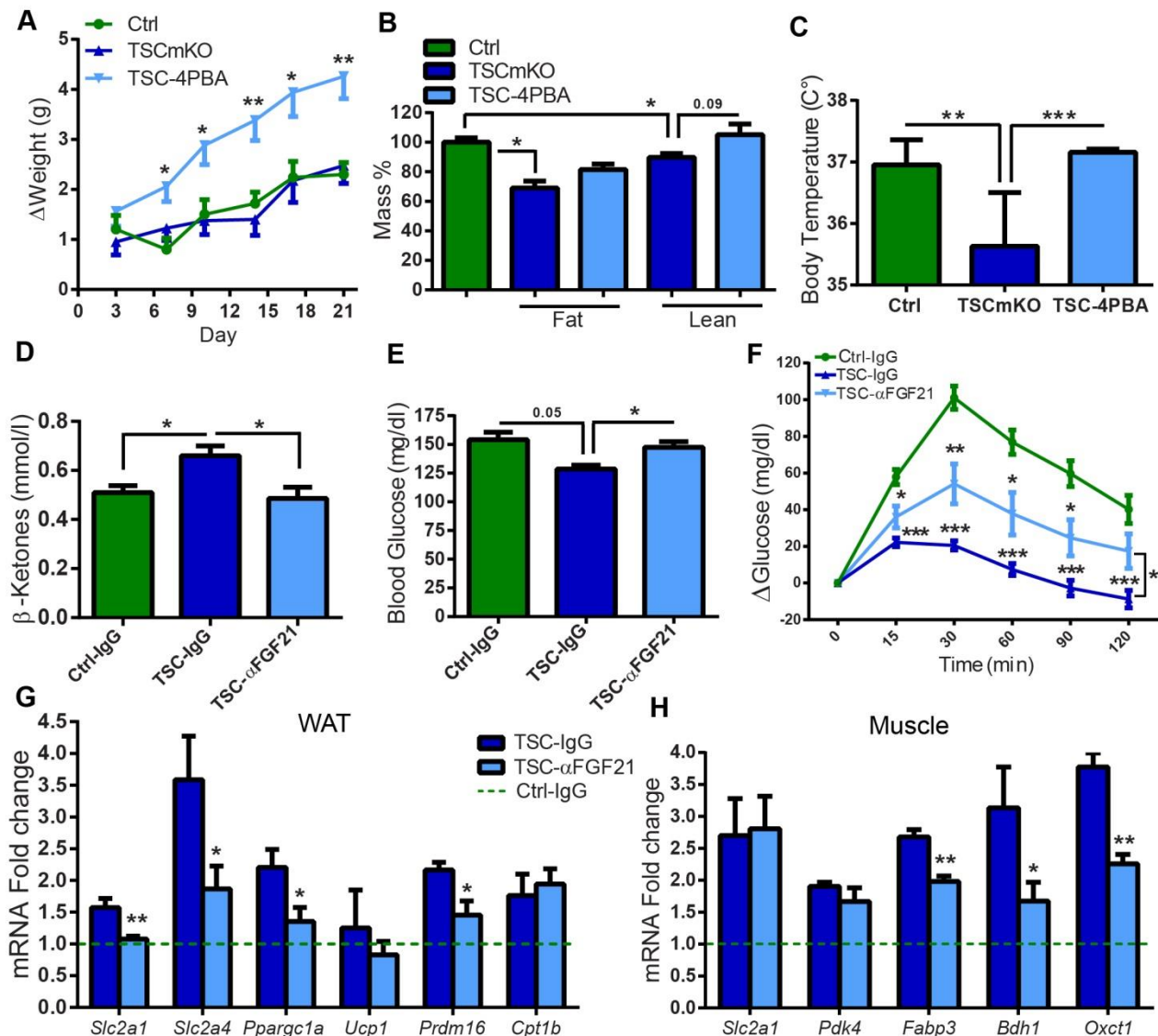


**Figure 6. Blocking FGF21 normalizes liver gluconeogenesis, plasma  $\beta$ -ketone and plasma glucose concentrations**

A. Body weight of TSCmKO mice significantly increased after 3 weeks 4-PBA treatment (n=5 mice per genotype and treatment). Linear regression analysis shows that the groups differed significantly (p=0.01).

B. Echo-MRI analysis of body composition showed changes in fat and lean mass percentage in TSCmKO mice upon 4 weeks 4-PBA treatment (n= 5 mice per genotype and treatment).

C. Body temperature was decreased in 14-week-old TSCmKO mice, but normalized after 4 weeks 4-PBA treatment (n= 7 mice per genotype and treatment).

D, E. Blood  $\beta$ -ketone (D) and glucose (E) concentrations were normalized in 11-week-old TSCmKO mice treated with FGF21-neutralizing antibody (n= 13), compared to mutant (n= 5) and control (n= 13) mice treated with rabbit IgG.

F. After treatment with FGF21-neutralizing antibody, gluconeogenesis was improved in TSCmKO mice (n= 6) when compared to mutant (n= 3) and control (n= 9) mice treated with rabbit IgG. Linear regression analysis shows that the groups differed significantly ( $p < 0.001$ ).

G. Expression of genes encoding glucose transporters (*Slc2a1* and *Slc2a4*), enzymes involved in fatty acid oxidation (*Ppargc1a*; *Cpt1b*) and browning markers (*Ucp1*; *Prdm16*) in WAT was normalized to varying extents after anti-FGF21 antibody treatment in 11-week-old TSCmKO mice (n= 7) when compared to TSCmKO (n= 5) and control mice treated with rabbit IgG (n= 8). Control line (Ctrl-IgG) represents normalized gene expression of the IgG-treated littermates.

H. Expression of genes encoding proteins involved in fatty acid and ketone body breakdown (*Fabp3*; *Bdh1*; *Oxct1*) in TA muscle was decreased after anti-FGF21 antibody treatment in 11-week-old TSCmKO mice (n= 7) when compared to TSCmKO (n= 5) and control mice (n= 8) treated with rabbit IgG. Control line (Ctrl-IgG) represents normalized gene expression of the IgG-treated littermates.

Data represent mean  $\pm$  SEM, \* $p < 0.05$ , \*\* $p < 0.01$ , \*\*\* $p < 0.001$ .

# Supplementary figures

## Figure S1

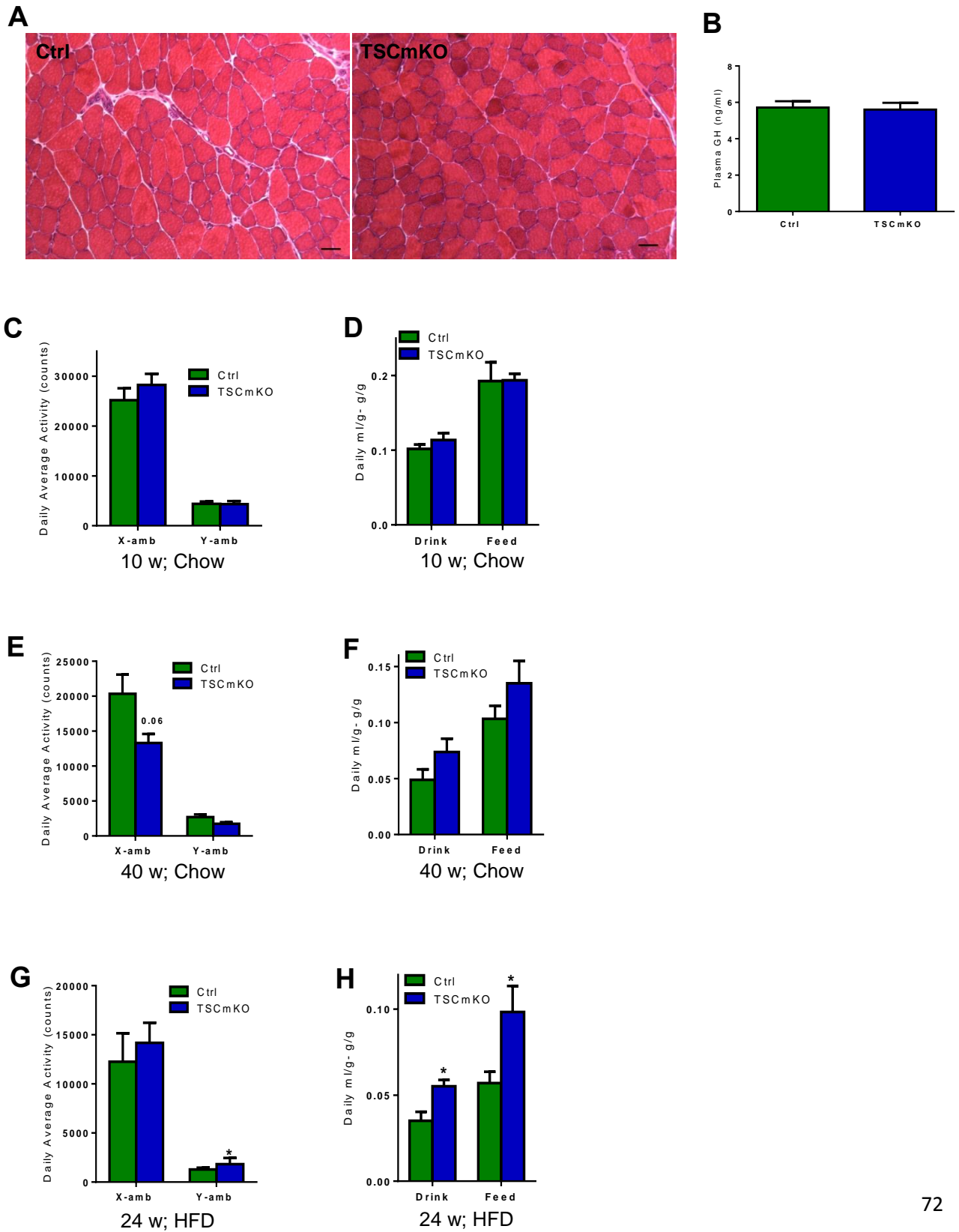




**Figure S1: TSCmKO mice do not show overt behavioral changes**

A. H&E staining of TA muscle from 12-week-old TSCmKO and control mice (n=3 mice per genotype). Scale bar, 100  $\mu$ m.

B. Plasma growth hormone (GH) concentration is similar in 10-week-old TSCmKO (n= 7) and control mice (n= 9).

C-H. CLAMS (Comprehensive Lab Animal Monitoring System) analysis of 10- (C-D, n= 6 mice per genotype) and 40- (E-F, n=6 mice per genotype) week-old TSCmKO and control mice on a chow diet, and of 16-week-old mutant and control mice during HFD (G-H, n= 6 mice per genotype). Activity, drinking and feeding were measured and normalized to body weight and daily average.

Data represent mean  $\pm$  SEM, \*p<0.05, \*\*p<0.01, \*\*\*p<0.001

**Figure S2**

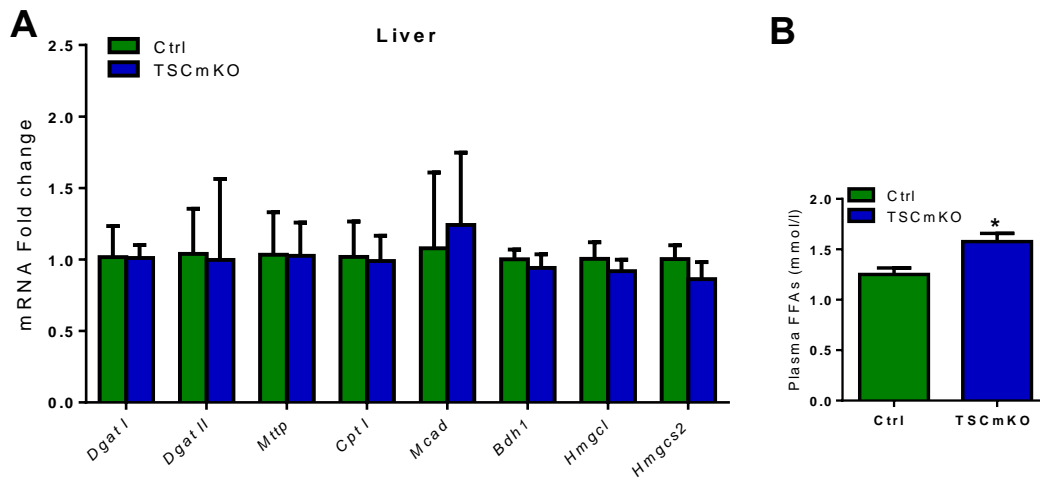


**Figure S2: Higher plasma concentrations of free fatty acids in TSCmKO mice**

A. Relative expression of genes involved in fatty acid metabolism in liver. mRNA was extracted from liver of 10-week-old TSCmKO and control mice (n= 4 mice per genotype).

B. Plasma free fatty acid concentrations after 24h starvation in 10-week-old TSCmKO and control mice (n= 4 mice per genotype).

Data represent mean  $\pm$  SEM, \*p<0.05.

Figure S3

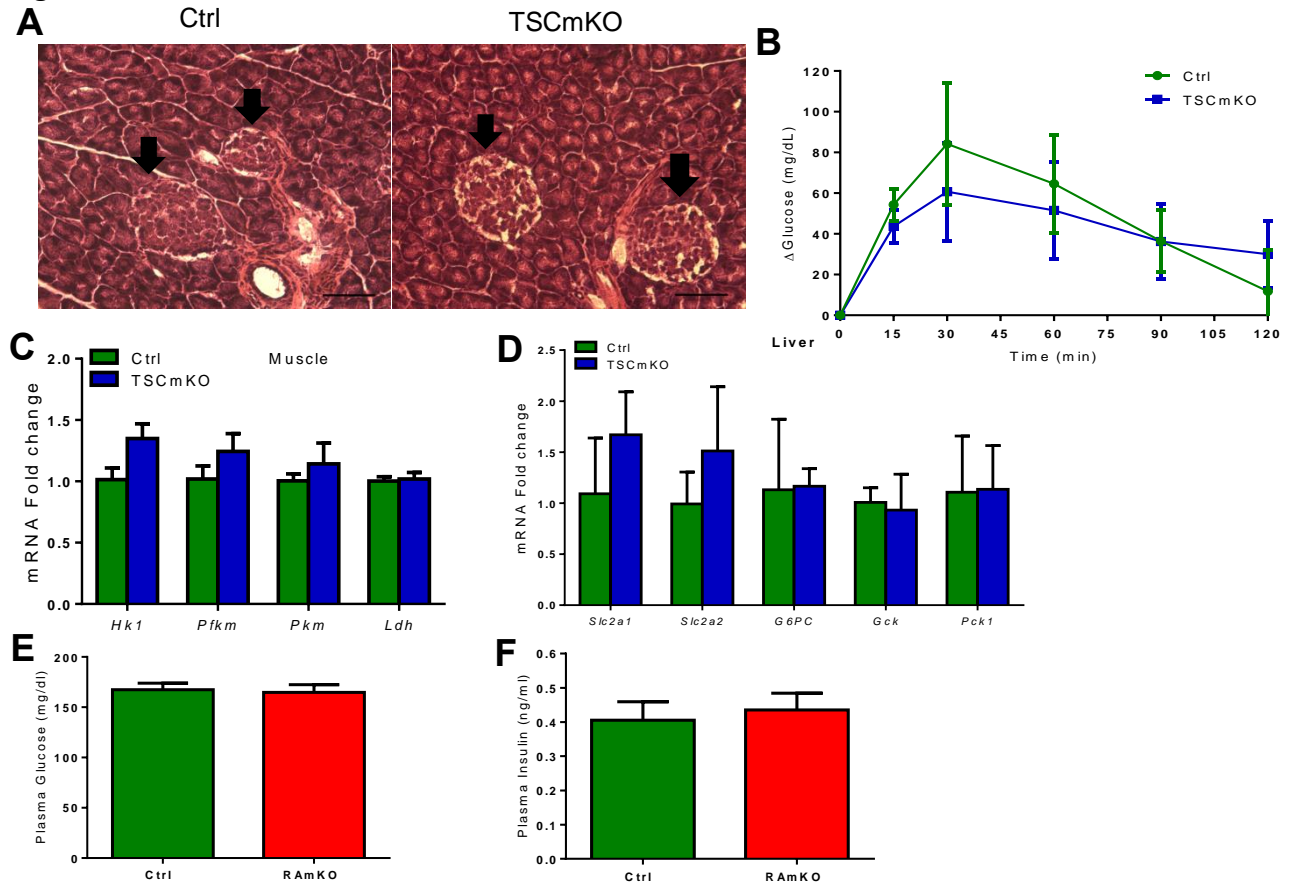


**Figure S3: TSCmKO mice do not show changes in the expression of genes encoding enzymes involved in glycolysis**

A. H&E staining of pancreas from 10-week-old TSCmKO and control mice (n=3 mice per genotype). Scale bar, 100  $\mu$ m. Arrows point at Langerhans islets.

B. Pyruvate tolerance test in 10-week-old TSCmKO and control mice (n= 6 mice per genotype). Linear regression analysis shows that the differences between the groups are not significant ( $p>0.05$ ).

C, D. Relative expression of genes involved in glucose metabolism in TA muscle (C) and in the liver (D) of 10-week-old TSCmKO and control mice (n=4 mice per genotype).

E, F. Plasma glucose (E) and insulin (F) concentrations in 10-week-old RAmKO and control mice (n= 6 mice per genotype). Data represent mean  $\pm$  SEM, \*p<0.05, \*\*p<0.01.

Figure S4

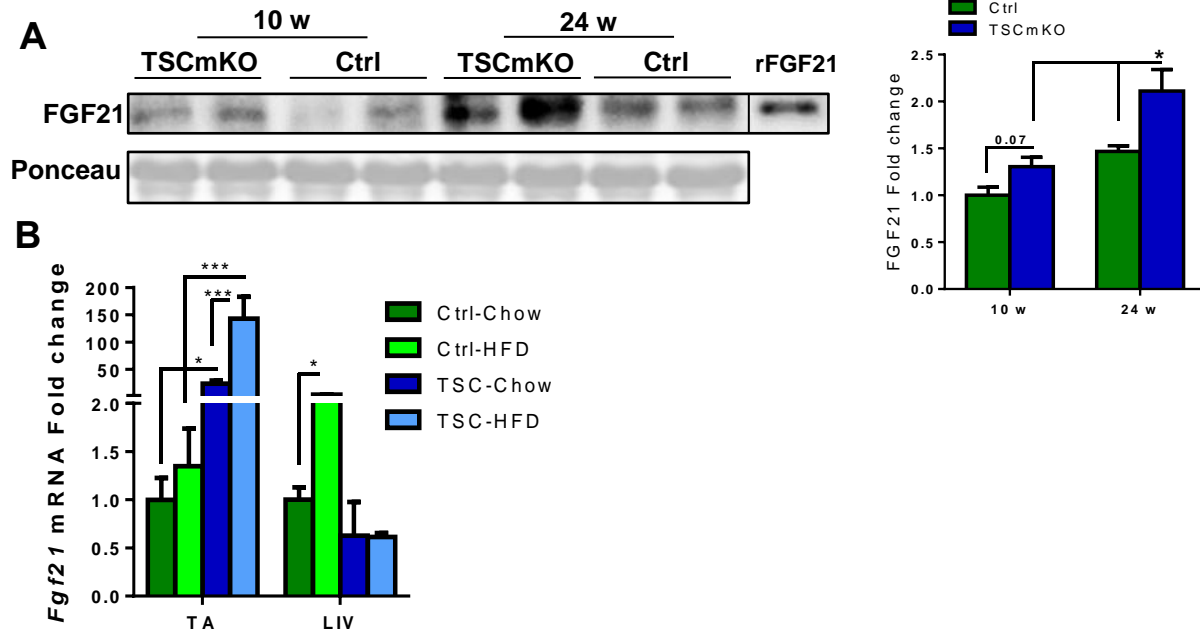


Figure S4: FGF21 abundance in muscle is increased in TSCmKO mice

A. Western blot analysis of plasma FGF21 after immunodepletion in 12- and 24-week-old fed TSCmKO and control mice (n= 4 mice per genotype and age). Ponceau staining was used as a loading control. 100 pg of recombinant FGF21 (rFGF21) were loaded as a control.

B. Relative expression of *Fgf21* in TA muscle and liver of Chow or HFD-fed 24-week-old control (Ctrl) and TSCmKO mice (n=3 mice per genotype and condition).

Data represent mean  $\pm$  SEM, \*p<0.05.

**Figure S5**

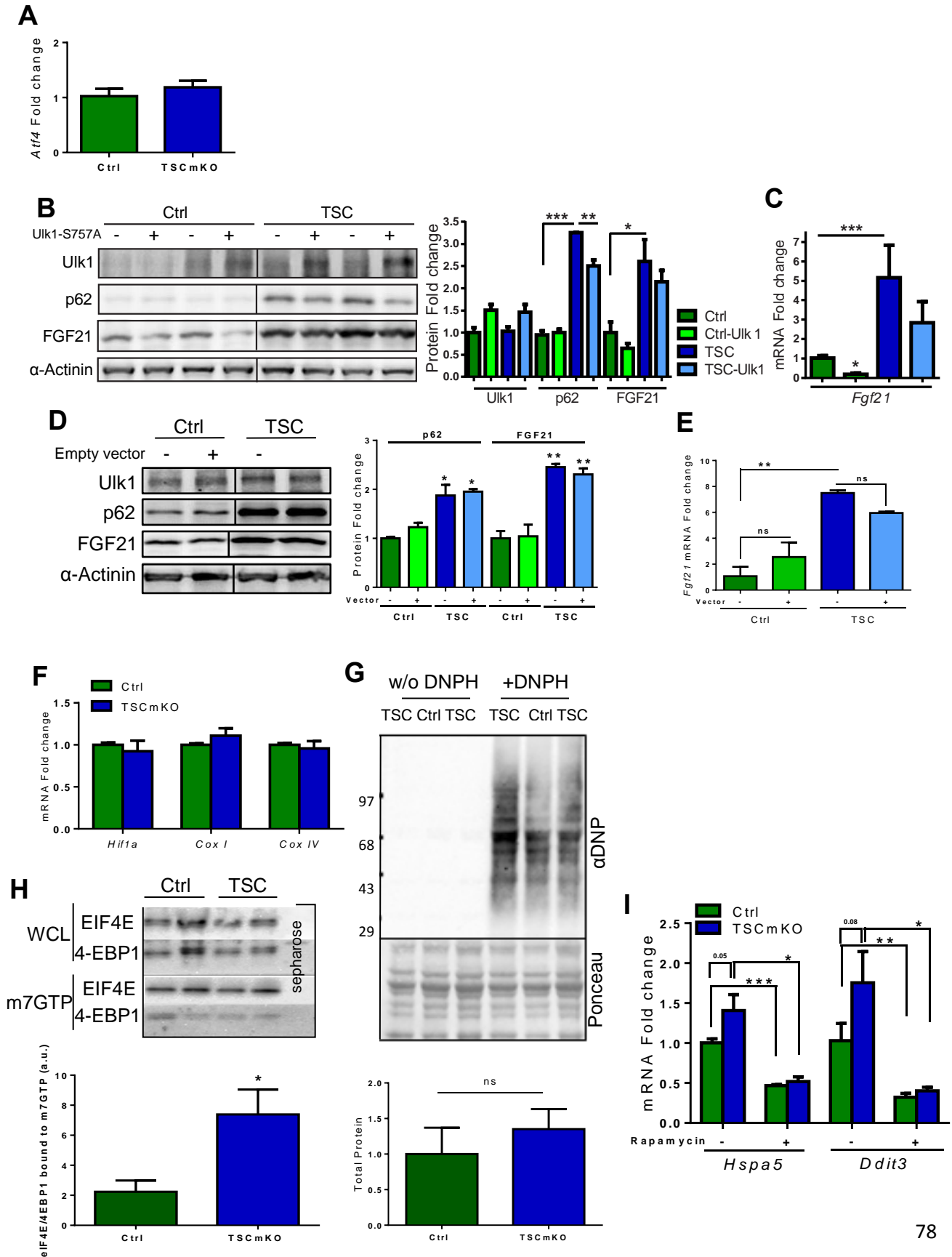


**Figure S5: FGF21 in TSCmKO mice is induced by ER stress, not autophagy impairment or mitochondrial dysfunction.**

A. Relative *Atf4* mRNA expression in TA muscle of 10-week-old TSCmKO and control mice (n= 4 mice per genotype).

B. Immunoblots of TA muscle electroporated with Ulk1-S757A (+) and non-electroporated contralateral muscle (-) from 20-week-old TSCmKO (TSC) and control (Ctrl) mice are shown for the indicated proteins (n= 3 mice per genotype and condition). Protein abundance is normalized to  $\alpha$ -actinin.

C. *Fgf21* expression is significantly decreased in TA electroporated with Ulk1-S757A in control mice, but not in the electroporated TSCmKO muscle when compared to respective contralateral legs (n= 3 mice per genotype and condition).

D. Immunoblots of TA muscle electroporated with an empty vector (+) and of the non-electroporated contralateral muscle (-) from 20-week-old TSCmKO (TSC) and control (Ctrl) mice are shown for the indicated proteins (n= 3 mice per genotype and condition). Protein abundance is normalized to  $\alpha$ -actinin.

E. *Fgf21* mRNA expression was quantified in TA muscle electroporated with an empty vector (+) and in the non-electroporated contralateral muscle (-) from 20-week-old TSCmKO (TSC) and control (Ctrl) mice (n=3 mice per genotype and condition).

F. Relative expression of mitochondrial genes in TA muscle from 10-week-old TSCmKO and control mice (n= 4 mice per genotype).

G. Protein oxidation status was quantified by Oxiblot assay in 10-week-old TSCmKO and control mice (n= 4 mice per genotype).

H. m7GTP binding assay reveals an increase in translation initiation in 10-week-old TSCmKO muscle, compared to control (n= 6 mice per genotype).

I. Relative expression of *Hspa5* and *Ddit3* in gastrocnemius muscle of 12-week-old TSCmKO and control mice with (+) and without (-) 3-day rapamycin treatment (n= 4 mice per genotype and treatment).

Data represent mean  $\pm$  SEM, \*p<0.05, \*\*p<0.01, \*\*\*p<0.001.



Figure S6

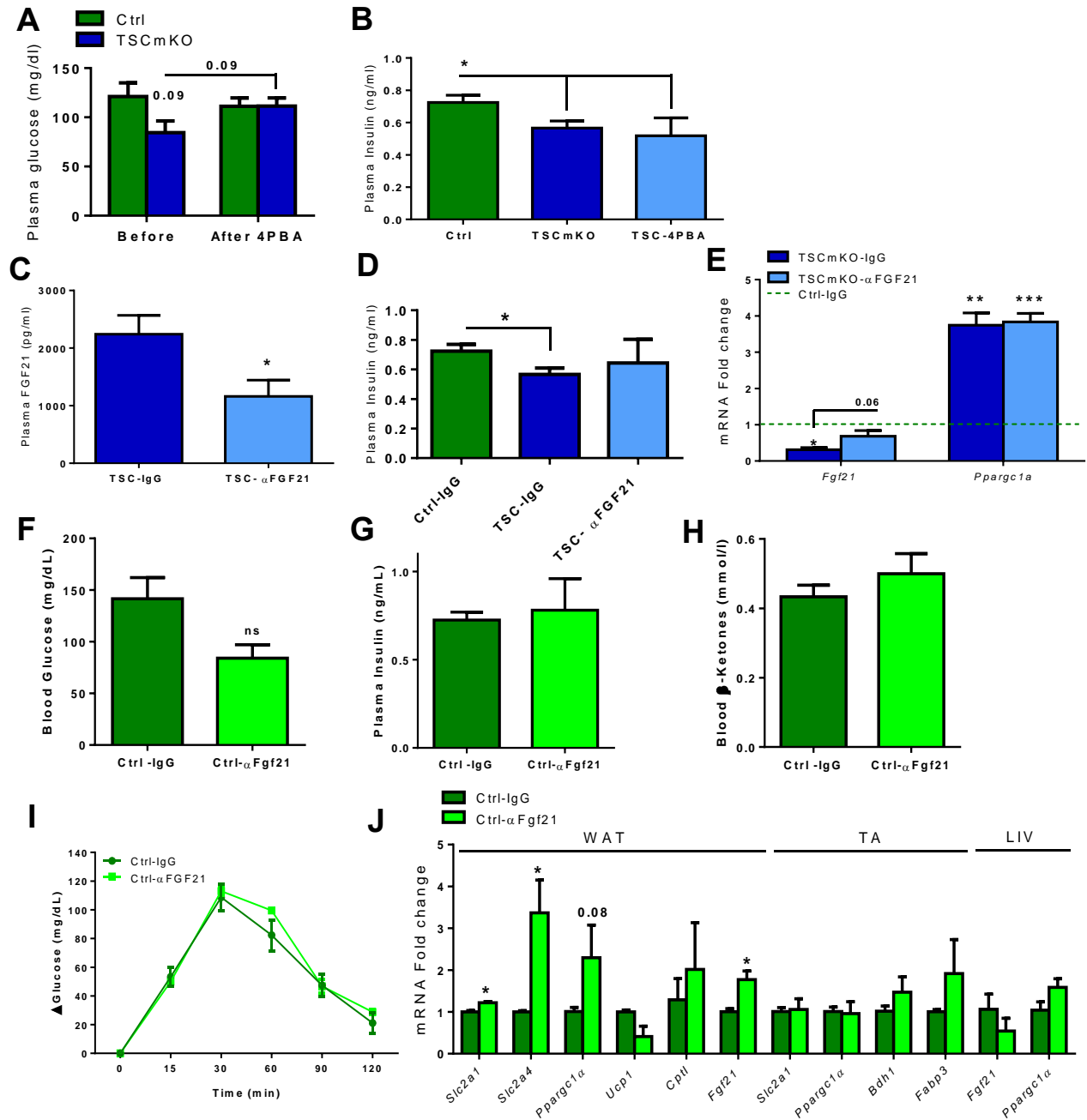


Figure S6: FGF21 blockade does not alter plasma insulin concentration in TSCmKO mice or metabolism in control mice

A. Plasma glucose concentrations from 10-week-old TSCmKO mice before and after 4-PBA treatment (n= 5 mice per genotype and treatment).

B. Plasma insulin concentrations in 14-week-old TSCmKO mice after 4-PBA treatment (n= 5) compared to untreated TSCmKO (n= 6) and control mice (n= 8).

C. Plasma FGF21 concentrations in 24-week-old TSCmKO mice treated with FGF21-neutralizing antibody and TSCmKO mice treated with non-immune IgG (n= 5 mice per genotype and treatment).

D. Plasma insulin concentrations from 12-week-old TSCmKO mice treated with FGF21-neutralizing antibody (n= 5) compared to TSCmKO (n= 6) and control mice (n= 8) treated with non-immune IgG.

E. Expression of *Fgf21* and *Ppargc1a* in liver from 10-week-old TSCmKO mice treated with FGF21-neutralizing antibody and TSCmKO and control mice treated with non-immune IgG (n= 4 mice per genotype and treatment). Control line (Ctrl-IgG) represents normalized *Fgf21* and *Ppargc1a* expression of the IgG treated littermates.

F-H. Plasma glucose (F), insulin (G) and ketone body (H) concentrations in anti-FGF21 or IgG antibody treated 10-week-old control (Ctrl) mice (n= 3 mice per genotype and treatment).

I. Pyruvate tolerance test in anti-FGF21 or IgG antibody treated 24-week-old control (Ctrl) mice (n= 3 mice per genotype and treatment). Linear regression analysis shows that the differences between the groups are not significant ( $p>0.05$ ).

J. Expression of genes involved in glucose, fatty acid or ketone metabolism in WAT, TA and Liver of anti-FGF21 or IgG antibody treated 10-week-old control (Ctrl) mice (n= 3 mice per genotype and treatment).

Data represent mean  $\pm$  SEM, \* $p<0.05$ , \*\* $p<0.01$ , \*\*\* $p<0.001$ .

**Table S1. Weight and size analysis in 10- and 40-week-old mice**

	10 weeks			40 weeks		
	Ctrl	TSCmKO		Ctrl	TSCmKO	
Weight (g)	25.3 ± 0.4	21.5 ± 0.7	***	27.8 ± 1.1	19.2 ± 0.7	***
Tibia (mm)	17.8 ± 0.1	17 ± 0.1	***	18.1 ± 0.1	17.3 ± 0.2	***

p values determined by Student's test are indicated by asterisks (n= 6-11 mice per genotype ).

Values represent mean ± SEM. \*\*\*p<0.001

---

**Table S2. COBAS plasma analysis of 10-week-old mice**

	Ctrl	TSCmKO
Triglycerides (mmol/l)	1.48 ± 0.14	1.84 ± 0.24
HDL-Cholesterol (mmol/l)	2.25 ± 0.09	2.08 ± 0.06
LDL-Cholesterol (mmol/l)	0.17 ± 0.01	0.22 ± 0.04
Cholesterol (mmol/l)	2.47 ± 0.08	2.28 ± 0.10

---

Values represent mean ± SEM (n= 5 mice per genotype)

---

**Table S3: Primers used for qPCR**

Gene	Forward primer	Reverse primer	Name of the gene
<i>Acac1</i>	ACC TTA CTG CCA TCC CAT GTG	GTG CCT GAT GAT CGC ACG AAC AAA	<i>Acetyl-CoA carboxylase 1</i>
<i>Acat1</i>	GTGAAGGAAGTCTACATGGGC	TGTGGTGCATGGAGTGGAAAT	<i>Acetyl CoA acyltransferase 1</i>
<i>Atf4</i>	AGCAAAACAAGACAGCAGCC	ACTCTCTCTCCCCCTTGC	<i>Activating transcription factor 4</i>
<i>Bdh1</i>	TTGAGCTGGATGTTCTCAGTC	TTTGCTGGCTGTTTGTGAAGG	<i>D-β-hydroxybutyrate dehydrogenase</i>
<i>Cidea</i>	TGGGATTGCAGACTAAGAAGGTC	CGGTCATGGTTTGAACCTGAAA	<i>Cell death-inducing DFFA-like effector a</i>
<i>Cox I</i>	GGT CAA CCA GGT GCA CTT TT	TGG GGC TCC GAT TAT TAG TG	<i>Cytochrome C-oxidase 1</i>
<i>Cox IV</i>	TACTTCGGTGTGCCTTCGA	TGACATGGGCCACATCAG	<i>Cytochrome C-oxidase 4</i>
<i>Cpt1b</i>	GGT CGA TTG CAT CCA GAG AT	GAC TCC GGT GGA GAA GAT GA	<i>Carnitine palmitoyltransferase 1</i>
<i>Ddit3</i>	CCACCACACTGAAAGCAGAA	AGGTGAAAGGCAGGGACTCA	<i>DNA-Damage-Inducible Transcript 3-CHOP</i>
<i>Dgat I</i>	CATGCGTGATTATTGCATCC	ACAGTTTGCATCCCGGTAG	<i>Diglyceride acyltransferase I</i>
<i>Dgat II</i>	GCGCTACTCCGAGACTACTT	GGGCCTTATGCCAGGAAACT	<i>Diglyceride acyltransferase II</i>
<i>Fabp3</i>	CCC CTCAGCTCAGCACCA	CAG AAA AAT CCC AAC CCA AGA AT	<i>Fatty acid binding protein 3</i>
<i>Fasn</i>	GCTGCGGAAACTTCAGGAAAT	AGAGACGTGTCCTCTGGACTT	<i>Fatty acid synthase</i>
<i>Fgf21</i>	TACACAGATGACGACCAAGA	GGCTTCAGACTGGTACACAT	<i>Fibroblast growth factor 21</i>
<i>Gck</i>	CCCTGAGTGGCTTACAGTTC	ACGGATGTGAGTGTGAAGC	<i>Glucokinase</i>
<i>G6pc</i>	AGC GGA ATG GGA GCA ACT TG	CAG AAT GGG TCC ACC TTG ACA C	<i>Glucose-6-phosphatase</i>
<i>Hif1α</i>	CAGTACAGGATGCTTGCCAAAA	ATACCACTACAACATAATTCACACACA	<i>Hypoxia inducible factor 1α</i>
<i>Hk1</i>	CCCTGCCACCAGACGAAA	GACTTGAACCCCTTAGTCCATGA	<i>hexokinase</i>
<i>Hmgcl</i>	GATGCCGGGAAACTTCTGAATG	CCAGCTTTGTTTCTCCAAAGTG	<i>3-hydroxymethyl-3-methylglutaryl-CoA lyase</i>
<i>Hmgcs2</i>	CCACAAGGTGAACCTCTCTCCA	TGCATCTCATCCACTCGTTCA	<i>3-hydroxy 3-methylglutaryl CoA synthase 2</i>
<i>Hspa5</i>	TTCAGCCAATTATCAGCAAACCTCT	TTTTCTGATGATCCTCTTACCAGT	<i>Heat shock 70kDa protein 5 -BiP</i>
<i>β-Klotho</i>	AGGGTCTCCGGGGAATGAAT	GATCTTTCAGTGCCTGTTG	<i>Beta-klotho receptor</i>
<i>Ldh</i>	TGTCTCCAGCAAAGACTACTGT	GACTGTACTTACAATGTTGGGA	<i>Lactate dehydrogenase</i>
<i>Mcad</i>	TCTCGAAGACGTCAGAGTGC	TGCGACTGTAGTCTGGTTC	<i>Medium-chain acyl-coenzyme A dehydrogenase</i>
<i>Mttp</i>	CGTCCACATACAGCCTTGAC	CCACCTGACTACCATGAAGC	<i>Microsomal triglyceride transport protein</i>
<i>Oxct1</i>	CCCATACCACTGAAAGACGAA	CTGGAGAAGAAAGAGGCTCCTG	<i>3-oxoacid-CoA transferase 1</i>
<i>Pck1</i>	CAT CCA GGC AAT GTC ATC GC	GCA TAA CTA ACC CG AAG GCA AG	<i>Phosphoenolpyruvate carboxikinase</i>
<i>Pdk4</i>	AAA ATT TCC AGG CCA ACC AA	CGA AGA GCA TGT GGT GAA GGT	<i>Pyruvate dehydrogenase kinase, isozyme 4</i>
<i>Pfkm</i>	CAGATCAGTGCCAACATAACCAA	CGG GAT GCA GAG CTC ATC A	<i>Phosphofruktokinase</i>
<i>Pkm</i>	CGATCTGTGGAGATGCTGAA	AATGGGATCAGATGCAAAGC	<i>Pyruvate kinase</i>
<i>Ppargc1α</i>	TGATGTGAATGACTTGGATACAGACA	GCTCATTGTTGACTGGTTGGATATG	<i>Peroxisome proliferator activated receptor gamma coactivator 1-alpha</i>
<i>Ppargc1β</i>	CCATGCTGTTGATGTTCCAC	GACGACTGACAGCACTTGGAA	<i>Peroxisome proliferator activated receptor gamma coactivator 1-beta</i>
<i>Prdm16</i>	AGCTGAGGAAGCATTGAAGTTA	ATATGCCTGGTCTTAGCCTGC	<i>PR domain containing 16</i>
<i>Scd1</i>	CAA GCTGGAGTACGTCTGGA	CAG AGC GCT GGT CAT GTA GT	<i>Stearoyl-CoA desaturase 1</i>
<i>Slc2a1</i>	CGAGGGACAGCCGATGTG	GCCGACCCTCTTCTTCAT	<i>Glucose transporter1</i>
<i>Slc2a4</i>	GATGAGAAACGGAAGTTGGAGAGA	GCACCACTGCGATGATCAGA	<i>Glucose transporter4</i>
<i>Trib3</i>	GGACAAGATGCGAGCCACAT	CCACAGCAGGTGACAAGTCT	<i>Tribbles homolog 3</i>
<i>Ucp1</i>	GGCCTCTACGACTCAGTCCA	TAAGCCGGCTGAGATCTTGT	<i>Uncoupling protein 1</i>
<i>Ucp2</i>	TCCCCTGTTGATGTGGTCAA	CAGTGACCTGCGCTGTGGTA	<i>Uncoupling protein 2</i>
<i>Xbp1</i>	TGGCCGGTCTGCTGAGTCCG	GTCCATGGGAAGATGTTCTGG	<i>X-box binding protein 1</i>

### 3.2. Manuscript 2

## Alterations to mTORC1 signaling in skeletal muscle differentially affect whole-body metabolism

Maitea Guridi<sup>1</sup>, Barbara Kupr<sup>1</sup>, Klaas Romanino<sup>1</sup>, Shuo Lin<sup>1</sup>, Denis Falcetta<sup>1</sup>, Lionel Tintignac<sup>1#</sup>, Markus A. Rüegg<sup>1\*</sup>

<sup>1</sup>Biozentrum, University of Basel, 4056 Basel, Switzerland

#### \*Corresponding author:

markus-a.ruegg@unibas.ch, Tel: +41 61 267 22 23, Fax: +41 61 267 22 08

Maitea Guridi: [m.guridi@unibas.ch](mailto:m.guridi@unibas.ch) ; Barbara Kupr: [barbara.kupr@unibas.ch](mailto:barbara.kupr@unibas.ch) ; Klaas Romanino: [k.romanino@gmx.ch](mailto:k.romanino@gmx.ch) ; Denis Falcetta: [d.falcetta@stud.unibas.ch](mailto:d.falcetta@stud.unibas.ch) ; Shuo Lin: [shuo.lin@unibas.ch](mailto:shuo.lin@unibas.ch) ; Lionel Tintignac: [lionel.tintignac@unibas.ch](mailto:lionel.tintignac@unibas.ch)

<sup>#</sup>Present address: Neuromuscular Research Center, Departments of Neurology and Biomedicine, Pharmazentrum, University of Basel, 4056 Basel, Switzerland

## **ABSTRACT**

**Background:** The mammalian target of rapamycin complex 1 (mTORC1) is a central node in a network of signaling pathways controlling cell growth and survival. This multiprotein complex integrates external signals and affects different nutrient pathways in various organs. However, it is not clear how alterations of mTORC1 signaling in skeletal muscle affect whole-body metabolism.

**Results:** We characterized the metabolic phenotype of young and old RAmKO (Raptor muscle knock-out) and TSCmKO (TSC1 muscle knock-out) mice, where mTORC1 activity in skeletal muscle is inhibited or constitutively activated, respectively. Ten week-old RAmKO mice are lean and insulin resistant with increased energy expenditure and they are resistant to a high-fat diet (HFD). This correlates with an increased expression of histone deacetylases (HDACs) and a down-regulation of genes involved in glucose and fatty acid metabolism. Ten week-old TSCmKO mice are also lean, glucose intolerant with a decreased activation of Akt/PKB targets that regulate glucose transporters in muscle. The mice are resistant to a HFD and show reduced accumulation of glycogen and lipids in the liver. Both mouse models suffer from a myopathy with age, with reduced fat and lean mass, and both RAmKO and TSCmKO mice develop insulin resistance and increased intramyocellular lipid content.

**Conclusions:** Our study shows that alterations of mTORC1 signaling in skeletal muscle differentially affect whole-body metabolism. While both, inhibition and constitutive activation of mTORC1 induce leanness and resistance to obesity, changes in the metabolism of muscle and

peripheral organs are distinct. These results indicate that a balanced mTORC1 signaling in the muscle is required for proper metabolic homeostasis.

**KEYWORDS:** Muscle/ Myopathy/ Metabolism/ Diabetes/ mTOR/ TSC1/ Raptor

## **BACKGROUND**

The highly conserved serine/threonine protein kinase mammalian target of rapamycin (mTOR) is known to control numerous cellular processes related to cell growth (Wullschleger et al, 2006). mTOR assembles into two functionally distinct multiprotein complexes, the rapamycin-sensitive mTOR complex 1 (mTORC1), and mTORC2, which is only sensitive to prolonged rapamycin treatment (Sarbassov et al, 2006). mTORC1 is a central sensor of growth factors and nutrients in various cell types and has been described to play an important role in different pathologies like cancer, metabolic diseases and aging (Laplante & Sabatini, 2012). Because of its central role in metabolism, the mTOR pathway is extensively studied for its function in type 2 diabetes (Polak & Hall, 2009). mTORC1 is also highly active in the liver and skeletal muscle of obese and high-fat-fed rodents (Khamzina et al, 2005; Um et al, 2004). Inhibition of mTOR signaling by rapamycin prolongs lifespan in several species including mice (Harrison et al., Nature, 2009), a treatment that has been proposed to mimic calorie restriction (Selman et al, 2009). Paradoxically, prolonged treatment with rapamycin causes glucose intolerance and insulin resistance (Cunningham et al, 2007; Fraenkel et al, 2008; Houde et al, 2010), which has been interpreted to be the result of the inactivation of mTORC2 (Lamming et al, 2012). In



skeletal muscle, mTORC1 regulates muscle mass by affecting both protein synthesis and degradation (Laplante & Sabatini, 2012).

As it is difficult to distinguish the contribution of different tissues on the systemic effects of rapamycin treatment, several laboratories have generated various mouse models with tissue-specific deletions of essential components of the mTORC1 pathway. White adipose tissue (WAT)-specific deletion of *rptor* (gene coding for raptor), which is essential for the activity of mTORC1, leads to improved insulin sensitivity and reduced adipocyte number and size (Polak et al, 2008a). Inactivation of mTORC1 in liver leads to resistance to hepatic steatosis and hypercholesteremia induced by a Western diet (Peterson et al, 2011). While those tissues are the primary sites controlling metabolism, skeletal muscle has also been shown to contribute to whole-body metabolism. For example, skeletal muscle is the major site of glucose uptake in response to food intake and insulin and thus can contribute to type 2 diabetes (DeFronzo & Tripathy, 2009). Accordingly, patients with muscular dystrophies often develop metabolic complications like glucose intolerance and insulin resistance (Rodriguez-Cruz et al, 2015; Savkur et al, 2001). Similarly, sustained activation of mTORC1 leads to metabolic changes at the whole-body level (Guridi et al, 2015).

In this study we compared as to how activation or inactivation of mTORC1 in skeletal muscle affect systemic energy homeostasis. We show that both fatty acid and glucose metabolism are dependent on proper mTORC1 signaling. In mice with muscle-specific depletion of raptor (i.e. inactive mTORC1), the metabolic changes correlate with up-regulation of class II histone deacetylases (HDACs). On the contrary, muscle-specific depletion of TSC1 (i.e. constant activation of mTORC1) leads to an up-regulation of transcripts involved in glucose and fatty acid

metabolism in various metabolic organs (Guridi et al, 2015), but causes glucose intolerance and late-onset damage in both the liver and the kidneys. These data thus provide evidence that mTORC1 signalling in skeletal muscle is a major regulator of whole-body metabolism and they suggest that muscle mTORC1 could be a valuable target for the treatment of metabolic complications associated with muscle diseases including muscular dystrophies.

## **MATERIAL AND METHODS**

**Animal experiments.** Generation of TSCmKO and RAmKO mice and their genotyping were described before (Bentzinger et al, 2008; Castets et al, 2013; Kwiatkowski et al, 2002). Control mice were littermates floxed for *Rptor* (gene encoding raptor) or *Tsc1* but not expressing Cre-recombinase. TSCmKO and RAmKO mice were always compared to a control group of littermates. Initial statistical analysis was always done separately using the respective controls. At the young age, control mice for RAmKO and TSCmKO mice were pooled as those mice had the same age and because statistics was not altered when experimental groups were compared to non-pooled controls. All data shown represent new cohorts of mice although some of the metabolic phenotype of TSCmKO mice have been published before (Guridi et al, 2015). The fact that those data are confirmatory is mentioned throughout the text. Mice were maintained in a conventional facility with a fixed light cycle (23°C – 12 hr dark-light cycle) and were fed standard chow (KLIBA NAFAG, 1304811) or a high-fat diet (HFD) containing 60% fat (KLIBA NAFAG, 2127.PH.A05) *ad libitum*. HFD was started at 8 or 10 weeks of age respectively for RAmKO and TSCmKO mice, and continued for 12 weeks. Body composition was determined by Magnetic Resonance with the EchoMRI-100H body composition analyzer (EchoMRI TM) in immobilized

conscious mice. In some experiments, mice were intraperitoneally injected with insulin at 2pm (0.75 U/kg Humalog, Eli Lilly) after a 5 hour fast, and euthanized 45 minutes after for tissue collection. Euthanasia in the rest of mice was performed at 10 am after food removal at 6 am of the same morning. Both male and female mice were used for this study after confirming that the phenotype observed was not dependent on gender. Data from male mice are shown in the main figures, whereas results from female mice, when available, are shown in Additional files. All procedures were performed in accordance with the Swiss regulations for animal experimentation and approved by the veterinary commission of the Canton Basel-Stadt.

**Metabolic measurements.** Glucose, lactate and insulin plasma levels were analyzed in tail vein blood after a 4 hour fast (6 am to 10 am) with One Touch Ultra Easy glucose meter (LifeScan, Inc.), Lactate-pro test strips (Arkray Factory, Inc.) and Ultra-Sensitive Mouse Insulin ELISA kit (Crystal Chem, Inc.), respectively. ATP content and glycogen amount in muscle and liver were determined by using a luminescence assay (CellTiter-Glo Luminescent Cell Viability Assay, Promega) and a Glycogen assay kit (SIGMA-ALDRICH), respectively. A full analysis of plasma parameters was performed with a Cobas C111 machine (Roche) after a 4 hour fast (6 am to 10 am).

**Indirect calorimetry by CLAMS (Comprehensive Lab Animal Monitoring System, Columbus Instruments).** Mice were acclimatized for two days (individual housing) followed by data acquisition over three to four days. Activity (i.e. ambulatory movement determined by laser counts in X and Y coordinates), feeding and drinking behaviors were measured daily over a

period of 4 days. Oxygen use and carbon dioxide production was measured and energy expenditure was calculated with the Weir equation. Respiratory exchange ratio (RER) was calculated as  $VCO_2/VO_2$ . Data were normalized to body weight.

**IP Insulin tolerance test (ITT) and glucose tolerance test (GTT).** After an overnight starvation for GTT and a 5 hour fast for ITT (from 9 am to 2pm), mice were intraperitoneally injected with 1.5 g/kg glucose (Merck) or 0.75 U/kg insulin (Humalog, Eli Lilly), respectively. Basal blood glucose was measured before the injection from tail vein blood and at the indicated time points after the intraperitoneal injection.

**Histology.** Liver and *tibialis anterior* (TA) muscle, frozen in liquid nitrogen-cooled isopentane, were cut into 10  $\mu$ m-thick cross-sections. Sections were stained with hematoxylin (Merck) - eosin (Sigma-Aldrich) and Oil Red-O (Sigma-Aldrich) and mounted with glycerol gelatin (Sigma-Aldrich).

**Quantitative real-time PCR.** Total RNA from RAMKO and control mice was isolated (SV Total RNA isolation System, Promega) and equal amounts of RNA were reverse transcribed using a mixture of oligodT and random hexamer primers (iScript cDNA Synthesis Kit, Bio-Rad). Quantitative real-time PCR was performed using SYBR Green (Power SYBR Green Master Mix, Applied Biosystems) and StepOne™ Software 2.1. (Applied Biosystems). Expression levels for each gene of interest were normalized to the mean cycle number using real-time PCR for the housekeeping gene encoding  $\beta$ -actin, whose expression was not altered between RAMKO and

control mice (Additional file 1: Figure S1A). All experiments were performed in triplicates. Primers used are listed in Additional file 2: Table S1.

**Western blotting.** Proteins were extracted from TA muscle, liver, WAT and BAT as described previously (Bentzinger et al, 2008). Total protein levels were determined using a reducing agent compatible BCA Protein Assay (Pierce). Signal was captured on a Fusion Fx machine (Vilber Lourmat), grey values were corrected for background and analyzed with the FUSION Capt FX software. Quantification of each protein was normalized to the loading control ( $\alpha$ -actinin or  $\beta$ -actin). To determine the extent of protein phosphorylation, relative intensity of the band using a phospho-specific antibody was divided by the amount of protein as determined by a pan-specific antibody. Samples from 4 groups of mice were all run together on the same gel, and quantification was done relative to the values of the control group for each genotype. Antibodies are listed in Additional file 1: Figure S1B.

**Statistical analyses.** Compiled data are expressed as mean  $\pm$  SEM and *n* (total number of knock-out mice). Measurements were performed at least in 3 independent sets of experiments. Statistical comparison of two conditions was performed using the Student's t- test, comparison of 3 or more groups was performed using the one-way or two-way ANOVA test with Tukey correction for multiple comparisons and data where time was a variable were analyzed by linear regression (GraphPad Prism Software). A 0.05 level of confidence was accepted for statistical significance.

## RESULTS

### Modification of skeletal muscle mTORC1 signaling affects whole-body metabolism

We have previously reported that inhibition of mTORC1 activity in skeletal muscle by raptor depletion (RAmKO mice) results in a lethal myopathy (Bentzinger et al, 2008). Interestingly, sustained activation of mTORC1 by depletion of TSC1 (TSCmKO mice) also results in a late-onset myopathy (Castets et al, 2013). In addition, RAmKO mice show alterations in glucose metabolism in the muscle (Bentzinger et al, 2008) whereas TSCmKO show strong changes in their fatty acid metabolism at the whole-body level (Guridi et al, 2015). As the skeletal muscle phenotypes of RAmKO and TSCmKO converge at older age, we decided to also perform a detailed characterization and comparison of RAmKO and TSCmKO mice at the whole-body level.

First, we analyzed the body composition by EchoMRI using 10-week-old mice, an age at which neither of the mice show myopathic signs (Bentzinger et al, 2013; Bentzinger et al, 2008; Castets et al, 2013; Guridi et al, 2015). Both, male and female TSCmKO mice were significantly lighter when compared to age-matched control mice (Figure 1A; Additional file 3: Figure S2A). In RAmKO mice, male mice were also lighter than their control littermates (Figure 1A) while this difference did not reach significance in females (Additional file 3: Figure S2A). This difference in the young RAmKO mice was due to a lower lean mass without affecting the amount of fat (Figure 1B and 1C; Additional file 3: Figure S2B and S2C). In young TSCmKO mice, lean mass was moderately changed whereas the amount of fat was strongly reduced (Figure 1B and 1C; Additional file 3: Figure S2B and S2C). RAmKO mice showed no changes in insulin (Figure 1D) and plasma glucose levels (Figure 1E; Additional file 3: Figure S2D) whereas those plasma parameters were lower in TSCmKO mice as previously reported (Guridi et al, 2015) and now

confirmed in a new set of mice (Figure 1D and 1E; Additional file 3: Figure S2D). Besides the changes in blood glucose and insulin, the concentration of lactate was also increased in TSCmKO mice but not in RAmKO mice (Figure 1F). As those plasma profiles suggest changes in the glucose uptake capacity, we next performed glucose and insulin tolerance tests. They revealed that TSCmKO mice were glucose intolerant (Figure 1G) and slightly more sensitive to insulin (Figure 1H). RAmKO mice had the reciprocal phenotype with normal glucose tolerance (Figure 1G) but insulin resistance (Figure 1H). A similar reciprocal phenotype was observed for the basal metabolism as energy expenditure was increased in 10-week-old RAmKO mice but not in TSCmKO mice (Table 1). Thus, these results show that some of the early changes in the whole-body metabolism are differentially affected in RAmKO and TSCmKO mice.

### **TSCmKO and RAmKO mice are both resistant to a high-fat diet**

To test how the mice perform under metabolic stress, we fed both RAmKO and TSCmKO mice a high-fat diet (HFD) for 12 weeks, starting at the age of 8 or 10 weeks, respectively. Neither TSCmKO nor RAmKO mice gained as much weight as the control mice (Figure 2A). RAmKO mice maintained significantly lower fat and lean mass while on a HFD (Additional file 3: Figure S2E and S2F) as did TSCmKO mice (Guridi et al, 2015). Control mice also developed hepatic steatosis whereas TSCmKO and RAmKO were resistant (Figure 2B). Prolonged HFD feeding causes type 2 diabetes (Winzell & Ahren, 2004). Consistent with the HFD resistance, plasma glucose levels were reduced in TSCmKO (Guridi et al, 2015) and RAmKO mice (Additional file 3: Figure S2G). In addition, RAmKO mice showed an improved glucose tolerance compared to TSCmKO and control mice under the HFD (Figure 2C). In contrast, TSCmKO showed an increased insulin

sensitivity during the HFD when compared to RAmKO and control mice (Figure 2D); (Guridi et al, 2015). As previously shown (Guridi et al, 2015), TSCmKO mice placed on HFD ate and drank more, showed increased activity and energy expenditure but decreased respiratory exchange ratio (Table 2). On the other hand, RAmKO mice showed a decrease in their activity and the respiratory exchange ratio (Table 2), indicating a preference for fatty acid metabolism as a source of energy (Even & Nadkarni, 2012). These results show that both activation and inhibition of mTORC1 in skeletal muscle conferred resistance to a HFD and they indicate that different mechanisms underlie this phenotype.

#### **TSCmKO but not RAmKO mice show changes in other metabolic organs**

The activation state of the serine/threonine kinase Akt/PKB is altered in RAmKO and TSCmKO mice because of the negative feedback loop from S6K on IRS1 (Um et al. 2004). Thus, in RAmKO mice, lack of activation of S6K causes increased phosphorylation of Akt/PKB (Bentzinger et al, 2008), whereas Akt/PKB phosphorylation is dampened in TSCmKO mice (Bentzinger et al, 2013). As Akt/PKB signaling is an important regulator of carbohydrate metabolism (Schultze et al, 2012), we next examined Akt/PKB targets involved in glucose absorption and storage. As previously shown (Bentzinger et al, 2008; Guridi et al, 2015; Romanino et al, 2011), we confirmed that glycogen phosphorylase levels were decreased in RAmKO muscle, as well as glycogen synthase phosphorylation (Figure 3A) while they were unchanged in TSCmKO muscle. Moreover, phosphorylation of the Akt/PKB substrate of 160 kDa (AS160/TBC1D4), responsible for GLUT4 translocation to the sarcolemma upon insulin stimulation (Cartee, 2015), was decreased in TSCmKO when measured relative to the amount of TBC1D4. Similarly,



phosphorylation of TBC1D1, another Akt/PKB substrate involved in basal glucose absorption into skeletal muscle (Cartee, 2015), was also reduced in TSCmKO muscle relative to the total amount of TBC1D1 (Figure 3A). Interestingly, both TBC1D4 and TBC1D1 protein levels were increased in TSCmKO muscle (Figure 3A). In contrast, phosphorylation of TBC1D4 was increased in RAmKO muscle and there was a trend for increased TBC1D1 phosphorylation (Figure 3A). Overall, the observed changes correlated well with the increased glycogen levels (Figure 3B and Additional file 4: Figure S3A). Thus, modifications of the mTORC1 activity in skeletal muscle lead to dysregulated Akt/PKB signaling that result in changes in glucose transport and storage.

We have previously reported that TSCmKO mice show browning of white adipose tissue and increased fatty acid oxidation in the liver (Guridi et al, 2015). In contrast to the decrease in lipids in TSCmKO mice (Figure 3C), lipid content seemed unchanged in RAmKO liver (Figure 3C). In agreement with this, plasma non-esterified fatty acids were decreased in TSCmKO mice but were the same as in controls in the RAmKO mice (Figure 3D). We decided to analyze Akt/PKB signaling in the liver because insulin is a key regulator of gluconeogenesis and glycogenolysis in this organ. While Akt/PKB and mTORC1 activities were unchanged in RAmKO mice, both were down-regulated in the liver of TSCmKO mice (Figure 3E). This is likely a consequence of the decreased plasma insulin levels of the TSCmKO mice and not lack of responsiveness, as liver from TSCmKO mice responded to insulin like controls (Additional file 4: Figure S3B). Moreover, the amount of glucose-6 phosphatase was higher in TSCmKO mice than in controls or RAmKO mice (Figure 3E). In correlation with these protein changes, the glycogen amount was reduced in livers from TSCmKO but not from RAmKO mice (Figure 3F). In addition, none of the genes that were reported to be changed in TSCmKO mice involved in fatty acid or glucose metabolism

in the liver, white adipose tissue or brown fat of TSCmKO mice (Guridi et al, 2015) were changed in RAmKO mice (Additional file 4. Liver: Figure S3C, S3E and S3F; white adipose tissue: Figure S3C; brown fat: Figure S3D). These results show that under a normal diet, mTORC1 activation in skeletal muscle causes changes in other metabolic organs, such as liver and adipose tissue. In contrast, the effect of its inhibition is limited to the targeted skeletal muscle.

### **Strong down-regulation of metabolic genes and increased levels of HDACs in RAmKO skeletal muscle**

Uncoupling proteins (UCPs) uncouple the proton gradient in the inner membrane of the mitochondria thereby regulating efficiency of ATP production and energy expenditure in cells (Azzu & Brand, 2010). In WAT, mTORC1 regulates UCP expression (Polak et al, 2008a). Thus, we determined mRNA and protein levels of UCP in skeletal muscle. Both mRNA and protein abundance of UCP2 and of the muscle-specific UCP3 were significantly increased in RAmKO mice (Figure 4A and B). Whereas ATP levels in TSCmKO mice are reduced, whose muscles also contain a higher amount of UCP2 (Guridi et al, 2015), the ATP content in the muscle of RAmKO mice was identical to controls (Additional file 5: FigureS4). Besides the changes in UCPs, expression of genes involved in fatty acid transport and oxidation, like *Fatp4*, *Fabp3* or *Cpt1b*, was decreased in the muscle of young RAmKO mice compared to control littermates (Figure 4C). In addition, expression of glucose transporters and genes involved in glycolysis was also reduced in RAmKO skeletal muscle (Figure 4D), as opposed to the increased expression of genes involved in glucose absorption and fatty acid oxidation seen in TSCmKO muscle (Guridi et al, 2015). To better understand the possible pathways involved in the regulation of those

metabolic genes, we next analyzed expression of class II histone deacetylases 4 and 5 (HDAC4 and HDAC5), which are known to regulate glycolytic proteins (McGee et al, 2008; Tang et al, 2009). HDAC4 and HDAC5 protein levels were increased in RAmKO mice, while there was only a slight, but significant increase of HDAC4 in TSCmKO muscle (Figure 4E). Thus, the strong increase in HDAC4 and HDAC5 in RAmKO skeletal muscle could contribute to the decreased expression of genes involved in fatty acid and glucose metabolism.

### **Myopathy pre-dominates the metabolic changes in the two animal models at older age**

Previous work has shown that both RAmKO and TSCmKO mice develop a myopathy (Bentzinger et al, 2008; Castets et al, 2013). To investigate whether the metabolic changes in peripheral organs would also converge at older age, we next compared the overall metabolism between 20-week-old RAmKO and 40-week-old TSCmKO mice, the age at which the myopathy is fully developed (Bentzinger et al, 2008; Castets et al, 2013). Body weights were significantly reduced in male and female TSCmKO and male RAmKO mice (Figure 5A; Additional file 6: Figure S5A), which was due to lower lean (Figure 5B; Additional file 6: Figure S5B) and fat mass (Figure 5C; Additional file 6: Figure S5C). Basal metabolic analysis revealed an increase in energy expenditure in 40-week-old TSCmKO mice, while in 20-week-old RAmKO mice the overall energy expenditure was now as in controls (Table 3). Analysis of the blood plasma revealed that insulin (Figure 5D) and glucose (Figure 5E) levels were reduced in both TSCmKO and RAmKO mice, while the increased plasma lactate levels of young TSCmKO mice (see Figure 1F) were normalized in the old mice (Figure 5F). It is well established that loss of muscle mass also affects glucose metabolism (Rodriguez-Cruz et al, 2015; Savkur et al, 2001). While glucose tolerance

was normal (Figure 5G), both TSCmKO and RAmKO mice were now insulin resistant (Figure 5H). Insulin resistance in muscle has been linked to the disruption of lipid dynamics and accumulation of intramyocellular, lipotoxic intermediates (Badin et al, 2013). Thus, we analyzed lipid content in muscle of the mutant mice and found that lipid droplets accumulated in RAmKO muscle and the amount of lipids was increased in TSCmKO muscle (Figure 5I). These results suggest that the myopathy in RAmKO and TSCmKO mice results in very similar overall perturbation of the metabolism.

We previously reported that the myopathy of RAmKO mice is particularly severe in the diaphragm, which led us to suggest that respiratory failure might be the cause of death (Bentzinger et al, 2008). Low respiration reduces oxygen saturation and causes the accumulation of carbon dioxide in the blood. Blood gas analysis revealed that oxygen and carbon dioxide pressure in the blood was the same as in the controls in 10-week-old RAmKO, but oxygen levels dropped and carbon dioxide increased in 20-week-old, myopathic RAmKO mice (Additional file 7: Table S2). The increase in carbon dioxide also resulted in the lowering of the blood pH indicative of respiratory acidosis (Additional file 7: Table S2). Although we cannot rule out respiratory complications in old, myopathic TSCmKO mice (Castets et al, 2013), we observed that 40-week-old TSCmKO mice also had polycystic kidneys (Additional file 6: Figure S5D), a frequent cause for acute kidney failure (Woo, 1995). In agreement with the conclusion that the kidneys were damaged, the amount of creatinine and lactate dehydrogenase (LDH) was significantly elevated in the blood of TSCmKO mice (Table 4). In addition, alanine aminotransferase (ALT) and aspartate aminotransferase (AST) were also increased in the plasma of 40-week-old TSCmKO mice (Table 4), which are commonly used as markers for liver

damage (Oh & Husted, 2011). We hypothesize that this kidney damage in old TSCmKO mice was the consequence of prolonged muscle breakdown or rhabdomyolysis (Torres et al, 2015). These results suggest that the disease is mainly restricted to skeletal muscle in the RAMKO mice and thus the mice are likely to die of respiratory failure. In contrast, TSCmKO mice show defects in several tissues and thus they might succumb to diseases in multiple organs, including skeletal muscle and kidney.

## **DISCUSSION**

The control of energy balance plays a central role in metabolic diseases such as type 2 diabetes and obesity. mTORC1 has been postulated to play an essential role in glucose homeostasis by fine-tuning insulin signaling through Akt/PKB and by controlling metabolic pathways in different tissues (Tremblay et al., 2005; Um et al., 2006). Likewise, mTORC1 has a central role in regulating lipid metabolism and adipogenesis by activating essential transcription factors like *Pparg* and *Srebp1* (Lamming & Sabatini, 2013). Skeletal muscle is a particularly important player in the regulation of energy balance in the body, serving both as a major glucose and energy-storing tissue, as well as an avid energy consumer during physical activity. mTORC1 also affects muscle mass and integrity by regulating both protein synthesis and degradation and it has been suggested to be involved in muscle wasting during aging (Tintignac et al, 2015). However, how mTORC1 activity in skeletal muscle affects whole-body metabolism has not yet been clarified in detail.

Consequences of mTORC1 perturbation have been described in other metabolic tissues, such as WAT or liver, and revealed differential effects of mTORC1 signaling on tissue and whole-

body metabolism, depending on the targeted organs and the mouse models used. For instance, although mTORC1 promotes lipogenesis in liver cells through SREBP activation, this effect was abolished in mice with liver-specific depletion of TSC1 and also resulted in insulin resistance, due to the simultaneous inhibition of Akt/PKB in this tissue (Li et al, 2010; Peterson et al, 2011; Yecies et al, 2011). Inactivation of mTORC1 in WAT caused the browning and reduction of fat, resulted in an increase in energy expenditure and Akt/PKB-dependent insulin sensitivity (Polak et al, 2008b).

In our study, we now report on the whole-body consequences of mTORC1 activation and inhibition in skeletal muscle (Figure 6). At a young age, mTORC1 inhibition had a stronger effect on skeletal muscle, causing a significant reduction in lean mass and muscle atrophy (Bentzinger et al, 2008). Only few changes were observed at the metabolic level in RAMKO mice, one being increased energy expenditure, most likely a consequence of the higher UCP2 and UCP3 mRNA and protein amount in the muscle. However, RAMKO mice were insulin resistant, which could be a direct consequence of the early muscle atrophy and dysfunctional muscle dynamics. Conversely, at this young age, activation of mTORC1 in skeletal muscle caused strong changes of the metabolism without yet affecting the structural integrity of skeletal muscle. We have previously shown that mTORC1 activation induces the release of FGF21 from skeletal muscle, which in turn is responsible for several of the metabolic changes, such as hypoglycemia, increased fatty acid oxidation and reduced body weight (Guridi et al, 2015). Despite the improved metabolic profile of TSCmKO mice, we now show that they are glucose intolerant. We suggest that this could be a consequence of dampened Akt/PKB signaling and the decreased translocation of glucose transporters to the plasma membrane (Cartee, 2015). Surprisingly,

Akt/PKB signaling was also decreased in the liver of TSCmKO, likely due to decreased plasma insulin concentrations. In addition, the glycogen amount in the liver was lower in TSCmKO mice, which correlated with an increase in glucose 6-phosphatase, suggesting increased liver glycogenolysis as compensation for the low plasma glucose concentration. In contrast to the TSCmKO mice, RAmKO mice showed no changes in their liver or plasma profile, indicating that the consequences of early mTORC1 inhibition are limited to skeletal muscle.

Interestingly, even if RAmKO and TSCmKO mice initially show an opposite metabolic phenotype, both mutant mice are resistant to HFD. Both mutant mice did not gain weight nor did they develop hepatic steatosis on a 12-week-long HFD. However, while TSCmKO mice showed increased insulin sensitivity and seemed to accelerate their metabolism by eating more and being more active, RAmKO mice showed improved glucose tolerance and slowed their metabolism by decreasing the activity and their respiratory exchange ratio. All these metabolic changes, compared to those previously reported, point to the specific consequences of mTORC1 deregulation depending on the metabolic organs in which the perturbation occurs.

Consistent with the inhibition of mTORC1 activity, RAmKO mice display a downregulation of glycolytic proteins and genes involved in fatty acid oxidation in the skeletal muscle. This correlated with the increase in class II HDACs, which have been described to regulate the transcription of glycolytic proteins (Cohen et al., 2007). The inefficient nutrient utilization and the increased energy demand might lead to beneficial systemic effects and to a resistance to diet-induced obesity in the RAmKO mice. This phenotype is paralleled by a reduction of the oxidative capacity of the muscles and by a reduction of the number of mitochondria (Romanino

et al, 2011). Similar to RAmKO mice, treatment with rapamycin leads to a reduced glucose uptake (Blattler et al., 2012a), which highlights the critical role of muscle mTORC1 signaling.

Changes in muscle integrity can affect whole body metabolism, as seen in patients with muscular dystrophies who often develop glucose intolerance and insulin resistance (Cruz Guzman Odel et al, 2012; Savkur et al, 2001). Both TSCmKO and RAmKO mice develop a myopathy and show a reduced body weight, which suggested that they are not able to gain lean and fat mass with age as control mice do. Interestingly, myopathic RAmKO and TSCmKO mice develop insulin resistance, show lower plasma glucose and plasma insulin concentrations. It has been proposed that whole-body insulin resistance is a consequence of lipotoxicity caused by aberrant lipid metabolism in the muscle and increased intramyocellular accumulation of ceramides and diacylglycerol (Badin et al, 2013). Accordingly, TSCmKO and RAmKO mice could suffer from lipotoxicity as they showed increased accumulation of lipids in the skeletal muscle. This accumulation of toxic lipid intermediates could be a result of endoplasmic reticulum stress in TSCmKO mice (Guridi et al, 2015; Salvado et al, 2015) and activation of inflammatory pathways in RAmKO mice (Bentzinger et al, 2008; Osborn & Olefsky, 2012). Nonetheless, the development of insulin resistance in both mouse models after the onset of the myopathy is well in line with the metabolic complications in muscular dystrophies. It will be interesting to see whether deregulation of mTORC1 signaling could also be at the onset of those metabolic complications in muscular dystrophies.

Our results indicate that mTORC1 is a central controller of metabolic properties of muscle tissue by affecting fatty acid and glucose metabolism, glycogen storage and oxidative capacity. We also show that skeletal muscle mTORC1 plays an essential role in whole-body homeostasis



and energy expenditure. Our data imply that the beneficial effects of rapamycin on systemic metabolism and longevity could in part be based on inhibition of mTORC1 in skeletal muscle. Therefore, further investigation should be conducted to determine whether mTORC1 deregulation in muscular dystrophies might be the cause of the overall changes in the whole-body metabolism.

## **CONCLUSION**

In this study we have confirmed that alterations to mTORC1 signaling pathway in skeletal muscle directly affect whole-body metabolism, which highlights the importance of this tissue in maintaining energy stability. Moreover, we show that a proper balance in mTORC1 signaling is essential for muscle integrity and metabolic homeostasis, as both long-term activation and inhibition originate a myopathy that mimics the main metabolic complications of dystrophic patients. Thus, muscle mTORC1 could serve as a potential target to treat those metabolic complications.

## **COMPETING INTERESTS**

The authors declare they do not have competing interests.

## **AUTHOR CONTRIBUTIONS**

M.G. designed and performed most of the experiments, analyzed the data and wrote the paper; B.K. and K.R. performed most of the molecular analysis in the RAMKO mice and helped write the paper; D.F. collaborated on the inorganic staining and analysis; S.L. collaborated on the tissue dissection; L.A.T collaborated on the experimental design and supervised the project and M.A.R. designed the experiments, supervised the entire project and wrote the paper. All authors contributed and commented on the manuscript.

**ACKNOWLEDGMENTS** We thank F. Olivieri and late M. Beer for technical assistance. This work was supported by the Cantons of Basel-Stadt and Basel-Land, grants from the Swiss National Science Foundation and the Swiss Foundation for Research on Muscle Disease.

## REFERENCES

- Badin PM, Langin D, Moro C (2013) Dynamics of skeletal muscle lipid pools. *Trends Endocrinol Metab* **24**: 607-615
- Bentzinger CF, Lin S, Romanino K, Castets P, Guridi M, Summermatter S, Handschin C, Tintignac LA, Hall MN, Ruegg MA (2013) Differential response of skeletal muscles to mTORC1 signaling during atrophy and hypertrophy. *Skelet Muscle* **3**: 6
- Bentzinger CF, Romanino K, Cloetta D, Lin S, Mascarenhas JB, Oliveri F, Xia J, Casanova E, Costa CF, Brink M, Zorzato F, Hall MN, Ruegg MA (2008) Skeletal muscle-specific ablation of raptor, but not of rictor, causes metabolic changes and results in muscle dystrophy. *Cell Metab* **8**: 411-424
- Cartee GD (2015) Roles of TBC1D1 and TBC1D4 in insulin- and exercise-stimulated glucose transport of skeletal muscle. *Diabetologia* **58**: 19-30
- Castets P, Lin S, Rion N, Di Fulvio S, Romanino K, Guridi M, Frank S, Tintignac LA, Sinnreich M, Ruegg MA (2013) Sustained activation of mTORC1 in skeletal muscle inhibits constitutive and starvation-induced autophagy and causes a severe, late-onset myopathy. *Cell Metab* **17**: 731-744
- Cruz Guzman Odel R, Chavez Garcia AL, Rodriguez-Cruz M (2012) Muscular dystrophies at different ages: metabolic and endocrine alterations. *Int J Endocrinol* **2012**: 485376
- Cunningham JT, Rodgers JT, Arlow DH, Vazquez F, Mootha VK, Puigserver P (2007) mTOR controls mitochondrial oxidative function through a YY1-PGC-1 $\alpha$  transcriptional complex. *Nature* **450**: 736-740
- DeFronzo RA, Tripathy D (2009) Skeletal muscle insulin resistance is the primary defect in type 2 diabetes. *Diabetes Care* **32 Suppl 2**: S157-163
- Even PC, Nadkarni NA (2012) Indirect calorimetry in laboratory mice and rats: principles, practical considerations, interpretation and perspectives. *Am J Physiol Regul Integr Comp Physiol* **303**: R459-476
- Fraenkel M, Ketzinel-Gilad M, Ariav Y, Pappo O, Karaca M, Castel J, Berthault MF, Magnan C, Cerasi E, Kaiser N, Leibowitz G (2008) mTOR inhibition by rapamycin prevents beta-cell adaptation to hyperglycemia and exacerbates the metabolic state in type 2 diabetes. *Diabetes* **57**: 945-957
- Guridi M, Tintignac LA, Lin S, Kupr B, Castets P, Ruegg MA (2015) Activation of mTORC1 in skeletal muscle regulates whole-body metabolism through FGF21. *Sci Signal* **8**: ra113

Houde VP, Brule S, Festuccia WT, Blanchard PG, Bellmann K, Deshaies Y, Marette A (2010) Chronic rapamycin treatment causes glucose intolerance and hyperlipidemia by upregulating hepatic gluconeogenesis and impairing lipid deposition in adipose tissue. *Diabetes* **59**: 1338-1348

Khamzina L, Veilleux A, Bergeron S, Marette A (2005) Increased activation of the mammalian target of rapamycin pathway in liver and skeletal muscle of obese rats: possible involvement in obesity-linked insulin resistance. *Endocrinology* **146**: 1473-1481

Kwiatkowski DJ, Zhang H, Bandura JL, Heiberger KM, Glogauer M, el-Hashemite N, Onda H (2002) A mouse model of TSC1 reveals sex-dependent lethality from liver hemangiomas, and up-regulation of p70S6 kinase activity in Tsc1 null cells. *Hum Mol Genet* **11**: 525-534

Lamming DW, Sabatini DM (2013) A Central role for mTOR in lipid homeostasis. *Cell Metab* **18**: 465-469

Lamming DW, Ye L, Katajisto P, Goncalves MD, Saitoh M, Stevens DM, Davis JG, Salmon AB, Richardson A, Ahima RS, Guertin DA, Sabatini DM, Baur JA (2012) Rapamycin-induced insulin resistance is mediated by mTORC2 loss and uncoupled from longevity. *Science* **335**: 1638-1643

Laplante M, Sabatini DM (2012) mTOR Signaling in Growth Control and Disease. *Cell* **149**: 274-293

Li S, Brown MS, Goldstein JL (2010) Bifurcation of insulin signaling pathway in rat liver: mTORC1 required for stimulation of lipogenesis, but not inhibition of gluconeogenesis. *Proc Natl Acad Sci U S A* **107**: 3441-3446

McGee SL, van Denderen BJ, Howlett KF, Mollica J, Schertzer JD, Kemp BE, Hargreaves M (2008) AMP-activated protein kinase regulates GLUT4 transcription by phosphorylating histone deacetylase 5. *Diabetes* **57**: 860-867

Oh RC, Husted TR (2011) Causes and evaluation of mildly elevated liver transaminase levels. *Am Fam Physician* **84**: 1003-1008

Osborn O, Olefsky JM (2012) The cellular and signaling networks linking the immune system and metabolism in disease. *Nat Med* **18**: 363-374

Peterson TR, Sengupta SS, Harris TE, Carmack AE, Kang SA, Balderas E, Guertin DA, Madden KL, Carpenter AE, Finck BN, Sabatini DM (2011) mTOR complex 1 regulates lipin 1 localization to control the SREBP pathway. *Cell* **146**: 408-420

Polak P, Cybulski N, Feige JN, Auwerx J, Ruegg MA, Hall MN (2008a) Adipose-specific knockout of raptor results in lean mice with enhanced mitochondrial respiration. *Cell Metab* **8**: 399-410

Polak P, Cybulski N, Feige JN, Auwerx J, Ruegg MA, Hall MN (2008b) Adipose-specific knockout of raptor results in lean mice with enhanced mitochondrial respiration. *Cell Metab* **8**: 399-410

Polak P, Hall MN (2009) mTOR and the control of whole body metabolism. *Curr Opin Cell Biol* **21**: 209-218

Rodriguez-Cruz M, Sanchez R, Escobar RE, Cruz-Guzman Odel R, Lopez-Alarcon M, Bernabe Garcia M, Coral-Vazquez R, Matute G, Velazquez Wong AC (2015) Evidence of Insulin Resistance and Other Metabolic Alterations in Boys with Duchenne or Becker Muscular Dystrophy. *Int J Endocrinol* **2015**: 867273

Romanino K, Mazelin L, Albert V, Conjard-Duplany A, Lin S, Bentzinger CF, Handschin C, Puigserver P, Zorzato F, Schaeffer L, Gangloff YG, Ruegg MA (2011) Myopathy caused by mammalian target of rapamycin complex 1 (mTORC1) inactivation is not reversed by restoring mitochondrial function. *Proc Natl Acad Sci U S A* **108**: 20808-20813

Salvado L, Palomer X, Barroso E, Vazquez-Carrera M (2015) Targeting endoplasmic reticulum stress in insulin resistance. *Trends Endocrinol Metab* **26**: 438-448

Sarbassov DD, Ali SM, Sengupta S, Sheen JH, Hsu PP, Bagley AF, Markhard AL, Sabatini DM (2006) Prolonged rapamycin treatment inhibits mTORC2 assembly and Akt/PKB. *Mol Cell* **22**: 159-168

Savkur RS, Philips AV, Cooper TA (2001) Aberrant regulation of insulin receptor alternative splicing is associated with insulin resistance in myotonic dystrophy. *Nat Genet* **29**: 40-47

Schultze SM, Hemmings BA, Niessen M, Tschopp O (2012) PI3K/AKT, MAPK and AMPK signalling: protein kinases in glucose homeostasis. *Expert Rev Mol Med* **14**: e1

Selman C, Tullet JM, Wieser D, Irvine E, Lingard SJ, Choudhury AI, Claret M, Al-Qassab H, Carmignac D, Ramadani F, Woods A, Robinson IC, Schuster E, Batterham RL, Kozma SC, Thomas G, Carling D, Okkenhaug K, Thornton JM, Partridge L, Gems D, Withers DJ (2009) Ribosomal protein S6 kinase 1 signaling regulates mammalian life span. *Science* **326**: 140-144

Tang H, Macpherson P, Marvin M, Meadows E, Klein WH, Yang XJ, Goldman D (2009) A histone deacetylase 4/myogenin positive feedback loop coordinates denervation-dependent gene induction and suppression. *Mol Biol Cell* **20**: 1120-1131

Tintignac LA, Brenner HR, Ruegg MA (2015) Mechanisms Regulating Neuromuscular Junction Development and Function and Causes of Muscle Wasting. *Physiol Rev* **95**: 809-852

Torres PA, Helmstetter JA, Kaye AM, Kaye AD (2015) Rhabdomyolysis: pathogenesis, diagnosis, and treatment. *Ochsner J* **15**: 58-69

Um SH, Frigerio F, Watanabe M, Picard F, Joaquin M, Sticker M, Fumagalli S, Allegrini PR, Kozma SC, Auwerx J, Thomas G (2004) Absence of S6K1 protects against age- and diet-induced obesity while enhancing insulin sensitivity. *Nature* **431**: 200-205

Winzell MS, Ahren B (2004) The high-fat diet-fed mouse - A model for studying mechanisms and treatment of impaired glucose tolerance and type 2 diabetes. *Diabetes* **53**: S215-S219

Woo D (1995) Apoptosis and loss of renal tissue in polycystic kidney diseases. *N Engl J Med* **333**: 18-25

Wullschlegel S, Loewith R, Hall MN (2006) TOR signaling in growth and metabolism. *Cell* **124**: 471-484

Yecies JL, Zhang HH, Menon S, Liu S, Yecies D, Lipovsky AI, Gorgun C, Kwiatkowski DJ, Hotamisligil GS, Lee CH, Manning BD (2011) Akt stimulates hepatic SREBP1c and lipogenesis through parallel mTORC1-dependent and independent pathways. *Cell Metab* **14**: 21-32

## ADDITIONAL FILES

Additional files include 5 figures in .pdf format and 2 additional tables in .doc format.

**Additional file 1: Figure S1. Expression of *Actb* is not altered between RAMKO and control mice.** (A) *Actb* (encoding  $\beta$ -actin) expression in muscle, liver, WAT and BAT of control (n= 5) and RAMKO mice (n= 5). (B) List of antibodies used.

**Additional file 2: Table S1. List of primers used.**

**Additional file 3: Figure S2. Metabolism of female TSCmKO and RAMKO mice.** (A) Body weight is lower in chow-fed female TSCmKO (n= 11) mice at 10 weeks of age compared to female RAMKO (n= 8) and control (Ctrl) mice (n= 10). (B) - (C) Lean mass (B) is lower in chow-fed female RAMKO mice (n= 11) compared to TSCmKO (n= 8) and control (n= 13) mice, while fat mass (C) is lower in female TSCmKO mice (n= 4) when compared to RAMKO (n= 4) and control (Ctrl) mice at 10 weeks of age (n= 6). (D) Plasma glucose levels are lower in 10-week-old chow-fed female TSCmKO mice (n= 7) while they are unchanged in 10-week-old female RAMKO mice (n= 6) when compared to control (Ctrl) mice (n= 13). (E) - (F) Fat (E) and lean mass (F) are lower in male RAMKO (n= 4) mice on a HFD compared to control (Ctrl) littermates (n= 6). (G) Plasma glucose levels are lower in male RAMKO (n= 4) mice on a HFD when compared to control (Ctrl) littermates (n= 6).

**Additional file 4: Figure S3. RAMKO mice do not show changes in other organs.** (A) Glycogen amount is increased in *gastrocnemius* muscle of 10-week-old TSCmKO mice (n= 3). (B) Western blot analysis of liver from 10-week-old TSCmKO and control (Ctrl) mice are shown for the indicated phospho (P)- proteins (n= 4). Mice were intraperitoneally injected with insulin (+; TSC-Insulin) or not (-). Protein expression is normalized to eEF2. (C) - (D) RAMKO mice do not show changes in *Ucp2* expression in liver and WAT upon starvation and re-feeding (C), or *Ucp1* and *Ucp2* in BAT (D) at 12 weeks of age when compared to control mice (n= 5). (E) - (F) RAMKO mice show no changes in liver expression of genes involved in lipid (E) and glucose (F) metabolism upon re-feeding (n= 5).

**Additional file 5: Figure S4. ATP levels in RAmKO muscle.** ATP content in soleus muscle of RAmKO mice is the same as in controls at 12 weeks of age (n= 5).

**Additional file 6: Figure S5. Body composition in myopathic TSCmKO and RAmKO mice.** (A) Body weight is lower in 40-week-old female TSCmKO (n= 9) mice when compared to control (Ctrl) littermates (n= 11), whereas it is unchanged in 20-week-old female RAmKO mice (n= 4). (B) - (C) Both lean mass (B) and fat mass (C) are lower in female TSCmKO (n= 10) and RAmKO (n= 4) mice at 40 and 20 weeks of age, respectively, when compared to control (Ctrl) littermates (n= 10). (D) Kidneys in TSCmKO mice appear polycystic at the age of 40 weeks. Cysts are indicated by arrows.

**Additional file 7: Table S2. RAmKO blood analysis.**



## **LIST OF ABBREVIATIONS USED**

**Akt/PKB:** Protein kinase B

**ALT:** Alanine transaminase

**AST:** Aspartate transaminase

**ATP:** Adenosine triphosphate

**BAT:** Brown adipose tissue

**FGF21:** Fibroblast growth factor 21

**GLUT4:** Glucose transporter 4

**GTT:** Glucose tolerance test

**HDAC:** Histone deacetylase

**HFD:** High-fat diet

**IP:** Intra-peritoneal

**ITT:** Insulin tolerance test

**LDH:** Lactate dehydrogenase

**mTORC1:** Mammalian target of rapamycin complex 1

**PPARG:** Peroxisome proliferator activated receptor gamma

**RAmKO:** Raptor muscle knock-out

**SREBP1:** Sterol regulatory element binding protein 1

**TA:** Tibialis anterior

**TBC1D1/TBC1D4:** TBC1 domain family member 1/4

**TSC1:** Tuberous sclerosis complex 1

**TSCmKO:** TSC1 muscle knock-out

**UCP:** Uncoupling protein

**VCO<sub>2</sub>:** Carbon dioxide volume

**VO<sub>2</sub>:** Oxygen volume

**WAT:** White adipose tissue

## Figure 1

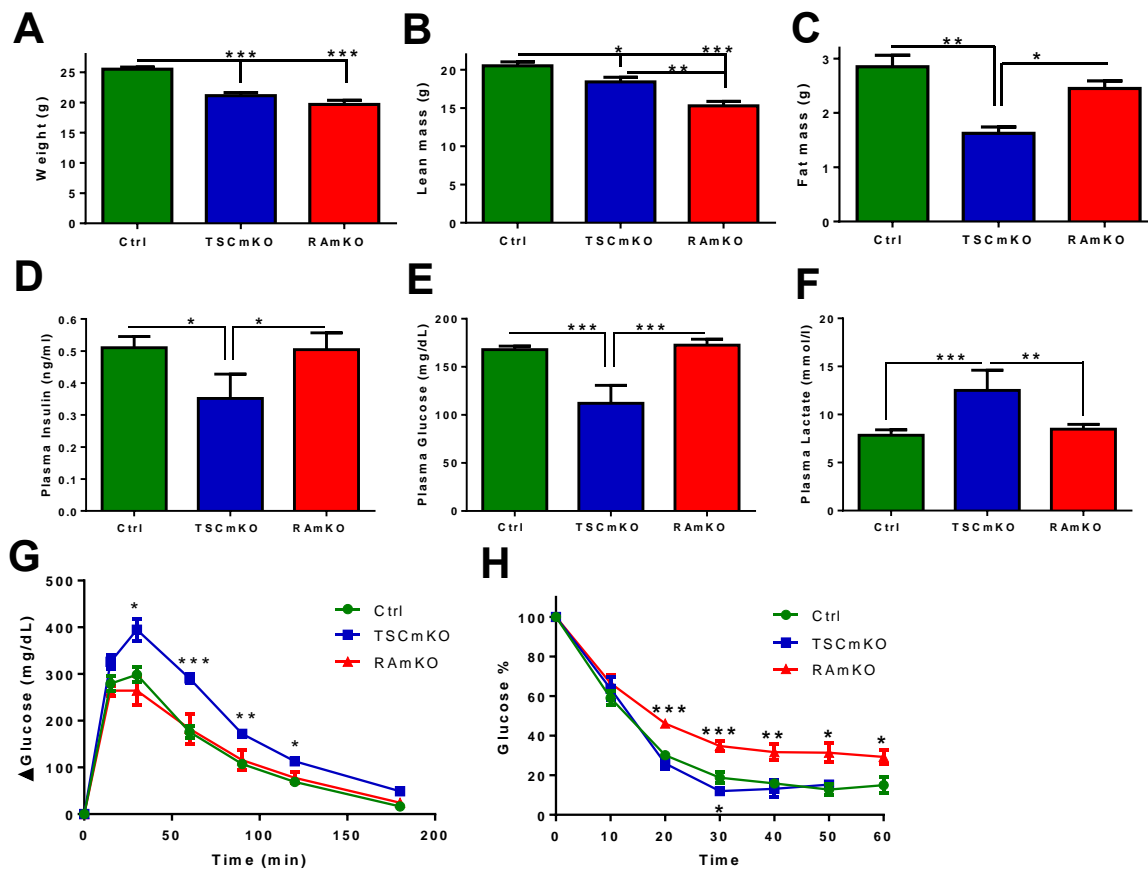


**Figure 1. Alterations of mTORC1 signaling in skeletal muscle affects whole-body metabolism**

(A) Body weight is lower in TSCmKO (n= 10) and RAmKO (n= 17) mice at 10 weeks of age when compared to control (Ctrl) mice (n= 14).

(B) - (C) Lean mass (B) is lower in TSCmKO (n= 13) and RAmKO (n= 16) mice while fat mass (C) is only decreased in TSCmKO mice (n= 6) when compared to control (Ctrl) mice at 10 weeks of age (n= 21).

(D) - (E) Plasma insulin levels (D) and glucose levels (E) are decreased in 10-week-old TSCmKO mice (n= 12) while they are unchanged in 10-week-old RAmKO mice (n= 6) when compared to control (Ctrl) mice (n= 10).

(F) Plasma lactate levels are increased in 10-week-old TSCmKO mice (n= 6) while they are unchanged in 10-week-old RAmKO mice (n= 6) when compared to control (Ctrl) mice (n= 12).

(G) - (H) TSCmKO (n= 6) but not RAmKO mice (n= 6) show glucose intolerance in a GTT (G) while RAmKO (n= 6) but not TSCmKO mice (n= 6) show insulin resistance in an ITT (H) at 10 weeks of age when compared to control (Ctrl) mice (n= 10).

Data presented are all from male mice of the indicated genotypes. Data represent mean  $\pm$  SEM. \* $p < 0.05$ , \*\* $p < 0.01$ , \*\*\* $p < 0.001$ .

**Figure 2**

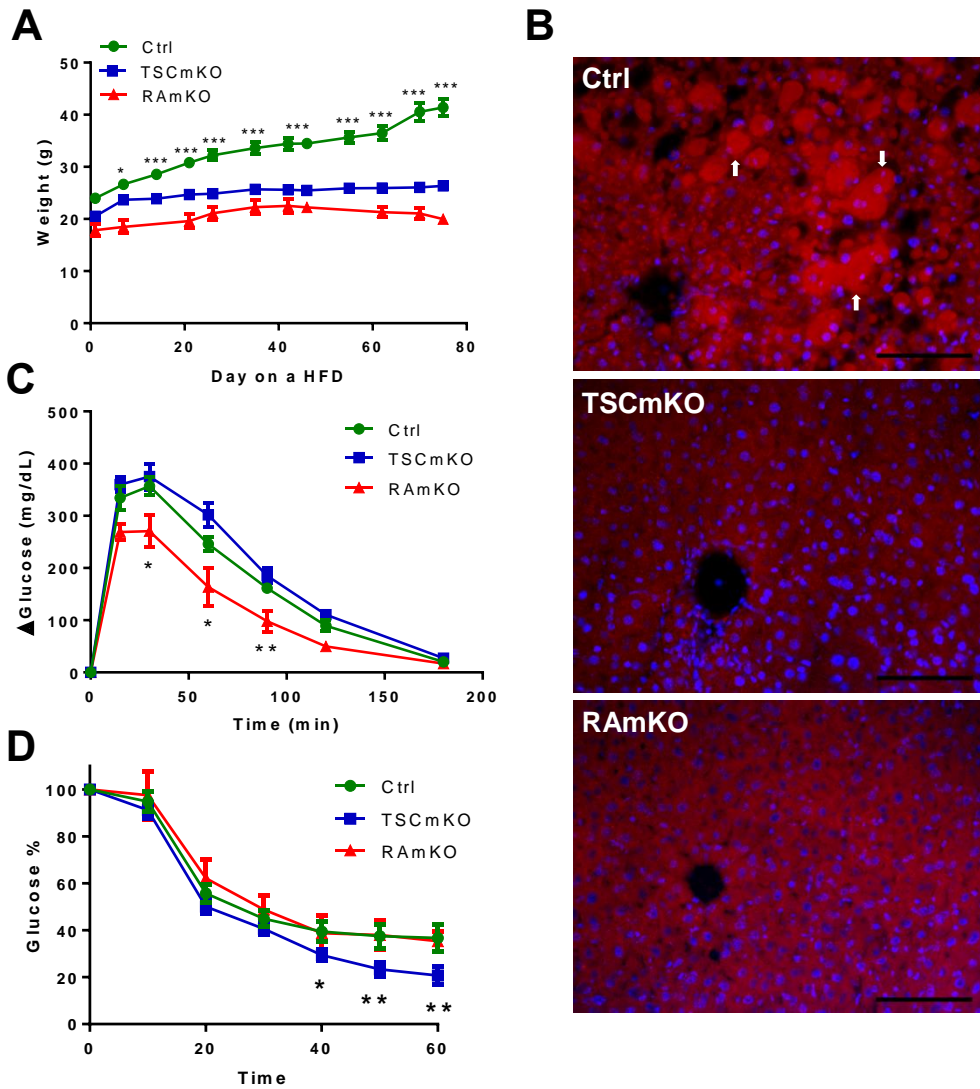


**Figure 2. TSCmKO and RAmKO mice are both resistant to a high-fat diet**

(A) TSCmKO (n= 7) and RAmKO (n= 5) mice do not gain significant weight on a HFD when compared to control (Ctrl) mice (n= 12).

(B) TSCmKO and RAmKO mice are resistant to HFD-induced hepatic steatosis, shown by decreased lipid accumulation in Oil-Red O stained liver (n= 3). Arrows indicate oil red-stained lipids. Scale bar 100  $\mu$ m.

(C) 20-week-old RAmKO mice (n= 5) show an increased glucose tolerance on a GTT after a HFD when compared to TSCmKO (n= 6) and control (Ctrl) mice (n= 12).

(D) 20-week-old TSCmKO mice (n= 6) show increased insulin sensitivity on an ITT after a HFD when compared to RAmKO (n= 5) and control (Ctrl) mice (n= 12).

Data presented are all from male mice of the indicated genotypes. Data represent mean  $\pm$  SEM.

\*p<0.05, \*\*p<0.01, \*\*\*p<0.001.

**Figure 3**

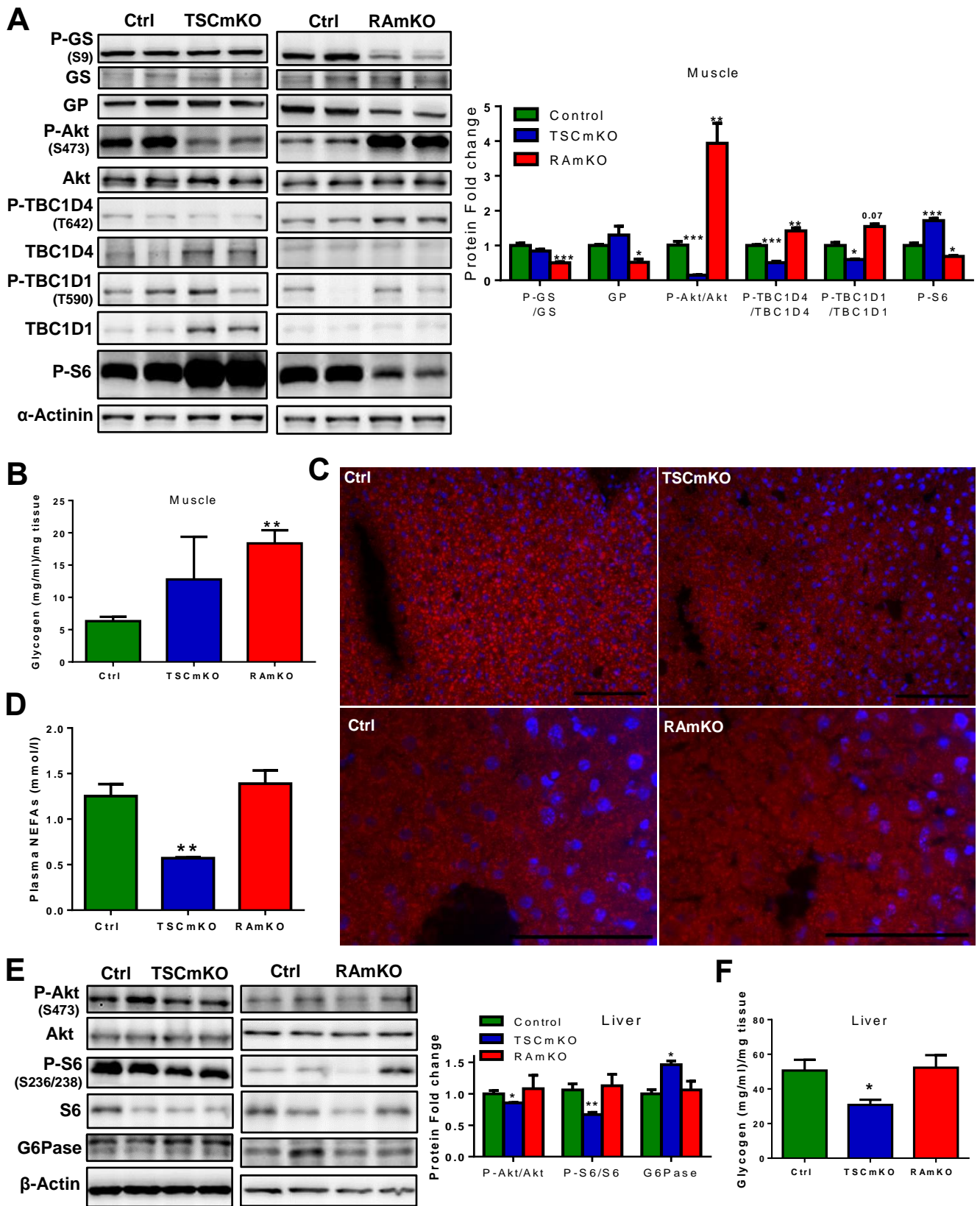


**Figure 3. TSCmKO but not RAmKO mice show changes in non-targeted metabolic organs**

(A) Immunoblots of TA muscle from 10-week-old TSCmKO, RAmKO and control (Ctrl) mice are shown for the indicated phospho (P)- and total proteins (n= 4). Protein expression is normalized to  $\alpha$ -actinin. Quantification of phosphorylation is shown relative to the total amount of each protein except for P-S6.

(B) Glycogen amount is increased in the *gastrocnemius* muscle of 12-week-old RAmKO mice (n= 5) compared to TSCmKO (n= 7) and control (Ctrl) mice (n= 13).

(C) Liver lipid content is decreased in 12-week-old TSCmKO as shown by oil red O staining, while it is unchanged in 10-week-old RAmKO mice (n= 3). Scale bar 100  $\mu$ m.

(D) The concentration of non-sterified fatty acids in the plasma is decreased in 10-week-old TSCmKO mice (n= 4) compared to RAmKO (n= 6) and control (Ctrl) mice (n= 8).

(E) Immunoblots of liver from 10-week-old TSCmKO, RAmKO and control (Ctrl) mice are shown for the indicated phospho (P)- and total proteins (n= 4). Protein expression is normalized to  $\beta$ -actin. Quantification of the phospho-protein is shown relative to the amount of each protein.

(F) Glycogen amount is decreased in liver from 12-week-old TSCmKO mice (n= 4) compared to RAmKO (n= 3) and control (Ctrl) mice (n= 6).

Data presented are all from male mice of the indicated genotypes. Data represent mean  $\pm$  SEM.

\*p<0.05, \*\*p<0.01, \*\*\*p<0.001.

**Figure 4**

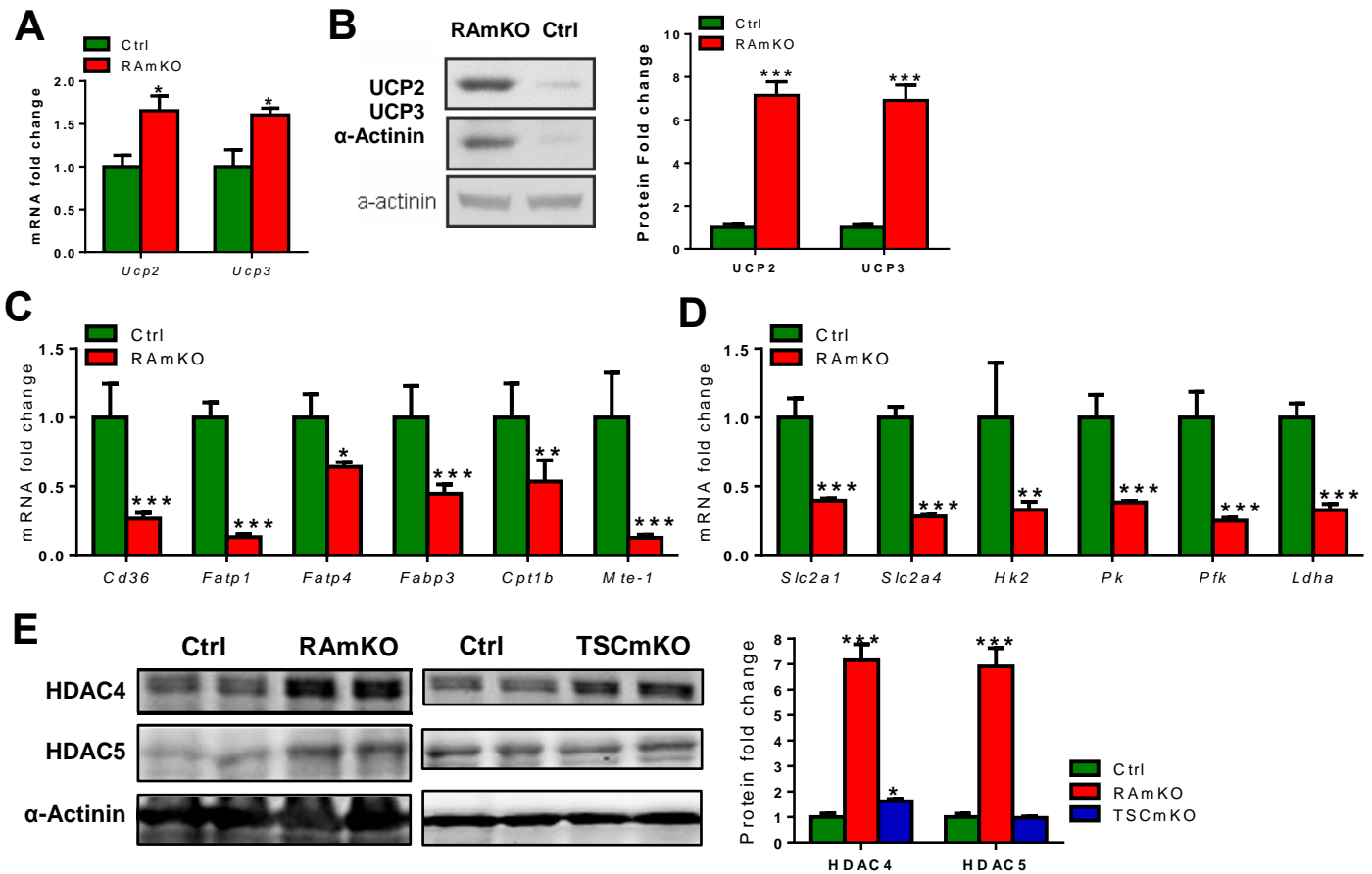


**Figure 4. Strong down-regulation of metabolic genes and increased levels of HDACs in RAMKO skeletal muscle**

(A) - (B) Increased expression (A) and protein levels (B) of UCP2 and UCP3 in skeletal muscle of 12-week-old RAMKO mice (n= 4) when compared to control (Ctrl) littermates (n= 4).

(C) - (D) Genes involved in fatty acid (C) and glucose metabolism (D) are expressed at lower levels in skeletal muscle of 12-week-old RAMKO mice (n= 4) when compared to control (Ctrl) littermates (n= 4).

(E) HDAC4 protein levels are higher in the TA muscles of RAMKO (n= 4) and TSCmKO (n= 4) at 12 weeks of age. In contrast, the levels of HDAC5 are only higher in RAMKO (n= 4) as shown by



immunoblot. Note: both bands of the HDAC proteins were included in the quantification.

Protein expression is normalized to  $\alpha$ -actinin.

Data presented are all from male mice of the indicated genotypes. Data represent mean  $\pm$  SEM.

\* $p < 0.05$ , \*\* $p < 0.01$ , \*\*\* $p < 0.001$ .

**Figure 5**

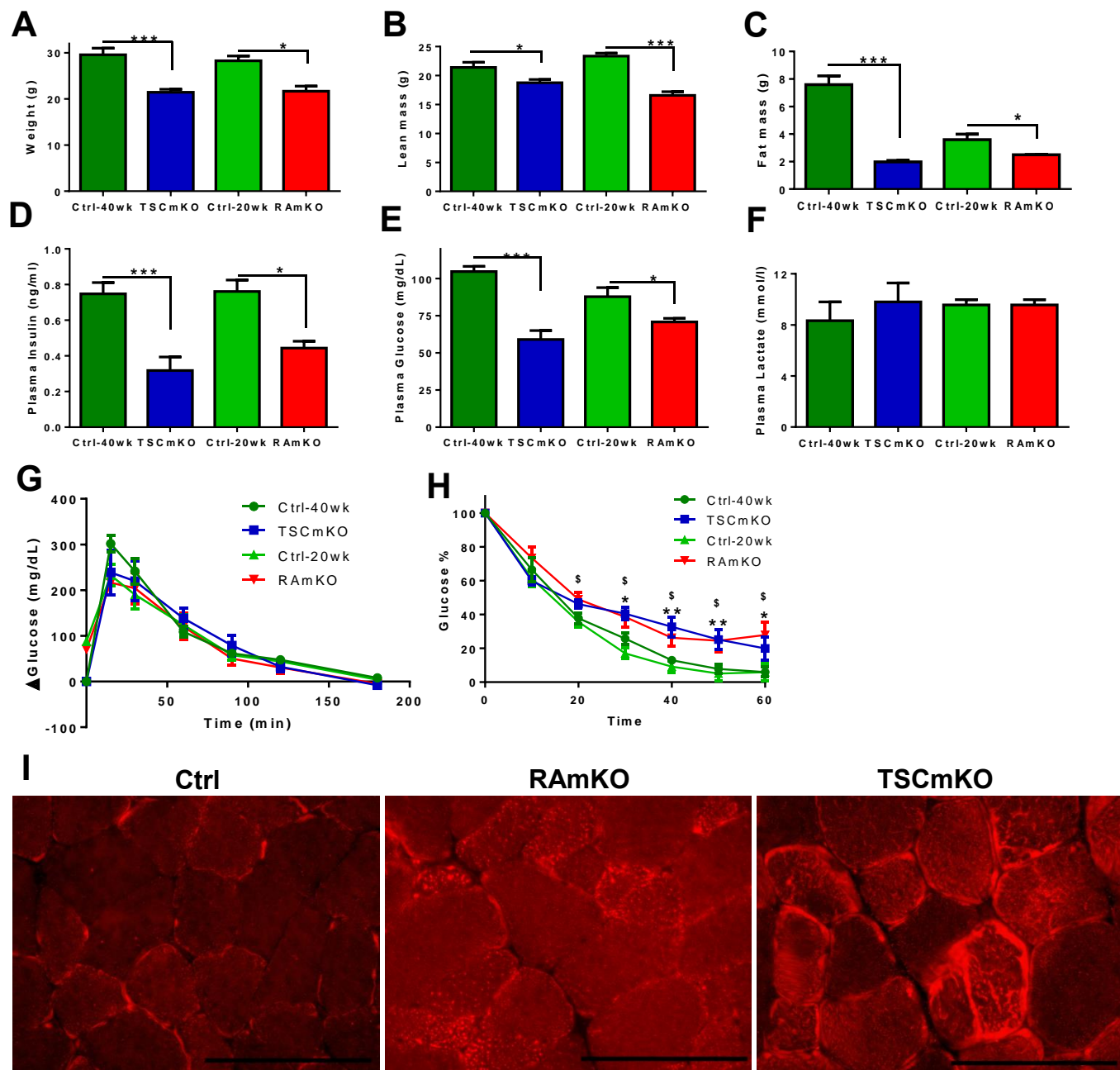


**Figure 5. Myopathy pre-dominates the metabolic changes at higher age**

(A) Body weight is decreased in both TSCmKO (n= 8) and RAmKO (n= 4) mice at 40 and 20 weeks of age, respectively, when compared to control (Ctrl) littermates (n= 9).

(B) - (C) Both lean mass (B) and fat mass (C) are decreased in TSCmKO (n= 10) and RAmKO (n= 8) mice at 40 and 20 weeks of age, respectively, when compared to control (Ctrl) littermates (n= 10).

(D) - (E) Both plasma insulin (D) and glucose (E) levels are decreased in TSCmKO (n= 8) and RAmKO (n= 5) mice at 40 and 20 weeks of age, respectively, when compared to control (Ctrl) littermates (n= 12).

(F) Plasma lactate levels are unchanged in 40-week-old TSCmKO (n= 3) and 20-week-old RAmKO (n= 3) mice compared to control (Ctrl) littermates (n= 6).

(G) - (H) TSCmKO (n= 5) and RAmKO mice (n= 5) show normal glucose tolerance (H) and develop insulin resistance (I) at 40 and 20 weeks of age, respectively, when compared to control (Ctrl) littermates (n= 10).

(I) Oil Red O staining of *gastrocnemius* muscle in 40-week-old TSCmKO and RamKO mice indicates increased lipid accumulation (n= 3). Scale bar, 100  $\mu$ m.

Data presented are all from male mice of the indicated genotypes. Data represent mean  $\pm$  SEM.

\*p<0.05, \*\*p<0.01, \*\*\*p<0.001.

**Figure 6**

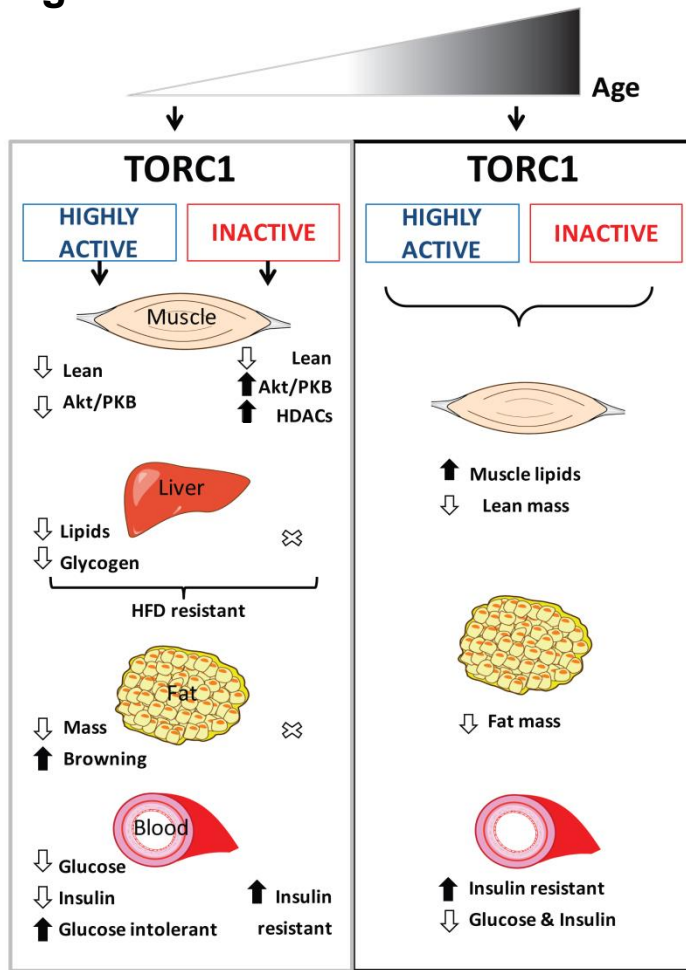


**Figure 6. Summary of metabolic changes induced by altered mTORC1 signaling in skeletal muscle of mice during aging.**

## TABLES

**Table 1. CLAMS analysis of 10-week-old TSCmKO and RAmKO mice**

	Ctrl	TSCmKO	P	Ctrl	RAmKO	P
Drink (ml/g/day)	0.31 ± 0.04	0.34 ± 0.06	ns	0.28 ± 0.04	0.30 ± 0.10	ns
Feed (g/g/day)	0.58 ± 0.17	0.58 ± 0.05	ns	0.42 ± 0.06	0.60 ± 0.14	*
CO2 (l/g/day)	0.37 ± 0.02	0.36 ± 0.03	ns	0.34 ± 0.04	0.41 ± 0.03	*
O2 (l/g/day)	0.39 ± 0.02	0.38 ± 0.02	ns	0.37 ± 0.05	0.44 ± 0.04	*
RER	0.94 ± 0.01	0.93 ± 0.03	ns	0.90 ± 0.01	0.91 ± 0.01	ns
Heat (kcal/h/g)	0.020 ± 0.00	0.019 ± 0.00	ns	0.026 ± 0.00	0.032 ± 0.00	*
X-amb (counts/h)	1078.9 ± 230.2	938.66 ± 314.8	ns	935.3 ± 357.3	938.7 ± 314.8	ns
Y-amb (counts/h)	187.9 ± 45.8	186.1 ± 51.6	ns	169.50 ± 93.17	140.19 ± 61.47	ns

Student's test \*p<0.05 (n= 6). Values represent mean ± SEM over a period of 3 days. Data presented are of male mice.

X-amb and Y-amb refer to ambulatory movement measured by laser counts in X and Y coordinates.

**Table 2. CLAMS analysis of TSCmKO and RAmKO mice on a HFD**

	Ctrl	TSCmKO	P	Ctrl	RAmKO	P
Drink (ml/g/day)	0.11 ± 0.04	0.16 ± 0.02	**	0.15 ± 0.03	0.15 ± 0.06	ns
Feed (g/g/day)	0.21 ± 0.06	0.36 ± 0.12	*	0.27 ± 0.02	0.29 ± 0.13	ns
CO2 (l/g/day)	0.24 ± 0.03	0.32 ± 0.02	***	0.29 ± 0.04	0.30 ± 0.04	ns
O2 (l/g/day)	0.31 ± 0.04	0.41 ± 0.02	**	0.36 ± 0.04	0.40 ± 0.06	ns
RER	0.75 ± 0.01	0.77 ± 0.01	**	0.79 ± 0.01	0.75 ± 0.01	**
Heat (kcal/h/g)	0.021 ± 0.00	0.028 ± 0.00	**	0.019 ± 0.00	0.020 ± 0.00	ns
X-amb (counts/h)	557.5 ± 122.4	616.9 ± 80.6	ns	601.2 ± 103.8	294.7 ± 71.1	**
Y-amb (counts/h)	55.5 ± 7.8	79.1 ± 25.1	0.05	49.4 ± 10.5	42.3 ± 15.9	ns

Student's test \*p<0.05, \*\*p<0.01, \*\*\*p<0.001 (n= 6). Values represent mean ± SEM over a period of 4 days. Data presented are of male mice.

X-amb and Y-amb refer to ambulatory movement measured by laser counts in X and Y coordinates.

**Table 3. CLAMS analysis of 40-week-old TSCmKO and 20-week-old RAmKO mice**

	Ctrl	TSCmKO	P	Ctrl	RAmKO	P
Drink (ml/g/day)	0.18 ± 0.05	0.22 ± 0.07	ns	0.23 ± 0.11	0.14 ± 0.03	ns
Feed (g/g/day)	0.31 ± 0.09	0.40 ± 0.12	ns	0.37 ± 0.19	0.44 ± 0.13	ns
CO2 (l/g/day)	0.28 ± 0.03	0.32 ± 0.04	*	0.25 ± 0.05	0.26 ± 0.02	ns
O2 (l/g/day)	0.32 ± 0.03	0.37 ± 0.04	*	0.28 ± 0.05	0.30 ± 0.03	ns
RER	0.85 ± 0.05	0.88 ± 0.05	ns	0.88 ± 0.04	0.87 ± 0.01	ns
Heat (kcal/h/g)	0.022 ± 0.00	0.028 ± 0.00	*	0.026 ± 0.00	0.028 ± 0.00	ns
X-amb (counts/h)	884.1 ± 316.4	578.1 ± 113.1	0.05	820.7 ± 247.7	856.6 ± 434.9	ns
Y-amb (counts/h)	117.1 ± 43.1	75.8 ± 19.5	0.09	100.2 ± 56.4	130.0 ± 48.8	ns

Student's test \*p<0.05 (n= 6). Values represent mean ± SEM over a period of 3 days. Data presented are of male mice.

X-amb and Y-amb refer to ambulatory movement measured by laser counts in X and Y coordinates.

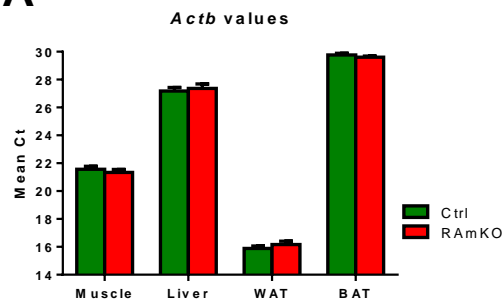
**Table 4. COBAS analysis of 40-week-old TSCmKO and 20-week old RAmKO plasma**

Group	ALTL (U/l)	ASTL (U/l)	Uric Acid (µmol/l)	Creatinine (µmol/l)	LDH (mmol/l)	TRIGL (mmol/l)	HDL-Chol (mmol/l)	LDL-Chol (mmol/l)	Chol (mmol/l)
Ctrl	40.5 ± 4.3	65.7 ± 10.5	220.8 ± 54.0	10.7 ± 1.7	256.5 ± 76.1	1.1 ± 0.2	2.5 ± 0.5	0.3 ± 0.0	2.7 ± 0.6
TSCmKO	85.4 ± 13.6	308.9 ± 53.3	244.1 ± 60.6	16.6 ± 0.6	567.2 ± 74.2	1.1 ± 0.2	2.26 ± 0.3	0.4 ± 0.0	2.6 ± 0.3
P	**	***	ns	***	***	ns	ns	**	ns
Ctrl	31.5 ± 4.7	60.3 ± 14.3	115.3 ± 24.6	16.1 ± 1.7	278.0 ± 99.3	0.7 ± 0.5	2.0 ± 0.3	0.2 ± 0.0	2.3 ± 0.3
RAmKO	38.4 ± 8.7	95.2 ± 12.8	118.8 ± 28.5	15.5 ± 1.9	412.4 ± 58.7	0.5 ± 0.4	1.9 ± 0.2	0.2 ± 0.0	2.3 ± 0.3
P	ns	*	ns	ns	ns	ns	ns	ns	ns

Values represent mean ± SEM of male mice. Student's test \*p<0.05, \*\*p<0.01, \*\*\*p<0.001 (n= 5).

## Additional file 1: Figure S1

**A**



**B**

The following antibodies were used for immunoblotting :  $\beta$ -actin (#4970), Phospho-GS Ser<sup>641</sup> (#3891), Phospho-Akt Ser<sup>473</sup> (#4058), Akt (#9272), Phospho-AS160 Thr<sup>642</sup> (#8881), AS160 (#2670), Phospho-TBC1D1 Thr<sup>590</sup> (#6927), TBC1D1 (#4629), eEF2 (#2232) and P-S6 Ser<sup>235/236</sup> (#2211) from Cell Signalling;  $\alpha$ -Actinin (7732) from Sigma; G6Pase (sc-134714) and HDAC-4 (sc-11418) from Santa Cruz; UCP2 (AB3040) and HDAC-5 (#07-045) from Millipore; and UCP3 (ab3477) from Abcam.

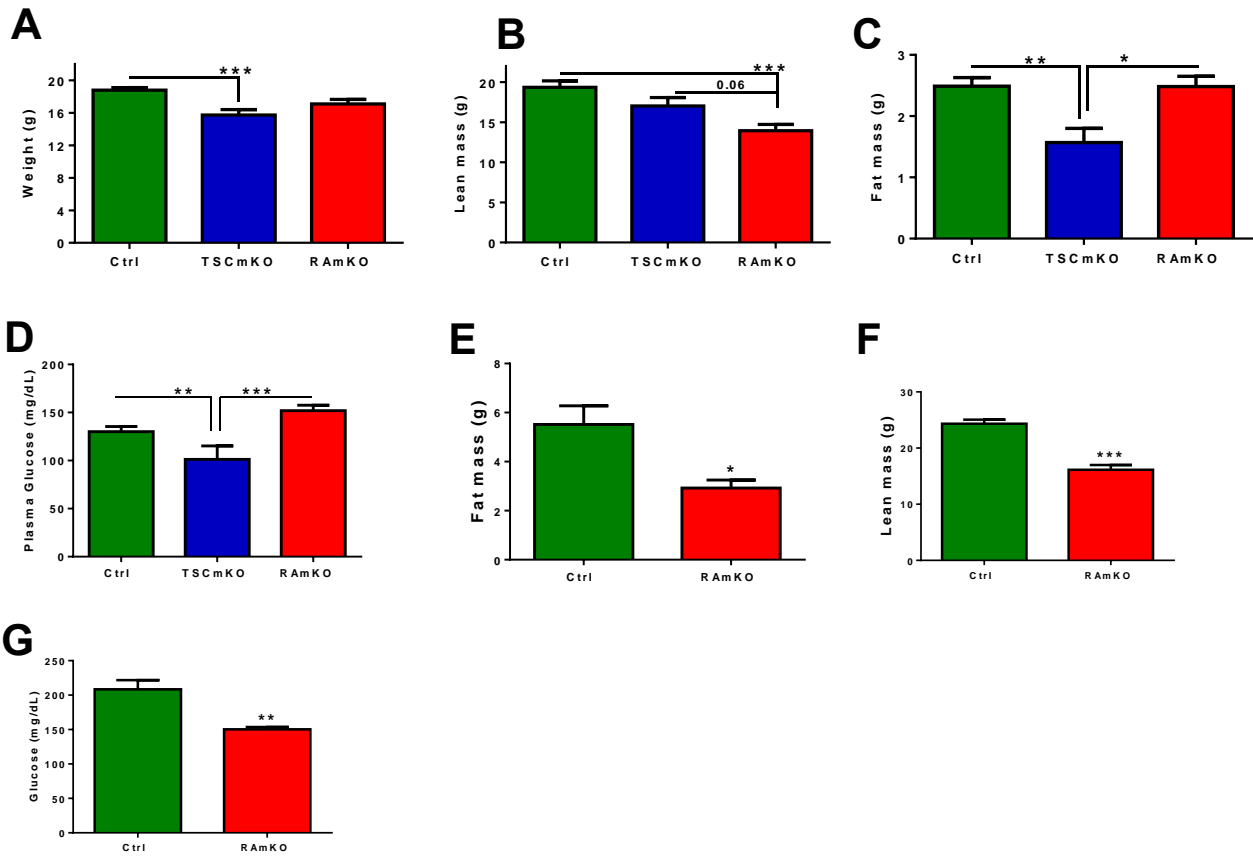
**Additional file 2.**

**Table S1. Primer list.**

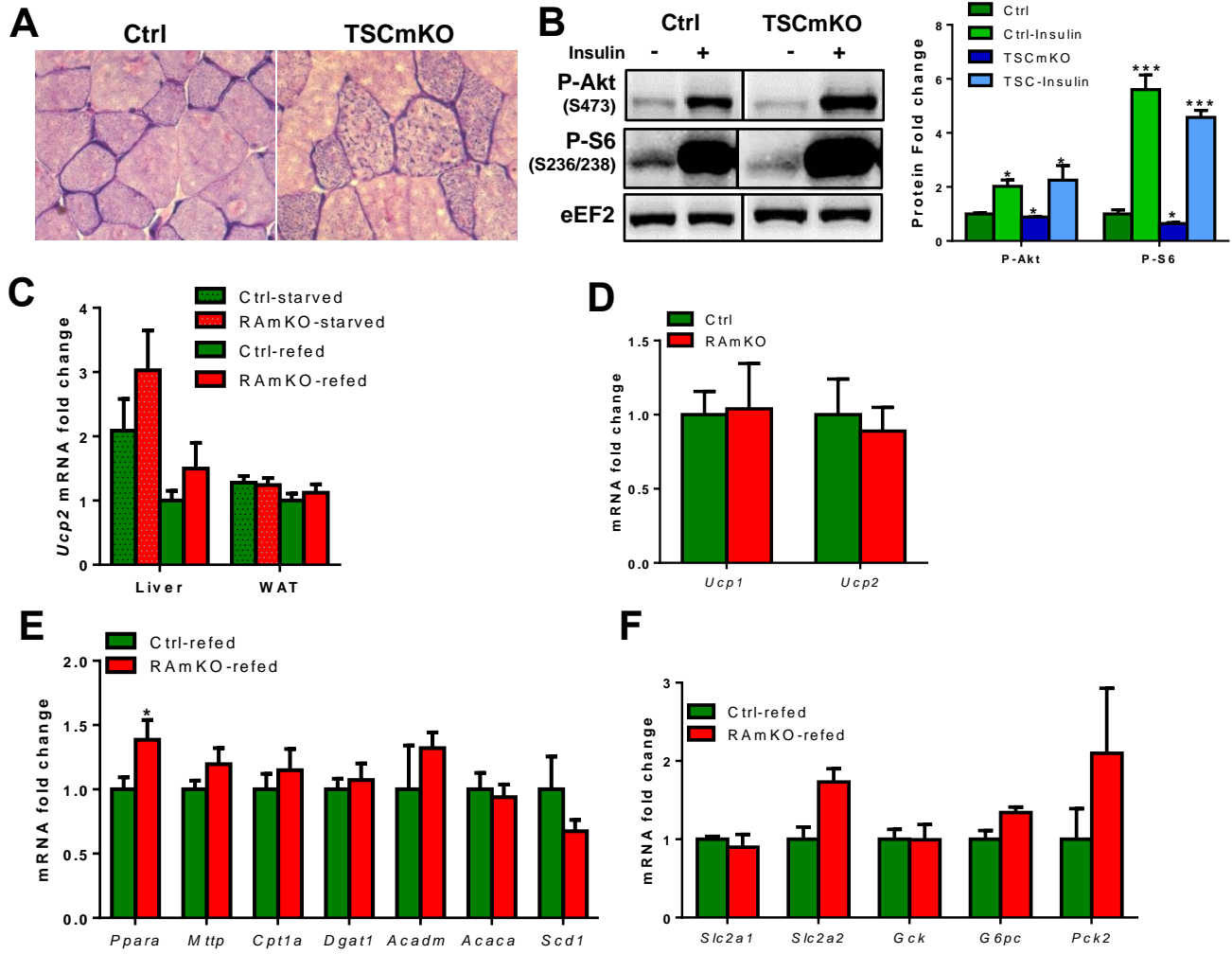
<i>Cd36</i>	fw: TGGCCTTACTTGGGATTGG	bw: CCAGTGTATATGTAGGCTCATCCA
<i>Sc127a1</i> (Fatp1)	fw: GGCTCCTGGAGCAGGAACA	bw: ACGGAAGTCCCAGAAACCA
<i>Slc27a4</i> (Fatp4)	fw: GGCTTCCCTGGTGTACTATGGAT	bw: ACGATGTTTCCTGCTGAGTGGTA
<i>Fabp3</i>	fw: CCCCTCAGCTCAGCACCA	bw: CAGAAAAATCCCAACCCAAGAAT
<i>Cpt1b</i>	fw: GGTCGATTGCATCCAGAGAT	bw: GACTCCGGTGGAGAAGATGA
<i>Acot2</i> (Mte1)	fw: TGGGAACACCATCTCTACAA	bw: CCACGACATCCAAGAGACCA
<i>Slc2a1</i> (Glut1)	fw: CGAGGGACAGCCGATGTG	bw: TGCCGACCCTCTTCTTTCAT
<i>Slc2a4</i> (Glut4)	fw: GATGAGAAACGGAAGTTGGAGAGA	bw: GCACCACTGCGATGATCAGA
<i>Hk2</i>	fw: CCCTGCCACCAGACGAAA	bw: GACTTGAACCCCTTAGTCCATGA
<i>Pkm</i>	fw: CGATCTGTGGAGATGCTGAA	bw: AATGGGATCAGATGCAAAGC
<i>Pfkm</i>	fw: CAGATCAGTGCCAACATAACCAA	bw: CGGGATGCAGAGCTCATCA
<i>Ldha</i>	fw: TGTCTCCAGCAAAGACTACTGT	bw: GACTGTACTTGACAATGTTGGGA
<i>Ucp2</i>	fw: ACCAAGGGCTCAGAGCATGCA	bw: TGGCTTTCAGGAGAGTATCTTTG
<i>Ucp3</i>	fw: ACTCCAGCGTCGCCATCAGGATTCT	bw: TAAACAGGTGAGACTCCAGCAACTT
<i>Actb</i> ( $\beta$ -actin)	fw: CAGCTTCTTTGCAGCTCCTT	bw: GCAGCGATATCGTCATCCA
<i>Scd1</i>	fw: CAAGCTGGAGTACGTCTGGA	bw: CAGAGCGCTGGTCATGTAGT
<i>Mttp</i>	fw: CGTCCACATACAGCCTTGAC	bw: CCACCTGACTACCATGAAGC
<i>Ucp1</i>	fw: GGCCTCTACGACTCAGTCCA	bw: TAAGCCGGCTGAGATCTTGT
<i>Dgat1</i>	fw: CATGCGTGATTATTGCATCC	bw: ACAGGTTGACATCCCGGTAG
<i>Acaca</i> (Acc1)	fw: ACCTTACTGCCATCCCATGTG	bw: GTGCCTGATGATCGCACGAACAAA
<i>Acadm</i> (Mcad)	fw: TCTCGAAGACGTCAGAGTGC	bw: TGCGACTGTAGGTCTGGTTC
<i>G6Pc</i>	fw: AGCGGAATGGGAGCAACTTG	bw: CAGAATGGGTCCACCTTGACAC
<i>Gck</i>	fw: CCCTGAGTGGCTTACAGTTC	bw: ACGGATGTGAGTGTTGAAGC
<i>Pck2</i> (Pepck)	fw: CATCCAGGCAATGTCATCGC	bw: GCATAACTAACCCGAAGGCAAG
<i>Slc2a2</i> (Glut2)	fw: GTCCAGAAAGCCCCAGATACC	bw: GTGACATCCTCAGTTCCTCTTAG
<i>Ppara</i>	fw: TGTTTGTGGCTGCTATAATTTGC	bw: GCAACTTCTCAATGTAGCCTATGTTT



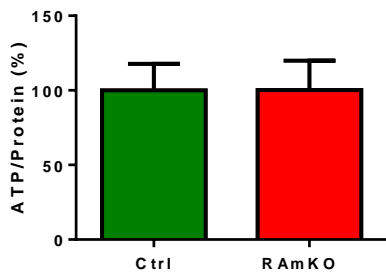
### Additional file 3: Figure S2



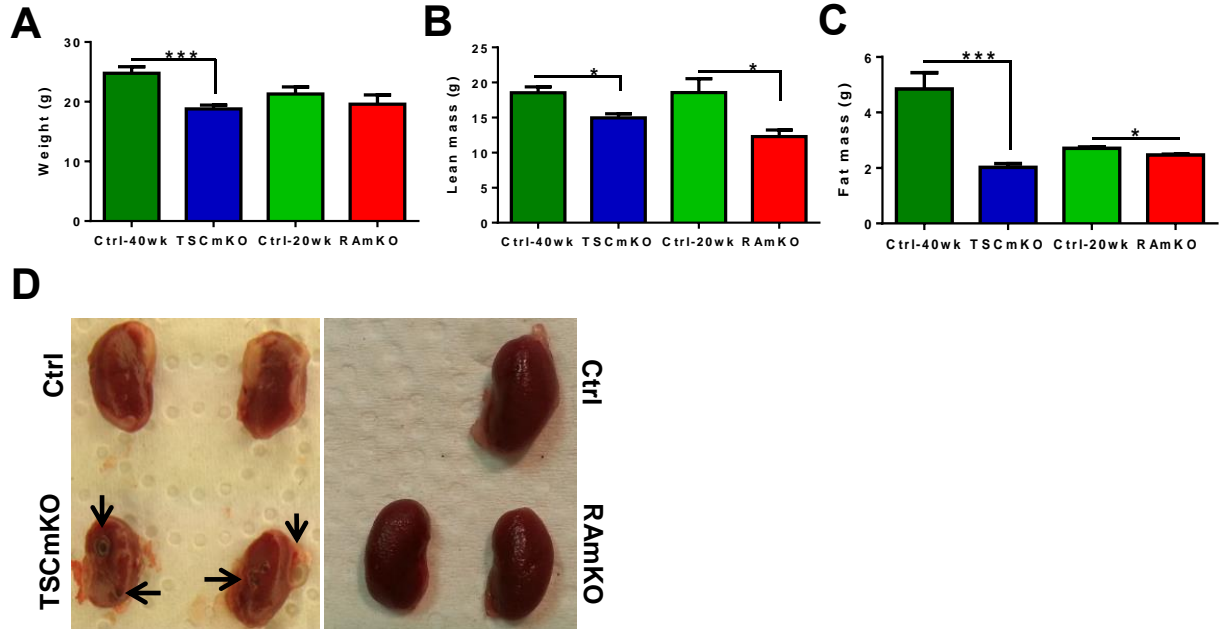
### Additional file 4: Figure S3



### Additional file 5: Figure S4



## Additional file 6: Figure S5



## Additional file 7.

**Table S2. RAmKO blood analysis**

	10-week-old			20-week-old		
	Ctrl	RAmKO	P	Ctrl	RAmKO	P
pO <sub>2</sub> [mm Hg]	82.8 ±16.3	97.3 ±17.1	ns	90.7 ±7.2	68.7 ±5.6	***
pCO <sub>2</sub> [mm Hg]	18.5 ±5.8	16.4 ±4.0	ns	18.45 ±2.3	32.8 ±8.2	**
pH	7.5 ±0.06	7.6 ±0.07	ns	7.5 ±0.07	7.4 ±0.05	*

Values represent mean ± SEM. Student's test \*p<0.05, \*\*p<0.01, \*\*\*p<0.001 (n= 4).

### 3.3. Creation and characterization of a new mouse model

#### FGF21 knock-out in skeletal muscle of the TSCmKO mice results in decreased survival

We were able to confirm with two different rescue experiments that muscle secreted FGF21 was responsible for most of the metabolic phenotype of TSCmKO mice. However, there was still another enigma to answer: was this stress-induced FGF21 a good myokine that helped compensate for the metabolic complications of a muscle myopathy? Was it helping with muscle survival? Or was its over-production actually contributing to the deterioration of the whole-body metabolism? Even more, could FGF21 or the consequent whole-body metabolic changes be somehow involved in the pathology of the late-onset myopathy developed by TSCmKO mice?

To address these questions, we generated a muscle specific FGF21 knock-out mouse model, by crossing FGF21 floxed mice, donated by Dr. David Mangelsdorf from University of Texas Southwestern Medical Center (generation of the mice detailed in (Potthoff et al, 2009)), with mice expressing Cre recombinase under the human skeletal actin (HSA) promoter, which knocked-out FGF21 specifically in skeletal muscle (Figure 1A). These mice, the FGF21mKO mice, were born at a normal Mendelian-ratio and were fertile. We designed primers outside the first and third exons of the *Fgf21* gene, outside the floxed sequence (Figure 1A), which allowed us to confirm by PCR the proper recombination of the *Fgf21* gene: in FGF21mKO muscle a small product would be amplified by PCR (approximately 200 bp), while the control mice would show a bigger amplification product (Figure 1B). We observed successful recombination in all muscles analyzed, with no recombination in liver or adipose tissue, while a partial recombination was present in the heart (Figure 1B). We also confirmed the correct elimination of *Fgf21* in skeletal muscle by a qPCR, which showed almost completely abolished expression of *Fgf21* in skeletal muscle (Figure 1C).

We then crossed the FGF21mKO with the TSCmKO mice, to knock-out FGF21 in the skeletal muscle of the TSCmKO mice, and created the double knock-out mouse line (DKO). This way, we would be able to distinguish the effect of muscle-secreted FGF21 upon stress (DKO) or basal (FGF21mKO) conditions. We confirmed elimination of the *Fgf21* gene by qPCR, which

showed significantly decreased expression in DKO muscle when compared to TSCmKO littermates (Figure 1D). DKO male and females were fertile, but were characteristically small and weak upon birth (Figure 1E), and had a 42% survival rate: out of 19 DKO mice born during one year, 11 were dead before reaching the first week of age and only 8 were able to reach adulthood. This would suggest that the initial post-natal induction of FGF21 is essential for the development of the TSCmKO mice. Surprisingly, even if 5-week-old DKO mice were smaller and lighter than their control and TSCmKO littermates, they progressed favorably and were significantly heavier than the TSCmKO littermates by 10 weeks of age (Figure 1F). On the other hand, 5-week-old FGF21mKO mice were already heavier than the control mice, and gained weight normally (Figure 1G). These results show that eliminating Fgf21 in skeletal muscle had aggravating consequences for the survival of TSCmKO mice, maybe due to its involvement in muscle development (Ribas et al, 2014). However, once they got over a possible critical stage, they were able to develop normally and even overcome weight issues seen before in TSCmKO mice.

### **Increased body weight, lean mass and plasma glucose levels are the physiological effects of muscle secreted FGF21**

Comparison of the FGF21mKO and DKO phenotypes would allow us to differentiate the effect of the over-secretion of FGF21 from muscle *versus* the basal FGF21 secretion on the whole-body metabolism. 10-week-old DKO mice had increased body weight when compared to TSCmKO littermates, which was almost normalized to control levels (Figure 2A). Likewise, 8-week-old FGF21mKO mice were heavier than their control littermates (Figure 2B). This increase in the body weight was most likely due to a significant increase in lean mass in both DKO (Figure 2C) and FGF21mKO mice (Figure 2D). Another recurrent feature of the TSCmKO phenotype that we hypothesized was a consequence of increased FGF21 was the decrease in plasma glucose levels. Accordingly, plasma glucose was significantly increased when we knocked-out muscle FGF21, both in DKO (Figure 2E) and FGF21mKO mice (Figure 2F). Interestingly, when we separated our data by sex groups, we could observe that plasma glucose was significantly increased in the female FGF21mKO mice (Figure 2G) while it only tended to higher amount in

male mice (Figure 2H). This sexual dimorphism could be the consequence of FGF21 acting on the hypothalamic-pituitary-ovarian axis (Owen et al, 2013), which could be lost in the FGF21mKO females. Blood FGF21 amount has been shown to be regulated by the liver upon starvation (Markan et al, 2014), but under stress conditions the muscle can increase the plasma FGF21 concentration (Keipert et al, 2014; Kim et al, 2013c). As a result, plasma FGF21 was normalized in DKO mice when compared to the increase shown by TSCmKO mice (Figure 2I). We also confirmed normalization of fed plasma FGF21 levels in DKO mice by a western blotting of immuno-depleted plasma (Figure 2J). However, under fed conditions FGF21 amount is very low and shows a high inter-individual variation (Angelin et al, 2012), so we starved FGF21mKO mice to measure the contribution of muscle to plasma FGF21. Plasma FGF21 tended to be lower in starved FGF21mKO mice (Figure 2K and 2L), which could account for the metabolic phenotype observed in these mice. However, when we starved the TSCmKO and DKO mice, plasma FGF21 levels seemed higher on both groups when compared to control mice (Figure 2M), which could account for a compensatory mechanism from the liver or another secretory organ. On the other hand, the decreased plasma IGF1 observed in the TSCmKO mice was not reversed in the DKO (Figure 2N), and the FGF21mKO mice showed no changes in their plasma IGF1 (Figure 2O). These results show that muscle secreted plasma FGF21 affects whole-body metabolism by increasing body weight, lean mass and plasma glucose levels, under basal or stress conditions.

### **Muscle FGF21 is involved in the fatty acid metabolism of skeletal muscle.**

We had previously shown that stress-secreted FGF21 from skeletal muscle had an impact on the whole-body metabolism, which was reversed when we knocked-out muscle FGF21 and normalized plasma FGF21 amount (Figure 2I). We next decided to check if muscle FGF21 could also affect the muscle itself. TSCmKO mice did not show any structural abnormalities in the muscle when compared to control littermates, as did the DKO muscles (Figure 3A). Likewise, we did not observe any problems in the structural integrity of FGF21mKO muscles (Figure 3B). TSCmKO mice were shown to have increased oxidative capacity (Bentzinger et al, 2013), which correlated with an increase in fatty acid oxidation (Guridi et al, 2015). In DKO mice, we could

still observe an increase in the oxidative capacity of the muscle when compared to control mice (Figure 3A), which would indicate that sustained mTORC1 activity is causing the changes in the oxidative capacity of muscle. On the other hand, FGF21mKO muscles showed an increased oxidative capacity when compared to control muscles, which correlated with a decreased lipid accumulation (Figure 3B). In parallel, the increase in the accumulation of intramyocellular lipids of TSCmKO muscle was reversed in the DKO muscle (Figure 3A). Beta-oxidation, a mitochondrial catabolic process, supplies the muscle of energy by oxidating fatty acids, thus the increased oxidative capacity of FGF21 depleted muscles likely caused an increased fatty acid oxidation and the consequent reduction in lipid content. These results suggest that FGF21 could regulate fatty acid metabolism in skeletal muscle.

#### **Differential effect of muscle secreted FGF21 on the whole-body metabolism upon mTORC1 activation or basal conditions**

We next decided to analyze the differences between the lack of basally secreted muscle FGF21 *versus* the lack of its over-secretion. Due to an increase in liver ketogenesis TSCmKO mice showed higher plasma  $\beta$ -ketone bodies, which we hypothesized was due to plasma FGF21 because they were normalized upon treatment with the FGF21 neutralizing antibody (Guridi et al, 2015). Accordingly, DKO mice showed a decrease in plasma  $\beta$ -ketone bodies (Figure 4A), while they were unchanged in FGF21mKO mice (Figure 4B). Another consequence of increased plasma FGF21, as seen in FGF21 transgenic mice (Inagaki et al, 2007) and TSCmKO mice is growth impairment and reduced body temperature. While tibia length was normalized in DKO mice (Figure 4C), it was unchanged in FGF21mKO mice (Figure 4D). Likewise, body temperature tended to increase in the DKO mice (Figure 4E) while it was normal in FGF21mKO mice (Figure 4F). In addition, while plasma insulin levels were significantly lower in TSCmKO mice when compared to control littermates, they were unchanged in DKO mice (Figure 4G). While increased plasma FGF21 might decrease insulin secretion, the lack of basally secreted muscle FGF21 did not change plasma insulin levels (Figure 4H). On the other hand, one of the most prominent features of TSCmKO mice we hypothesized as a consequence of increased FGF21 was the loss of fat mass, which was still significantly decreased in DKO mice (Figure 4I).

However, the lack of muscle FGF21 did cause a moderate but significant increase of fat mass in FGF21mKO mice (Figure 4J). These results would suggest that muscle secreted FGF21 can reduce whole-body fat mass, but the loss of adipose tissue in the TSCmKO mice could be aggravated by other consequences of increased muscle mTORC1 activity. Interestingly, muscle secreted FGF21 did not only have an effect on the global metabolism, but also affected the development of skeletal muscle (Figure 2G-2H). On the other hand, muscle force was not affected by eliminating FGF21 in skeletal muscle (Figure 4K-4N). Thus, these results suggest that consequences of muscle secreted FGF21 on the whole-body metabolism are different depending on the basal secretion or stress-induced over-secretion. For instance, changes in plasma insulin, ketone bodies, body temperature and growth could be caused by muscle FGF21 over-secretion, while they were not dependent on basal muscle FGF21 secretion. However, basal muscle FGF21 could cause changes on the fat mass, while further research is needed to determine if over-secretion of muscle FGF21 can contribute to the decrease of adipose tissue.

#### **Deletion of muscle FGF21 caused a diabetic phenotype**

FGF21 was discovered as an anti-obesity and anti-diabetic drug, and whole-body FGF21 knock-out mice showed increased gain in body weight and adiposity upon a ketogenic diet (Badman et al, 2009). Skeletal muscle FGF21 over-expression protected mice against diet induced obesity and promoted a lean phenotype (Keipert et al, 2014; Kim et al, 2013c), which corroborated the beneficial effects of FGF21 and pointed at skeletal muscle as being an important source of FGF21. Eliminating FGF21 in skeletal muscle caused an increase in body weight (Figure 2B), higher plasma glucose levels (Figure 2D) and increased fat mass (Figure 4J), which are characteristic traits of obesity induced type II diabetes. Diabetic patients often develop peripheral tissue insulin resistance and glucose intolerance due to increased adiposity (Kahn et al, 2006). While FGF21mKO mice had normal insulin sensitivity (Figure 5A), they showed a slight glucose intolerance (Figure 5B), which is another feature in diabetic and obese individuals. Interestingly, when we separated glucose tolerance by sex groups, female FGF21mKO mice showed significantly reduced glucose tolerance when compared to female control littermates (Figure 5C), which correlated with the previous observation of predominantly female



FGF21mKO mice showing increased plasma glucose levels (Figure 2D). We next tested if the glucose intolerance in FGF21mKO mice could be due to an insulin secretion problem, but the pancreas histology of FGF21mKO was normal compared to control mice (Figure 5D) and when stimulated with glucose FGF21mKO mice were able to increase plasma insulin levels the same way as control mice did (Figure 5E). On the other hand, glucose absorption into WAT and liver were normal in the FGF21mKO mice, while it tended to be reduced in skeletal muscle (Figure 5F), which could contribute to the glucose intolerance.

We next analyzed basal metabolism of FGF21mKO mice, and observed that female mice ate significantly less than their control littermates (Figure 5F), while water drinking was normal (Figure 5G). On the other hand, both male and female FGF21mKO mice were more active (Figure 5H-5J), while respiratory exchange ratio was unchanged (Figure 5K). FGF21mKO mice tended to show increased heat production (Figure 5L) and higher oxygen consumption (Figure 5M), while carbon dioxide volume was normal when compared to control mice (Figure 5N). The increased activity of FGF21mKO mice was likely causing this tendency to higher energy expenditure (Figure 5O). We also challenged the metabolism of the mice by feeding them a HFD for 12 weeks, and observed a similar increase in body weight in both groups (Figure 5P). In addition, WAT of FGF21mKO mice showed an increased *TNF $\alpha$*  expression, which would correlate with obesity inducing inflammation in the adipose tissue (Figure 5Q).

### **Eliminating muscle FGF21 in TSCmKO mice normalized browning and glucose absorption in WAT while it decreased ketolysis and altered fatty acid oxidation in skeletal muscle**

Many of the whole-body metabolic characteristics of TSCmKO were reverted when we knocked-out FGF21 in skeletal muscle. So we next analyzed the molecular changes in muscle, WAT and liver of DKO mice. ER stress was still high in DKO skeletal muscle, comparable to TSCmKO mice, as seen by increased expression of ER stress markers *Hspa5*, *Ddit3*, *Xbp1* and *Trib3* (Figure 6A). Expression of genes involved in ketogenesis, *Acat1* and *Hmgcs2*, were still significantly decreased in muscle of DKO mice (Figure 6B). On the other hand, while *Oxct1* was still increased, expression of ketolytic gene *Bdh1* was significantly decreased when compared to TSCmKO muscle (Figure 6B), which correlated with the decrease in plasma ketone bodies

(Figure 4A). In parallel, the expression of genes involved in fatty acid oxidation, such as *Ppargc1a*, *Fabp3* and *Ucp3* were significantly up-regulated in DKO muscle when compared to TSCmKO (Figure 6C), which could mean that an increase in fatty acid oxidation could cause the decreased accumulation of lipids in the muscle (Figure 3A) and contribute to the wasting of fat mass (Figure 4I). On the contrary, while FGF21 seemed to be involved in regulating fatty acid metabolism of skeletal muscle, its elimination had no effect on glucose metabolism, because *Glut1* glucose transporter and glucokinase remained significantly up-regulated in DKO muscle (Figure 6D). In addition, glycogen storage, most likely a consequence of increased *Glut1* expression, was still increased in DKO mice when compared to TSCmKO muscle (Figure 6E). On the other hand, while *Ppargc1a* was unchanged in DKO liver when compared to TSCmKO mice, glucokinase expression was increased in DKO liver (Figure 6F), correlating with the increased availability of glucose in their plasma. Increased phospho-S6 in DKO muscles indicated no changes in mTORC1 activity and Akt activation still remained low as in TSCmKO mice, while phospho-AMPK was normalized in DKO muscles to a control level (Figure 6G). We hypothesized that AMPK activity was higher in TSCmKO mice due to an energetic depletion of muscle and decreased ATP content, which was normalized when we depleted FGF21 in skeletal muscle (Figure 6H). On the other hand, expression of atrogenes *Murf1* and *Atg1*, involved in the increased proteasomal degradation in TSCmKO muscle (Bentzinger et al, 2013), was still up-regulated in DKO muscle, while  $\beta$ -Klotho, the essential co-receptor of FGF21, was significantly reduced (Figure 6D). Together, these results suggest that while muscle FGF21 does not affect ER stress, proteasomal degradation, ketogenesis or glucose metabolism, it has a role in regulating fatty acid metabolism of skeletal muscle.

The main effect of increased plasma FGF21 in TSCmKO mice was observed in WAT, as it showed increased expression of markers for adipose tissue browning and glucose transporters, correlating with the increased browning and glucose absorption into WAT. Interestingly, glucose transporters (*Glut1* and *Glut4*) were significantly down-regulated in the DKO WAT when compared to TSCmKO (Figure 6I), which would indicate that the decrease glucose absorption into WAT could cause the increase in plasma glucose levels observed in DKO mice (Figure 2C). In addition, expression of browning markers, *Ppargc1a*, *Cidea*, *Ucp1* and *Fabp3* were also

significantly down-regulated in WAT of DKO (Figure 6I), confirming the role of muscle secreted FGF21. Furthermore, similar to skeletal muscle, expression of both *Fgf21* and  *$\beta$ -Klotho* was significantly down-regulated in WAT of DKO mice (Figure 6I), which would confirm a possible feed-forward effect of FGF21 signaling in the affected tissue. Thus, these results demonstrate that the changes observed in TSCmKO WAT were due to the effect of muscle-secreted FGF21, because markers for browning and glucose absorption are normalized in this tissue.

### **Potential involvement of muscle FGF21 in the development of the myopathy in TSCmKO mice**

We next decided to analyze the progression of the metabolic and muscle phenotype of DKO mice with age. 10-month-old DKO female mice tended to weight more than TSCmKO littermates, which were significantly lighter than the control mice (Figure 7A). Likewise, 10-month-old FGF21mKO female mice were significantly heavier than the control mice (Figure 7A). This increase in body weight was not due to changes in fat mass, which was significantly lower in TSCmKO and DKO mice (Figure 7B), but a consequence of a significant increase in lean mass observed both in 10-month-old DKO female mice compared to TSCmKO littermates, and in FGF21mKO mice when compared to control littermates (Figure 7C). In addition, tibia length was normalized in 10-month old DKO mice (Figure 7D), while it remained unchanged in FGF21mKO mice (data not shown). Plasma glucose and insulin were normalized in younger DKO mice (Figure 2C and 4G), but both glucose (Figure 7E) and insulin (Figure 7F) remained low in 10-month-old DKO mice when compared to control littermates.

TSCmKO mice develop a late-onset myopathy with age, characterized by changes in fiber size, vacuoles and swollen nuclei (Castets et al, 2013). While fiber size distribution was still affected, we did not observe any vacuoles or swollen nuclei in the skeletal muscle of 10-month-old female DKO mice (Figure 7G). In addition, while oxidative capacity was still increased, intramyocellular lipid content was normalized in DKO skeletal muscle (Figure 7G). These results, similar to the observations in young DKO mice, would suggest that FGF21 could regulate fatty acid metabolism in muscle, and that eliminating muscle FGF21 is favorable for the outcome of TSCmKO skeletal muscle development.

**Figure 1**

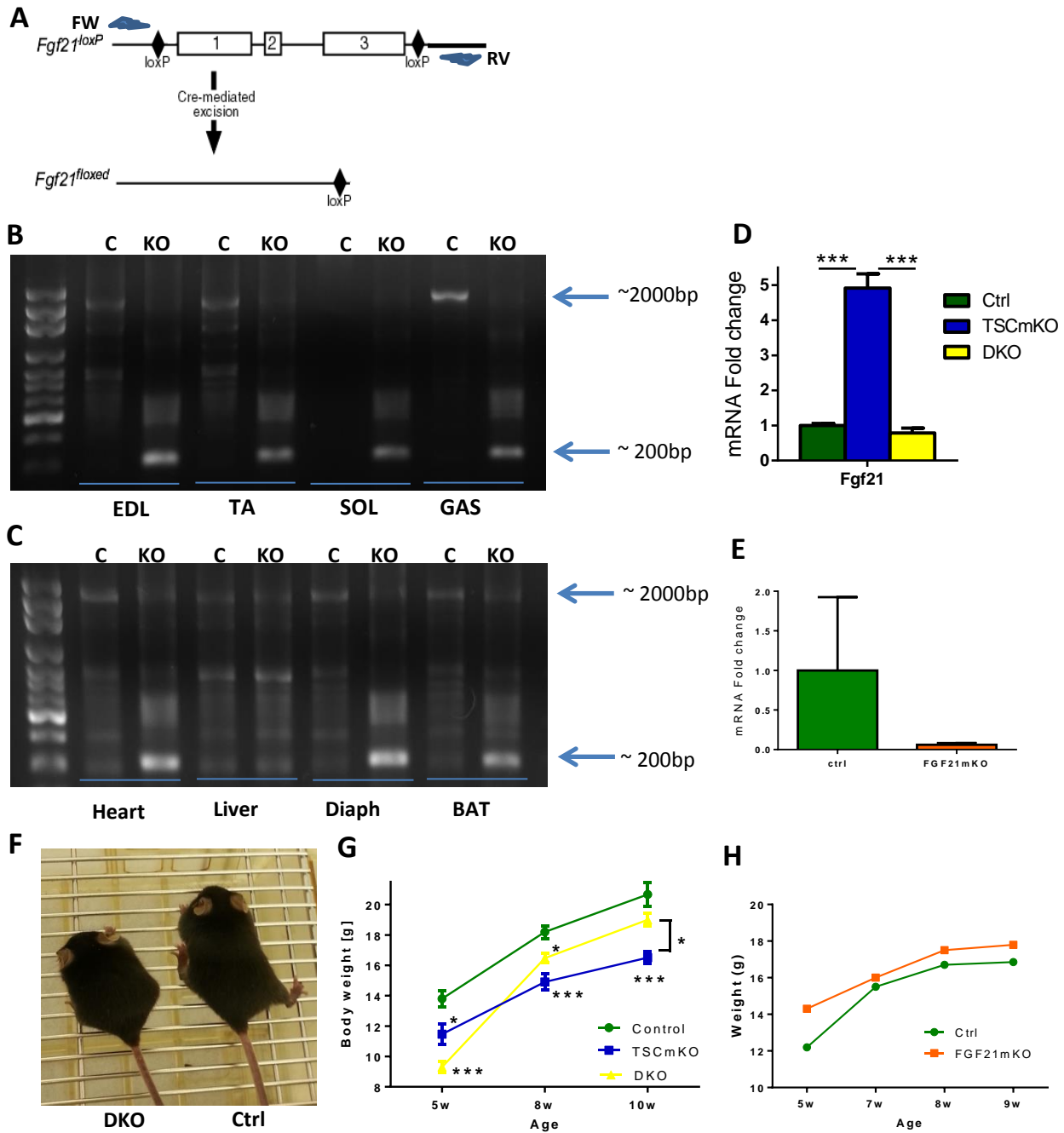


**Figure 1. FGF21 knock-out in skeletal muscle of the TSCmKO mice results in decreased survival**

A) Representation of the p lox insertion sites before exon 1 and after exon 3 of the *Fgf21* gene, and the Cre mediated excision of the three exons in the DKO and FGF21mKO mice. Adapted from REF Inagaki et al

B) Amplification of the *Fgf21* gene in control (C) and FGF21mKO (KO) mice, for EDL, TA, Soleus and Gastrocnemius muscles. Forward: CCT CCA GAT TTA GGA GTG CAG A and reverse: AGG GAG GCA GAG GCA AGT GAT T primers used amplified an approximately 2000 base pair (bp) product in the wild type group, while they amplified an approximately 200 bp product in the KO mice (n= 2).

C) Amplification of the *Fgf21* gene in control (C) and FGF21mKO (KO) mice, for Heart, Liver, Diaphragm and Brown adipose tissue (BAT). Forward: CCT CCA GAT TTA GGA GTG CAG A and reverse: AGG GAG GCA GAG GCA AGT GAT T primers used amplified an approximately 2000 base pair (bp) product in all of the organs, while they also partially amplified an approximately 200 bp product in the heart, Diaphragm and BAT (n= 2).

D) Real-time PCR amplification showed increased expression of *Fgf21* in TA muscle of TSCmKO mice when compared to the control (Ctrl) group, while it was normalized in the DKO group (n= 5).

E) Real-time PCR amplification showed lack of *Fgf21* expression in TA muscle of FGF21mKO mice when compared to the control (Ctrl) mice (n= 4).

F) 5-week-old DKO mice appear smaller and weaker than their wild type control (Ctrl) littermates. Image is representative of n=5 mice.

G) Body weight progression from 5-week-old to 10-week-old control (Ctrl), TSCmKO and DKO mice (n=5).

H) Body weight progression from 6-week-old to 9-week-old control (Ctrl) and FGF21mKO mice (n=2).

**Figure 2**

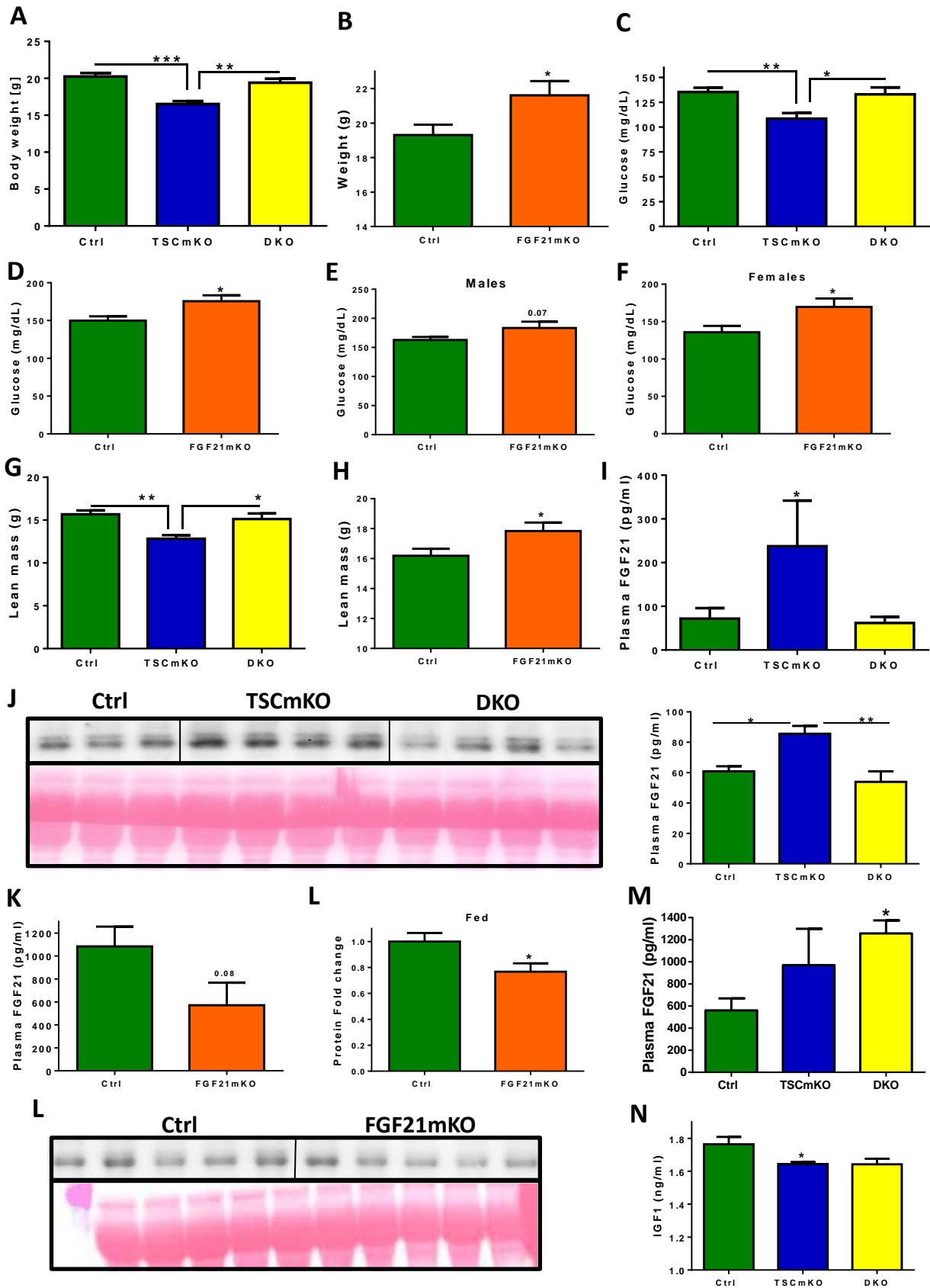


**Figure 2. Increased body weight, lean mass and plasma glucose levels are the physiological effects of muscle secreted FGF21**

A-B) Body weight was increased in 10-week-old DKO (n= 5) (A) and 8-week-old FGF21mKO (n= 18) (B) mice when compared to control (Ctrl) littermates.

C-D) Plasma glucose levels were increased in 10-week-old DKO (n= 5) (A) and 8-week-old FGF21mKO (n= 14) (B) mice when compared to control (Ctrl) littermates.

E-F) Plasma glucose levels tended to be higher in 8-week-old male FGF21mKO mice (n=6) (E) while they were significantly increased in 8-week-old female FGF21mKO mice (n= 8) (F) when compared to age-matched control (Ctrl) mice.

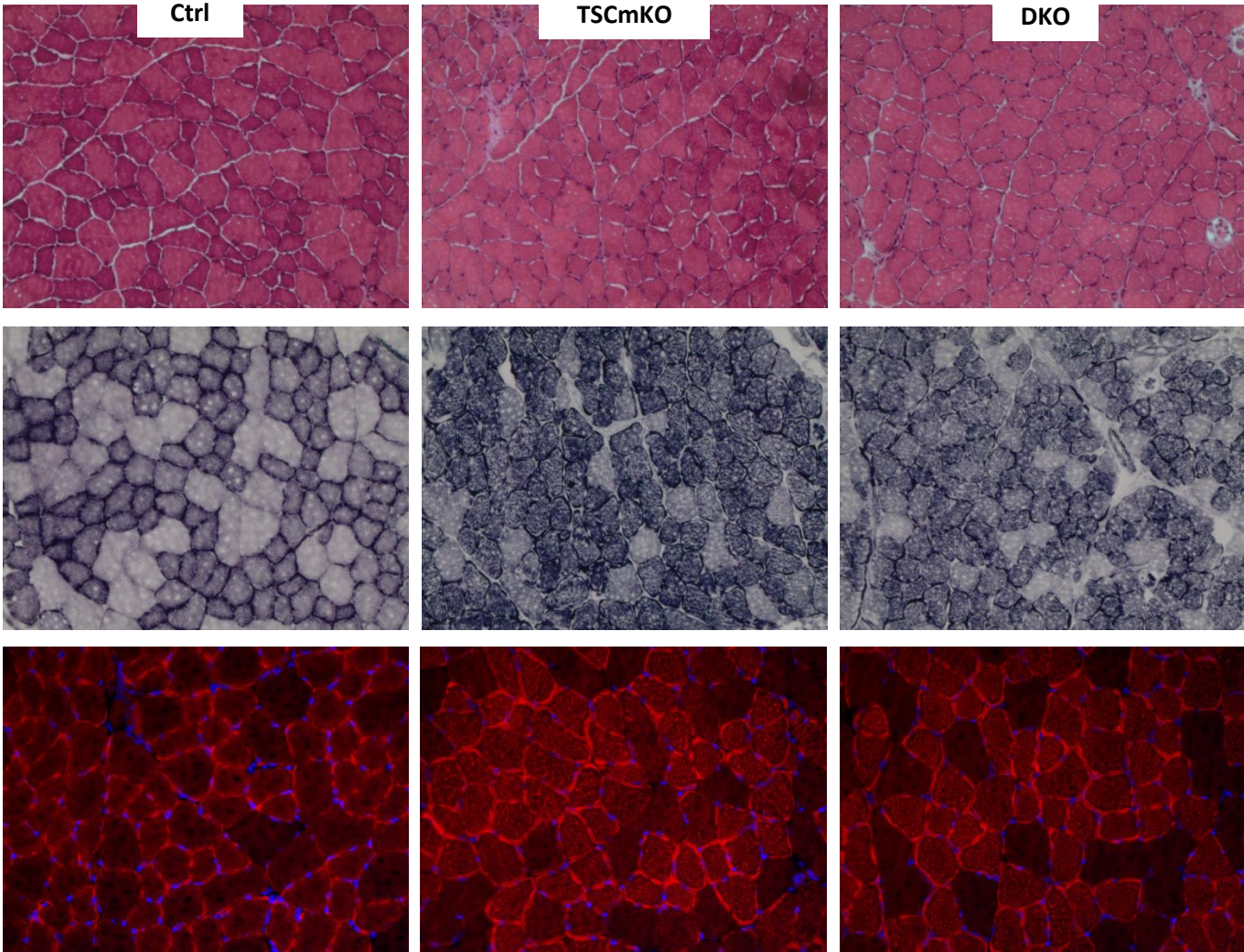
G-H) Lean mass was significantly increased in 10-week-old DKO (n= 5) (G) and 8-week-old FGF21mKO mice (n= 22) (H) when compared to control (Ctrl) mice.

I-M) Plasma FGF21 levels were normalized in 10-week-old fed DKO mice (n=5), as seen by ELISA (I) and immuno-depleted plasma western blot analysis (J), while they tended to be lower in overnight-starved 10-week-old FGF21mKO mice (K) and were lower in fed FGF21mKO mice (L) when compared to control (Ctrl) littermates (n= 10). On the other hand, plasma FGF21 levels were significantly higher in overnight-starved DKO mice (n= 3) (M).

N) Plasma IGF-1 levels were not changed between 10-week-old TSCmKO and DKO mice, which were lower than in control (Ctrl) mice (n= 5).

**Figure 3**

**A**



**B**

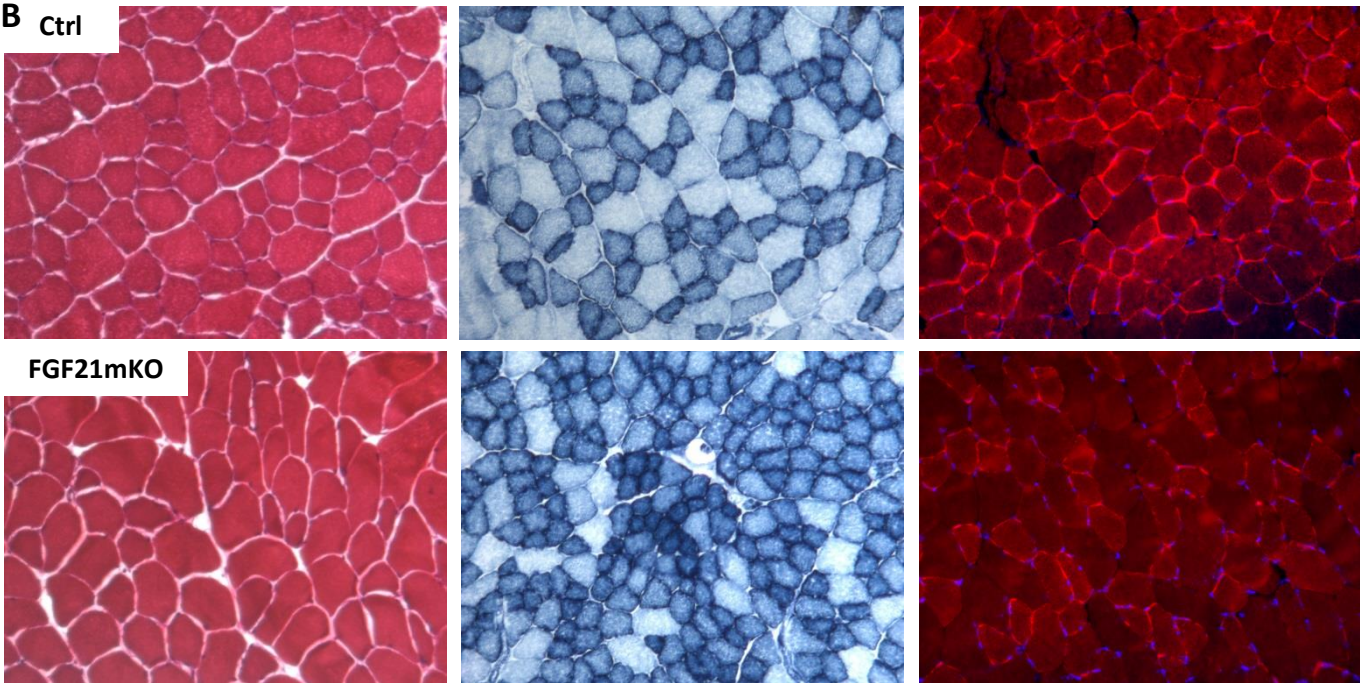




**Figure 3. Muscle FGF21 involved in fatty acid metabolism of skeletal muscle.**

A) H&E staining (top panel) didn't show any structural changes in 10-week-old TSCmKO or DKO TA muscle. NADH staining (middle panel) revealed an increased oxidative capacity of TSCmKO TA muscle, which remained increased in DKO TA muscle compared to control (Ctrl) mice. Oil Red-O staining (bottom panel) showed increased lipid accumulation in TSCmKO TA muscle, while lipid accumulation was reduced in DKO TA muscle when compared to TSCmKO mice. Images are representative of 4 sections from n=3 mice.

B) H&E staining (left panel) didn't show any structural changes in 10-week-old FGF21mKO gastrocnemius muscle. NADH staining (middle panel) revealed increased oxidative capacity of FGF21mKO TA muscle. Oil Red-O staining (right panel) showed reduced lipid accumulation in FGF21mKO gastrocnemius muscle. Images are representative of 4 sections from n=3 mice.

**Figure 4**

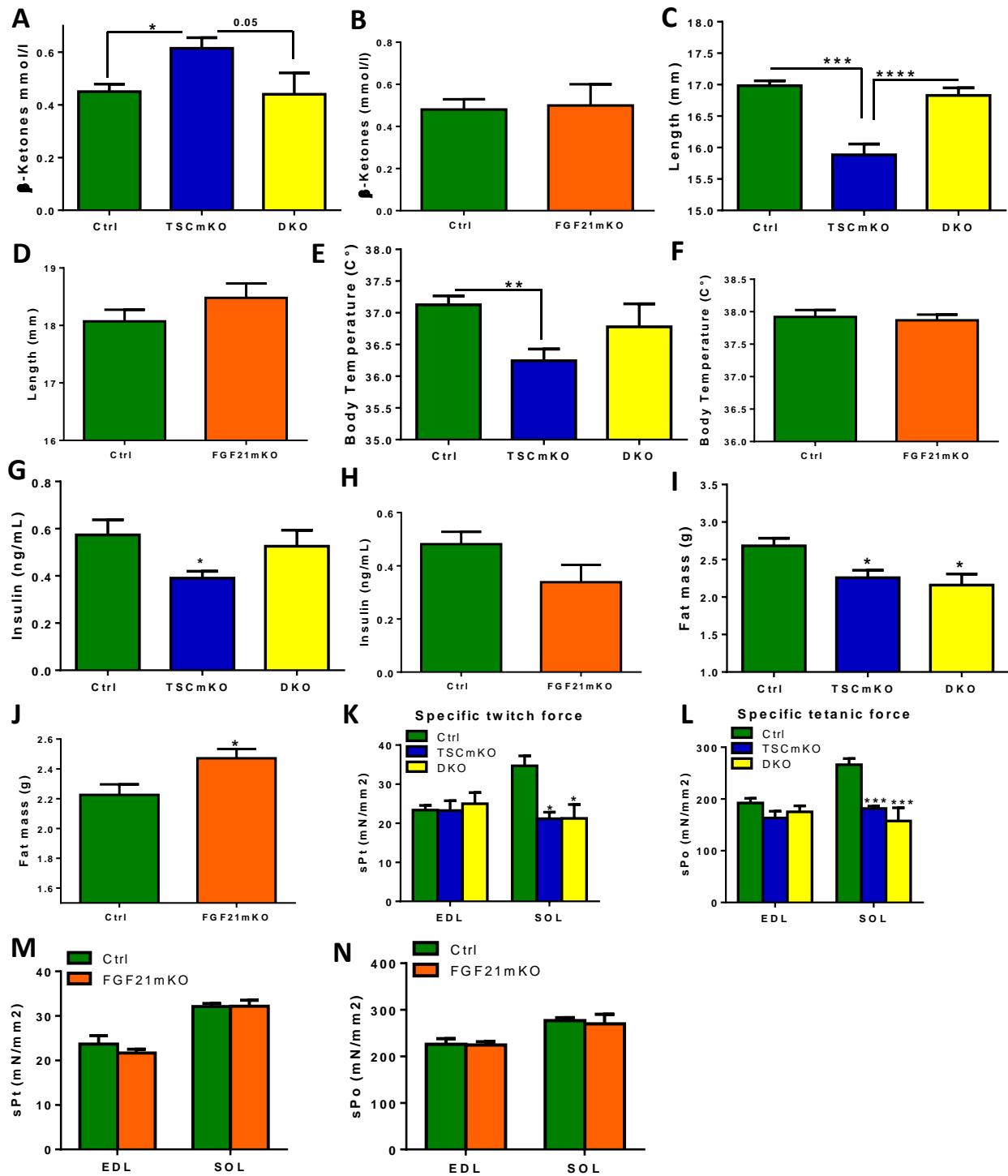


**Figure 4. Differential effect of muscle secreted FGF21 on the whole-body metabolism upon mTORC1 activation or basal conditions**

A-B) Increased plasma β-ketone concentrations in 10-week-old TSCmKO were normalized in DKO mice (n= 5) (A), while they remained unchanged in FGF21mKO mice (n= 3) (B).

C-D) Reduced tibia length in 10-week-old TSCmKO mice was normalized in DKO mice (n= 5) (C), while it remained unchanged in FGF21mKO mice (n= 3) (D) when compared to control (Ctrl) mice.

E-F) Body temperature in 10-week-old TSCmKO mice was reduced, while it was unchanged in DKO mice (n= 5) (E) or FGF21mKO mice (n= 3) (F) when compared to control (Ctrl) littermates.

G-H) Plasma insulin concentrations were significantly lower in 10-week-old TSCmKO mice, while they were unchanged in DKO mice (n= 5) (G) or FGF21mKO mice (n= 6) (H) when compared to control (Ctrl) littermates.

I-J) Fat mass was significantly decreased in 10-week-old TSCmKO and DKO mice (n= 5) (I), while it was significantly increased in 10-week-old FGF21mKO mice (n= 22) (J).

K-L) Specific twitch force (K) and specific tetanic force (L) were unchanged in TSCmKO and DKO EDL muscles, while they remained decreased in TSCmKO and DKO soleus muscles (n= 5).

M-N) Specific twitch force (m) and specific tetanic force (N) were unchanged in 10-week-old FGF21mKO EDL or soleus muscles (n= 5).

**Figure 5**

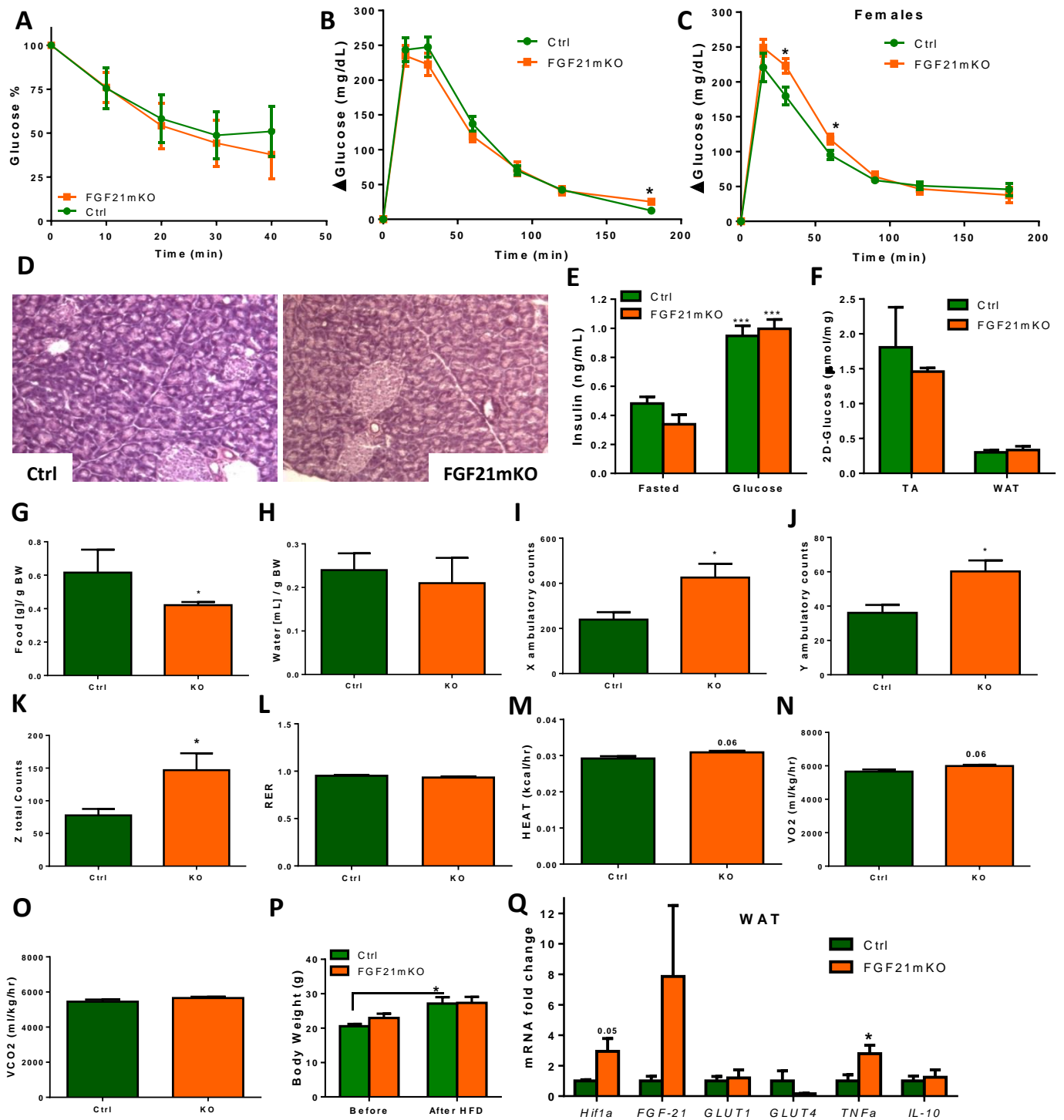


**Figure 5. Deletion of muscle FGF21 caused a diabetic phenotype**

A) Unchanged insulin sensitivity in 14-week-old male and female FGF21mKO mice (n= 6)

B-C) Glucose tolerance was normal in 14-week-old male and female FGF21mKO mice, while it was significantly impaired in 14-week-old female FGF21mKO mice (n= 5).

D) Pancreas histology was normal in 14-week-old FGF21mKO mice, as seen by H&E staining of 10µm cross-sections. Images are representative of 4 sections of 3 mice per genotype.

E) Plasma insulin levels are efficiently increased upon glucose stimulation in 12-week-old FGF21mKO mice (n= 4).

F) Glucose absorption was unchanged in TA muscle or WAT of 12-week-old FGF21mKO mice, as seen by a 2 deoxy-glucose uptake test (n= 4).

G-O) CLAMS analysis exposed the basal metabolism of 12-week-old FGF21mKO mice: female FGF21mKO mice ate significantly less food than control (Ctrl) mice (G); both male and female mice were more active than their control littermates (I-K); FGF21mKO mice had normal respiratory exchange ratio (RER) (L); energy expenditure (M) tended to be higher in male and female FGF21mKO mice, as well as oxygen consumption (N), while CO<sub>2</sub> respiratory values (O) were normal (n= 6).

P) Body weight was significantly higher in control mice after 10 weeks of HFD feeding, while it tended to increase in male and female FGF21mKO mice (n= 6).

Q) Increased *TNFα* expression in WAT of 14-week-old FGF21mKO mice when compared to control (Ctrl) littermates (n= 4).

**Figure 6**

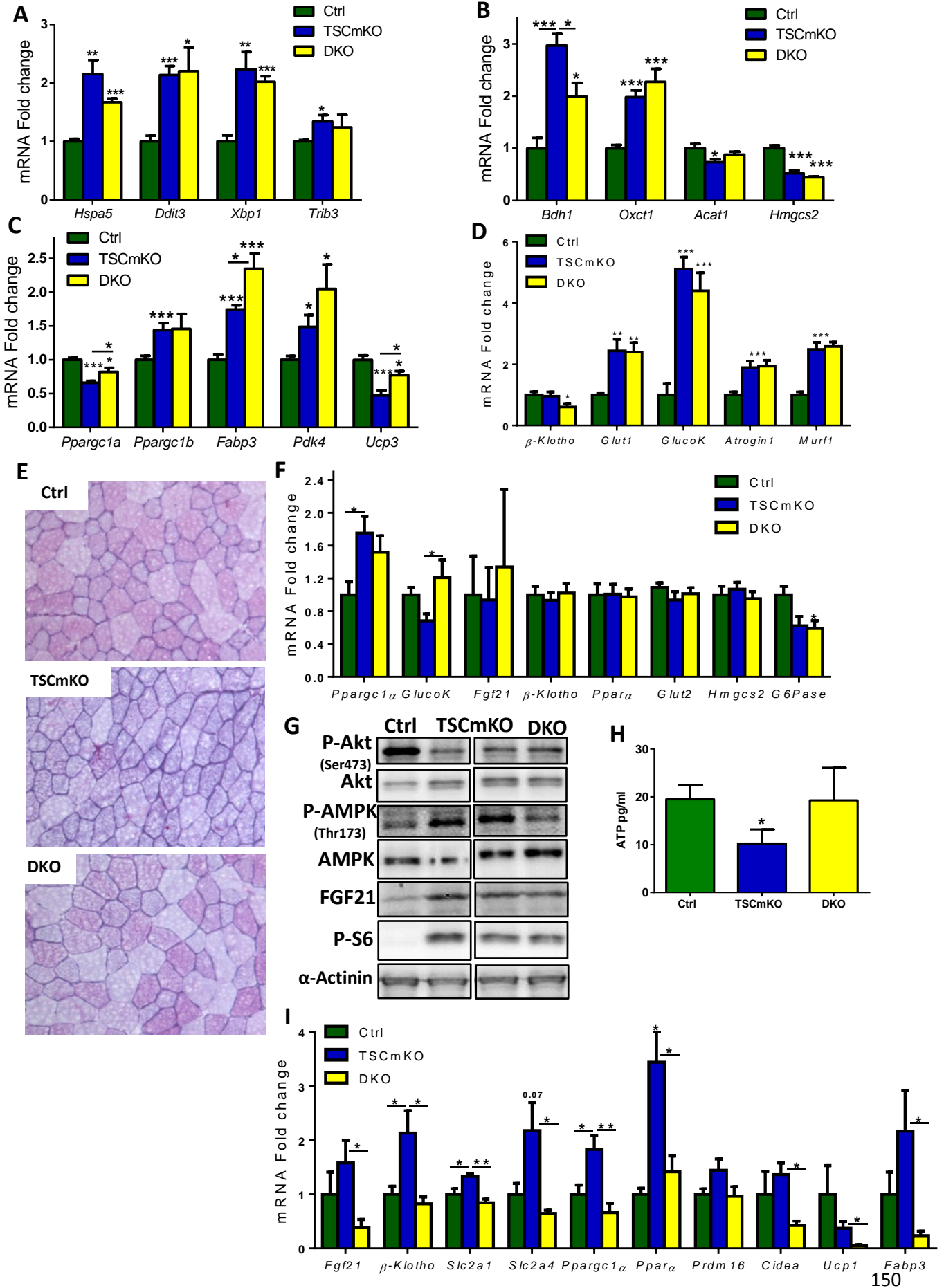


**Figure 6. Eliminating muscle FGF21 in TSCmKO mice normalized browning and glucose absorption in WAT while it decreased ketolysis and altered fatty acid oxidation in skeletal muscle**

A) 10-week-old TSCmKO and DKO mice showed increased expression of ER stress markers in TA muscle (*Hspa5; Ddit3; Xbp1; Trib3*) (n= 5).

B) Increased expression of ketolytic gene *Bdh1* observed in 10-week-old TSCmKO TA muscle was significantly decreased in DKO TA muscle, while other genes involved in ketolysis (*Oxct1*) and ketogenesis (*Acat1; Hmgcs2*) were unchanged (n= 5).

C) 10-week-old DKO mice showed increased expression of genes involved in fatty acid oxidation and mitochondria biogenesis (*Ppargc1a; Ppargc1b; Fabp3; Pdk4; Ucp3*) in TA muscle when compared to TSCmKO mice (n= 5).

D) Expression of genes involved in glucose absorption (*Slc2a1; GlucoK*) or proteasome degradation (*Atrogin1; Murf1*) was still increased in TA muscle of DKO mice when compared to 10-week-old TSCmKO mice (n= 5).

E) Glycogen storage was increased in muscle from 10-week-old TSCmKO and DKO mice when compared to control (Ctrl) littermates, as seen by PAS staining of TA muscles. Images are representative of 4 sections from 3 mice per genotype.

F) Expression of *glucokinase* was increased in liver from 10-week-old DKO mice when compared to TSCmKO and control (Ctrl) littermates (n=5).

G) Immunoblots of TA muscle from 10-week-old TSCmKO, DKO and control (Ctrl) mice are shown for the indicated phospho (P-) and total proteins (n= 5). Protein levels are normalized to  $\alpha$ -actinin.

H) ATP content is decreased in EDL muscle of TSCmKO mice while it is unchanged in DKO mice (n= 4).

l) Expression of genes involved in *Fgf21* signaling (*Fgf21*; *β-Klotho*) was up-regulated in WAT of 10-week-old TSCmKO mice, while they were normalized in DKO mice; expression of glucose transporters (*Slc2a1*; *Slc2a4*) was significantly down-regulated in DKO WAT when compared to TSCmKO mice, as well as the expression of genes involved in browning of WAT (*Ppargc1a*; *Prdm16*; *Cidea*; *Ucp1*; *Fabp3*) (n= 5).



**Figure 7**

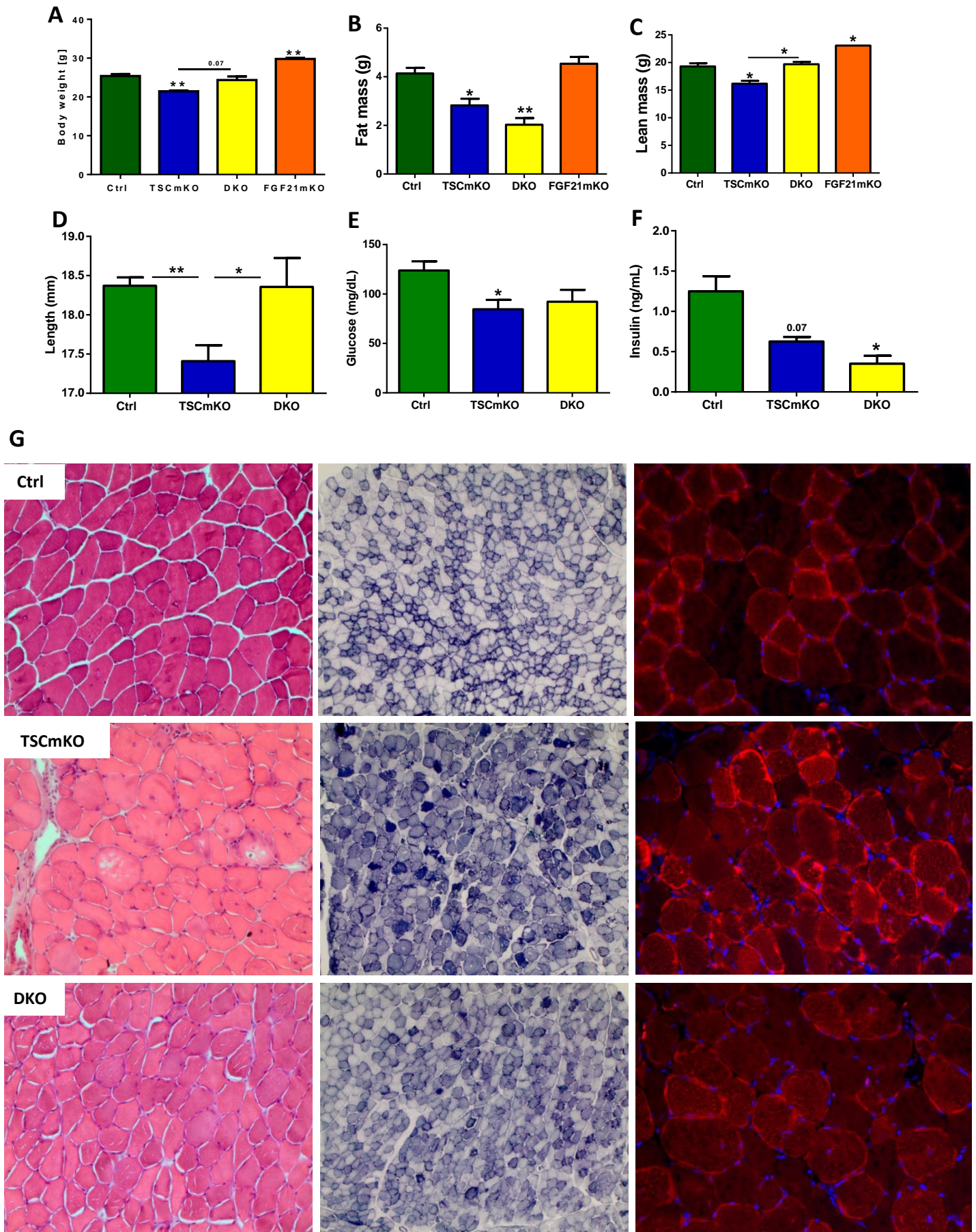


**Figure 7. Potential involvement of muscle FGF21 in the development of the myopathy in TSCmKO mice**

A) Body weight tended to increase in 10-month-old female DKO mice when compared to TSCmKO mice, while 10-month-old female FGF21mKO were significantly heavier than the control (Ctrl) littermates (n= 2).

B) Fat mass was reduced in 10-month-old female TSCmKO and DKO mice, while it was unchanged in 10-month-old female FGF21mKO mice when compared to control (Ctrl) littermates (n= 2).

C) Lean mass was higher in 10-month-old female DKO mice when compared to TSCmKO mice, while it was also significantly higher in 10-month-old female FGF21mKO mice when compared to control (Ctrl) mice (n= 2).

D) Reduced tibia length of 10-month-old TSCmKO mice was normalized in male and female DKO mice (n= 3).

E) Plasma glucose levels remained low in 10-month-old male and female TSCmKO and DKO mice (n= 3).

F) Plasma insulin levels remained reduced in 10-month-old male and female TSCmKO and DKO mice (n= 2).

G) H&E staining showed lack of vacuoles and reduced centralized nuclei in TA muscle from 10-month-old female DKO mice when compared to TSCmKO mice (left panel line). NADH staining revealed increased oxidative capacity in 10-month-old female TSCmKO and DKO TA muscles (middle panel line). Oil Red-O staining (right panel) showed reduced lipid accumulation in TA muscle from 10-month-old female DKO mice when compared to the increased lipid accumulation observed in TSCmKO mice. Images are representative of 4 sections from 3 mice per genotype.

#### 4. CONCLUDING REMARKS

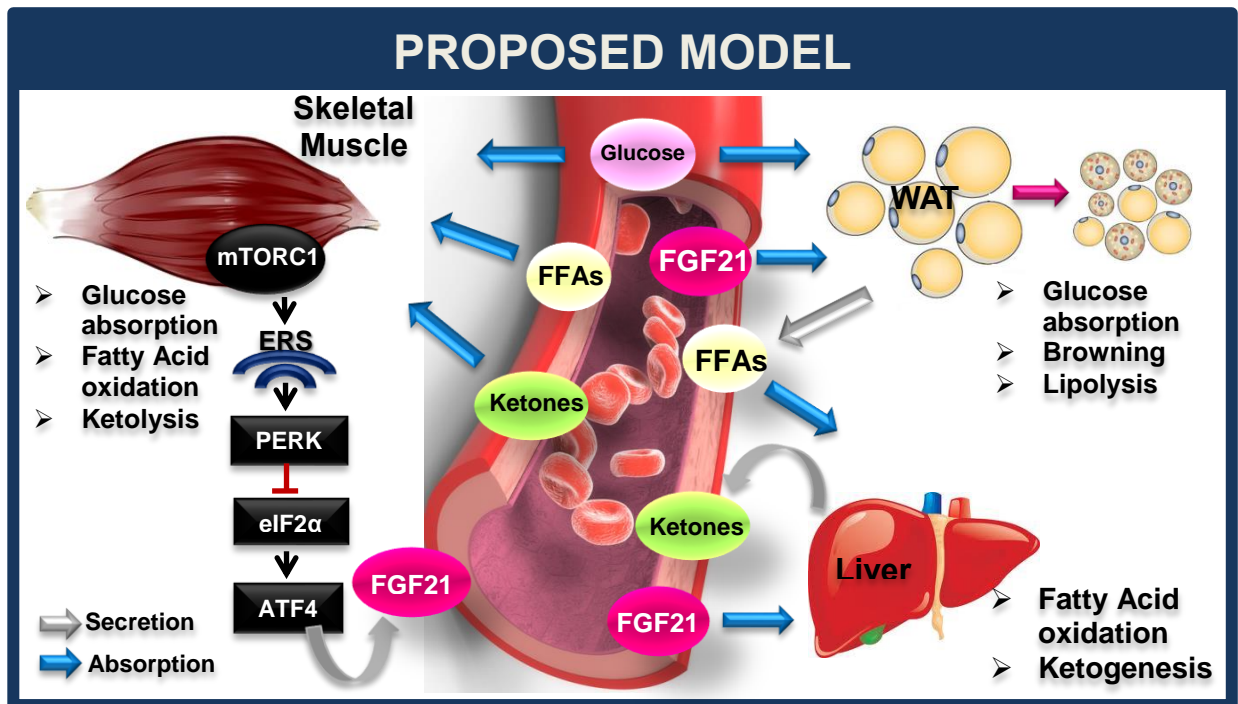


**Figure 8. Representative scheme of the metabolic changes caused by increased FGF21 in TSCmKO mice**

Increased mTORC1 activity in skeletal muscle caused the activation of the ER stress due to increased protein synthesis and energy depletion. This led to the production and secretion of FGF21 from skeletal muscle. FGF21 acted predominantly on white adipose tissue (WAT) to induce increased glucose absorption, which together with the increased glucose absorption into skeletal muscle reduced the plasma glucose levels of the mice. In addition, FGF21 induced the browning of WAT, which likely contributed to the increased energy expenditure of the TSCmKO mice. On the other hand, WAT was broken down by excessive lipolysis into free fatty acids (FFA), which were delivered to skeletal muscle as an extra source of energy for increased fatty acid oxidation, and also to the liver, where we observed an increase in fatty acid oxidation and ketogenesis, with the subsequent delivery of ketone bodies into the circulation. These ketone bodies were also taken up by skeletal muscle for energy production through ketolysis. The plasma glucose and ketone bodies, as well as WAT glucose absorption and browning were normalized when we knocked-out FGF21 in the skeletal muscle of TSCmKO mice, confirming our proposed model of whole-body metabolic changes caused by muscle-secreted FGF21.

## **Muscle mTORC1 and metabolism**

Obesity and overweight are fast-growing metabolic diseases reaching epidemic proportions in the developed world. The World Health Organization estimates that almost 30% of the adult population is overweight, of which 10% is obese, which is a preventable disease. Obesity-related conditions include heart disease, stroke, type-2 diabetes and certain types of cancer, some of the leading causes of preventable death. Thus, it is critical to try to figure out new ways to decrease the prevalence and risk factors leading to un-balanced metabolic features. For this, understanding all of the components that regulate whole-body metabolism is crucial. It is widely known and accepted that key metabolic organs, like the liver or the pancreas, have essential roles in maintaining metabolic homeostasis, adapting the body's response to outside stimuli like feeding, starvation or exercise and energy demand. However, the role of skeletal muscle in regulating whole-body metabolism is less obvious.

We decided to study the insulin-signaling pathway in skeletal muscle, and more specifically the role of muscle mTORC1 in regulating whole-body metabolism. We observed that inhibition of mTORC1 activity by depletion of raptor in skeletal muscle caused predominantly a muscle phenotype of the RAmKO mice, with decreased expression of metabolic genes involved in glucose absorption and fatty acid oxidation. This was a consequence of denervation induced increase in class II HDACs, which rendered the muscle incapable of efficiently utilizing energy substrates. In addition, inflammation markers were increased and NF- $\kappa$ B pathway was activated, which likely contributed to the insulin resistance observed in RAmKO mice. On the other hand, constitutive activation of mTORC1 in skeletal muscle by depletion of its inhibitor TSC1, caused a strong phenotypic change not only in the muscle, but also at the whole-body level of young mice, with changes arising in other organs like the liver and adipose tissues. TSCmKO mice were lean and showed a progressive loss of fat mass. They also had changes in their plasma profile, with lower insulin and glucose levels, while ketone bodies were increased, which were likely a consequence of increased insulin sensitivity and fatty acid oxidation respectively. They showed an up-regulation of the expression of several metabolic genes involved in glucose absorption and fatty acid oxidation predominantly in WAT and muscle.

Thus, while metabolism was virtually being “shut-down” in the skeletal muscle of RAmKO mice, muscle of TSCmKO mice were showing an accelerated metabolic profile with increased energetic demands. Interestingly, while at the young age of 10 weeks RAmKO and TSCmKO mice showed the opposite metabolic profile, likely a consequence of inverse mTORC1 signaling in the muscle, both mouse models developed the same metabolic phenotype with age and myopathy onset. They had lower plasma glucose and insulin levels, with increased glycogen storage in the muscle and they both developed insulin resistance as a consequence of increased intramyocellular lipid content. These metabolic changes are frequently observed in patients with muscular dystrophies (Cruz Guzman Odel et al, 2012), as a consequence of the altered muscle integrity. These observations would suggest that skeletal muscle mTORC1 could serve as a potential target to treat metabolic complications of diseases like diabetes, obesity and muscle dystrophies.

### **Muscle secreted FGF21**

We were able to figure out the main reason behind the extension of the metabolic phenotype from skeletal muscle to liver and adipose tissue happening in the TSCmKO mice. It was the result of the induction and secretion into circulation of the myokine FGF21. We were first able to demonstrate the involvement of FGF21 in the metabolic phenotype of TSCmKO mice by overnight neutralization of plasma FGF21 with an antibody treatment. It not only normalized plasma glucose and ketone bodies, but it largely normalized the altered expression of metabolic genes in WAT, which confirmed that FGF21 would control metabolism by transcriptional regulation in this key target tissue. It was reported that FGF21 was induced in skeletal muscle upon oxidative stress or mitophagy defects (Keipert et al, 2014; Kim et al, 2013c), and we now demonstrate that in addition, endoplasmic reticulum stress can also activate FGF21 secretion through PERK-eIF2 $\alpha$  activation of its transcription factor ATF4. Increased mTORC1 activity overwhelmed the folding capacity of the ER by increasing protein synthesis and translation. We demonstrated this molecular mechanism by treating the TSCmKO with the chemical chaperone 4-PBA, which besides decreasing ER stress it also significantly reduced FGF21 production in skeletal muscle. Interestingly, 4-PBA treatment also prompted a significant weight gain in

TSCmKO, mostly due to an increase in lean mass, while it also normalized their body temperature. Thus, increased mTORC1 activity in skeletal muscle induced FGF21 secretion through ER stress activation, which in turn modified the whole-body metabolism of TSCmKO mice.

The remaining question was to figure out what is the goal of the increase in plasma FGF21. One interpretation is that it could represent a protective response to a metabolic overload originated in skeletal muscle that would lead to modulation of glucose and lipid metabolism at the whole-body level. The alternative is that increased levels of FGF21 in such situations may reflect a “spill-over” from cells subject to a “metabolic stress”. This excessive FGF21 could actually be contributing to the wasting and deterioration of the organism, and may even participate in the decline of skeletal muscle by altering the metabolic dynamics. To be able to answer to this question we generated the DKO mice, which also allowed us to identify the key parameters in the TSCmKO mice that were directly a consequence of muscle secreted FGF21. A first observation revealed that these mice had decreased survival, as they appeared to be extremely small and weak upon birth. This would suggest that the initial increase of FGF21 was required for early development. One possibility is that it was necessary for skeletal muscle growth and differentiation upon TSC1 deletion, as MyoD regulates FGF21 expression in differentiating myotubes (Ribas et al, 2014), suggesting that it could promote muscle development. On the other hand, neonatal DKO mice could be having problems with temperature regulation, because FGF21 is known to protect BAT and improve thermogenesis (Fisher et al, 2012). Brown adipocytes and myocytes share a common Myf5-lineage progenitor cell (Seale et al, 2008), thus the communication between these two tissues might be essential for proper thermodynamics upon birth, and FGF21 could be a mediator. However, this was specific to mTORC1 activation in DKO mice, as FGF21mKO mice did not have survival problems and were already bigger than their control littermates by 5 weeks of age. Nevertheless, once the DKO mice got over an un-identified “critical period” 5 weeks after birth, they were able to develop favorably and indeed gained more weight than the TSCmKO mice by 10 weeks of age. This demonstrates that the initial impairment of TSCmKO mice to gain weight was due to increased FGF21 in these mice. Surprisingly, this higher body weight was not due to changes in

fat mass as hypothesized, but a consequence of an increase in lean mass. The increase and normalization of lean mass remained in 40-week-old DKO mice, which draws attention to a previously unidentified role of FGF21 in skeletal muscle. Furthermore, 10-month-old female DKO mice did not develop the vacuoles or giant nuclei observed in muscle of TSCmKO mice, which would suggest that FGF21 could be involved in the progression of the myopathy. It was originally thought that skeletal muscle is not a target tissue for FGF21 action due to a lack of expression of the  $\beta$ -Klotho receptor (Yang et al, 2012). However, we not only detected expression of  $\beta$ -Klotho in skeletal muscle (as did Keipert *et al.* in their study), but DKO muscles showed a significant down-regulation of its expression. In parallel, WAT of TSCmKO mice showed an increased expression of  $\beta$ -Klotho receptor that was normalized in DKO mice. These results suggest that FGF21 might have a positive feedback to regulate its own signaling, and that it does act on skeletal muscle to regulate muscle mass. FGF21 could be involved in regulating fatty acid metabolism in muscle, as seen by changes in oxidative capacity and lipid content in muscles of both DKO and FGF21mKO mice. Interestingly, the higher expression of genes coding for mediators of fatty acid oxidation in muscle suggested that DKO muscles relied more in fatty acid metabolism. This correlated with reduced lipid content in muscles from DKO mice, which suggests that instead of promoting fatty acid oxidation, FGF21 would actually be promoting lipid storage. In parallel, FGF21mKO muscles also showed a decrease in lipid content and increased oxidative capacity. FGF21 was proposed to have a protective role against excessive lipolysis upon starvation (Arner et al, 2008; Badman et al, 2007; Chen et al, 2011), and it reduces growth and promotes hibernation as energy preserving means (Inagaki et al, 2007; Ishida, 2009). Accordingly, it could be stopping excessive growth prompted by hyperactive mTORC1 in the skeletal muscle of TSCmKO mice, and promoting lipid-form energy storage. Thus, muscle seems to be a target of the autocrine action of FGF21, which inhibits its growth, reduces fatty acid oxidation and contributes to an intramyocellular lipid accumulation, likely as a protective mechanism to preserve energy. As a consequence, eliminating muscle FGF21 facilitated the deregulated fatty acid oxidation induced by sustained mTORC1 activity, which might contribute to the ongoing WAT tissue lipolysis and wasting. In parallel, expression of genes involved in glucose absorption and browning of WAT were normalized in DKO, which

would corroborate that in TSCmKO mice, muscle FGF21 was causing these changes in WAT by transcriptional regulation.

On the other hand, markers for ER stress remained increased in skeletal muscle of DKO mice, as did the expression of atrogenes and glucose transporters. This would suggest that increased Glut1 expression in muscle of TSCmKO was not a consequence of FGF21, but likely the result of decreased Akt activity and its downstream target TBC1D1 (Zhou et al, 2008). As a consequence, DKO muscle, where Akt phosphorylation was still low, also showed increased glycogen accumulation. Expression of enzymes involved in ketogenesis remained low in DKO muscles, which would point at mTORC1 being involved in their regulation. Expression of *Bdh1* however, involved in ketone body breakdown, was down-regulated in the muscle of DKO mice, similar to when FGF21 was neutralized in the plasma of TSCmKO mice. This correlated with the normalization of plasma ketone bodies in DKO mice, which would suggest that lower availability of this metabolite could regulate the “ketolysis” response in skeletal muscle. Ketone bodies are synthesized in the liver in response to low glucose and increased fatty acid oxidation (Newman & Verdin). Although expression of genes involved in ketogenesis was unchanged in the liver of TSCmKO mice, it showed an increased expression of the gene encoding for PGC1 $\alpha$ , involved in fatty acid oxidation. The fact that PGC1 $\alpha$  was still increased in DKO would suggest that the changes in liver metabolism present in TSCmKO mice might not be a direct consequence of FGF21, but rather a secondary effect of the increased lipolysis and availability of free fatty acids in the plasma. In DKO liver we observed an increased expression of the gene encoding for the liver-specific enzyme glucokinase, which regulates the first step of glycolysis after glucose absorption into the hepatocyte (Massa et al, 2011). This correlated with an increased abundance of plasma glucose in the DKO mice, which was likely a consequence of decreased absorption of glucose into WAT. Thus, eliminating muscle FGF21 in TSCmKO mice normalized plasma glucose and insulin levels, and as a consequence liver metabolism could rely more on carbohydrates which would reduce fatty acid oxidation and ketogenesis.

Plasma glucose and ketone bodies were thus normalized in DKO mice. However, IGF-1 remained low, while the growth retardation of TSCmKO was corrected in DKO. This would



contradict our initial hypothesis that FGF21 caused GH resistance in the liver to reduce IGF-1 synthesis. Because tibia was significantly longer in DKO mice while IGF-1 was still decreased, this would suggest that muscle secreted FGF21 was impairing normal growth in TSCmKO independent of IGF-1. This was likely a consequence of the reduced action of FGF21 on chondrocytes, as this was hypothesized to reduce growth during chronic undernutrition by inducing the expression of LEPROT and LEPROT1 (Wu et al, 2013).

### **FGF21 and obesity**

The origin of circulating FGF21 remained controversial, with studies reporting that all of plasma FGF21 was secreted from liver (Markan et al, 2014). However, a recent report showed that skeletal muscle can also contribute to the abundance of plasma FGF21 and in turn regulate whole-body metabolism (Kim et al, 2013c). We decided to analyze specifically the effect of muscle-secreted FGF21 by creating a muscle FGF21 KO mouse model. These mice were viable and fertile, and showed an increase in body weight as early as 5 weeks of age. The higher body weight was due to an increase in both lean and fat mass, which would correlate with the anti-obesity effect of FGF21. In parallel, the reduced plasma FGF21 in FGF21mKO mice caused an increase in plasma glucose levels and glucose intolerance, which would point to the development of obesity-induced diabetes. Interestingly, expression of TNF $\alpha$  was increased in WAT of FGF21mKO mice, which could be linked to the activation of inflammatory pathways in adipose tissue as a consequence of obesity (Osborn & Olefsky, 2012).

Interestingly, global FGF21 KO mice develop a very similar phenotype to that of FGF21mKO mice, with increases in body weight, lean and fat mass, plasma glucose and glucose intolerance (Badman et al, 2009). On the other hand, liver or adipose tissue FGF21 KO mice do not show a strong phenotype, but only a slight decrease in plasma glucose levels (Markan et al, 2014). This would suggest that muscle FGF21 would be a major contributor of the global FGF21 KO phenotype, which is similar to the FGF21mKO, even with normal liver FGF21 secretion. Thus, muscle would constitute an important FGF21 secretory organ, which can alter whole-body metabolism. FGF21 is known to cross the blood-brain barrier and act on the suprachiasmatic-nucleus of the hypothalamus to regulate metabolic homeostasis on a circadian fashion

(Bookout et al, 2013). The FGF21mKO mice showed various evidence of muscle FGF21 acting on the brain, as they were significantly more active than the control mice, and ate higher amounts of food. This would correlate with the “hibernating” effect of FGF21, because it can induce torpor, reduce food intake and activity as energy preserving means. Thus, in FGF21mKO mice, this muscle-brain communication would be lost, and the mice would appear to be in a constant fed and high energy status. Furthermore, the action of FGF21 on the brain, and more specifically on the hypothalamic-pituitary-ovarian axis can reduce female fertility (Owen et al, 2013), which would suggest that it could have a distinct effect on the female mice. In parallel, FGF21mKO female mice showed a stronger phenotype than male mice, with higher plasma glucose levels, becoming glucose intolerant and decreasing their food intake.

In conclusion, we were able to demonstrate that muscle-secreted FGF21 is a major contributor to circulating plasma FGF21 levels, which in turn can alter whole-body metabolism to regulate the organism’s response against obesity and diabetes. Moreover, there appears to be a straight communication between muscle and brain mediated by FGF21 to establish and coordinate the body’s energetic status, which seemed to show a sexual dimorphism as the phenotype was stronger in female mice. Furthermore, when FGF21 was eliminated in skeletal muscle the mice showed an increase in lean mass and changes in oxidative capacity of the muscle, correlating with the increased lean mass of global FGF21 KO mice, which would point at FGF21 having a significant role in skeletal muscle. Thus, this opens new and exciting possibilities for FGF21 action in muscle that need further studying.

## 5. REFERENCES

- Adams AC, Cheng CC, Coskun T, Kharitonov A (2012a) FGF21 requires betaklotho to act in vivo. *PLoS One* **7**: e49977
- Adams AC, Coskun T, Rovira AR, Schneider MA, Raches DW, Micanovic R, Bina HA, Dunbar JD, Kharitonov A (2012b) Fundamentals of FGF19 & FGF21 action in vitro and in vivo. *PLoS One* **7**: e38438
- Akiyama M, Hatanaka M, Ohta Y, Ueda K, Yanai A, Uehara Y, Tanabe K, Tsuru M, Miyazaki M, Saeki S, Saito T, Shinoda K, Oka Y, Tanizawa Y (2009) Increased insulin demand promotes while pioglitazone prevents pancreatic beta cell apoptosis in Wfs1 knockout mice. *Diabetologia* **52**: 653-663
- Albert V, Hall MN (2015) mTOR signaling in cellular and organismal energetics. *Curr Opin Cell Biol* **33**: 55-66
- Altomare DA, Guo K, Cheng JQ, Sonoda G, Walsh K, Testa JR (1995) Cloning, chromosomal localization and expression analysis of the mouse Akt2 oncogene. *Oncogene* **11**: 1055-1060
- Angelin B, Larsson TE, Rudling M (2012) Circulating fibroblast growth factors as metabolic regulators--a critical appraisal. *Cell Metab* **16**: 693-705
- Appenzeller-Herzog C, Hall MN (2012) Bidirectional crosstalk between endoplasmic reticulum stress and mTOR signaling. *Trends Cell Biol* **22**: 274-282
- Arner P, Pettersson A, Mitchell PJ, Dunbar JD, Kharitonov A, Ryden M (2008) FGF21 attenuates lipolysis in human adipocytes - a possible link to improved insulin sensitivity. *FEBS Lett* **582**: 1725-1730
- Badin PM, Langin D, Moro C (2013) Dynamics of skeletal muscle lipid pools. *Trends Endocrinol Metab* **24**: 607-615
- Badman MK, Koester A, Flier JS, Kharitonov A, Maratos-Flier E (2009) Fibroblast growth factor 21-deficient mice demonstrate impaired adaptation to ketosis. *Endocrinology* **150**: 4931-4940
- Badman MK, Pissios P, Kennedy AR, Koukos G, Flier JS, Maratos-Flier E (2007) Hepatic fibroblast growth factor 21 is regulated by PPARalpha and is a key mediator of hepatic lipid metabolism in ketotic states. *Cell Metab* **5**: 426-437
- Bartelt A, Heeren J (2014) Adipose tissue browning and metabolic health. *Nature reviews Endocrinology* **10**: 24-36

Beenken A, Mohammadi M (2009) The FGF family: biology, pathophysiology and therapy. *Nat Rev Drug Discov* **8**: 235-253

Bellinger AM, Mongillo M, Marks AR (2008) Stressed out: the skeletal muscle ryanodine receptor as a target of stress. *J Clin Invest* **118**: 445-453

Bentzinger CF, Lin S, Romanino K, Castets P, Guridi M, Summermatter S, Handschin C, Tintignac LA, Hall MN, Ruegg MA (2013) Differential response of skeletal muscles to mTORC1 signaling during atrophy and hypertrophy. *Skelet Muscle* **3**: 6

Bentzinger CF, Romanino K, Cloetta D, Lin S, Mascarenhas JB, Oliveri F, Xia J, Casanova E, Costa CF, Brink M, Zorzato F, Hall MN, Ruegg MA (2008a) Skeletal muscle-specific ablation of raptor, but not of rictor, causes metabolic changes and results in muscle dystrophy. *Cell metabolism* **8**: 411-424

Bentzinger CF, Romanino K, Cloetta D, Lin S, Mascarenhas JB, Oliveri F, Xia J, Casanova E, Costa CF, Brink M, Zorzato F, Hall MN, Ruegg MA (2008b) Skeletal muscle-specific ablation of raptor, but not of rictor, causes metabolic changes and results in muscle dystrophy. *Cell Metab* **8**: 411-424

Berglund ED, Li CY, Bina HA, Lynes SE, Michael MD, Shanafelt AB, Kharitononkov A, Wasserman DH (2009) Fibroblast growth factor 21 controls glycemia via regulation of hepatic glucose flux and insulin sensitivity. *Endocrinology* **150**: 4084-4093

Bodine SC, Stitt TN, Gonzalez M, Kline WO, Stover GL, Bauerlein R, Zlotchenko E, Scrimgeour A, Lawrence JC, Glass DJ, Yancopoulos GD (2001) Akt/mTOR pathway is a crucial regulator of skeletal muscle hypertrophy and can prevent muscle atrophy in vivo. *Nat Cell Biol* **3**: 1014-1019

Bookout AL, de Groot MH, Owen BM, Lee S, Gautron L, Lawrence HL, Ding X, Elmquist JK, Takahashi JS, Mangelsdorf DJ, Kliewer SA (2013) FGF21 regulates metabolism and circadian behavior by acting on the nervous system. *Nat Med* **19**: 1147-1152

Bostrom P, Wu J, Jedrychowski MP, Korde A, Ye L, Lo JC, Rasbach KA, Bostrom EA, Choi JH, Long JZ, Kajimura S, Zingaretti MC, Vind BF, Tu H, Cinti S, Hojlund K, Gygi SP, Spiegelman BM (2012) A PGC1-alpha-dependent myokine that drives brown-fat-like development of white fat and thermogenesis. *Nature* **481**: 463-468

Brodbeck D, Cron P, Hemmings BA (1999) A human protein kinase Bgamma with regulatory phosphorylation sites in the activation loop and in the C-terminal hydrophobic domain. *J Biol Chem* **274**: 9133-9136

Cartee GD (2015) Roles of TBC1D1 and TBC1D4 in insulin- and exercise-stimulated glucose transport of skeletal muscle. *Diabetologia* **58**: 19-30

Castets P, Lin S, Rion N, Di Fulvio S, Romanino K, Guridi M, Frank S, Tintignac LA, Sinnreich M, Ruegg MA (2013) Sustained activation of mTORC1 in skeletal muscle inhibits constitutive and starvation-induced autophagy and causes a severe, late-onset myopathy. *Cell Metab* **17**: 731-744

Chau MD, Gao J, Yang Q, Wu Z, Gromada J (2010) Fibroblast growth factor 21 regulates energy metabolism by activating the AMPK-SIRT1-PGC-1alpha pathway. *Proc Natl Acad Sci U S A* **107**: 12553-12558

Chavez AO, Molina-Carrion M, Abdul-Ghani MA, Folli F, DeFronzo RA, Tripathy D (2009) Circulating fibroblast growth factor-21 is elevated in impaired glucose tolerance and type 2 diabetes and correlates with muscle and hepatic insulin resistance. *Diabetes Care* **32**: 1542-1546

Chen W, Hoo RL, Konishi M, Itoh N, Lee PC, Ye HY, Lam KS, Xu A (2011) Growth hormone induces hepatic production of fibroblast growth factor 21 through a mechanism dependent on lipolysis in adipocytes. *J Biol Chem* **286**: 34559-34566

Chen WS, Xu PZ, Gottlob K, Chen ML, Sokol K, Shiyanova T, Roninson I, Weng W, Suzuki R, Tobe K, Kadowaki T, Hay N (2001) Growth retardation and increased apoptosis in mice with homozygous disruption of the Akt1 gene. *Genes Dev* **15**: 2203-2208

Cornu M, Oppliger W, Albert V, Robitaille AM, Trapani F, Quagliata L, Fuhrer T, Sauer U, Terracciano L, Hall MN (2014) Hepatic mTORC1 controls locomotor activity, body temperature, and lipid metabolism through FGF21. *Proc Natl Acad Sci U S A* **111**: 11592-11599

Cruz Guzman Odel R, Chavez Garcia AL, Rodriguez-Cruz M (2012) Muscular dystrophies at different ages: metabolic and endocrine alterations. *Int J Endocrinol* **2012**: 485376

Cunningham JT, Rodgers JT, Arlow DH, Vazquez F, Mootha VK, Puigserver P (2007) mTOR controls mitochondrial oxidative function through a YY1-PGC-1alpha transcriptional complex. *Nature* **450**: 736-740

D'Amico A, Bertini E (2013) Metabolic neuropathies and myopathies. *Handb Clin Neurol* **113**: 1437-1455

Dasarathy S, Yang Y, McCullough AJ, Marczewski S, Bennett C, Kalhan SC (2011) Elevated hepatic fatty acid oxidation, high plasma fibroblast growth factor 21, and fasting bile acids in nonalcoholic steatohepatitis. *Eur J Gastroenterol Hepatol* **23**: 382-388

De Palma S, Capitanio D, Vasso M, Braghetta P, Scotton C, Bonaldo P, Lochmuller H, Muntoni F, Ferlini A, Gelfi C (2014) Muscle proteomics reveals novel insights into the pathophysiological mechanisms of collagen VI myopathies. *J Proteome Res* **13**: 5022-5030

DeFronzo RA, Tripathy D (2009) Skeletal muscle insulin resistance is the primary defect in type 2 diabetes. *Diabetes Care* **32 Suppl 2**: S157-163

Deldicque L, Hespel P, Francaux M (2012) Endoplasmic reticulum stress in skeletal muscle: origin and metabolic consequences. *Exerc Sport Sci Rev* **40**: 43-49

DePirro R, Lauro R, Testa I, Ferretti I, De Martinis C, Dellattonio R (1982) Decreased insulin receptors but normal glucose metabolism in Duchenne muscular dystrophy. *Science* **216**: 311-313

Ding X, Boney-Montoya J, Owen BM, Bookout AL, Coate KC, Mangelsdorf DJ, Kliewer SA (2012) betaKlotho is required for fibroblast growth factor 21 effects on growth and metabolism. *Cell Metab* **16**: 387-393

Domingo P, Gallego-Escuredo JM, Domingo JC, Gutierrez Mdel M, Mateo MG, Fernandez I, Vidal F, Giralt M, Villarroya F (2010) Serum FGF21 levels are elevated in association with lipodystrophy, insulin resistance and biomarkers of liver injury in HIV-1-infected patients. *Aids* **24**: 2629-2637

Dushay J, Chui PC, Gopalakrishnan GS, Varela-Rey M, Crawley M, Fisher FM, Badman MK, Martinez-Chantar ML, Maratos-Flier E (2010) Increased fibroblast growth factor 21 in obesity and nonalcoholic fatty liver disease. *Gastroenterology* **139**: 456-463

Duvel K, Yecies JL, Menon S, Raman P, Lipovsky AI, Souza AL, Triantafellow E, Ma Q, Gorski R, Cleaver S, Vander Heiden MG, MacKeigan JP, Finan PM, Clish CB, Murphy LO, Manning BD (2010) Activation of a metabolic gene regulatory network downstream of mTOR complex 1. *Mol Cell* **39**: 171-183

Easton RM, Cho H, Roovers K, Shineman DW, Mizrahi M, Forman MS, Lee VM, Szabolcs M, de Jong R, Oltersdorf T, Ludwig T, Efstratiadis A, Birnbaum MJ (2005) Role for Akt3/protein kinase Bgamma in attainment of normal brain size. *Mol Cell Biol* **25**: 1869-1878

Ebert SM, Dyle MC, Kunkel SD, Bullard SA, Bongers KS, Fox DK, Dierdorff JM, Foster ED, Adams CM (2012) Stress-induced skeletal muscle Gadd45a expression reprograms myonuclei and causes muscle atrophy. *J Biol Chem* **287**: 27290-27301

Ebert SM, Monteys AM, Fox DK, Bongers KS, Shields BE, Malmberg SE, Davidson BL, Suneja M, Adams CM (2010) The transcription factor ATF4 promotes skeletal myofiber atrophy during fasting. *Mol Endocrinol* **24**: 790-799

Emanuelli B, Vienberg SG, Smyth G, Cheng C, Stanford KI, Arumugam M, Michael MD, Adams AC, Kharitononkov A, Kahn CR (2014) Interplay between FGF21 and insulin action in the liver regulates metabolism. *J Clin Invest* **124**: 515-527

Even PC, Nadkarni NA (2012) Indirect calorimetry in laboratory mice and rats: principles, practical considerations, interpretation and perspectives. *Am J Physiol Regul Integr Comp Physiol* **303**: R459-476

Feldman BJ, Streeper RS, Farese RV, Jr., Yamamoto KR (2006) Myostatin modulates adipogenesis to generate adipocytes with favorable metabolic effects. *Proc Natl Acad Sci U S A* **103**: 15675-15680

Fisher FM, Chui PC, Antonellis PJ, Bina HA, Kharitononkov A, Flier JS, Maratos-Flier E (2010) Obesity is a fibroblast growth factor 21 (FGF21)-resistant state. *Diabetes* **59**: 2781-2789

Fisher FM, Kleiner S, Douris N, Fox EC, Mepani RJ, Verdeguer F, Wu J, Kharitononkov A, Flier JS, Maratos-Flier E, Spiegelman BM (2012) FGF21 regulates PGC-1alpha and browning of white adipose tissues in adaptive thermogenesis. *Genes Dev* **26**: 271-281

Flamment M, Hajduch E, Ferre P, Foufelle F (2012) New insights into ER stress-induced insulin resistance. *Trends Endocrinol Metab* **23**: 381-390

Fox DK, Ebert SM, Bongers KS, Dyle MC, Bullard SA, Dierdorff JM, Kunkel SD, Adams CM (2014) p53 and ATF4 mediate distinct and additive pathways to skeletal muscle atrophy during limb immobilization. *Am J Physiol Endocrinol Metab* **307**: E245-261

Fraenkel M, Ketzinel-Gilad M, Ariav Y, Pappo O, Karaca M, Castel J, Berthault MF, Magnan C, Cerasi E, Kaiser N, Leibowitz G (2008) mTOR inhibition by rapamycin prevents beta-cell adaptation to hyperglycemia and exacerbates the metabolic state in type 2 diabetes. *Diabetes* **57**: 945-957

Gaich G, Chien JY, Fu H, Glass LC, Deeg MA, Holland WL, Kharitononkov A, Bumol T, Schilske HK, Moller DE (2013) The effects of LY2405319, an FGF21 analog, in obese human subjects with type 2 diabetes. *Cell Metab* **18**: 333-340

Ge X, Chen C, Hui X, Wang Y, Lam KS, Xu A (2011) Fibroblast growth factor 21 induces glucose transporter-1 expression through activation of the serum response factor/Ets-like protein-1 in adipocytes. *J Biol Chem* **286**: 34533-34541

Gimeno RE, Moller DE (2014) FGF21-based pharmacotherapy - potential utility for metabolic disorders. *Trends Endocrinol Metab*

Goodman CA, Mayhew DL, Hornberger TA (2011) Recent progress toward understanding the molecular mechanisms that regulate skeletal muscle mass. *Cell Signal* **23**: 1896-1906

Guertin DA, Stevens DM, Thoreen CC, Burds AA, Kalaany NY, Moffat J, Brown M, Fitzgerald KJ, Sabatini DM (2006) Ablation in mice of the mTORC components raptor, rictor, or mLST8 reveals that mTORC2 is required for signaling to Akt-FOXO and PKCalpha, but not S6K1. *Dev Cell* **11**: 859-871

Guridi M, Tintignac LA, Lin S, Kupr B, Castets P, Rüegg MA (2015) Activation of mTORC1 in skeletal muscle regulates whole-body metabolism through FGF21. *Sci Signal* **8**

Hagiwara A, Cornu M, Cybulski N, Polak P, Betz C, Trapani F, Terracciano L, Heim MH, Ruegg MA, Hall MN (2012) Hepatic mTORC2 activates glycolysis and lipogenesis through Akt, glucokinase, and SREBP1c. *Cell Metab* **15**: 725-738

Hamrick M (2010) JMNI special issue: basic science and mechanisms of muscle-bone interactions. *J Musculoskelet Neuronal Interact* **10**: 1-2

Harding HP, Novoa I, Zhang Y, Zeng H, Wek R, Schapira M, Ron D (2000) Regulated translation initiation controls stress-induced gene expression in mammalian cells. *Mol Cell* **6**: 1099-1108

Hetz C (2012) The unfolded protein response: controlling cell fate decisions under ER stress and beyond. *Nat Rev Mol Cell Biol* **13**: 89-102

Holland WL, Adams AC, Brozinick JT, Bui HH, Miyauchi Y, Kusminski CM, Bauer SM, Wade M, Singhal E, Cheng CC, Volk K, Kuo MS, Gordillo R, Kharitonov A, Scherer PE (2013) An FGF21-adiponectin-ceramide axis controls energy expenditure and insulin action in mice. *Cell Metab* **17**: 790-797

Hondares E, Rosell M, Gonzalez FJ, Giralt M, Iglesias R, Villarroya F (2010) Hepatic FGF21 expression is induced at birth via PPARalpha in response to milk intake and contributes to thermogenic activation of neonatal brown fat. *Cell Metab* **11**: 206-212

Houde VP, Brule S, Festuccia WT, Blanchard PG, Bellmann K, Deshaies Y, Marette A (2010) Chronic rapamycin treatment causes glucose intolerance and hyperlipidemia by upregulating hepatic gluconeogenesis and impairing lipid deposition in adipose tissue. *Diabetes* **59**: 1338-1348

Huang X, Yu C, Jin C, Yang C, Xie R, Cao D, Wang F, McKeehan WL (2006) Forced expression of hepatocyte-specific fibroblast growth factor 21 delays initiation of chemically induced hepatocarcinogenesis. *Mol Carcinog* **45**: 934-942



Huang Y, Li X, Wang Y, Wang H, Huang C, Li J (2014) Endoplasmic reticulum stress-induced hepatic stellate cell apoptosis through calcium-mediated JNK/P38 MAPK and Calpain/Caspase-12 pathways. *Mol Cell Biochem* **394**: 1-12

Iannitti T, Palmieri B (2011) Clinical and experimental applications of sodium phenylbutyrate. *Drugs R D* **11**: 227-249

Inagaki T, Dutchak P, Zhao G, Ding X, Gautron L, Parameswara V, Li Y, Goetz R, Mohammadi M, Esser V, Elmquist JK, Gerard RD, Burgess SC, Hammer RE, Mangelsdorf DJ, Kliewer SA (2007) Endocrine regulation of the fasting response by PPARalpha-mediated induction of fibroblast growth factor 21. *Cell Metab* **5**: 415-425

Inagaki T, Lin VY, Goetz R, Mohammadi M, Mangelsdorf DJ, Kliewer SA (2008) Inhibition of growth hormone signaling by the fasting-induced hormone FGF21. *Cell Metab* **8**: 77-83

Inoki K, Zhu T, Guan KL (2003) TSC2 mediates cellular energy response to control cell growth and survival. *Cell* **115**: 577-590

Ishida N (2009) Role of PPARalpha in the control of torpor through FGF21-NPY pathway: From circadian clock to seasonal change in mammals. *PPAR Res* **2009**: 412949

Izumiya Y, Bina HA, Ouchi N, Akasaki Y, Kharitonov A, Walsh K (2008a) FGF21 is an Akt-regulated myokine. *FEBS Lett* **582**: 3805-3810

Izumiya Y, Hopkins T, Morris C, Sato K, Zeng L, Viereck J, Hamilton JA, Ouchi N, LeBrasseur NK, Walsh K (2008b) Fast/Glycolytic muscle fiber growth reduces fat mass and improves metabolic parameters in obese mice. *Cell Metab* **7**: 159-172

Jiang S, Yan C, Fang QC, Shao ML, Zhang YL, Liu Y, Deng YP, Shan B, Liu JQ, Li HT, Yang L, Zhou J, Dai Z, Jia WP (2014) Fibroblast growth factor 21 is regulated by the IRE1alpha-XBP1 branch of the unfolded protein response and counteracts endoplasmic reticulum stress-induced hepatic steatosis. *J Biol Chem* **289**: 29751-29765

Johnson CL, Weston JY, Chadi SA, Fazio EN, Huff MW, Kharitonov A, Koester A, Pin CL (2009) Fibroblast growth factor 21 reduces the severity of cerulein-induced pancreatitis in mice. *Gastroenterology* **137**: 1795-1804

Joseph A, Neff K, Richard J, Gao L, Bangari D, Joly M, Culm-Merdek K, Garman R, Williams J, Richards S, Ruzek M (2012) Transient low-dose methotrexate induces tolerance to murine anti-thymocyte globulin and together they promote long-term allograft survival. *J Immunol* **189**: 732-743

Jung DY, Chalasani U, Pan N, Friedline RH, Prosdocimo DA, Nam M, Azuma Y, Maganti R, Yu K, Velagapudi A, O'Sullivan-Murphy B, Sartoretto JL, Jain MK, Cooper MP, Urano F, Kim JK, Gray S (2013) KLF15 is a molecular link between endoplasmic reticulum stress and insulin resistance. *PLoS One* **8**: e77851

Kahn SE, Hull RL, Utzschneider KM (2006) Mechanisms linking obesity to insulin resistance and type 2 diabetes. *Nature* **444**: 840-846

Kato H, Nakajima S, Saito Y, Takahashi S, Katoh R, Kitamura M (2012) mTORC1 serves ER stress-triggered apoptosis via selective activation of the IRE1-JNK pathway. *Cell Death Differ* **19**: 310-320

Keipert S, Ost M, Johann K, Imber F, Jastroch M, van Schothorst EM, Keijer J, Klaus S (2014) Skeletal muscle mitochondrial uncoupling drives endocrine cross-talk through the induction of FGF21 as a myokine. *Am J Physiol Endocrinol Metab* **306**: E469-482

Kenerson HL, Subramanian S, McIntyre R, Kazami M, Yeung RS (2015) Livers with constitutive mTORC1 activity resist steatosis independent of feedback suppression of Akt. *PLoS One* **10**: e0117000

Khamzina L, Veilleux A, Bergeron S, Marette A (2005) Increased activation of the mammalian target of rapamycin pathway in liver and skeletal muscle of obese rats: possible involvement in obesity-linked insulin resistance. *Endocrinology* **146**: 1473-1481

Khan RJ, Andermann E, Fantus IG (1986) Glucose intolerance in Friedreich's ataxia: association with insulin resistance and decreased insulin binding. *Metabolism* **35**: 1017-1023

Kharitonov A (2009) FGFs and metabolism. *Curr Opin Pharmacol* **9**: 805-810

Kharitonov A, Beals JM, Micanovic R, Strifler BA, Rathnachalam R, Wroblewski VJ, Li S, Koester A, Ford AM, Coskun T, Dunbar JD, Cheng CC, Frye CC, Bumol TF, Moller DE (2013) Rational design of a fibroblast growth factor 21-based clinical candidate, LY2405319. *PLoS One* **8**: e58575

Kharitonov A, Shiyanova TL, Koester A, Ford AM, Micanovic R, Galbreath EJ, Sandusky GE, Hammond LJ, Moyers JS, Owens RA, Gromada J, Brozinick JT, Hawkins ED, Wroblewski VJ, Li DS, Mehrbod F, Jaskunas SR, Shanafelt AB (2005) FGF-21 as a novel metabolic regulator. *J Clin Invest* **115**: 1627-1635

Kim HJ, Jamart C, Deldicque L, An GL, Lee YH, Kim CK, Raymackers JM, Francaux M (2011) Endoplasmic reticulum stress markers and ubiquitin-proteasome pathway activity in response to a 200-km run. *Med Sci Sports Exerc* **43**: 18-25

Kim HW, Lee JE, Cha JJ, Hyun YY, Kim JE, Lee MH, Song HK, Nam DH, Han JY, Han SY, Han KH, Kang YS, Cha DR (2013a) Fibroblast growth factor 21 improves insulin resistance and ameliorates renal injury in db/db mice. *Endocrinology* **154**: 3366-3376

Kim I, Xu W, Reed JC (2008) Cell death and endoplasmic reticulum stress: disease relevance and therapeutic opportunities. *Nat Rev Drug Discov* **7**: 1013-1030

Kim KH, Jeong YT, Kim SH, Jung HS, Park KS, Lee HY, Lee MS (2013b) Metformin-induced inhibition of the mitochondrial respiratory chain increases FGF21 expression via ATF4 activation. *Biochem Biophys Res Commun* **440**: 76-81

Kim KH, Jeong YT, Oh H, Kim SH, Cho JM, Kim YN, Kim SS, Kim do H, Hur KY, Kim HK, Ko T, Han J, Kim HL, Kim J, Back SH, Komatsu M, Chen H, Chan DC, Konishi M, Itoh N, Choi CS, Lee MS (2013c) Autophagy deficiency leads to protection from obesity and insulin resistance by inducing Fgf21 as a mitokine. *Nat Med* **19**: 83-92

Kim KH, Lee MS (2014) FGF21 as a Stress Hormone: The Roles of FGF21 in Stress Adaptation and the Treatment of Metabolic Diseases. *Diabetes Metab J* **38**: 245-251

Kim SH, Kim KH, Kim HK, Kim MJ, Back SH, Konishi M, Itoh N, Lee MS (2015) Fibroblast growth factor 21 participates in adaptation to endoplasmic reticulum stress and attenuates obesity-induced hepatic metabolic stress. *Diabetologia* **58**: 809-818

Kong XC, Barzaghi P, Rugg MA (2004) Inhibition of synapse assembly in mammalian muscle in vivo by RNA interference. *EMBO Rep* **5**: 183-188

Kramer HF, Witczak CA, Taylor EB, Fujii N, Hirshman MF, Goodyear LJ (2006) AS160 regulates insulin- and contraction-stimulated glucose uptake in mouse skeletal muscle. *J Biol Chem* **281**: 31478-31485

Kubicky RA, Wu S, Kharitonov A, De Luca F (2012) Role of fibroblast growth factor 21 (FGF21) in undernutrition-related attenuation of growth in mice. *Endocrinology* **153**: 2287-2295

Kurosu H, Kuro OM (2009) Endocrine fibroblast growth factors as regulators of metabolic homeostasis. *Biofactors* **35**: 52-60

Kwiatkowski DJ, Zhang H, Bandura JL, Heiberger KM, Glogauer M, el-Hashemite N, Onda H (2002) A mouse model of TSC1 reveals sex-dependent lethality from liver hemangiomas, and up-regulation of p70S6 kinase activity in Tsc1 null cells. *Hum Mol Genet* **11**: 525-534

Lamming DW, Sabatini DM (2013) A Central role for mTOR in lipid homeostasis. *Cell Metab* **18**: 465-469

Lamming DW, Ye L, Katajisto P, Goncalves MD, Saitoh M, Stevens DM, Davis JG, Salmon AB, Richardson A, Ahima RS, Guertin DA, Sabatini DM, Baur JA (2012) Rapamycin-induced insulin resistance is mediated by mTORC2 loss and uncoupled from longevity. *Science* **335**: 1638-1643

Laplanche M, Sabatini DM (2012) mTOR signaling in growth control and disease. *Cell* **149**: 274-293

Laplanche M, Sabatini DM (2013) Regulation of mTORC1 and its impact on gene expression at a glance. *J Cell Sci* **126**: 1713-1719

Lavery GG, Walker EA, Turan N, Rogoff D, Ryder JW, Shelton JM, Richardson JA, Falciani F, White PC, Stewart PM, Parker KL, McMillan DR (2008) Deletion of hexose-6-phosphate dehydrogenase activates the unfolded protein response pathway and induces skeletal myopathy. *J Biol Chem* **283**: 8453-8461

LeRoith D, Yakar S (2007) Mechanisms of Disease: metabolic effects of growth hormone and insulin-like growth factor 1. *Nat Clin Pract End Met* **3**: 302-310

Li S, Brown MS, Goldstein JL (2010) Bifurcation of insulin signaling pathway in rat liver: mTORC1 required for stimulation of lipogenesis, but not inhibition of gluconeogenesis. *Proc Natl Acad Sci U S A* **107**: 3441-3446

Lieberman AP, Puertollano R, Raben N, Slaugenhaupt S, Walkley SU, Ballabio A (2012) Autophagy in lysosomal storage disorders. *Autophagy* **8**: 719-730

Lin Z, Tian H, Lam KS, Lin S, Hoo RC, Konishi M, Itoh N, Wang Y, Bornstein SR, Xu A, Li X (2013) Adiponectin mediates the metabolic effects of FGF21 on glucose homeostasis and insulin sensitivity in mice. *Cell Metab* **17**: 779-789

Lindegaard B, Hvid T, Grondahl T, Frosig C, Gerstoft J, Hojman P, Pedersen BK (2013) Expression of fibroblast growth factor-21 in muscle is associated with lipodystrophy, insulin resistance and lipid disturbances in patients with HIV. *PLoS One* **8**: e55632

Llagostera E, Catalucci D, Marti L, Liesa M, Camps M, Ciaraldi TP, Kondo R, Reddy S, Dillmann WH, Palacin M, Zorzano A, Ruiz-Lozano P, Gomis R, Kaliman P (2007) Role of myotonic dystrophy protein kinase (DMPK) in glucose homeostasis and muscle insulin action. *PLoS One* **2**: e1134

Luo Y, McKeenan WL (2013) Stressed Liver and Muscle Call on Adipocytes with FGF21. *Front Endocrinol (Lausanne)* **4**: 194

Ma Y, Hendershot LM (2004) ER chaperone functions during normal and stress conditions. *J Chem Neuroanat* **28**: 51-65

Maffucci T, Falasca M (2001) Specificity in pleckstrin homology (PH) domain membrane targeting: a role for a phosphoinositide-protein co-operative mechanism. *FEBS Lett* **506**: 173-179

Mammucari C, Milan G, Romanello V, Masiero E, Rudolf R, Del Piccolo P, Burden SJ, Di Lisi R, Sandri C, Zhao J, Goldberg AL, Schiaffino S, Sandri M (2007) FoxO3 controls autophagy in skeletal muscle in vivo. *Cell Metab* **6**: 458-471

Marciniak SJ, Ron D (2006) Endoplasmic reticulum stress signaling in disease. *Physiol Rev* **86**: 1133-1149

Mariano A, Henning A, Han R (2013) Dysferlin-deficient muscular dystrophy and innate immune activation. *Febs J* **280**: 4165-4176

Markan KR, Naber MC, Ameka MK, Anderegg MD, Mangelsdorf DJ, Kliewer SA, Mohammadi M, Potthoff MJ (2014) Circulating FGF21 is liver derived and enhances glucose uptake during refeeding and overfeeding. *Diabetes* **63**: 4057-4063

Mashili FL, Austin RL, Deshmukh AS, Fritz T, Caidahl K, Bergdahl K, Zierath JR, Chibalin AV, Moller DE, Kharitonov A, Krook A (2011) Direct effects of FGF21 on glucose uptake in human skeletal muscle: implications for type 2 diabetes and obesity. *Diabetes Metab Res Rev* **27**: 286-297

Massa ML, Gagliardino JJ, Francini F (2011) Liver glucokinase: An overview on the regulatory mechanisms of its activity. *IUBMB Life* **63**: 1-6

McGee SL, van Denderen BJ, Howlett KF, Mollica J, Schertzer JD, Kemp BE, Hargreaves M (2008) AMP-activated protein kinase regulates GLUT4 transcription by phosphorylating histone deacetylase 5. *Diabetes* **57**: 860-867

McGuinness OP, Ayala JE, Laughlin MR, Wasserman DH (2009) NIH experiment in centralized mouse phenotyping: the Vanderbilt experience and recommendations for evaluating glucose homeostasis in the mouse. *Am J Physiol Endocrinol Metab* **297**: E849-855

McPherron AC, Lawler AM, Lee SJ (1997) Regulation of skeletal muscle mass in mice by a new TGF-beta superfamily member. *Nature* **387**: 83-90

Meyer C, Dostou JM, Welle SL, Gerich JE (2002) Role of human liver, kidney, and skeletal muscle in postprandial glucose homeostasis. *Am J Physiol Endocrinol Metab* **282**: E419-427

Moll J, Barzaghi P, Lin S, Bezakova G, Lochmuller H, Engvall E, Muller U, Ruegg MA (2001) An agrin minigene rescues dystrophic symptoms in a mouse model for congenital muscular dystrophy. *Nature* **413**: 302-307

Moorwood C, Barton ER (2014) Caspase-12 ablation preserves muscle function in the mdx mouse. *Hum Mol Genet* **23**: 5325-5341

Mounir Z, Krishnamoorthy JL, Wang S, Papadopoulou B, Campbell S, Muller WJ, Hatzoglou M, Koromilas AE (2011) Akt determines cell fate through inhibition of the PERK-eIF2alpha phosphorylation pathway. *Sci Signal* **4**: ra62

Moxley RT, 3rd, Griggs RC, Goldblatt D, VanGelder V, Herr BE, Thiel R (1978) Decreased insulin sensitivity of forearm muscle in myotonic dystrophy. *J Clin Invest* **62**: 857-867

Moxley RT, Corbett AJ, Minaker KL, Rowe JW (1984) Whole body insulin resistance in myotonic dystrophy. *Ann Neurol* **15**: 157-162

Muise ES, Azzolina B, Kuo DW, El-Sherbeini M, Tan Y, Yuan X, Mu J, Thompson JR, Berger JP, Wong KK (2008) Adipose fibroblast growth factor 21 is up-regulated by peroxisome proliferator-activated receptor gamma and altered metabolic states. *Mol Pharmacol* **74**: 403-412

Newman JC, Verdin E Ketone bodies as signaling metabolites. *Trends in Endocrinology & Metabolism* **25**: 42-52

Newman JC, Verdin E (2014) Ketone bodies as signaling metabolites. *Trends Endocrinol Metab* **25**: 42-52

Nielsen AR, Mounier R, Plomgaard P, Mortensen OH, Penkowa M, Speerschneider T, Pilegaard H, Pedersen BK (2007) Expression of interleukin-15 in human skeletal muscle effect of exercise and muscle fibre type composition. *J Physiol* **584**: 305-312

Nishimura T, Nakatake Y, Konishi M, Itoh N (2000) Identification of a novel FGF, FGF-21, preferentially expressed in the liver. *Biochimica et biophysica acta* **1492**: 203-206

O'Neill BT, Lauritzen HP, Hirshman MF, Smyth G, Goodyear LJ, Kahn CR (2015) Differential Role of Insulin/IGF-1 Receptor Signaling in Muscle Growth and Glucose Homeostasis. *Cell Rep* **11**: 1220-1235

Ogawa Y, Kurosu H, Yamamoto M, Nandi A, Rosenblatt KP, Goetz R, Eliseenkova AV, Mohammadi M, Kuro-o M (2007) BetaKlotho is required for metabolic activity of fibroblast growth factor 21. *Proc Natl Acad Sci U S A* **104**: 7432-7437

Ohoka N, Yoshii S, Hattori T, Onozaki K, Hayashi H (2005) TRB3, a novel ER stress-inducible gene, is induced via ATF4-CHOP pathway and is involved in cell death. *Embo J* **24**: 1243-1255

Omar BA, Andersen B, Hald J, Raun K, Nishimura E, Ahren B (2014) Fibroblast growth factor 21 (FGF21) and glucagon-like peptide 1 contribute to diabetes resistance in glucagon receptor-deficient mice. *Diabetes* **63**: 101-110

Osborn O, Olefsky JM (2012) The cellular and signaling networks linking the immune system and metabolism in disease. *Nat Med* **18**: 363-374

Osowski CM, Urano F (2011a) The binary switch that controls the life and death decisions of ER stressed beta cells. *Curr Opin Cell Biol* **23**: 207-215

Osowski CM, Urano F (2011b) Measuring ER stress and the unfolded protein response using mammalian tissue culture system. *Methods Enzymol* **490**: 71-92

Owen BM, Bookout AL, Ding X, Lin VY, Atkin SD, Gautron L, Kliewer SA, Mangelsdorf DJ (2013) FGF21 contributes to neuroendocrine control of female reproduction. *Nat Med* **19**: 1153-1156

Owen BM, Ding X, Morgan DA, Coate KC, Bookout AL, Rahmouni K, Kliewer SA, Mangelsdorf DJ (2014) FGF21 acts centrally to induce sympathetic nerve activity, energy expenditure, and weight loss. *Cell Metab* **20**: 670-677

Ozcan U, Ozcan L, Yilmaz E, Duvel K, Sahin M, Manning BD, Hotamisligil GS (2008) Loss of the tuberous sclerosis complex tumor suppressors triggers the unfolded protein response to regulate insulin signaling and apoptosis. *Mol Cell* **29**: 541-551

Ozcan U, Yilmaz E, Ozcan L, Furuhashi M, Vaillancourt E, Smith RO, Gorgun CZ, Hotamisligil GS (2006) Chemical chaperones reduce ER stress and restore glucose homeostasis in a mouse model of type 2 diabetes. *Science* **313**: 1137-1140

Pedersen BK, Febbraio MA (2008) Muscle as an endocrine organ: focus on muscle-derived interleukin-6. *Physiol Rev* **88**: 1379-1406

Pedersen BK, Febbraio MA (2012) Muscles, exercise and obesity: skeletal muscle as a secretory organ. *Nat Rev Endocrinol* **8**: 457-465

Peterson TR, Laplante M, Thoreen CC, Sancak Y, Kang SA, Kuehl WM, Gray NS, Sabatini DM (2009) DEPTOR is an mTOR inhibitor frequently overexpressed in multiple myeloma cells and required for their survival. *Cell* **137**: 873-886

Peterson TR, Sengupta SS, Harris TE, Carmack AE, Kang SA, Balderas E, Guertin DA, Madden KL, Carpenter AE, Finck BN, Sabatini DM (2011) mTOR complex 1 regulates lipin 1 localization to control the SREBP pathway. *Cell* **146**: 408-420

Polak P, Cybulski N, Feige JN, Auwerx J, Ruegg MA, Hall MN (2008a) Adipose-specific knockout of raptor results in lean mice with enhanced mitochondrial respiration. *Cell Metab* **8**: 399-410

Polak P, Cybulski N, Feige JN, Auwerx J, Ruegg MA, Hall MN (2008b) Adipose-specific knockout of raptor results in lean mice with enhanced mitochondrial respiration. *Cell metabolism* **8**: 399-410

Polak P, Hall MN (2009) mTOR and the control of whole body metabolism. *Curr Opin Cell Biol* **21**: 209-218

Potthoff MJ, Inagaki T, Satapati S, Ding X, He T, Goetz R, Mohammadi M, Finck BN, Mangelsdorf DJ, Kliewer SA, Burgess SC (2009) FGF21 induces PGC-1 $\alpha$  and regulates carbohydrate and fatty acid metabolism during the adaptive starvation response. *Proc Natl Acad Sci U S A* **106**: 10853-10858

Puigserver P (2005) Tissue-specific regulation of metabolic pathways through the transcriptional coactivator PGC1- $\alpha$ . *Int J Obes (Lond)* **29 Suppl 1**: S5-9

Ramos FJ, Chen SC, Garelick MG, Dai DF, Liao CY, Schreiber KH, MacKay VL, An EH, Strong R, Ladiges WC, Rabinovitch PS, Kaerberlein M, Kennedy BK (2012) Rapamycin reverses elevated mTORC1 signaling in lamin A/C-deficient mice, rescues cardiac and skeletal muscle function, and extends survival. *Sci Transl Med* **4**: 144ra103

Reaven GM, Hollenbeck C, Jeng CY, Wu MS, Chen YD (1988) Measurement of plasma glucose, free fatty acid, lactate, and insulin for 24 h in patients with NIDDM. *Diabetes* **37**: 1020-1024

Reyes ET, Perurena OH, Festoff BW, Jorgensen R, Moore WV (1984) Insulin resistance in amyotrophic lateral sclerosis. *J Neurol Sci* **63**: 317-324

Ribas F, Villarroya J, Hondares E, Giralt M, Villarroya F (2014) FGF21 expression and release in muscle cells: involvement of MyoD and regulation by mitochondria-driven signalling. *Biochem J* **463**: 191-199

Riggs AC, Bernal-Mizrachi E, Ohsugi M, Wasson J, Fatrai S, Welling C, Murray J, Schmidt RE, Herrera PL, Permutt MA (2005) Mice conditionally lacking the Wolfram gene in pancreatic islet beta cells exhibit



diabetes as a result of enhanced endoplasmic reticulum stress and apoptosis. *Diabetologia* **48**: 2313-2321

Risson V, Mazelin L, Roceri M, Sanchez H, Moncollin V, Corneloup C, Richard-Bulteau H, Vignaud A, Baas D, Defour A, Freyssenet D, Tanti JF, Le-Marchand-Brustel Y, Ferrier B, Conjard-Duplany A, Romanino K, Bauche S, Hantai D, Mueller M, Kozma SC, Thomas G, Ruegg MA, Ferry A, Pende M, Bigard X, Koulmann N, Schaeffer L, Gangloff YG (2009a) Muscle inactivation of mTOR causes metabolic and dystrophin defects leading to severe myopathy. *The Journal of cell biology* **187**: 859-874

Risson V, Mazelin L, Roceri M, Sanchez H, Moncollin V, Corneloup C, Richard-Bulteau H, Vignaud A, Baas D, Defour A, Freyssenet D, Tanti JF, Le-Marchand-Brustel Y, Ferrier B, Conjard-Duplany A, Romanino K, Bauche S, Hantai D, Mueller M, Kozma SC, Thomas G, Ruegg MA, Ferry A, Pende M, Bigard X, Koulmann N, Schaeffer L, Gangloff YG (2009b) Muscle inactivation of mTOR causes metabolic and dystrophin defects leading to severe myopathy. *J Cell Biol* **187**: 859-874

Rodriguez-Cruz M, Sanchez R, Escobar RE, Cruz-Guzman Odel R, Lopez-Alarcon M, Bernabe Garcia M, Coral-Vazquez R, Matute G, Velazquez Wong AC (2015) Evidence of Insulin Resistance and Other Metabolic Alterations in Boys with Duchenne or Becker Muscular Dystrophy. *Int J Endocrinol* **2015**: 867273

Romanino K, Mazelin L, Albert V, Conjard-Duplany A, Lin S, Bentzinger CF, Handschin C, Puigserver P, Zorzato F, Schaeffer L, Gangloff YG, Ruegg MA (2011) Myopathy caused by mammalian target of rapamycin complex 1 (mTORC1) inactivation is not reversed by restoring mitochondrial function. *Proc Natl Acad Sci U S A* **108**: 20808-20813

Rommel C, Bodine SC, Clarke BA, Rossman R, Nunez L, Stitt TN, Yancopoulos GD, Glass DJ (2001) Mediation of IGF-1-induced skeletal myotube hypertrophy by PI(3)K/Akt/mTOR and PI(3)K/Akt/GSK3 pathways. *Nat Cell Biol* **3**: 1009-1013

Sabatini DM, Erdjument-Bromage H, Lui M, Tempst P, Snyder SH (1994) RAFT1: a mammalian protein that binds to FKBP12 in a rapamycin-dependent fashion and is homologous to yeast TORs. *Cell* **78**: 35-43

Saito K, Lee S, Shiuchi T, Toda C, Kamijo M, Inagaki-Ohara K, Okamoto S, Minokoshi Y (2011) An enzymatic photometric assay for 2-deoxyglucose uptake in insulin-responsive tissues and 3T3-L1 adipocytes. *Anal Biochem* **412**: 9-17

Salvado L, Palomer X, Barroso E, Vazquez-Carrera M (2015) Targeting endoplasmic reticulum stress in insulin resistance. *Trends Endocrinol Metab* **26**: 438-448

Sammons MF, Price DA (2014) Modulation of adipose tissue thermogenesis as a method for increasing energy expenditure. *Bioorg Med Chem Lett* **24**: 425-429

Sandri M, Sandri C, Gilbert A, Skurk C, Calabria E, Picard A, Walsh K, Schiaffino S, Lecker SH, Goldberg AL (2004) Foxo transcription factors induce the atrophy-related ubiquitin ligase atrogin-1 and cause skeletal muscle atrophy. *Cell* **117**: 399-412

Sano H, Kane S, Sano E, Miinea CP, Asara JM, Lane WS, Garner CW, Lienhard GE (2003) Insulin-stimulated phosphorylation of a Rab GTPase-activating protein regulates GLUT4 translocation. *J Biol Chem* **278**: 14599-14602

Santalla A, Nogales-Gadea G, Ortenblad N, Brull A, de Luna N, Pinos T, Lucia A (2014) McArdle disease: a unique study model in sports medicine. *Sports Med* **44**: 1531-1544

Sarbassov DD, Ali SM, Sengupta S, Sheen JH, Hsu PP, Bagley AF, Markhard AL, Sabatini DM (2006) Prolonged rapamycin treatment inhibits mTORC2 assembly and Akt/PKB. *Mol Cell* **22**: 159-168

Savkur RS, Philips AV, Cooper TA (2001) Aberrant regulation of insulin receptor alternative splicing is associated with insulin resistance in myotonic dystrophy. *Nat Genet* **29**: 40-47

Schaap FG, Kremer AE, Lamers WH, Jansen PL, Gaemers IC (2013) Fibroblast growth factor 21 is induced by endoplasmic reticulum stress. *Biochimie* **95**: 692-699

Schroder M, Kaufman RJ (2005) The mammalian unfolded protein response. *Annu Rev Biochem* **74**: 739-789

Schultze SM, Hemmings BA, Niessen M, Tschopp O (2012) PI3K/AKT, MAPK and AMPK signalling: protein kinases in glucose homeostasis. *Expert Rev Mol Med* **14**: e1

Seale P, Bjork B, Yang W, Kajimura S, Chin S, Kuang S, Scime A, Devarakonda S, Conroe HM, Erdjument-Bromage H, Tempst P, Rudnicki MA, Beier DR, Spiegelman BM (2008) PRDM16 controls a brown fat/skeletal muscle switch. *Nature* **454**: 961-967

Seale P, Conroe HM, Estall J, Kajimura S, Frontini A, Ishibashi J, Cohen P, Cinti S, Spiegelman BM (2011) Prdm16 determines the thermogenic program of subcutaneous white adipose tissue in mice. *J Clin Invest* **121**: 96-105

Selman C, Tullet JM, Wieser D, Irvine E, Lingard SJ, Choudhury AI, Claret M, Al-Qassab H, Carmignac D, Ramadani F, Woods A, Robinson IC, Schuster E, Batterham RL, Kozma SC, Thomas G, Carling D, Okkenhaug K, Thornton JM, Partridge L, Gems D, Withers DJ (2009) Ribosomal protein S6 kinase 1 signaling regulates mammalian life span. *Science* **326**: 140-144

Serrano AL, Baeza-Raja B, Perdiguero E, Jardi M, Munoz-Canoves P (2008) Interleukin-6 is an essential regulator of satellite cell-mediated skeletal muscle hypertrophy. *Cell Metab* **7**: 33-44

Spitali P, Grumati P, Hiller M, Chrisam M, Aartsma-Rus A, Bonaldo P (2013) Autophagy is Impaired in the Tibialis Anterior of Dystrophin Null Mice. *PLoS Curr* **5**

Suomalainen A (2013) Fibroblast growth factor 21: a novel biomarker for human muscle-manifesting mitochondrial disorders. *Expert Opin Med Diagn* **7**: 313-317

Suomalainen A, Elo JM, Pietilainen KH, Hakonen AH, Sevastianova K, Korpela M, Isohanni P, Marjavaara SK, Tyni T, Kiuru-Enari S, Pihko H, Darin N, Ounap K, Kluijtmans LA, Paetau A, Buzkova J, Bindoff LA, Annunen-Rasila J, Uusimaa J, Rissanen A, Yki-Jarvinen H, Hirano M, Tulinius M, Smeitink J, Tyynismaa H (2011) FGF-21 as a biomarker for muscle-manifesting mitochondrial respiratory chain deficiencies: a diagnostic study. *Lancet Neurol* **10**: 806-818

Tan SX, Ng Y, Burchfield JG, Ramm G, Lambright DG, Stockli J, James DE (2012) The Rab GTPase-activating protein TBC1D4/AS160 contains an atypical phosphotyrosine-binding domain that interacts with plasma membrane phospholipids to facilitate GLUT4 trafficking in adipocytes. *Mol Cell Biol* **32**: 4946-4959

Tang H, Macpherson P, Marvin M, Meadows E, Klein WH, Yang XJ, Goldman D (2009) A histone deacetylase 4/myogenin positive feedback loop coordinates denervation-dependent gene induction and suppression. *Mol Biol Cell* **20**: 1120-1131

Thedieck K, Polak P, Kim ML, Molle KD, Cohen A, Jenö P, Arriemerlou C, Hall MN (2007) PRAS40 and PRR5-like protein are new mTOR interactors that regulate apoptosis. *PLoS One* **2**: e1217

Thoreen CC, Chantranupong L, Keys HR, Wang T, Gray NS, Sabatini DM (2012) A unifying model for mTORC1-mediated regulation of mRNA translation. *Nature* **485**: 109-113

Torres PA, Helmstetter JA, Kaye AM, Kaye AD (2015) Rhabdomyolysis: pathogenesis, diagnosis, and treatment. *Ochsner J* **15**: 58-69

Touvier T, De Palma C, Rigamonti E, Scagliola A, Incerti E, Mazelin L, Thomas JL, D'Antonio M, Politi L, Schaeffer L, Clementi E, Brunelli S (2015) Muscle-specific Drp1 overexpression impairs skeletal muscle growth via translational attenuation. *Cell Death Dis* **6**: e1663

Um SH, D'Alessio D, Thomas G (2006) Nutrient overload, insulin resistance, and ribosomal protein S6 kinase 1, S6K1. *Cell Metab* **3**: 393-402

Um SH, Frigerio F, Watanabe M, Picard F, Joaquin M, Sticker M, Fumagalli S, Allegrini PR, Kozma SC, Auwerx J, Thomas G (2004) Absence of S6K1 protects against age- and diet-induced obesity while enhancing insulin sensitivity. *Nature* **431**: 200-205

Unterberger U, Hoftberger R, Gelpi E, Flicker H, Budka H, Voigtlander T (2006) Endoplasmic reticulum stress features are prominent in Alzheimer disease but not in prion diseases in vivo. *J Neuropathol Exp Neurol* **65**: 348-357

Varadarajan S, Bampton ET, Smalley JL, Tanaka K, Caves RE, Butterworth M, Wei J, Pellecchia M, Mitcheson J, Gant TW, Dinsdale D, Cohen GM (2012) A novel cellular stress response characterised by a rapid reorganisation of membranes of the endoplasmic reticulum. *Cell Death Differ* **19**: 1896-1907

Vitadello M, Doria A, Tarricone E, Ghirardello A, Gorza L (2010) Myofiber stress-response in myositis: parallel investigations on patients and experimental animal models of muscle regeneration and systemic inflammation. *Arthritis Res Ther* **12**: R52

Wan XS, Lu XH, Xiao YC, Lin Y, Zhu H, Ding T, Yang Y, Huang Y, Zhang Y, Liu YL, Xu ZM, Xiao J, Li XK (2014) ATF4- and CHOP-Dependent Induction of FGF21 through Endoplasmic Reticulum Stress. *Biomed Res Int* **2014**: 807874

Wang C, Dai J, Yang M, Deng G, Xu S, Jia Y, Boden G, Ma ZA, Yang G, Li L (2014) Silencing of FGF-21 expression promotes hepatic gluconeogenesis and glycogenolysis by regulation of the STAT3-SOCS3 signal. *Febs J* **281**: 2136-2147

Wang H, Qiang L, Farmer SR (2008) Identification of a domain within peroxisome proliferator-activated receptor gamma regulating expression of a group of genes containing fibroblast growth factor 21 that are selectively repressed by SIRT1 in adipocytes. *Mol Cell Biol* **28**: 188-200

Wei W, Dutchak PA, Wang X, Ding X, Bookout AL, Goetz R, Mohammadi M, Gerard RD, Dechow PC, Mangelsdorf DJ, Kliewer SA, Wan Y (2012) Fibroblast growth factor 21 promotes bone loss by potentiating the effects of peroxisome proliferator-activated receptor gamma. *Proc Natl Acad Sci U S A* **109**: 3143-3148

Winzell MS, Ahren B (2004) The high-fat diet-fed mouse - A model for studying mechanisms and treatment of impaired glucose tolerance and type 2 diabetes. *Diabetes* **53**: S215-S219

Wu S, Grunwald T, Kharitonov A, Dam J, Jockers R, De Luca F (2013) Increased expression of fibroblast growth factor 21 (FGF21) during chronic undernutrition causes growth hormone insensitivity in chondrocytes by inducing leptin receptor overlapping transcript (LEPROT) and leptin receptor overlapping transcript-like 1 (LEPROTL1) expression. *J Biol Chem* **288**: 27375-27383

Wu Z, Puigserver P, Andersson U, Zhang C, Adelmant G, Mootha V, Troy A, Cinti S, Lowell B, Scarpulla RC, Spiegelman BM (1999) Mechanisms controlling mitochondrial biogenesis and respiration through the thermogenic coactivator PGC-1. *Cell* **98**: 115-124

Wullschlegel S, Loewith R, Hall MN (2006) TOR signaling in growth and metabolism. *Cell* **124**: 471-484

Xu C, Bailly-Maitre B, Reed JC (2005) Endoplasmic reticulum stress: cell life and death decisions. *J Clin Invest* **115**: 2656-2664

Xu J, Lloyd DJ, Hale C, Stanislaus S, Chen M, Sivits G, Vonderfecht S, Hecht R, Li YS, Lindberg RA, Chen JL, Jung DY, Zhang Z, Ko HJ, Kim JK, Veniant MM (2009) Fibroblast growth factor 21 reverses hepatic steatosis, increases energy expenditure, and improves insulin sensitivity in diet-induced obese mice. *Diabetes* **58**: 250-259

Yang C, Jin C, Li X, Wang F, McKeenan WL, Luo Y (2012) Differential specificity of endocrine FGF19 and FGF21 to FGFR1 and FGFR4 in complex with KLB. *PLoS One* **7**: e33870

Yang C, Lu W, Lin T, You P, Ye M, Huang Y, Jiang X, Wang C, Wang F, Lee MH, Yeung SC, Johnson RL, Wei C, Tsai RY, Frazier ML, McKeenan WL, Luo Y (2013) Activation of Liver FGF21 in hepatocarcinogenesis and during hepatic stress. *BMC Gastroenterol* **13**: 67

Ye L, Varamini B, Lamming DW, Sabatini DM, Baur JA (2012) Rapamycin has a biphasic effect on insulin sensitivity in C2C12 myotubes due to sequential disruption of mTORC1 and mTORC2. *Front Genet* **3**: 177

Yecies JL, Zhang HH, Menon S, Liu S, Yecies D, Lipovsky AI, Gorgun C, Kwiatkowski DJ, Hotamisligil GS, Lee CH, Manning BD (2011) Akt stimulates hepatic SREBP1c and lipogenesis through parallel mTORC1-dependent and independent pathways. *Cell Metab* **14**: 21-32

Yilmaz Y, Eren F, Yonal O, Kurt R, Aktas B, Celikel CA, Ozdogan O, Imeryuz N, Kalayci C, Avsar E (2010) Increased serum FGF21 levels in patients with nonalcoholic fatty liver disease. *Eur J Clin Invest* **40**: 887-892

Young RM, Ackerman D, Quinn ZL, Mancuso A, Gruber M, Liu L, Giannoukos DN, Bobrovnikova-Marjon E, Diehl JA, Keith B, Simon MC (2013) Dysregulated mTORC1 renders cells critically dependent on desaturated lipids for survival under tumor-like stress. *Genes Dev* **27**: 1115-1131

Zhang X, Yeung DC, Karpisek M, Stejskal D, Zhou ZG, Liu F, Wong RL, Chow WS, Tso AW, Lam KS, Xu A (2008) Serum FGF21 levels are increased in obesity and are independently associated with the metabolic syndrome in humans. *Diabetes* **57**: 1246-1253

Zhang Y, Nicholatos J, Dreier JR, Ricoult SJ, Widenmaier SB, Hotamisligil GS, Kwiatkowski DJ, Manning BD (2014) Coordinated regulation of protein synthesis and degradation by mTORC1. *Nature* **513**: 440-443

Zhang Y, Xie Y, Berglund ED, Coate KC, He TT, Katafuchi T, Xiao G, Potthoff MJ, Wei W, Wan Y, Yu RT, Evans RM, Kliewer SA, Mangelsdorf DJ (2012) The starvation hormone, fibroblast growth factor-21, extends lifespan in mice. *Elife* **1**: e00065

Zhou QL, Jiang ZY, Holik J, Chawla A, Hagan GN, Leszyk J, Czech MP (2008) Akt substrate TBC1D1 regulates GLUT1 expression through the mTOR pathway in 3T3-L1 adipocytes. *Biochem J* **411**: 647-655

## 6. APPENDIX

### 6.1. Publication 3

Cell Metabolism  
Article



## Sustained Activation of mTORC1 in Skeletal Muscle Inhibits Constitutive and Starvation-Induced Autophagy and Causes a Severe, Late-Onset Myopathy

Perrine Castets,<sup>1,2,5</sup> Shuo Lin,<sup>1,5</sup> Nathalie Rion,<sup>1</sup> Sabrina Di Fulvio,<sup>2</sup> Klaas Romanino,<sup>1</sup> Maitea Guridi,<sup>1</sup> Stephan Frank,<sup>3</sup> Lionel A. Tintignac,<sup>1,4</sup> Michael Sinnreich,<sup>2,\*</sup> and Markus A. Ruegg<sup>1,\*</sup>

<sup>1</sup>Biozentrum, University of Basel, 4056 Basel, Switzerland

<sup>2</sup>Neuromuscular Research Center, Departments of Neurology and Biomedicine, Pharmazentrum

<sup>3</sup>Institute of Pathology, Division of Neuropathology

Basel University Hospital, 4056 Basel, Switzerland

<sup>4</sup>INRA, UMR866, Université Montpellier 1, Université Montpellier 2, 34060 Montpellier, France

<sup>5</sup>These authors contributed equally to this work

\*Correspondence: msinnreich@uhbs.ch (M.S.), markus-a.ruegg@unibas.ch (M.A.R.)

<http://dx.doi.org/10.1016/j.cmet.2013.03.015>

#### SUMMARY

Autophagy is a catabolic process that ensures homeostatic cell clearance and is deregulated in a growing number of myopathological conditions. Although FoxO3 was shown to promote the expression of autophagy-related genes in skeletal muscle, the mechanisms triggering autophagy are unclear. We show that TSC1-deficient mice (TSCmKO), characterized by sustained activation of mTORC1, develop a late-onset myopathy related to impaired autophagy. In young TSCmKO mice, constitutive and starvation-induced autophagy is blocked at the induction steps via mTORC1-mediated inhibition of Ulk1, despite FoxO3 activation. Rapamycin is sufficient to restore autophagy in TSCmKO mice and improves the muscle phenotype of old mutant mice. Inversely, abrogation of mTORC1 signaling by depletion of raptor induces autophagy regardless of FoxO inhibition. Thus, mTORC1 is the dominant regulator of autophagy induction in skeletal muscle and ensures a tight coordination of metabolic pathways. These findings may open interesting avenues for therapeutic strategies directed toward autophagy-related muscle diseases.

#### INTRODUCTION

Muscle wasting, a hallmark of genetic and acquired muscle pathologies, is also associated with aging, cancer, AIDS, and chronic diseases of the heart, lung, or kidney. Muscle size depends on the balance between protein synthesis and protein degradation, the latter being ensured by the ubiquitin-proteasome pathway and the autophagy process (Rüegg and Glass, 2011). Despite the identification of the main molecular pathways involved in the regulation of this homeostatic balance, our understanding of the integrated signaling network remains limited.

Muscle growth is a costly process restricted to optimal nutrient and energy availability. The mammalian target of rapamycin complex 1 (mTORC1), which includes mTOR and regulatory associated protein of mTOR (raptor), is a conserved regulator of cell growth that integrates cellular inputs to ensure translation, lipid synthesis, and organelle biogenesis (Laplante and Sabatini, 2012). Most of these signals converge on the heterodimer TSC1/TSC2 (tuberous sclerosis complex 1 and 2) that functions as a GTPase-activating protein for the mTORC1 activator, the Ras-related binding protein Rheb (Inoki et al., 2003; Tee et al., 2003). Sensing of amino acids is, by contrast, independent of TSC1/TSC2 but mediated by the Ragulator-Rag complex that recruits mTORC1 to lysosomal membranes and promotes its activation by Rheb (Sancak et al., 2010).

Macroautophagy, hereafter referred to as autophagy, is involved in the constitutive turnover of organelles and macromolecules, as well as in the adaptive degradation of cellular components in response to different stresses such as low nutrient or energy supply. Upon autophagy induction, double-membrane vesicles, called autophagosomes, engulf large parts of the cytoplasm and release degraded components following fusion with lysosomes, thus ensuring metabolite recycling (Lum et al., 2005). In most cell types, autophagy induction relies on the release of the inhibition of the Ulk1-Atg13-FIP200 complex by mTORC1 (Kim et al., 2011). By contrast, in skeletal muscle, autophagy was suggested to be independent of mTORC1 but controlled by the forkhead box O3 protein (FoxO3), which promotes the transcriptional induction of atrogenes (notably encoding the E3 ubiquitin ligases atrogin1/MAFbx and MuRF1) and autophagy-related genes (Mammucari et al., 2007; Zhao et al., 2007).

In contrast to this apparent clear-cut separation between mTORC1-dependent anabolism and FoxO-dependent catabolism, integration of the entire regulatory network responsible for muscle homeostasis appears to be more complicated. In particular, the common control of mTORC1 and FoxO pathways by the upstream Akt protein and the existing feedback loops make it difficult to predict the physiological consequences of their modulation. We previously showed that inactivation of mTORC1 in skeletal muscle by deleting raptor (RAMKO mice)



Cell Metabolism 17, 731–744, May 7, 2013 ©2013 Elsevier Inc. 731

leads to muscle atrophy (Bentzinger et al., 2008). Inversely, activation of Akt promotes muscle growth. Although this effect can be blocked by rapamycin, the contribution of the inhibition of FoxO-dependent catabolism to this hypertrophy response is not clear (Bodine et al., 2001; Lai et al., 2004). Importantly, deletion of *Tsc1* in skeletal muscle (TSCmKO mice), which leads to simultaneous activation of mTORC1 and FoxO pathways, causes atrophy of most muscles (Bentzinger et al., 2013).

Here, we investigated the relative importance of mTORC1 and FoxO signaling for muscle homeostasis and their role in the regulation of autophagy. We show that sustained activation of mTORC1 in TSCmKO mice leads to a severe, late-onset phenotype reminiscent of myopathies caused by impaired autophagy. Despite simultaneous activation of FoxO3 signaling in TSCmKO mice, induction of constitutive and starvation-dependent autophagy is inhibited in mutant animals. This autophagy blockade and the myopathy of old TSCmKO mice are largely reversible by rapamycin. We also establish that mTORC1 inactivation, in RAmKO mice, is sufficient to induce autophagy. Our data thus demonstrate that mTORC1 is the dominant regulator of autophagy in skeletal muscle.

## RESULTS

### TSCmKO Mice Develop a Severe, Late-Onset Myopathy

TSCmKO mice, obtained by deleting *Tsc1* specifically in muscle tissues and characterized by constant activation of the mTORC1 pathway, are macroscopically indistinguishable from control animals at an early age (Bentzinger et al., 2013). However, after 9 months of age, mutant mice developed a severe kyphosis (Figure 1A) and eventually died around one year of age (data not shown). They were significantly lighter than control mice, which was largely related to a loss in fat and lean body mass (Table 1). Like in young mutant mice (Bentzinger et al., 2013), *tibialis anterior* (TA), *extensor digitorum longus* (EDL), *quadriceps*, and *gastrocnemius* muscles from 12-month-old TSCmKO mice were lighter than in control mice, while *soleus* was significantly heavier (Table 1). The mTORC1 pathway remained activated in 12-month-old TSCmKO mice as indicated by the increased phosphorylation of the mTORC1 target ribosomal protein S6 (Figure S1A). Moreover, phosphorylation of Akt was dampened (Figure S1A), consistent with the negative feedback loop exerted by mTORC1 signaling onto IRS1 (Harrington et al., 2004; Bentzinger et al., 2008).

The loss of fat and lean body mass in old TSCmKO mice was due to the genetic depletion of TSC1 in muscle, as TSC1 expression and/or the levels of phospho-S6 were not modified in other tissues such as liver, fat, or kidney (Figure S1A). Although levels of blood glucose were slightly lower in old TSCmKO mice than in age-matched controls, insulin levels and the two cachexia markers TNF $\alpha$  and IL6 (Späte and Schulze, 2004; Tisdale, 2010) were not significantly changed (Figure S1B).

Histological examination of muscles from 12-month-old TSCmKO mice revealed vacuolated fibers, basophilic fibers, and intracellular inclusions (Figures 1B and S1C). Most inclusions were positive for acid phosphatase, nicotinamide adenine dinucleotide (NADH), and COX, but were devoid of adenosine triphosphatase (ATPase) activity, indicating the presence of mitochondria, sarcoplasmic reticulum, and lysosomes and the

loss of myofibrillar elements in these regions (Figure S1D). As reported in human vacuolar myopathies (De Bleecker et al., 1993), some, but not all, vacuoles were positive for sarcolemmal components such as dystrophin or  $\beta$ -dystroglycan (Figure S1E). Abnormally large myonuclei were often observed in hematoxylin and eosin (H&E)-stained muscle sections (Figure 1B) or by immunohistological staining with anti-lamin C antibody (Figure 1C). These pathological changes in skeletal muscle were absent in 3-month-old mice but became visible in 6-month-old TSCmKO mice (Figure S1F).

Ultrastructural analysis by electron microscopy confirmed the presence of enlarged myonuclei and vacuoles in EDL and *soleus* muscles from 9-month-old TSCmKO mice (Figure 1D). Contractile compartments of some muscle fibers were shrunken with an enlarged peripheral region containing giant and vacuolated mitochondria or accumulation of aberrant membrane structures (Figures 1D and S1G). Sarcomeres were sometimes disorganized with accumulation of mitochondria (Figure S1G).

Immunostaining against type I and II myosin heavy chain (MHC) on TA sections from 12-month-old TSCmKO mice revealed a marked atrophy of type IIb fibers, whereas type IIa/IIx fibers were significantly hypertrophic (Figure 1E). The number of fibers and the fiber-type proportions were unchanged compared to control (data not shown). In *soleus*, type I fibers were significantly smaller than in control mice, whereas type IIa/IIx fibers varied from atrophic to hypertrophic fibers (Figure 1F). Such atrophic fibers likely resulted from fiber splitting, consistent with an increased number of fibers in *soleus* from 12-month-old mutant mice compared to controls (data not shown).

To determine whether the pathological changes correlated with impaired muscle function, we measured the *in vitro* force of the atrophic EDL and the hypertrophic *soleus* from 12-month-old mice. As shown in Table 1, specific twitch (sPt) and tetanic (sPo) forces were reduced to less than 50% in both mutant muscles compared to controls. Thus, constant activation of mTORC1 results in muscle weakness that is decoupled from muscle size. A similar decline in sPt and sPo was found in *soleus* from 3-month-old TSCmKO mice, indicating that the loss of muscle force precedes the detection of the myopathic alterations (Table 1).

Together, these observations indicate that sustained activation of mTORC1 in skeletal muscle results in a multifaceted myopathy characterized by the presence of vacuoles and the accumulation of abnormal organelles.

### Muscle Alterations in TSCmKO Mice Are Related to Impaired Autophagy

The similarity of the phenotype to mice with impaired autophagy (Masiero et al., 2009) prompted us to evaluate autophagy markers in TSCmKO mice at different ages. Because Akt was inhibited in TSCmKO mice, one could expect activation of FoxO3 signaling, another regulator of autophagy (Mammucari et al., 2007; Zhao et al., 2007). Nonetheless, we did not detect a major decrease in the phosphorylation of FoxO1/FoxO3 proteins in muscles from 6- or 12-month-old mutant mice (Figure 2A), and expression of *MuRF1* and *Atrogin1*, which were significantly induced in TA from 3-month-old mice, was not changed in older mutant mice (Figure 2B and data not shown).



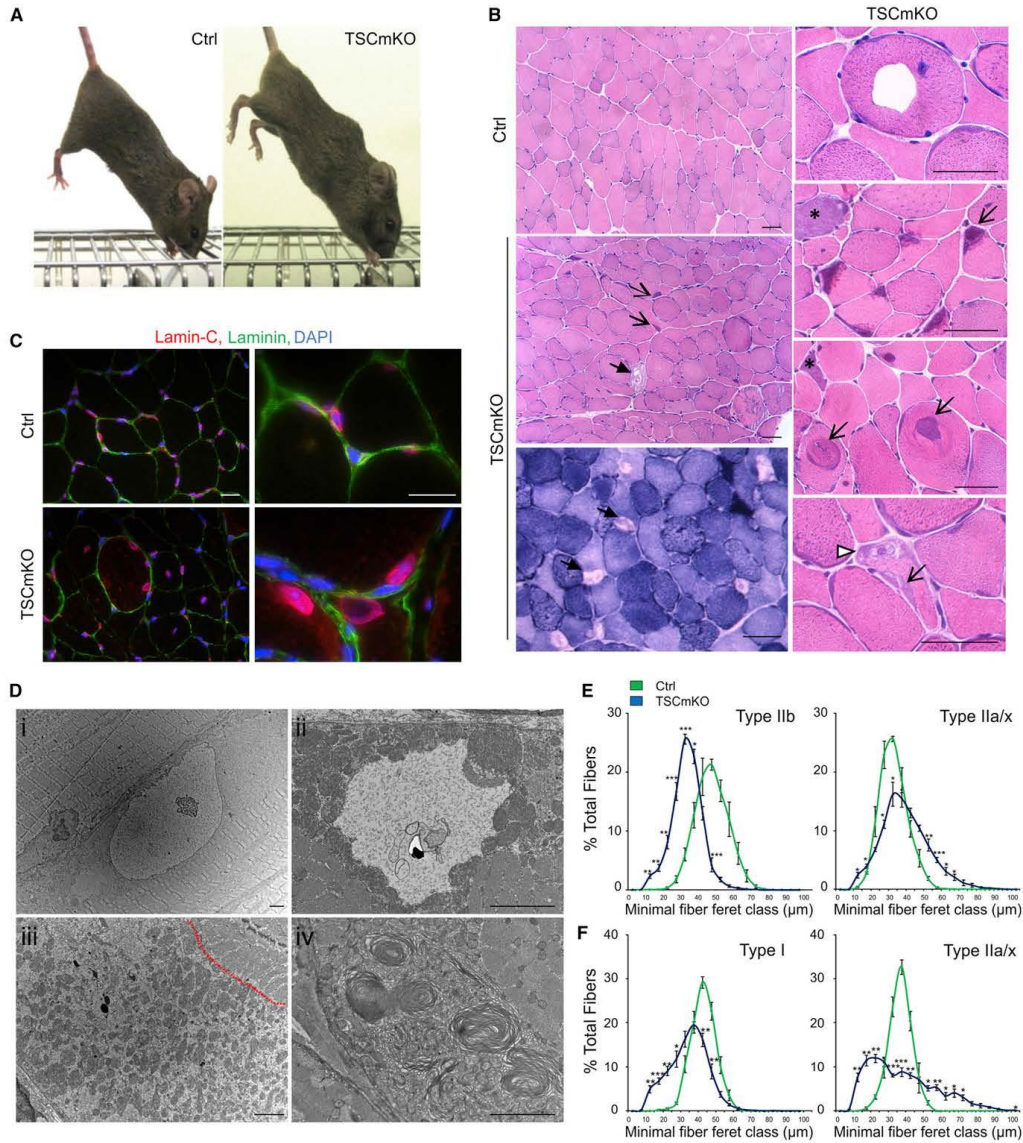


**Figure 1. TSCmKO Mice Develop a Late-Onset Phenotype with Severe Muscle Alterations**

(A) TSCmKO mice display severe kyphosis at 9 months of age.  
 (B) H&E and NADH stains reveal accumulation of vacuolated (arrow) and basophilic (asterisk) fibers, intracellular inclusions (open arrow), and abnormally large myonuclei (arrowhead) in TA muscle from 12-month-old TSCmKO mice. Scale bar = 50  $\mu$ m.  
 (C) Immunostaining against laminin-C and laminin reveals giant nuclei in muscle from 12-month-old TSCmKO mice. Scale bar = 20  $\mu$ m.  
 (D) Electron micrographs show inflated myonuclei (i), vacuoles (ii), intracellular accumulation of abnormal mitochondria (iii), and aberrant membrane structures (iv) in muscles from 12-month-old TSCmKO mice. The dotted line in (iii) indicates the limit of the contractile region of the fiber. Scale bar = 2  $\mu$ m.  
 (E and F) Fiber size distribution in TA (E) and *soleus* (F) from 12-month-old TSCmKO mice reveals atrophy of type IIb and I fibers and hypertrophy of type IIa/ix fibers. Values are mean  $\pm$  SEM; \* $p$  < 0.05, \*\* $p$  < 0.005, \*\*\* $p$  < 0.0005.

**Table 1. TSCmKO Mice Are Characterized by Reduction in Body Weight and in Muscle Force**

	Ctrl	TSCmKO
Body mass (g)		
Whole body	24.2 ± 0.7	19.6 ± 0.5***
Lean	16.8 ± 0.3	14.9 ± 0.38***
Fat	4.8 ± 0.5	2.2 ± 0.1***
Muscle mass (mg)		
TA	53.2 ± 1.9	44.0 ± 3.2*
EDL	13.6 ± 0.6	9.3 ± 0.6**
<i>Quadriceps</i>	212.8 ± 5.9	178.4 ± 14.9
<i>Gastrocnemius</i>	138.6 ± 5.7	95.6 ± 6.3**
<i>Soleus</i>	10.3 ± 0.9	13.8 ± 0.7**
Specific Twitch Force (sPt; mN/mm <sup>2</sup> )		
3 month		
EDL	51.4 ± 2.3	42.7 ± 6.6
<i>Soleus</i>	45.6 ± 4.2	11.9 ± 1.3***
12 month		
EDL	38.9 ± 3.7	16.0 ± 4.6**
<i>Soleus</i>	37.4 ± 3.1	10.2 ± 3.1***
Specific Tetanic Force (sPo; mN/mm <sup>2</sup> )		
3 month		
EDL	480.0 ± 22.7	328.8 ± 68.8
<i>Soleus</i>	390.4 ± 11.4	185.3 ± 16.3***
12 month		
EDL	355.0 ± 22.8	120.0 ± 10.3***
<i>Soleus</i>	316.2 ± 12.3	86.6 ± 20.0***

Body and muscle masses are given for 12-month-old TSCmKO and control (Ctrl) mice. The lean and fat mass was measured by EchoMRI. TA, *tibialis anterior*; EDL, *extensor digitorum longus*. p values determined by Student's t test are indicated by asterisks (n ≥ 3). Values represent mean ± SEM. \*p < 0.05, \*\*p < 0.005, \*\*\*p < 0.0005.

The SQSTM1/p62 protein is an autophagy-specific substrate, the accumulation of which is used as a readout for autophagy impairment (Klionsky et al., 2012). In 12-month-old TSCmKO mice, p62 accumulated in the cytoplasm or as focal aggregates in most muscle fibers (Figure 2C) irrespective of their fiber type (data not shown). Basophilic cells and intracellular inclusions located in the periphery of the cells were positive for p62, whereas vacuoles and central inclusions were mostly negative (Figure S2A). p62 levels were increased in both the detergent-soluble and -insoluble fractions from TA and *soleus* muscles, confirming the presence of aggregates in muscle fibers (Figure 2D and data not shown). Concomitantly, levels of ubiquitinated proteins were increased in muscles from 12-month-old TSCmKO mice and p62 aggregates were generally positive for ubiquitin (Figures S2B and S2C). p62 also accumulated in muscle from younger TSCmKO mice (Figure 2D), but aggregates were not detected in 3-month-old mice and were less frequent in 6-month-old mice than in 12-month-old animals (Figure 2C). This indicates that p62 accumulates prior to morphological muscle alterations.

Because accumulation of p62 is a hallmark of impaired autophagy flux, we next evaluated levels of the soluble (LC3I) and autophagosome-associated (LC3II) forms of the widely used LC3 (microtubule-associated protein light chain 3) autophagy marker. The conversion of LC3I to LC3II is representative of the accumulation of autophagosomes in cells (Klionsky et al.,

2012). In TA from 3- and 6-month-old TSCmKO mice, levels of LC3I were increased compared to control, while both LC3I and LC3II forms tended to accumulate in 12-month-old TSCmKO mice. By contrast, LC3I and LC3II were not altered in *soleus* muscles (Figure 2D). It is noteworthy that lysosome-related vesicles, marked with the lysosomal-associated membrane protein 1 or 2 (Lamp1/Lamp2), also accumulated in muscle fibers from 12-month-old TSCmKO mice, especially at the periphery of the cells and around myonuclei (Figures 2E and S2D). These lysosomal structures rarely colocalized with p62 aggregates (Figure S2E). Expression of Cathepsin L, a lysosomal enzyme involved in the degradation of autophagic content, was increased in TA and even more so in *soleus* from TSCmKO mice at all ages (Figure 2D). Transcript levels of *Cathepsin L* and *p62* were increased in TA and *soleus* muscles from 3-month-old TSCmKO mice, consistent with FoxO activation, but their expression normalized in older mice, as observed for *MuRF1*. *LC3* messenger RNA (mRNA) levels were not changed at any age (Figures 2F and 2G). Together with the morphological alterations described above, these observations indicate that autophagy is perturbed in TSCmKO mice.

#### Induction of Constitutive and Starvation-Dependent Autophagy Is Blocked in Skeletal Muscle from TSCmKO Mice

To better understand the autophagy-related defects detected in TSCmKO mice, we explored the ability of 2-month-old mutant mice to increase autophagy flux in muscle when submitted to a physiological stimulus like fasting (Mizushima et al., 2004). To distinguish between constitutive and starvation-induced autophagy, mice were examined in fed or basal conditions and following food deprivation (starved). Fed mice were sacrificed in the late evening when they were actively eating, while basal conditions refer to the early morning during the light-on circadian period. Fed mice showed activation of Akt and S6 similar to mice that were fasted overnight and then refed for 4 hr in the morning (data not shown). In control muscle, autophagy was induced in basal conditions, as shown by the conversion of LC3I to LC3II, compared to fed conditions (Figure S3A). This induction of autophagy correlated with Akt/mTORC1 inhibition (Figure S3A), whereas transcription of the main autophagy-related genes remained unchanged (Figure S3B). After 24 or 48 hr of starvation, autophagy was greatly induced, as reflected by a major increase in the LC3II/LC3I ratio (Figure S3A), and was paralleled by upregulation of autophagy-related genes (Figure S3B). Levels of phospho-Akt and phospho-S6 were not significantly reduced compared to basal conditions (Figure S3A).

In stark contrast to controls, TSCmKO mice showed constant high phosphorylation of S6 and low levels of phospho-Akt regardless of their nutritional status (Figure 3A). Interestingly, the energy-sensing 5' AMP-activated protein kinase (AMPK) was similarly activated upon starvation in control and mutant mice (Figure S3C). Starvation increased the percentage of myonuclei positive for FoxO3, indicative of its active state (Figure S3D); mRNA expression of *MuRF1* and *Atrogin1* (Figure 3B) was also increased in TA muscle of control and TSCmKO mice. It should be noted, however, that the percentage of FoxO3-positive myonuclei was higher in TSCmKO mice than in controls in both basal and starved conditions (Figure S3D). These results

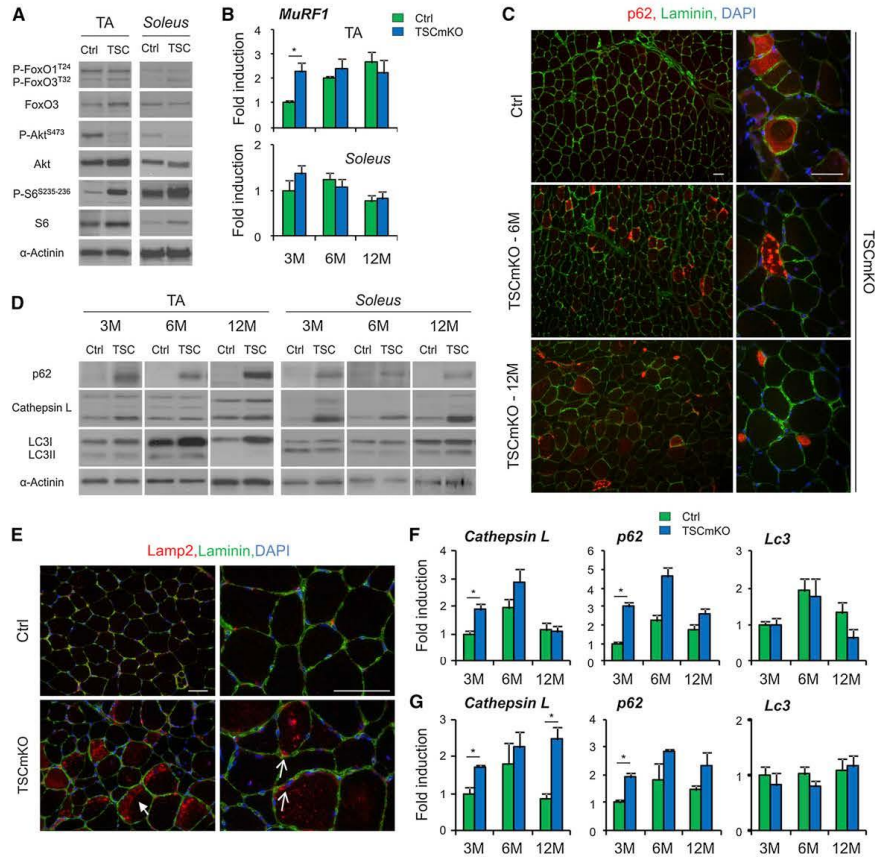


**Figure 2. Autophagy Flux Is Impaired in TSCmKO Muscles**

(A) Immunoblots of TA and *soleus* muscles from 12-month-old TSCmKO (TSC) and control (Ctrl) mice are shown for the indicated phospho- (P)- and total proteins. (B) *MuRF1* mRNA expression was quantified by qPCR in TA and *soleus* from 3-, 6-, and 12-month-old (M, month) TSCmKO and control mice and normalized to  $\beta$ -*actin* expression. Levels are presented as mean  $\pm$  SEM relative to 3-month-old control mice; \* $p < 0.05$ . (C) p62 accumulates within the cytoplasm or as focal aggregates in muscle fibers from 6- and 12-month-old (M, month) TSCmKO mice. Scale bar = 50  $\mu$ m. (D) Immunoblots for autophagy-related proteins reveal impaired autophagy flux in TA and *soleus* muscles from TSCmKO (TSC) mice at different ages compared to control (Ctrl). The proprotein (37 kDa), intermediate (30 kDa), and mature (25 kDa) forms of Cathepsin L are shown. Data are normalized to  $\alpha$ -actinin and represent at least three independent experiments; quantification is given in Table S1. M, month. (E) Lysosomal vesicles stained with anti-Lamp2 antibody accumulate in muscle fibers, especially in the periphery of muscle fibers (arrow) and around myonuclei (open arrow) in 12-month-old (M, month) TSCmKO mice, but not in control (Ctrl) animals. Scale bar = 50  $\mu$ m. (F and G) Expression of some autophagy-related genes is significantly increased in TA (F) and *soleus* (G) from 3-month-old TSCmKO mice compared to control mice. This difference becomes less prominent in 6- and 12-month-old mice. Values are mean  $\pm$  SEM of data normalized to  $\beta$ -*actin* levels; \* $p < 0.05$ . M, month.

are consistent with the strong inhibition of Akt and the normal activation of AMPK in TSCmKO mice. Together, these data support the idea that starvation-induced activation of FoxO3 not only depends on Akt inhibition, but further requires AMPK activation, consistent with recent *in vitro* results obtained in muscle cells (Sanchez et al., 2012).

When TSCmKO mice were starved for 12, 24, or even 48 hr, loss of body weight was comparable to that in control mice

(data not shown). Starvation did not lead to major muscle alterations in mutant mice, although a few fibers from *soleus* muscle of TSCmKO mice contained small vacuoles and abnormally large myonuclei that were not observed in control mice or fed mutant mice (Figure S3E). Starvation increased the levels of p62 protein in mutant muscle (Figure 3A), but the protein did not form large aggregates like in 12-month-old mice (Figure S3F). Interestingly, in TA muscle from TSCmKO mice, levels

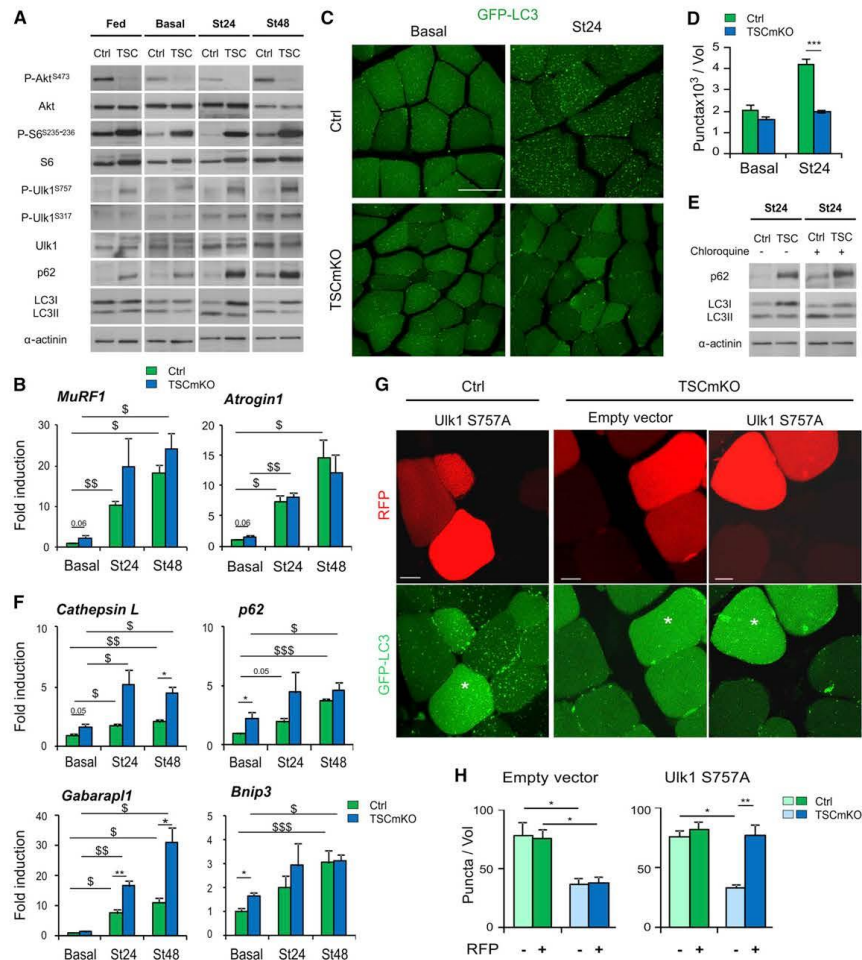


**Figure 3. Autophagy Induction Is Blocked in TSCmKO Muscles**

(A) Two-month-old TSCmKO (TSC) and control (Ctrl) mice were examined in fed, basal, and starved (St24 or St48 hr) conditions. Immunoblots using antibodies to detect Akt and S6 protein, specific phosphorylation sites (P) in the respective proteins, and autophagy-related proteins show that mutant TA muscle was resistant to starvation-mediated autophagy induction. Data are normalized to  $\alpha$ -actinin and representative of three independent experiments; for quantification, see Table S2.

(B) Transcript expression of *MuRF1* and *Atrogin1* is efficiently upregulated in TA from TSCmKO mice after 24 or 48 hr of starvation (St). Expression levels are normalized to  $\beta$ -actin. Values are mean  $\pm$  SEM; <sup>s</sup>p < 0.05, <sup>ss</sup>p < 0.005 compared to same genotype in basal conditions.

(C and D) TSCmKO mice expressing GFP-LC3 display a reduced number of GFP-positive puncta in TA muscle compared to control (Ctrl) after 24 hr of starvation (St24) (C). This effect is confirmed by quantifying the number of GFP-LC3 puncta in a volume unit (Vol) of  $3.6 \times 10^5 \mu\text{m}^3$  (D). Data are mean  $\pm$  SEM; <sup>\*\*\*</sup>p < 0.0005. Scale bar = 50  $\mu\text{m}$ .

(E) Treatment with chloroquine (+) leads to only a mild increase in LC3II levels in TA muscle from starved TSCmKO (TSC) mice, indicating that LC3I accumulation in these mice is due to impaired induction steps.

(F) Expression of autophagy-related genes is upregulated after 24 or 48 hr of starvation (St) in TA from TSCmKO mice. Data are normalized to  $\beta$ -actin levels and relative to control mice in basal conditions. Values are mean  $\pm$  SEM; <sup>\*</sup>p < 0.05, <sup>\*\*</sup>p < 0.005 compared to control mice in the same condition; <sup>s</sup>p < 0.05, <sup>ss</sup>p < 0.005, <sup>sss</sup>p < 0.0005 compared to same genotype in basal conditions.

(G and H) Overexpression of the Ulk1 mutant S757A, together with construct expressing tdRFP, restores the induction of GFP-LC3 puncta in electroporated TSCmKO fibers (\*) (G); quantification of the results are shown in (H). No effect is observed with the empty plasmid or in control (Ctrl) muscle. Scale bar = 10  $\mu\text{m}$ . A volume unit (Vol) is  $3.6 \times 10^5 \mu\text{m}^3$ . Values are mean  $\pm$  SEM. <sup>\*</sup>p < 0.05; <sup>\*\*</sup>p < 0.005.

of LC3I and LC3II remained unchanged between fed, basal, and starved conditions (even after prolonged fasting for 48 hr), and they were comparable to those observed in fed control mice (Figure 3A). To confirm this result, we crossed TSCmKO mice with GFP-LC3 transgenic mice (Mizushima et al., 2004) and examined the number of green fluorescent protein (GFP)-positive puncta, representative of autophagosomes, in control and mutant muscle. In basal conditions, the number of GFP-LC3 puncta in TA was similar in TSCmKO and control mice. However, the number of GFP-LC3 puncta did not increase in TSCmKO muscles after 24 hr of starvation, while, as expected, the number of puncta more than doubled in control mice (Figures 3C and 3D). These results are consistent with either a blockade in autophagy induction or an excessive exhaustion of the vesicles. To discriminate between the two possibilities, starved mice were treated with chloroquine, a lysosomal inhibitor that prevents the degradation of the autophagic content. While chloroquine treatment strongly increased LC3II levels in control mice, LC3II was only slightly increased in TSCmKO mice, indicating that the reduced number of autophagosomes in mutant muscles is due to impaired autophagy induction (Figure 3E).

We next addressed whether this defect in autophagy induction was caused by abnormal expression of autophagy-related genes (Mammucari et al., 2007). Consistent with FoxO being active, mRNA expression of *Cathepsin L*, *p62*, *Gabarrap1*, and *Bnip3* was efficiently increased after 24 or 48 hr of starvation in TSCmKO mice compared to control mice (Figures 3F and S3G). *Cathepsin L* and the two positive regulators of autophagy, *Bnip3* and *Beclin 1*, also showed normal or higher protein expression in mutant mice (Figure S3C). Similar results were obtained in *soleus* muscle (Figures S3H and S3I). These results show that sustained activation of mTORC1 blocks the induction of constitutive and starvation-induced autophagy despite FoxO3 activation.

In cultured cells, mTORC1 has been shown to phosphorylate Ulk1 and thereby inhibit its activation by AMPK (Kim et al., 2011). We therefore assessed the phosphorylation state of Ulk1 in TSCmKO muscles and found that the amount of the inactive, phosphorylated form of Ulk1 at S757 was markedly increased in all conditions compared to control, while there was no major change in the AMPK-dependent phosphorylation at S317 of Ulk1 in mutant mice (Figure 3A). To test whether this hyperphosphorylation of Ulk1 was responsible for the effect on autophagy, TA muscles from control and TSCmKO mice were coelectroporated with a tandem-dimer (td) red fluorescent protein (RFP) expression construct and a plasmid encoding the Ulk1 mutant S757A, which is insensitive to mTORC1 (Kim et al., 2011). After 8 days and starvation of the mice for the final 36 hr, the number of GFP-LC3 puncta was significantly higher in RFP-positive fibers compared to RFP-negative fibers in TSCmKO muscle and became similar to that detected in control muscle (Figures 3G and 3H). Similar results were obtained when the wild-type form of Ulk1 was electroporated into TA muscle (Figure S3J). In contrast, no effect was observed using the empty plasmid, and electroporation of empty vector or Ulk1 encoding plasmid into control muscle did not affect the number of GFP-LC3 puncta (Figure 3G and 3H). These results indicate that mTORC1 mediates its inhibitory function on autophagy via

Ulk1 and that restoration of Ulk1 is sufficient to normalize autophagy in TSCmKO muscle.

#### Hyperactivation of mTORC1 Is Sufficient to Block Autophagy Both In Vivo and In Vitro

To test whether acute depletion of the TSC complex could also block autophagy, we electroporated control muscles with small hairpin RNA (shRNA) constructs directed against *Tsc1* and *Tsc2* together with tdRFP expression plasmids. After 8 days, muscles were examined following starvation of the mice for the last 36 hr. Compared to muscle electroporated with control shRNA to *Cd4*, knockdown of *Tsc1/Tsc2* in *soleus* muscle resulted in lower levels of TSC1 and TSC2 and higher levels of phospho-S6 (Figure 4A). Indicative of reduced autophagy induction, the LC3II/LC3I ratio was reduced (Figure 4A) and the number of GFP-LC3 puncta was significantly decreased in RFP-positive fibers of TA muscle electroporated with *Tsc1/Tsc2* shRNA compared to RFP-negative fibers in the same muscle (Figures 4B and 4C). No effect was detected with control shRNA directed against *Cd4*. In a similar experiment, when examining *soleus* muscle 4 weeks after electroporation of shRNA directed against *Tsc2* together with an expression construct for nuclear GFP (nuGFP), TSC2 levels were reduced and high levels of phospho-S6 were detected (Figure 4D). Notably, the amount of p62 was increased in the examined muscles, and p62 accumulation was further observed by immunostaining in nuGFP-positive fibers expressing *Tsc2* shRNA (Figure 4E). These results demonstrate that autophagy is also impaired following acute perturbation of mTORC1 signaling in adult mice.

In an additional step, we investigated whether sustained activation of mTORC1 would impair autophagy in vitro by isolating single fibers from EDL muscle of TSCmKO mice expressing GFP-LC3. Compared to fibers placed in growth medium, a strong increase in the number of GFP-positive puncta was observed when control fibers were incubated with medium depleted of amino acids and glucose. In contrast, the number of GFP-LC3 puncta remained low in TSCmKO fibers even after amino acid and glucose depletion (Figures 4F, 4G, and S4A). In addition, control fibers contained large, Lamp2-positive vesicles after starvation, whereas only few such structures could be detected in TSCmKO fibers (Figure 4F). Levels of p62 were slightly increased in mutant fibers compared to control, and as observed in vivo, TSCmKO fibers maintained high levels of phospho-S6 and low levels of phospho-Akt irrespective of the culture conditions (Figures 4H and S4B). These results demonstrate that the release of TSC1/TSC2 inhibition onto mTORC1 is sufficient to fully activate the pathway both in vivo and in vitro, hence contrasting with in vitro evidence suggesting that amino acid supply is absolutely required for mTORC1 activation, irrespective of other positive stimuli (Smith et al., 2005).

#### Inactivation of mTORC1 Promotes LC3 Lipidation in Spite of FoxO Inhibition

Having established that sustained activation of mTORC1 impairs autophagy, we asked whether its inactivation would promote the autophagy flux by examining the response of 2-month-old RAmKO mice to food deprivation. Mutant mice displayed reduced phospho-S6 levels in fed, basal, and starved conditions compared to controls, in accordance with mTORC1 inactivation

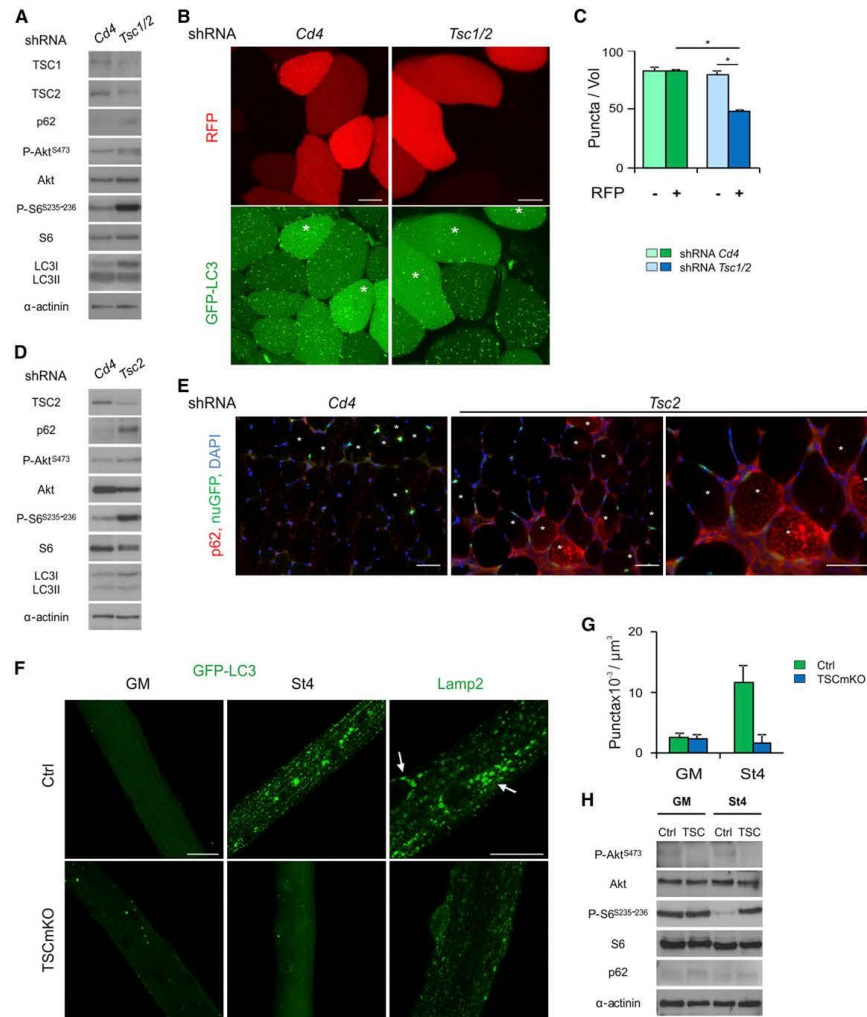


**Figure 4. Hyperactivation of mTORC1 Impairs Autophagy in Muscle Fibers**

(A–C) Coelectroporation of tdRFP and shRNA constructs directed against *Tsc1* and *Tsc2* results in hyperactivation of mTORC1 signaling after 8 days (A) and in a decreased number of GFP-LC3 puncta in transfected RFP-positive fibers (\*) when mice were previously starved for 36 hr (B). GFP-LC3 puncta were quantified in a volume unit (Vol) of  $3.6 \times 10^3 \mu\text{m}^3$  (C). Scale bar = 10  $\mu\text{m}$ . Values are mean  $\pm$  SEM. \* $p < 0.05$ .

(D and E) Four weeks after electroporating *Tsc2* shRNA together with nuGFP in TA muscle, levels of phospho-S6 and p62 are increased compared to muscle electroporated with control *Cd4* shRNA (D). Accumulation of p62 is detected by immunostaining in nuGFP-positive fibers in muscle electroporated with *Tsc2* shRNA (E). Scale bar = 50  $\mu\text{m}$ .

(F and G) Single muscle fibers isolated from GFP-LC3 expressing control mice (Ctrl) show induction of GFP-positive puncta and large Lamp2 vesicles (arrow) after 4 hr in glucose- and amino acid-deprived medium (S14) compared to fibers placed in growth medium (GM). These vesicles remain rare in fibers isolated from TSCmKO mice (F). Quantification of the number of GFP-LC3 puncta/ $\mu\text{m}^3$  (G). Scale bar = 25  $\mu\text{m}$ . Values are mean  $\pm$  SEM.

(H) Immunoblots using antibodies that detect Akt and S6 protein and their phosphorylated forms reveal hyperactivation of mTORC1 signaling in TSCmKO fibers (TSC) in growth medium (GM) and after 4 hr without glucose and amino acid (S14).

(Figure 5A). Conversely, phosphorylation of Akt (Figure 5A) and FoxO1/FoxO3 (Figure S5A) was maintained at high levels in starved mutant mice, and transcript levels of *MuRF1* and *Atrogin1* were markedly lower than in starved control mice (Figure 5B).

After 12 or 24 hr of starvation, a similar loss of body mass was measured in RAmKO and control mice, and H&E staining revealed no obvious muscle alterations compared to basal conditions (data not shown). p62 protein accumulated in only a few muscle fibers from starved mutant mice, although the number and the size of these aggregates were increased compared to basal conditions (Figure 5C). Western blot analysis revealed similar low levels of p62 in TA from mutant and control mice (Figure 5D). Interestingly, elevated levels of LC3II, similar to those in starved control mice, were detected in RAmKO muscle, regardless of the nutritive status of the mice (Figure 5D). To further evaluate the number of autophagosomes in muscle fibers, RAmKO mice were crossed with GFP-LC3 transgenic mice (Mizushima et al., 2004). In basal conditions, the number of GFP-positive puncta in TA sections from RAmKO mice was significantly higher compared to control mice and similar to the number in TA from starved control mice (Figures 5E and 5F). After 24 hr of starvation, the number of GFP-LC3 puncta was not further increased in RAmKO mice, and we noticed that GFP-LC3 puncta were not distributed homogeneously in mutant muscle compared to control (Figure 5F). While in basal and starved conditions, chloroquine treatment enhanced LC3II levels in both mutant and control mice; in fed conditions, the amount of LC3II was only increased in RAmKO mice, supporting the idea that autophagy is permanently induced in mutant mice (Figure 5D). Contrasting with this result, transcript levels of autophagy-related genes were strongly reduced in muscles from starved mutant mice, consistent with increased Akt-dependent inhibition of FoxO compared to control mice (Figures 5G and S5B). Nevertheless, expression of most autophagy-related genes was significantly increased after starvation in mutant muscles, which could be related to starvation-induced activation of AMPK (Figure S5A). Cathepsin L, Cathepsin D, and *Bnip3* protein levels were also reduced in mutant mice compared to control animals, while no major change was detected in the amount of Beclin 1 and phospho-Ulk1<sup>S757</sup> (Figures 5D and S5A). In contrast, phosphorylation of Ulk1 at S317 was strongly increased in RAmKO mice, suggesting that mTORC1 inactivation facilitates AMPK-dependent activation of Ulk1 in muscle (Figure S5A). Similar results were obtained in *soleus* muscle (Figures S5C and S5D). Together, these data indicate that autophagy is induced in RAmKO muscles despite reduced FoxO-dependent transcription of autophagy genes.

To go further, autophagy markers were assessed in 6-month-old RAmKO mice: like in 2-month-old mice, mRNA levels of *Cathepsin L*, *LC3*, and *Bnip3* were significantly decreased in mutant mice, and the amount of LC3II was increased (Figures S5E–S5G). In parallel, protein expression of *Cathepsin L* was strongly reduced while the levels of *Cathepsin D* and *Lamp1* were only slightly lowered in mutant TA muscle compared to control (Figure S5G). No major difference was observed in the acid phosphatase activity of RAmKO and control muscles, except in regenerative fibers, which were strongly reactive to the staining (Figure S5H). While p62 levels were unchanged in

detergent-soluble and -insoluble protein fractions from mutant muscle, p62 aggregates were observed in many myofibers (Figures S5G and S5I). Similarly, *Lamp1/Lamp2*-positive structures accumulated in a few fibers but did not colocalize with p62 aggregates (Figures S5J and S5K). Lastly, the amount of ubiquitinated proteins was increased in TA muscle from starved 2-month-old ( $100 \pm 4\%$  in control;  $122 \pm 7\%$  in mutant) and 6-month-old ( $100 \pm 2\%$  in control;  $191 \pm 17\%^{**}$  in mutant,  $^{**}p < 0.005$ ) RAmKO mice (Figures S5L and S5M). Together, these results suggest that lysosomal activity may be slowed down in RAmKO muscles, thereby limiting the final degradation steps of autophagy and resulting in the accumulation of autophagic substrates.

Lastly, as mTOR complex 2 (mTORC2), characterized by the rapamycin-insensitive companion of mTOR (rictor), was also reported to indirectly regulate autophagy via Akt in muscle cells (Mammucari et al., 2007), we examined whether mice specifically depleted for rictor in skeletal muscle (RImKO; Bentzinger et al., 2008) would show changes in autophagy. No difference in the number of GFP-LC3 puncta was observed in muscles of RImKO mice compared to control mice in basal and starved conditions (Figures S5N and S5O). Furthermore, LC3I, LC3II, and p62 levels in 3- and 6-month-old RImKO mice were similar to control animals (Figures S5P and S5Q). These results indicate that autophagy in skeletal muscle is not regulated by mTORC2.

#### Rapamycin Restores the Autophagy Flux and Reverses Muscle Alterations in TSCmKO Mice

Having shown that mTORC1 inhibition is required and sufficient to trigger autophagy induction, we assessed whether inhibition of mTORC1 would restore autophagy and reverse the myopathic phenotype of TSCmKO mice. In TA muscle, rapamycin normalized phospho-Akt and phospho-S6 levels in starved 2-month-old and 12-month-old mutant mice, indicating that mTORC1 was efficiently inhibited by the treatment (Figure 6A). Rapamycin treatment decreased the amount of p62 in both 2- and 12-month-old TSCmKO mice and restored the conversion of LC3I to LC3II and the number of GFP-LC3 puncta in starved TSCmKO mice (Figures 6A–6C). Levels of phospho-Ulk1<sup>S757</sup> and Beclin 1 were normalized by rapamycin (Figures 6A and S6A), while mRNA expression of the autophagy-related genes in starved mice was not significantly affected (Figures 6D and S6B). Similar results were obtained in *soleus* muscles (Figures S6C and S6D). These results show that mTORC1 inhibition by rapamycin in TSCmKO mice is sufficient to restore autophagy induction.

Morphological analyses of TA and *soleus* muscles revealed an improvement of the myopathy in 12-month-old TSCmKO mice when treated with rapamycin (Figure 6E). In particular, fibers with vacuoles or hematoxylin-positive inclusions were less frequent, and the accumulation of p62 aggregates was strongly reduced in rapamycin-treated mice (Figure 6E). Moreover, rapamycin reversed, at least partially, the atrophy of type IIb fibers in TA (Figure 6F) and the hypertrophy of type IIa/IIx fibers in *soleus* (Figure S6E). Most importantly, rapamycin normalized mass, specific twitch force (sPt), and specific tetanic force (sPo) of the TSCmKO *soleus* muscle (Figures 6G and 6H). Altogether, these data indicate that rapamycin is sufficient to ameliorate the myopathy observed in old TSCmKO mice, which is likely due to the normalization of the autophagy flux.

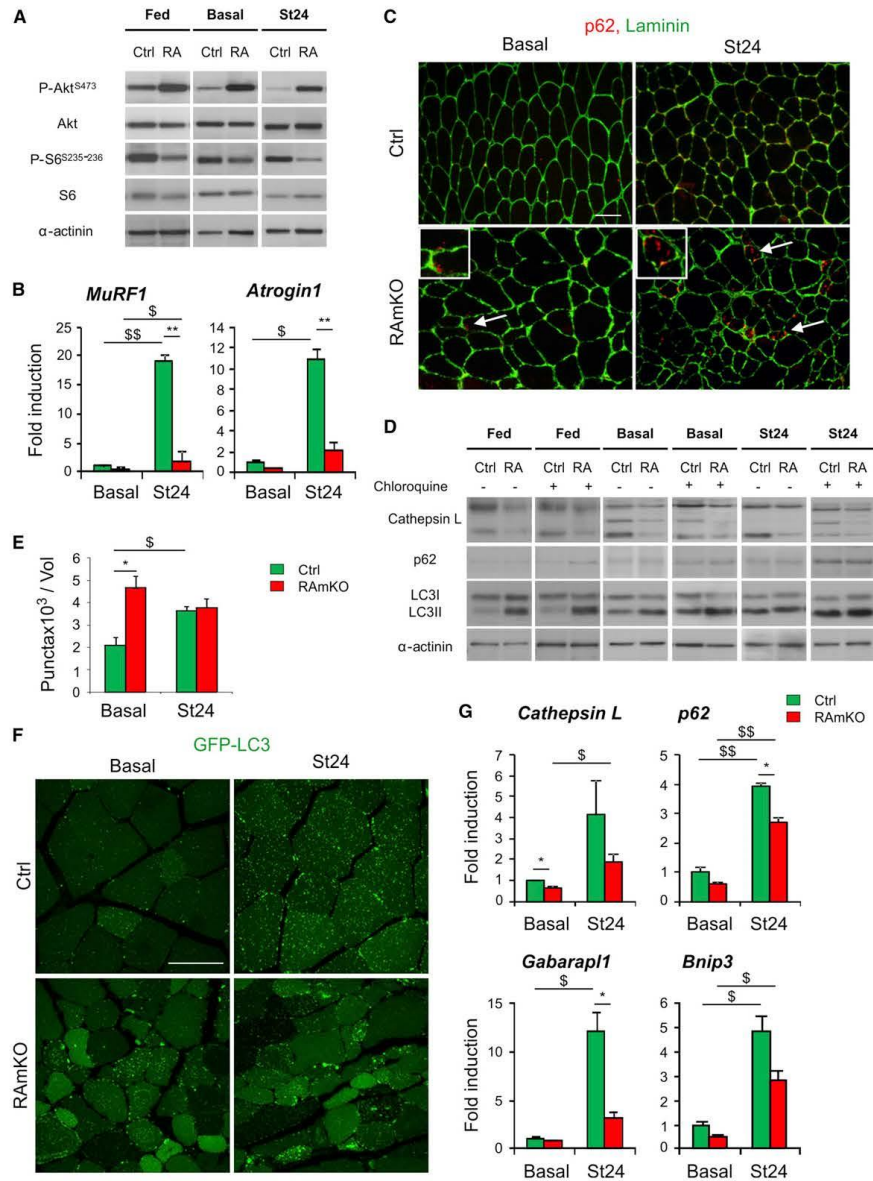


**Figure 5. Autophagy Is Induced in RAmKO Mice Despite Reduced FoxO3 Activity**  
(A) Immunoblots using antibodies that detect Akt and S6 protein and their phosphorylated forms show resistance of RAmKO (RA) TA to food intake and deprivation compared to control (Ctrl). Data are normalized to  $\alpha$ -actinin and are representative of three independent experiments; quantification is given in Table S4.  
(B) Transcript levels of *MuRF1* and *Atrogin1* in TA from starved RAmKO mice are reduced compared to starved control mice. Expressions are normalized to  $\beta$ -actin levels. Values are mean  $\pm$  SEM; \*\*p < 0.05 compared to control mice under the same condition; \$p < 0.05, \$\$p < 0.005 compared to same genotype in basal conditions.  
(legend continued on next page)



## DISCUSSION

Autophagy impairment has been positioned as a central pathomechanism related to neurodegenerative diseases, cancer, and aging-associated dysfunctions. By generating mice depleted for TSC1 in skeletal muscle (TSCmKO), we show that sustained activation of the mTORC1 pathway leads to a late-onset myopathy with muscle atrophy and severe muscle weakness. Previous reports established that excessive, as well as insufficient, autophagy flux damage muscle tissue (Mammucari et al., 2007; Masiero et al., 2009). Accordingly, TSCmKO muscles progressively accumulate p62 aggregates, vacuoles, and damaged organelles with age, supporting the idea that muscle atrophy in TSCmKO mice is at least partly caused by impaired autophagy flux. *Soleus* muscle was the only muscle analyzed with increased muscle weight, but this gain of mass was nonfunctional, as its force-drop was even higher than in EDL muscle. Although slow muscles were reported to have lower autophagy flux compared to fast muscles (Ogata et al., 2010), *soleus* muscle was not spared from the accumulation of autophagic substrates in TSCmKO mice. Hence, whether the distinct muscle growth response to mTORC1 activation relies on differential autophagy impairment remains unclear, but one can hypothesize that it may be more complex than a simple fast versus slow muscle distinction and may also combine specific modulation of anabolism and proteasomal activity.

Contrasting the current view that autophagy is independent of mTORC1 in skeletal muscle and strictly depends on FoxO3 (Mammucari et al., 2007; Zhao et al., 2007), we find here that sustained activation of mTORC1 blocks the induction of autophagy, despite increased FoxO3 activity, both in vivo and in vitro. As described in other cell types, this inhibitory effect of mTORC1 on autophagy in skeletal muscle was related to phosphorylation of Ulk1 protein at S757, which prevents its activation by AMPK in response to energy deprivation (Kim et al., 2011). Inhibition of mTORC1 with rapamycin or overexpression of the Ulk1 mutant S757A in TSCmKO mice was sufficient to restore autophagy in vivo. Inversely, the sustained induction of autophagy in RAmKO mice, in spite of the strong activation of Akt, indicates that LC3 lipidation is also dictated by mTORC1 inactivation and does not require FoxO3 activation. This autophagy induction correlated with higher AMPK-dependent phosphorylation of Ulk1 at S317, which is likely facilitated by mTORC1 abrogation as established in mouse embryonic fibroblast (MEF) cells (Kim et al., 2011). These seemingly different results to previous studies conducted in muscle

likely stem from experimental procedures, which may not reproduce the blocking effect of mTORC1 (Mammucari et al., 2007; Zhao et al., 2007). However, the described inability of rapamycin to increase the number of autophagosomes in mice that express a constitutively active form of Akt is more surprising (Mammucari et al., 2007). This may be due to the complete inhibition of the FoxO pathway, thereby constituting a limiting factor for autophagy induction. In RAmKO mice, expression of Bnip3 and Beclin 1 proteins, which are essential for FoxO3-dependent activation of autophagy (Mammucari et al., 2007; Grumati et al., 2010), was still detected, suggesting that FoxO3 activity is not completely blocked. Nonetheless, RAmKO mice did not respond to starvation by further inducing autophagy, which may be due to the limited upregulation of autophagy-related genes. Similarly, heterogeneous distribution of autophagosomes in muscle fibers from starved RAmKO mice and accumulation of p62 aggregates with age may reflect insufficient autophagy flux. Notably, we cannot rule out that the degradation steps of autophagy are limited in RAmKO mice due to restricted lysosomal activity, which may be related to FoxO inhibition in these mice. Hence, our findings strongly support the idea that constitutive autophagy, related to circadian feeding and activity, depends on the inhibition of the Akt/mTORC1 axis, a condition required for further stress-induced autophagy associated with the AMPK/FoxO3 axis (Sanchez et al., 2012). In this system, mTORC1 constitutes the major upstream-limiting safety catch for autophagy that coordinates changes in catabolism and anabolism in a transcription-independent manner.

Growing evidence incriminates the decline of autophagy capacity in the age-related dysfunction of several tissues (Salmiinen and Kaarniranta, 2009). Accordingly, the muscle phenotype described in TSCmKO mice is reminiscent of age-related loss of muscle mass and function, identified as sarcopenia. The concomitant loss of fat and changes in plasma glucose levels are also observed in mice with a muscle-specific deletion of *Atg7* in which autophagy in skeletal muscle is blocked (Kim et al., 2013), suggesting that similar mechanisms may account for the metabolic perturbation in TSCmKO mice. Notwithstanding, it is now well established that restoring autophagy flux, for instance by caloric restriction or by inhibiting the mTORC1 pathway, is sufficient to reverse some age-related alterations and to increase lifespan in different organisms (Mizushima et al., 2008; Harrison et al., 2009; Wohlgemuth et al., 2010). Consistently, rapamycin improves the morphological and functional muscle phenotype of old TSCmKO mice. This effect was not driven by indirect activation of FoxO3 through

(C) Accumulation of p62 (arrow) is observed rarely in muscle fibers in 2-month-old RAmKO mice in basal conditions and is slightly increased after 24 hr of starvation. Scale bar = 50  $\mu$ m.

(D) Two-month-old RAmKO (RA) and control (Ctrl) mice were submitted to fed, basal, or starved conditions (S124) with (+) or without (-) chloroquine treatment. Notably, immunoblots of TA mutant muscle reveal stronger LC3I-to-LC3II conversion, which is further increased with chloroquine. Data are normalized to  $\alpha$ -actinin and represent three independent experiments; quantification is given in Table S4.

(E and F) Quantification of the number of GFP puncta in TA muscle of GFP-LC3-expressing RAmKO and control (Ctrl) under basal conditions and after 24 hr starvation (E) and visualization of the GFP puncta in cross-sections (F). In basal conditions, the number of GFP-positive puncta is significantly higher in RAmKO than in control mice but fails to further increase upon starvation (S124). A volume unit (Vol) displayed in (E) corresponds to  $3.6 \times 10^5 \mu\text{m}^3$ . Data are mean  $\pm$  SEM; \* $p < 0.05$  compared to control mice in same conditions; <sup>§</sup> $p < 0.05$  compared to same genotype in basal conditions. Scale bar = 50  $\mu$ m (F).

(G) Expression of autophagy-related genes in TA from starved RAmKO mice is reduced compared to starved control mice but upregulated compared to basal conditions. Expressions are normalized to  $\beta$ -actin levels. Values are mean  $\pm$  SEM; \* $p < 0.05$  compared to control mice under the same condition; <sup>§</sup> $p < 0.05$ , <sup>§§</sup> $p < 0.005$  compared to same genotype in basal conditions.

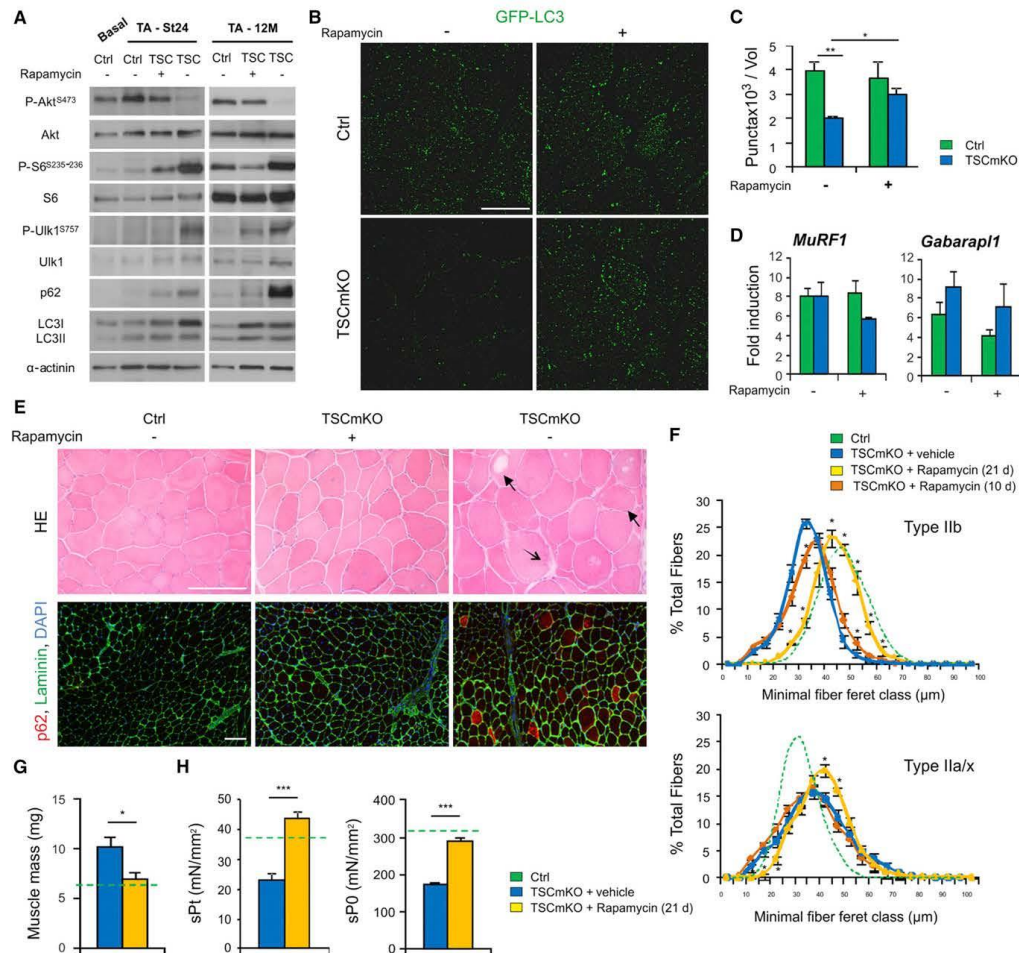


**Figure 6. Rapamycin Restores Starvation-Induced Autophagy and Ameliorates the Muscle Phenotype in TSCmKO Mice**  
 (A) Rapamycin (+) normalizes levels of phosphorylation (P) of Akt and S6 and reduces the accumulation of phospho (P)-Ulk1<sup>S3757</sup> and p62 in TA from 2-month-old starved (St24) and from 12-month-old (M, month) TSCmKO mice. The treatment also promotes the conversion of LC3I to LC3II in starved TSCmKO mice. Data are normalized to  $\alpha$ -actinin and are representative of three independent experiments; for quantification, see Table S2.  
 (B and C) Rapamycin is sufficient to increase the number of GFP-positive puncta in TA muscle from 2-month-old starved TSCmKO mice expressing GFP-LC3 (B). Scale bar = 50  $\mu$ m. GFP-LC3 puncta were quantified in a volume unit (Vol) of  $3.6 \times 10^5 \mu\text{m}^3$  (C). Values are mean  $\pm$  SEM. \* $p < 0.05$ ; \*\* $p < 0.005$ .  
 (D) Expression of the E3 ligase *MuRF1* and the autophagy-related gene *Gabarapl1* is unchanged in TA from rapamycin-treated (+) starved mice compared to sham-treated (-) mice. Data are normalized to  $\alpha$ -actinin and relative to control mice in basal conditions. Values are mean  $\pm$  SEM.  
 (E) H&E and immunostaining against p62 show reduced accumulation of vacuolated fibers (arrow), intracellular inclusions (open arrow), and p62 aggregates in TA from 12-month-old TSCmKO mice treated with rapamycin (+) compared to untreated (-) mutant mice. Scale bar = 100  $\mu$ m.  
 (F) Rapamycin treatment for 10 or 21 days (d) ameliorates the atrophy of type IIb fibers, but not the hypertrophy of type IIa/IIx fibers, in TA from 12-month-old TSCmKO mice. Values are mean  $\pm$  SEM; \* $p < 0.05$  compared to sham-treated TSCmKO mice.  
 (G and H) Muscle mass (G), specific twitch (sPt), and tetanic (sPo) forces (H) of *soleus* muscle from 12-month-old rapamycin-treated TSCmKO mice are improved compared to sham-treated mutant mice. Control values are indicated for reference by the dotted green line. Values are mean  $\pm$  SEM; \* $p < 0.05$ ; \*\*\* $p < 0.0005$ .

mTORC2-dependent regulation of Akt (Guertin et al., 2006), as Akt tends to be more activated and autophagy-related genes were unchanged. These results may foster the development of therapies modulating mTORC1 as a strategy for the treatment of sarcopenia and for muscle pathologies linked to impaired autophagy. Given our findings, therapeutic inhibition of mTORC1

will only make sense in pathological conditions where autophagy is prevented by hyperactivation of mTORC1. Accordingly, rapamycin treatment of collagen VI-deficient mice, characterized by increased Akt activation, was sufficient to restore autophagy and partly ameliorated the phenotype of the animals (Grumati et al., 2010). Other muscle pathologies with impaired autophagy related to Akt/mTORC1 misregulation may constitute potential targets for the therapeutic modulation of the mTORC1 pathway, though this will require great care given the complexity of the integrated signaling network.

#### EXPERIMENTAL PROCEDURES

##### Animal Experiments

Generation and genotyping of RAmKO, RimKO, and GFP-LC3 transgenic mice were described previously (Mizushima et al., 2004; Bentzinger et al., 2008). TSCmKO mice were obtained by crossing *Tsc1*-floxed mice (Kwiatkowski et al., 2002) from Jackson Laboratory with transgenic mice expressing Cre recombinase under the control of the human skeletal actin promoter (Schwander et al., 2003). For starvation experiments, mice were euthanized in the following conditions: ad libitum; at 10 pm (fed) or 10 am (basal); or after 12, 24, 36, or 48 hr with food deprivation (starved) but free access to water. In some experiments, mice were intraperitoneally injected with chloroquine (50 mg/kg; Sigma-Aldrich) or rapamycin (1.5 mg/kg; LC Laboratories) as described previously (Bodine et al., 2001; Grumati et al., 2010). In vitro force measurements of *soleus* and EDL muscles were conducted as described previously (Bentzinger et al., 2008). All procedures were performed in accordance with the Swiss regulations for animal experimentation and approved by the veterinary commission of the Canton Basel-Stadt.

##### In Vivo Muscle Electroporation

The constructs have been described previously (Kong et al., 2004; Bentzinger et al., 2013) or are detailed in the Supplemental Experimental Procedures. Plasmid for wild-type Ulk1 (Yan et al., 1998) was obtained from Addgene; mutagenesis (S757A) was conducted with QuikChange II XL Site-Directed Mutagenesis Kit (Agilent). Electroporation into muscle fibers was performed as described before (Kong et al., 2004).

##### Isolated Single Fibers

Single muscle fibers were isolated from EDL and TA muscles as described previously (Rosenblatt et al., 1995) and incubated for 4 hr in growth medium or PBS before protein extraction or methanol fixation.

##### Transcript Expression Analyses

Gene expression was quantified by quantitative PCR. Results were normalized to  $\beta$ -actin or  $\alpha$ -actinin expression and relative to expression in control mice. Primers are listed in Table S6.

##### Western Blotting

Proteins were extracted from TA and *soleus* muscles as described previously (Bentzinger et al., 2008). The detergent-insoluble protein fraction was solubilized in lysis buffer supplemented with 2% SDS. Antibodies used for immunoblotting are listed in the Supplemental Experimental Procedures.

##### Histology and Electron Microscopy

Inorganic colorations, immunostaining, and GFP-LC3 detection were conducted on muscle cryosections as described previously (Mizushima et al., 2004; Bentzinger et al., 2008). Antibodies are listed in the Supplemental Experimental Procedures. Transmission electron microscopy was performed as described (Moll et al., 2001).

##### Images and Statistical Analyses

Images were analyzed with the analySIS (Soft Imaging System) and imaris software. Results are expressed as mean  $\pm$  SEM of independent animals, with *n* (number of individual experiments)  $\geq$  3. Statistical comparison of two

conditions was performed using Student's *t* test with a 0.05 level of confidence accepted for statistical significance.

Detailed experimental procedures are given in Supplemental Experimental Procedures.

#### SUPPLEMENTAL INFORMATION

Supplemental information includes seven figures, six tables, and Supplemental Experimental Procedures and can be found with this article online at <http://dx.doi.org/10.1016/j.cmet.2013.03.015>.

#### ACKNOWLEDGMENTS

We thank Dr. V. Allamand for her remarks on the manuscript and Drs. T. Wiktorowicz, A. Bertrand, A.S. Arnold, R.M. Lustenberger as well as B. Erne, F. Oliveri, B. Kupr, and U. Sauder for technical assistance. MHC and Lamp antibodies, developed by H.M. Blau and J.T. August, respectively, were obtained from DSHB (Iowa, USA). We acknowledge Professor Muramatsu for the Ulk1 plasmid deposited at Addgene. This work was supported by the Cantons of Basel-Stadt and Baselland, grants from the Swiss National Science Foundation, the Swiss Foundation for Research on Muscle Disease, Swiss Life, the Association Française contre les Myopathies, the University of Basel, and Myosuisse.

Received: July 31, 2012  
Revised: November 22, 2012  
Accepted: March 21, 2013  
Published: April 18, 2013

#### REFERENCES

- Bentzinger, C.F., Romanino, K., Cloëtta, D., Lin, S., Mascarenhas, J.B., Oliveri, F., Xia, J., Casanova, E., Costa, C.F., Brink, M., et al. (2008). Skeletal muscle-specific ablation of raptor, but not of rictor, causes metabolic changes and results in muscle dystrophy. *Cell Metab.* 8, 411–424.
- Bentzinger, C.F., Lin, S., Romanino, K., Castets, P., Guridi, M., Summermatter, S., Handschin, C., Tintignac, L.A., Hall, M.N., and Rüegg, M.A. (2013). Differential response of skeletal muscles to mTORC1 signaling during atrophy and hypertrophy. *Skelet Muscle* 3, 6.
- Bodine, S.C., Stitt, T.N., Gonzalez, M., Kline, W.O., Stover, G.L., Bauerlein, R., Zlotchenko, E., Scrimgeour, A., Lawrence, J.C., Glass, D.J., and Yancopoulos, G.D. (2001). Akt/mTOR pathway is a crucial regulator of skeletal muscle hypertrophy and can prevent muscle atrophy in vivo. *Nat. Cell Biol.* 3, 1014–1019.
- De Bleecker, J.L., Engel, A.G., and Winkelmann, J.C. (1993). Localization of dystrophin and beta-spectrin in vacuolar myopathies. *Am. J. Pathol.* 143, 1200–1208.
- Grumati, P., Coletto, L., Sabatelli, P., Cescon, M., Angelin, A., Bertaggia, E., Blaauw, B., Urciuolo, A., Tiepolo, T., Merlini, L., et al. (2010). Autophagy is defective in collagen VI muscular dystrophies, and its reactivation rescues myofiber degeneration. *Nat. Med.* 16, 1313–1320.
- Guertin, D.A., Stevens, D.M., Thoreen, C.C., Burdts, A.A., Kalaany, N.Y., Moffat, J., Brown, M., Fitzgerald, K.J., and Sabatini, D.M. (2006). Ablation in mice of the mTORC components raptor, rictor, or mTORC2 reveals that mTORC2 is required for signaling to Akt-FOXO and PKC $\alpha$ , but not S6K1. *Dev. Cell* 11, 859–871.
- Harrington, L.S., Findlay, G.M., Gray, A., Tolkacheva, T., Wigfield, S., Rebholz, H., Barnett, J., Leslie, N.R., Cheng, S., Shepherd, P.R., et al. (2004). The TSC1-2 tumor suppressor controls insulin-Pi3K signaling via regulation of IRS proteins. *J. Cell Biol.* 166, 213–223.
- Harrison, D.E., Strong, R., Sharp, Z.D., Nelson, J.F., Astle, C.M., Flurkey, K., Nadon, N.L., Wilkinson, J.E., Frenkel, K., Carter, C.S., et al. (2009). Rapamycin fed late in life extends lifespan in genetically heterogeneous mice. *Nature* 460, 392–395.
- Inoki, K., Li, Y., Xu, T., and Guan, K.L. (2003). Rheb GTPase is a direct target of TSC2 GAP activity and regulates mTOR signaling. *Genes Dev.* 17, 1829–1834.

- Kim, J., Kundu, M., Viollet, B., and Guan, K.L. (2011). AMPK and mTOR regulate autophagy through direct phosphorylation of Ulk1. *Nat. Cell Biol.* **13**, 132–141.
- Kim, K.H., Jeong, Y.T., Oh, H., Kim, S.H., Cho, J.M., Kim, Y.N., Kim, S.S., Kim, H., Hur, K.Y., Kim, H.K., et al. (2013). Autophagy deficiency leads to protection from obesity and insulin resistance by inducing Fgf21 as a mitokine. *Nat. Med.* **19**, 83–92.
- Klionsky, D.J., Abdalla, F.C., Abeliovich, H., Abraham, R.T., Acevedo-Arozena, A., Adeli, K., Agholme, L., Agnello, M., Agostinis, P., Aguirre-Ghiso, J.A., et al. (2012). Guidelines for the use and interpretation of assays for monitoring autophagy. *Autophagy* **8**, 445–544.
- Kong, X.C., Barzaghi, P., and Ruedig, M.A. (2004). Inhibition of synapse assembly in mammalian muscle in vivo by RNA interference. *EMBO Rep.* **5**, 183–188.
- Kwiatkowski, D.J., Zhang, H., Bandura, J.L., Heiberger, K.M., Glogauer, M., el-Hashemite, N., and Onda, H. (2002). A mouse model of TSC1 reveals sex-dependent lethality from liver hemangiomas, and up-regulation of p70S6 kinase activity in Tsc1 null cells. *Hum. Mol. Genet.* **11**, 525–534.
- Lai, K.M., Gonzalez, M., Poueymirou, W.T., Kline, W.O., Na, E., Zlotchenko, E., Stitt, T.N., Economides, A.N., Yancopoulos, G.D., and Glass, D.J. (2004). Conditional activation of akt in adult skeletal muscle induces rapid hypertrophy. *Mol. Cell. Biol.* **24**, 9295–9304.
- Laplanche, M., and Sabatini, D.M. (2012). mTOR signaling in growth control and disease. *Cell* **149**, 274–293.
- Lum, J.J., DeBerardinis, R.J., and Thompson, C.B. (2005). Autophagy in metabolism: cell survival in the land of plenty. *Nat. Rev. Mol. Cell Biol.* **6**, 439–448.
- Mammucari, C., Milan, G., Romanello, V., Masiero, E., Rudolf, R., Del Piccolo, P., Burden, S.J., Di Lisi, R., Sandri, C., Zhao, J., et al. (2007). FoxO3 controls autophagy in skeletal muscle in vivo. *Cell Metab.* **6**, 458–471.
- Masiero, E., Agatea, L., Mammucari, C., Blaauw, B., Loro, E., Komatsu, M., Metzger, D., Reggiani, C., Schiaffino, S., and Sandri, M. (2009). Autophagy is required to maintain muscle mass. *Cell Metab.* **10**, 507–515.
- Mizushima, N., Yamamoto, A., Matsui, M., Yoshimori, T., and Ohsumi, Y. (2004). In vivo analysis of autophagy in response to nutrient starvation using transgenic mice expressing a fluorescent autophagosome marker. *Mol. Biol. Cell* **15**, 1101–1111.
- Mizushima, N., Levine, B., Cuervo, A.M., and Klionsky, D.J. (2008). Autophagy fights disease through cellular self-digestion. *Nature* **451**, 1069–1075.
- Moll, J., Barzaghi, P., Lin, S., Bezakova, G., Lochmüller, H., Engvall, E., Müller, U., and Ruedig, M.A. (2001). An agrin minigene rescues dystrophic symptoms in a mouse model for congenital muscular dystrophy. *Nature* **413**, 302–307.
- Ogata, T., Oishi, Y., Higuchi, M., and Muraoka, I. (2010). Fasting-related autophagic response in slow- and fast-twitch skeletal muscle. *Biochem. Biophys. Res. Commun.* **394**, 136–140.
- Rosenblatt, J.D., Lunt, A.I., Parry, D.J., and Partridge, T.A. (1995). Culturing satellite cells from living single muscle fiber explants. *In Vitro Cell. Dev. Biol. Anim.* **31**, 773–779.
- Rüegg, M.A., and Glass, D.J. (2011). Molecular mechanisms and treatment options for muscle wasting diseases. *Annu. Rev. Pharmacol. Toxicol.* **51**, 373–395.
- Salminen, A., and Kaamiranta, K. (2009). Regulation of the aging process by autophagy. *Trends Mol. Med.* **15**, 217–224.
- Sancak, Y., Bar-Peled, L., Zoncu, R., Markhard, A.L., Nada, S., and Sabatini, D.M. (2010). Ragulator-Rag complex targets mTORC1 to the lysosomal surface and is necessary for its activation by amino acids. *Cell* **141**, 290–303.
- Sanchez, A.M., Csibi, A., Raibon, A., Cornille, K., Gay, S., Bernardi, H., and Candau, R. (2012). AMPK promotes skeletal muscle autophagy through activation of forkhead FoxO3a and interaction with Ulk1. *J. Cell. Biochem.* **113**, 695–710.
- Schwander, M., Leu, M., Stumm, M., Dorchies, O.M., Ruedig, U.T., Schittny, J., and Müller, U. (2003). Beta1 integrins regulate myoblast fusion and sarcomere assembly. *Dev. Cell* **4**, 673–685.
- Smith, E.M., Finn, S.G., Tee, A.R., Browne, G.J., and Proud, C.G. (2005). The tuberous sclerosis protein TSC2 is not required for the regulation of the mammalian target of rapamycin by amino acids and certain cellular stresses. *J. Biol. Chem.* **280**, 18717–18727.
- Spätle, U., and Schulze, P.C. (2004). Proinflammatory cytokines and skeletal muscle. *Curr. Opin. Clin. Nutr. Metab. Care* **7**, 265–269.
- Tee, A.R., Manning, B.D., Roux, P.P., Cantley, L.C., and Blenis, J. (2003). Tuberous sclerosis complex gene products, Tuberin and Hamartin, control mTOR signaling by acting as a GTPase-activating protein complex toward Rheb. *Curr. Biol.* **13**, 1259–1268.
- Tisdale, M.J. (2010). Cancer cachexia. *Curr. Opin. Gastroenterol.* **26**, 146–151.
- Wohlgemuth, S.E., Seo, A.Y., Marzetti, E., Lees, H.A., and Leeuwenburgh, C. (2010). Skeletal muscle autophagy and apoptosis during aging: effects of calorie restriction and life-long exercise. *Exp. Gerontol.* **45**, 138–148.
- Yan, J., Kuroyanagi, H., Kuroiwa, A., Matsuda, Y., Tokumitsu, H., Tomoda, T., Shirasawa, T., and Muramatsu, M. (1998). Identification of mouse ULK1, a novel protein kinase structurally related to *C. elegans* UNC-51. *Biochem. Biophys. Res. Commun.* **246**, 222–227.
- Zhao, J., Brault, J.J., Schild, A., Cao, P., Sandri, M., Schiaffino, S., Lecker, S.H., and Goldberg, A.L. (2007). FoxO3 coordinately activates protein degradation by the autophagic/lysosomal and proteasomal pathways in atrophying muscle cells. *Cell Metab.* **6**, 472–483.

## 6.2. Publication 4

Bentzinger et al. *Skeletal Muscle* 2013, **3**:6  
<http://www.skeletalmusclejournal.com/content/3/1/6>



### RESEARCH

### Open Access

# Differential response of skeletal muscles to mTORC1 signaling during atrophy and hypertrophy

C Florian Bentzinger<sup>1†</sup>, Shuo Lin<sup>1†</sup>, Klaas Romanino<sup>1</sup>, Perrine Castets<sup>1,2</sup>, Maitea Guridi<sup>1</sup>, Serge Summermatter<sup>1</sup>, Christoph Handschin<sup>1</sup>, Lionel A Tintignac<sup>1,3</sup>, Michael N Hall<sup>1</sup> and Markus A Rüegg<sup>1\*</sup>

#### Abstract

**Background:** Skeletal muscle mass is determined by the balance between protein synthesis and degradation. Mammalian target of rapamycin complex 1 (mTORC1) is a master regulator of protein translation and has been implicated in the control of muscle mass. Inactivation of mTORC1 by skeletal muscle-specific deletion of its obligatory component raptor results in smaller muscles and a lethal dystrophy. Moreover, raptor-deficient muscles are less oxidative through changes in the expression PGC-1 $\alpha$ , a critical determinant of mitochondrial biogenesis. These results suggest that activation of mTORC1 might be beneficial to skeletal muscle by providing resistance to muscle atrophy and increasing oxidative function. Here, we tested this hypothesis by deletion of the mTORC1 inhibitor tuberous sclerosis complex (TSC) in muscle fibers.

**Method:** Skeletal muscles of mice with an acute or a permanent deletion of raptor or TSC1 were examined using histological, biochemical and molecular biological methods. Response of the muscles to changes in mechanical load and nerve input was investigated by ablation of synergistic muscles or by denervation.

**Results:** Genetic deletion or knockdown of raptor, causing inactivation of mTORC1, was sufficient to prevent muscle growth and enhance muscle atrophy. Conversely, short-term activation of mTORC1 by knockdown of TSC induced muscle fiber hypertrophy and atrophy-resistance upon denervation, in both fast *tibialis anterior* (TA) and slow *soleus* muscles. Surprisingly, however, sustained activation of mTORC1 by genetic deletion of *Tsc1* caused muscle atrophy in all but *soleus* muscles. In contrast, oxidative capacity was increased in all muscles examined. Consistently, TSC1-deficient *soleus* muscle was atrophy-resistant whereas TA underwent normal atrophy upon denervation. Moreover, upon overloading, *plantaris* muscle did not display enhanced hypertrophy compared to controls. Biochemical analysis indicated that the atrophy response of muscles was based on the suppressed phosphorylation of PKB/Akt via feedback inhibition by mTORC1 and subsequent increased expression of the E3 ubiquitin ligases *MuRF1* and *atrogin-1/MAFbx*. In contrast, expression of both E3 ligases was not increased in *soleus* muscle suggesting the presence of compensatory mechanisms in this muscle.

**Conclusions:** Our study shows that the mTORC1- and the PKB/Akt-FoxO pathways are tightly interconnected and differentially regulated depending on the muscle type. These results indicate that long-term activation of the mTORC1 signaling axis is not a therapeutic option to promote muscle growth because of its strong feedback induction of the E3 ubiquitin ligases involved in protein degradation.

**Keywords:** Skeletal muscle, Hypertrophy, Atrophy, Mammalian target of rapamycin complex 1 (mTORC1), Raptor, Tuberous sclerosis complex (TSC), PKB/Akt, FoxO, MuRF1, Atrogin-1/MAFbx

\* Correspondence: [markus-a.ruegg@unibas.ch](mailto:markus-a.ruegg@unibas.ch)

<sup>†</sup>Equal contributors

<sup>3</sup>Biozentrum, University of Basel, Basel CH-4056, Switzerland

Full list of author information is available at the end of the article



© 2013 Bentzinger et al.; licensee BioMed Central Ltd. This is an Open Access article distributed under the terms of the Creative Commons Attribution License (<http://creativecommons.org/licenses/by/2.0>), which permits unrestricted use, distribution, and reproduction in any medium, provided the original work is properly cited.

## Background

Skeletal muscle is the largest organ, accounting for 30 to 40% of the total body weight. Muscle tissue is highly plastic and adapts its size to physical demand. For example, increase in load causes hypertrophy whereas unloading causes atrophy. Importantly, muscle atrophy and subsequent wasting are also hallmarks of pathology in muscular dystrophies or in cachexia, the latter being a secondary consequence of a primary disease (for example, AIDS, cancer or sepsis). Several lines of evidence indicate that muscle mass is controlled by the balance between protein synthesis and protein degradation [1,2]. In skeletal muscle, protein synthesis can be induced by IGF1 (insulin-like growth factor-1), which in turn, activates PI3K (phosphatidylinositol 3-kinase) and PKB (protein kinase B; also called Akt). Activated PKB/Akt inhibits the protein complex TSC1-TSC2 (tuberous sclerosis complex), which inactivates the small GTPase protein Rheb (Ras homolog enriched in brain). Rheb activates mammalian target of rapamycin complex 1 (mTORC1), which causes an increase in protein translation by phosphorylating its two best characterized targets S6K (p70S6 kinase) and 4EBP (eIF-4E-binding protein). This IGF1-PI3K-PKB/Akt-mTOR signaling pathway controls protein synthesis and cell size in several tissues [3,4].

Activation of PKB/Akt also negatively regulates protein degradation by phosphorylating the FoxO (Forkhead box O) transcription factors. Protein degradation is mainly carried out by enzymes of the ubiquitin-proteasomal and autophagosomal-lysosomal pathways [5,6]. Dephosphorylated FoxOs in the nuclei promote the expression of the two E3 ubiquitin ligases *atrogen-1/MAFbx* and *MuRF1* [7,8]. FoxOs have also been described to drive expression of autophagy-related genes [6,9]. The function of active PKB/Akt to simultaneously stimulate protein synthesis and inhibit protein degradation may explain the profound hypertrophic effect of constitutively active PKB/Akt [10,11].

mTOR belongs to the PI3/PI4-kinase family; it is highly conserved from yeast to human and assembles into two structurally and functionally distinct multi-protein complexes, called mTORC1 and mTORC2 [12,13]. An essential component of mTORC1 is the protein raptor (regulatory-associated protein of mTOR), whereas rictor (rapamycin-insensitive companion of mTOR) is an essential subunit of mTORC2 [3,4]. Most functions of mTORC1 are acutely inhibited by the immunosuppressant rapamycin, whereas mTORC2 is only repressed by long-term application of rapamycin [14]. In skeletal muscle, the function of mTORC2 seems to not be essential because mice deficient for rictor have no overt phenotype [15,16]. In contrast, mTORC1 participates in the control of muscle size. For example,

rapamycin prevents IGF1-induced growth of myotubes [17], inhibits compensatory hypertrophy in rat skeletal muscle [5] and blocks the growth-stimulating activity of clenbuterol [18]. Moreover, transgenic overexpression of TSC1 causes muscle atrophy in mice [19], while acute overexpression of Rheb induces muscle hypertrophy [20]. Finally, mice deficient for S6K1 show a reduction of muscle fiber size and a blunted response to IGF1 [21].

In agreement with these findings, we recently showed that mice with a skeletal muscle-specific knockout for raptor (called RAmKO for raptor muscle knockout) have a reduced muscle mass and suffer from a progressive dystrophy, which causes their death at the age of four to six months [16]. Muscles of RAmKO mice also have a decreased oxidative capacity, which can be restored by transgenic expression of PGC-1 $\alpha$  [22]. In addition, RAmKO mice show sustained activation of PKB/Akt because of relieved feedback inhibition onto IRS1 (insulin receptor substrate-1) by the diminished activation of S6K [16].

Here we investigated the contribution of mTORC1 to muscle atrophy and hypertrophy by targeting *raptor* (the gene encoding raptor) or *Tsc1* (encoding TSC1) specifically in mouse skeletal muscle. We show that deletion of *raptor* prevents muscle hypertrophy and enhances muscle atrophy. Surprisingly, sustained activation of mTORC1 by the genetic deletion of *Tsc1* does not induce hypertrophy but rather causes atrophy in all but *soleus* muscles. While the TSC1-deficient, hypertrophic *soleus* muscle is also resistant to denervation-induced atrophy, *tibialis anterior* (TA) muscle atrophies like controls. Biochemical characterization shows that regulation of the two E3 ligases *atrogen-1/MAFbx* and *MuRF1* differs between TA and *soleus* muscles. Furthermore, we demonstrate that all muscles show an increase in their oxidative capacity upon mTORC1 activation. In summary, we demonstrate that the oxidative capacity in all skeletal muscles is controlled by mTORC1, whereas the effect of sustained activation of mTORC1 on muscle size differs between muscles. Hence, our studies decipher a mechanism of biological robustness that balances the two major metabolic pathways involved in the control of skeletal muscle mass.

## Methods

### Mice

Mice were maintained in a conventional facility with a fixed dark–light cycle. Studies were carried out according to criteria outlined for the care and use of laboratory animals and with approval of the Swiss authorities. RAmKO mice were generated and genotyped as described before [16]. Floxed *Tsc1* mice [23] were obtained from The Jackson Laboratory (Bar Harbor, Maine, USA) and mated with mice expressing Cre recombinase under the human

skeletal actin (HSA) promoter [24]. Genotyping for the conditional *Tsc1* allele was performed as described [23]. TSC-RAmKO mice were generated by intercrossing mice carrying floxed *rptor* and *Tsc1* alleles. Mice homozygous for both floxed alleles were mated with double heterozygotes, which also carried the *HSA-Cre* transgene. Except for overloading experiments and Western blot analysis, only male TSCmKO mice were used. Both genders were used in RAmKO and TSC-RAmKO mice. All procedures were performed in accordance with the Swiss regulations for animal experimentation and they were approved by the veterinary commission of the Canton Basel-Stadt.

#### Rapamycin treatment of mice

Rapamycin treatment began three days before the mice were challenged with functional overload (FO) or electroporation and continued until mice were sacrificed. Rapamycin (LC Laboratories, Woburn, MA, USA), dissolved in saline containing 2% carboxymethylcellulose (Sigma-Aldrich, St. Louis, MO, USA), was delivered once daily by i.p. (intraperitoneal) injection at a dose of 1.5 mg/kg [5].

#### shRNA constructs

The methods to construct plasmids encoding shRNA and the sequences of the *Cd4* control shRNA and the NLS-GFP construct have been described elsewhere [25]. The murine 19 nucleotide target sequences correspond to: GTT GAT GCG TAA CCT TCT G (*Tsc2*), GAT GGA CAC TGA TGT TGT G (*Tsc1*) and GAA TTT TGC TGA TTT GGA A (*rptor*).

#### Tissue culture, transfections and shRNA efficiency

Adenoviruses encoding shRNA against *Tsc2* and *Cd4* were created by cloning the respective shRNA sequence and H1 promoter from pSuper into pAd-DEST (Life Technologies Europe B.V., Zug, Switzerland). To test the efficiency of the *Tsc2* shRNA, C2C12 myoblasts, cultured under standard conditions, were transfected with the *Tsc2* and *Cd4* shRNA viruses. The efficiency of the *rptor* shRNA was tested by co-transfection with an expression plasmid encoding HA-tagged raptor into COS7 cells using Lipofectamine 2000 (Life Technologies). For PGC1 $\beta$  overexpression and knockdown, myoblasts were permitted to fuse into multinucleated myotubes for 48 hr and cells were infected with adenovirus preparations for an additional 48 hr. Adenoviruses (Ad-GFP, Ad-PGC1 $\beta$ , Ad-scrambled or Ad-siPGC1 $\beta$ ) were kindly provided by BM Spiegelman (Harvard University, Boston, MA, USA).

#### Electroporation of muscle

Plasmids encoding shRNA constructs were electroporated into muscle fibers as described before [25]. Briefly, *soleus* or TA muscle of anesthetized mice was exposed and

injected with 10 to 30  $\mu$ l of a mixture containing the respective shRNA plasmid and a plasmid coding for NLS-GFP (2 mg/ml of each construct). The fascia and the skin were sutured and the electroporation was performed using an ECM 830 electroporation system (BTX Instruments Division, Harvard Apparatus Inc., Holliston, MA, USA). Eight pulses lasting 20 ms with the frequency of 1 Hz and the voltage set to 180 V/cm were applied. Mice were analyzed four to six weeks after electroporation.

#### Denervation, nerve crush and overloading

Mice were anesthetized with ketamine (111 mg/kg) and xylazine (22 mg/kg) by intra-peritoneal injection and surgery was performed under aseptic conditions. For denervation, a segment (approximately 5 mm) of the sciatic nerve at the mid-thigh level was excised [26]. To induce muscle re-growth, the nerve was crushed with No 5 Dupont forceps (Fine Science Tools GmbH, Heidelberg, Germany) for 10 seconds at mid-thigh [27]. To induce muscle hypertrophy, a functional overload of *plantaris* muscle was introduced by surgical removal of *soleus* and *gastrocnemius* muscles [28]. Surgery was performed on one leg only. The *plantaris* muscle of the contralateral leg served as control.

#### Antibodies

The antibodies used were from the following sources: rabbit polyclonal antibodies directed to 4E-BP1 (Phas-I) from Zymed (Life Technologies); those recognizing Phospho-4E-BP1 (Ser65), PKB/Akt, mTOR, S6 Ribosomal Protein or Phospho-S6 Ribosomal Protein (Ser235/236) were all from Cell Signaling Technology Inc. (Danvers, MA, USA); those against FoxO1a were from Abcam plc. (Cambridge, UK); those against TSC1 were from Bethyl Laboratories (Montgomery, TX, USA). Rabbit monoclonal antibodies directed against Phospho-Akt (Ser473), IRS-1, FoxO3a (75D8) and phospho-FoxO1(Thr24)/FoxO3a(Thr32) (#9466) were from Cell Signaling Technology Inc. Mouse monoclonal antibodies to  $\alpha$ -actinin were purchased from Sigma and antibodies against HA from Covance Inc. (Geneva, Switzerland). Rat monoclonal antibodies directed to the Laminin B2 Chain (MAB1914) were from Chemicon and sold by Millipore AG (Zug, Switzerland). The TSC2 antibodies used were described elsewhere [29]. Mouse monoclonal antibodies against myosin heavy chain: slow (A4.840), IIa/IIx (A4.74) and IIb (BF-F3) were purchased from The Developmental Studies Hybridoma Bank (University of Iowa, Iowa City, Iowa, USA). Antibodies to puromycin [30] were a kind gift of Dr. Philippe Pierre (CIML Parc Scientifique de Luminy, Marseille, France).

#### Histology and immunohistochemistry

Muscles frozen in liquid nitrogen-cooled isopentane were cut into 12  $\mu\text{m}$  cross-sections. Cross-sections were fixed with 2% paraformaldehyde (PFA) and permeabilized with 1% Triton/PBS for 5 minutes, washed with 100 mM glycine/PBS for 15 minutes, blocked with 1% BSA/PBS for 30 minutes, and incubated with the primary antibody overnight at 4°C. Samples were subsequently washed three times for 10 minutes each with 1% BSA/PBS and stained with the appropriate fluorescence labeled secondary antibodies for 1 hr at room temperature. After washing with PBS, samples were mounted with Citifluor (Citifluor Ltd. London, UK). General histology on cross-sections was performed using hematoxylin and eosin (H&E; Merck, Zug, Switzerland). NADH-TR (Nicotinamide adenine dinucleotide hydrogen-tetrazolium reductase) staining was done as described [31]. Methods of SDH and COX staining were described elsewhere [22]. Samples were dehydrated and mounted with DePeX mounting medium (Gurr, BDH, VWR International GmbH, Dietikon, Switzerland).

#### In vivo protein synthesis

Protein synthesis was measured using the surface sensing of translation (SUnSET) method [30] by i.p. injection of 0.040  $\mu\text{mol/g}$  puromycin dissolved in 100  $\mu\text{l}$  of PBS. Mice were sacrificed 30 minutes later and muscles were snap-frozen in liquid nitrogen. Muscles were lysed as described below and proteins were separated on 8 to 16% SDS-PAGE (Bio-Rad Laboratories AG, Cressier, Switzerland). After transfer to polyvinylidene difluoride membranes and blocking of free binding sites with 5% milk powder in Tris-buffered saline with 0.1% Tween 20 (TBST), the mouse IgG2a monoclonal anti-puromycin antibody (clone 12D10; 1:5,000) was incubated for 1 hr at room temperature. After incubation with the appropriate HRP-coupled secondary antibody, blots were developed using enhanced chemiluminescence reagent. Coomassie Blue staining was used to verify equal loading.

#### Tissue homogenization, SDS-PAGE and Western blot

Muscles frozen in liquid nitrogen were powdered on dry ice and lysed in cold RIPA buffer supplemented with 1% Triton-X, 10% glycerol, protease inhibitor cocktail tablets (Roche Diagnostics AG, Rotkreuz, Switzerland), and phosphatase inhibitor cocktail I and II (Sigma). Cell lysates were incubated on ice for 2 hr, sonicated two times for 15 s and centrifuged at 13,600 g for 30 minutes at 4°C. Cleared lysates were then used to determine total protein levels (BCA Protein Assay, Pierce, Rockford, IL, USA). After dilution with sample buffer, equal protein amounts were loaded onto SDS gels.

#### Real-time PCR

Total RNA was isolated (SV Total RNA Isolation System, Promega AG, Dübendorf, Switzerland) from *soleus* muscles. RNA concentrations were adjusted between samples and reverse transcription was carried out using a mixture of oligodT and random hexamer primers (iScript cDNA Synthesis Kit, Bio-Rad Laboratories AG). Sybr Green, real-time PCR analysis (Power SYBR Green Master Mix, Life Technologies) was performed using the ABI Prism 7000 Sequence Detector. Expression levels for each gene of interest were normalized to the expression of the housekeeping protein  $\beta$ -actin. The following primers were used:  $\beta$ -actin sense primer: 5' CAG CTT CTT TGC AGC TCC TT, antisense primer: 5' GCA GCG ATA TCG TCA TCC A; *atrogen-1/MAFbx* sense primer: 5' CTC TGT ACC ATG CCG TTC CT, antisense primer: 5' GGC TGC TGA ACA GAT TCT CC; *MuRF-1* sense primer: 5' ACC TGC TGG TGG AAA ACA TC, antisense primer: 5' AGG AGC AAG TAG GCA CCT CA; *Pgc1 $\alpha$*  sense primer: 5' TGA TGT GAA TGA CTT GGA TAC AGA CA, antisense primer: 5' GCT CAT TGT TGT ACT GGT TGG ATA TG; *Pgc1 $\beta$*  sense primer: 5' GGC AGG TTC AAC CCC GA, antisense primer: 5' CTT GCT AAC ATC ACA GAG GAT ATC TTG. Quantification of mitochondrial DNA copy numbers was done as described [22].

#### Quantifications and statistics

For muscle fiber size quantification, muscle cross-sections were stained either for laminin- $\gamma$ 1 or fluorescence labeled wheat-germ agglutinin. Images were acquired using a Leica DM5000B fluorescence microscope with 10x objective, a digital camera (F-View; Soft Imaging System, Olympus Soft Imaging Solutions GmbH, Münster, Germany), and analysis software (Soft Imaging System). Images of the entire *soleus* or *tibialis anterior* (TA) muscles were aligned with Adobe Photoshop (Adobe Systems Incorporated, San Jose, CA, USA). The minimum distance of parallel tangents at opposing particle borders (minimal feret's diameter) and cross-section area (CSA) were measured with analysis software as described [32]. Data are expressed as mean  $\pm$  SEM. For statistical comparison of two conditions, the Student's *t*-test was used. The level of significance is indicated as follows: \*\*\*  $P < 0.001$ , \*\*  $P < 0.01$ , \*  $P < 0.05$ .

#### Results

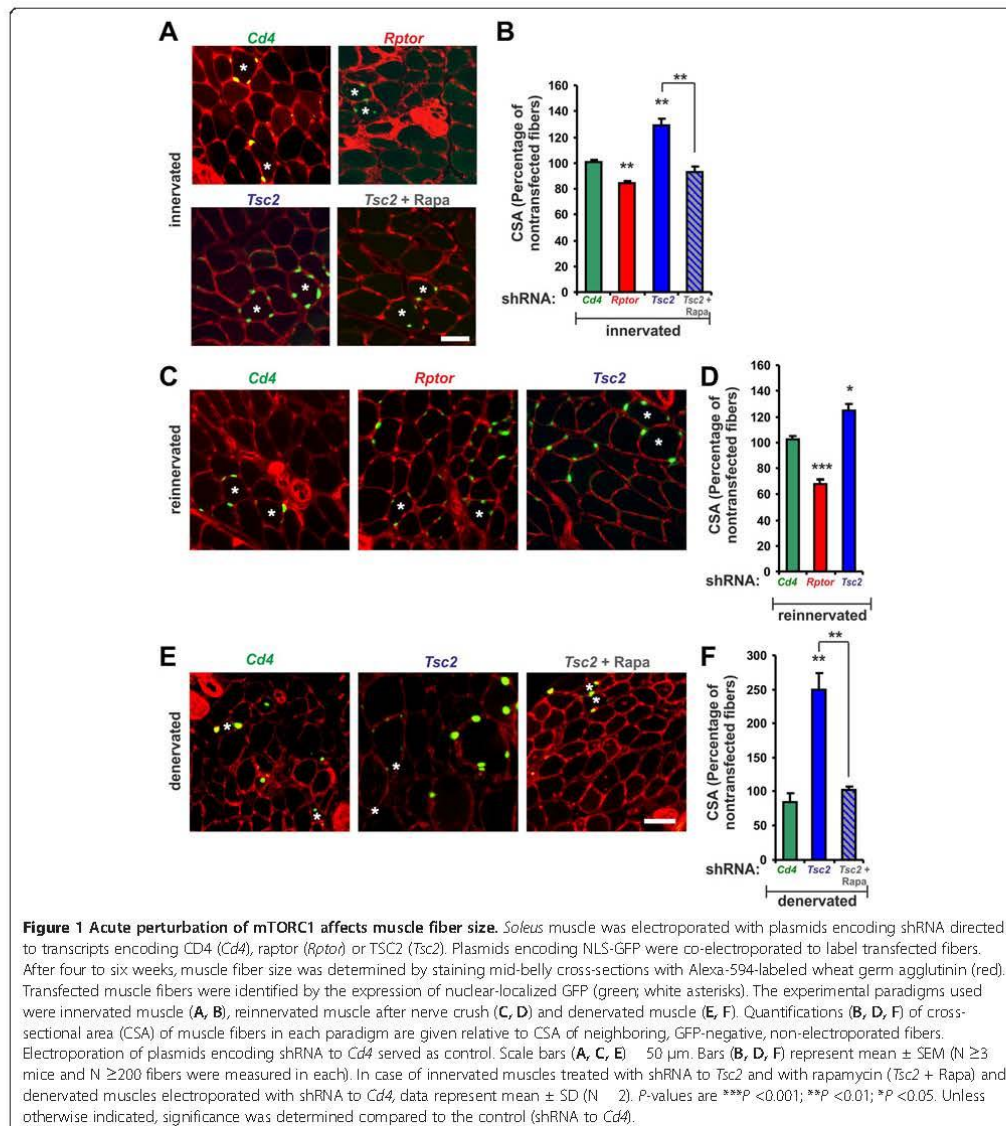
##### Acute changes in mTORC1 activity affect muscle fiber size

To evaluate the potential of mTORC1 in regulating muscle fiber size, we first tested the effect of mTORC1 inhibition or activation in normal weight-bearing muscles and in acute models of muscle hypertrophy and atrophy. To this end, we electroporated plasmids encoding an shRNA directed against *rptor* (to inactivate mTORC1) or *Tsc2* (to activate mTORC1) into muscle



fibers of mouse *soleus* muscle using the methods described [25]. As a negative control, shRNA constructs directed against *Cd4* were used. To label targeted muscle fibers, a plasmid coding for nuclear-localized GFP (NLS-GFP) was co-electroporated with all shRNA constructs. Before electroporation into muscle, each shRNA construct was tested in tissue culture using either COS cells co-transfected with the corresponding expression plasmid

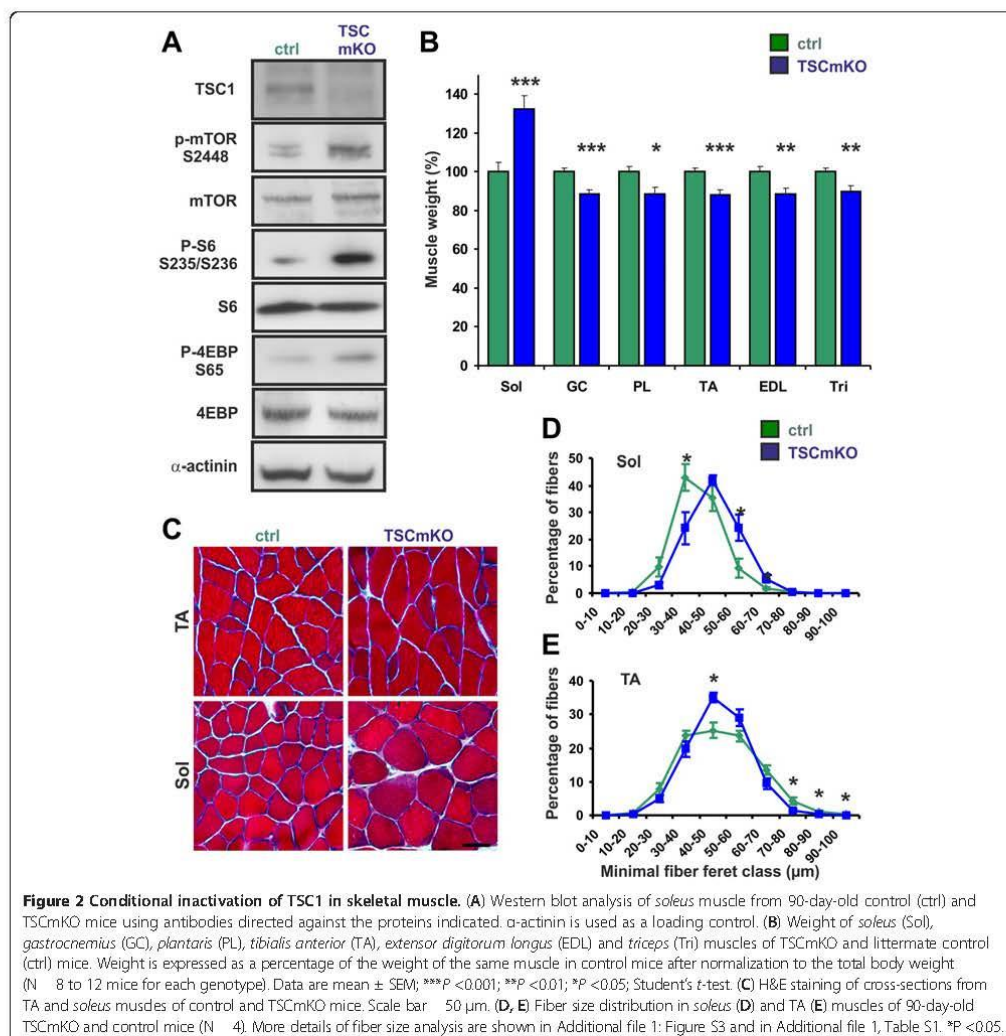
(Additional file 1: Figure S1A) or by infecting myoblasts with adenovirus expressing the corresponding shRNA construct (Additional file 1: Figure S1B). Four to six weeks after electroporation, transfected muscle fibers were identified by their expression of NLS-GFP in myonuclei (Figure 1) and the size of GFP-positive fibers was compared with that of neighboring, non-transfected fibers. Knockdown of raptor resulted in a small but significant



decrease in muscle fiber size, whereas knockdown of TSC2 resulted in a significant increase (Figure 1A, B). Consistent with the notion that TSC1/2 acts via mTORC1, rapamycin fully prevented the muscle hypertrophy observed in TSC2 knockdown fibers (Figure 1A, B). As expected, electroporation of shRNA constructs targeting *Tsc1* resulted in a hypertrophy response very similar to the *Tsc2* knockdown (Additional file 1: Figure S1C, D).

To test the role of mTORC1 in muscle plasticity, we crushed the sciatic nerve unilaterally immediately after electroporation, which causes a transient denervation-

induced atrophy, followed by fiber re-innervation and re-growth to normal size [27,33,34]. Such “hypertrophy on recovery” (HOR) was significantly less in muscle fibers expressing shRNA to *rptor* and significantly higher in fibers expressing shRNA to *Tsc2* (Figure 1C, D). To test whether shRNA-targeting acted on the initial atrophy or on re-growth, we also examined electroporated muscle fibers in a pure denervation-induced atrophy paradigm. No difference between non-electroporated and electroporated fibers was detected in *Cd4* controls (Figure 1E, F). In contrast, muscle fibers expressing



shRNA to *Tsc2* were much bigger than non-electroporated fibers and, like in innervated muscle, the effect of TSC2 knockdown was abrogated by rapamycin (Figure 1E, F). Similar results were obtained by electroporating *tibialis anterior* (TA) muscle (Additional file 1, Figure S1E, F). These results thus show that acute alteration of mTORC1 activity affects the response of both, the slow oxidative *soleus* and fast glycolytic TA muscles to growth-stimulating and atrophy-inducing conditions.

#### Constitutive deletion of *Tsc1* in skeletal muscle fibers affects muscles differentially

To examine whether sustained activation of mTORC1 would lead to the same effects observed in our electroporation paradigm, mice carrying floxed alleles for *Tsc1* [23] were crossed with mice that express Cre recombinase under the control of the muscle fiber-specific human skeletal actin (HSA) promoter [24]. Mice lacking TSC1 in skeletal muscle (herein called TSCmKO, for TSC muscle knockout) were born at the expected Mendelian ratio and, at birth, could not be visually distinguished from their littermate controls. Muscle extracts from TSCmKO mice were largely devoid of TSC1 (Figure 2A). Moreover, they showed the expected increase in

phosphorylation of mTOR at the mTORC1-selective site Serine 2448 and of the mTORC1 targets S6 and 4EBP (Figure 2A; Table 1 for quantification). These data are similar to those obtained in other tissues where *Tsc1* or *Tsc2* were conditionally ablated [23,35-37].

Consistent with the activation of the mTORC1 targets and the role of mTORC1 in the control of protein translation, protein synthesis in EDL muscle of TSCmKO was increased (Additional file 1: Figure S2A). However, TSCmKO mice gained less weight than their control littermates. Starting from the age of five weeks, male TSCmKO mice were significantly lighter (Additional file 1: Figure S2B), whereas the weight difference in females did not reach significance (Additional file 1: Figure S2C). At least part of this weight difference was due to alteration in muscle mass as all but *soleus* muscles were significantly lighter than in control mice (Figure 2B). Thus, despite increased protein synthesis, all but *soleus* muscles are lighter in TSCmKO mice than in control mice.

To investigate the reason for these muscle-specific differences in weight, we focused on *soleus* and TA muscles in three-month-old mice. Hematoxylin & eosin (H&E) staining did not reveal any major alterations in either of the muscles (Figure 2C). The difference in the muscle

**Table 1 Quantification of Western blot analysis**

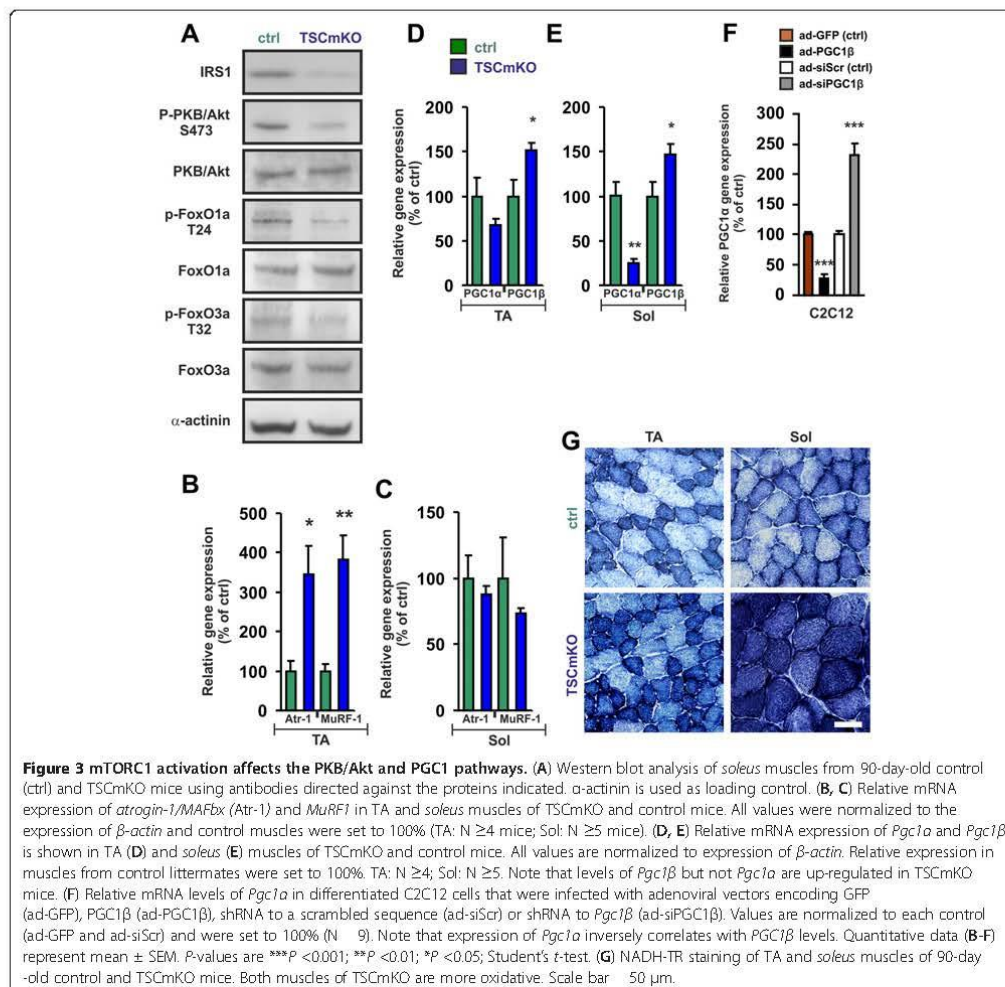
	TSCmKO	Ctrl	Ratio	Number of replicates
p-mTOR <sup>S2448</sup>	19 ± 2***	10 ± 1	1.9	4
mTOR	31 ± 6	28 ± 5	1.1	4
P-4E-BP1 <sup>S65</sup>	23 ± 5***	12 ± 3	1.9	4
4E-BP1	34 ± 6	39 ± 6	0.9	4
P-S6 <sup>S235/S236</sup>	53 ± 1***	13 ± 6	4	4
S6	48 ± 11	42 ± 17	1.1	4
IRS-1	6 ± 2***	24 ± 1	0.3	4
P-PKB/ Akt <sup>S473</sup>	4 ± 2***	22 ± 3	0.2	4
PKB/ Akt	28 ± 7	22 ± 6	1.2	4
FoxO1	23 ± 5	18 ± 3	1.3	4
FoxO3a	16 ± 7	17 ± 5	0.9	4
P-FoxO1 <sup>T24/3aT23</sup>	2 ± 7*/ 8 ± 3*	11 ± 2/ 20 ± 5	0.2/ 0.4	4
P-PKB/ Akt <sup>S473</sup> (Den. TA)	n.d.	n.d.	n.d.	3
P-S6 <sup>S235/S236</sup> (Den. TA)	47 ± 12***	5 ± 2	9.4	3
P-PKB/ Akt <sup>S473</sup> (Den. Sol)	n.d.	n.d.	n.d.	3
P-S6 <sup>S235/S236</sup> (Den. Sol)	41 ± 10**	3 ± 5	13.7	3
	RAmKO	Ctrl	ratio	number of replicates
P-PKB/ Akt <sup>S473</sup> (Den. TA)	12 ± 2	2 ± 1	6	3
P-S6 <sup>S235/S236</sup> (Den. TA)	n.d.	n.d.	n.d.	3
P-PKB/ Akt <sup>S473</sup> (Den. Sol)	19 ± 3	3 ± 2	6.3	3
P-S6 <sup>S235/S236</sup> (Den. Sol)	n.d.	n.d.	n.d.	3

Proteins were extracted from *soleus* (Sol) and *tibialis anterior* (TA) muscles of 90-day-old TSCmKO, RAmKO or control (Ctrl) littermates. "Den." denotes: denervated. "n.d." denotes: not detectable. The amount of total protein loaded onto the SDS-PAGE was adjusted and Western blots were additionally normalized to  $\alpha$ -actinin levels. Numbers given represent average gray values  $\pm$  SEM after subtraction of the background. "Ratio" represents the average gray value obtained from a knockout animal divided by the gray values from the control littermates. "Number of replicates" represents the number of knockout animals analyzed. The number of Ctrl littermates was always the same or higher than the values given. P-values were determined by Student's *t*-test; \* *P* <0.05, \*\* *P* <0.01, \*\*\**P* <0.001.

weight was matched by changes in the muscle fiber size in *soleus* and TA muscle (Figure 2D, E). Detailed analysis of fiber types showed that both type I and type IIa fibers were larger in *soleus* muscle (Additional file 1: Figure S3; Additional file 1: Table S1). In TA muscle, the glycolytic type IIb fibers were significantly smaller whereas the oxidative type IIa/x fibers were not affected (Additional file 1: Figure S3, Additional file 1: Table S1). In summary, these data show that the response to the activation of mTORC1 differs between muscles and fiber types.

We have previously shown that deletion of *rptor* not only affects the immediate downstream targets of mTORC1, S6K and 4EBP, but also causes a strong increase

in the phosphorylation of PKB/Akt [16]. As shown in Figure 3A, IRS1 levels were low in *soleus* muscle of TSCmKO mice compared to control (Figure 3A; Table 1). In addition, phosphorylation of PKB/Akt and of FoxO1/3 was substantially decreased in TSCmKO mice compared to controls (Figure 3A; Table 1). The same alterations in expression levels and phosphorylation of the examined proteins were detected in TA muscle of TSCmKO mice (data not shown). Consistent with the low phosphorylation levels of FoxO1a and FoxO3a, transcript levels of *atrogen-1/MAFbx* or *MuRF-1* were much higher in TA muscle of TSCmKO than in control mice (Figure 3B). Surprisingly, in *soleus* muscle, transcript levels of *atrogen-1/*



*MAFbx* and *MuRF1* did not differ from controls (Figure 3C) despite the low levels of phosphorylation of PKB/Akt. These data argue that the differential expression of the two E3 ligases might be responsible for the selective hypertrophy in *soleus* muscle.

#### Sustained activation of mTORC1 increases the oxidative capacity in all muscles

Additional factors that are regulated by mTORC1 [16,22,38] and have been implicated in the control of muscle size are the transcriptional coactivators PGC1 $\alpha$  and PGC1 $\beta$  [39,40]. Moreover, PGC1 $\alpha$  and PGC1 $\beta$  are major regulators of mitochondrial biogenesis [41]. To test whether deletion of *Tsc1* would also affect the PGC1 pathway and the oxidative capacity of skeletal muscle, we next compared expression of *Pgc1 $\alpha$*  and *Pgc1 $\beta$*  in TA and *soleus* muscles of TSCmKO mice with littermate controls. Contrary to the expectation, transcript levels of *Pgc1 $\alpha$*  were decreased in mutant muscles compared to controls (Figure 3D, E). The down-regulation of *Pgc1 $\alpha$*  was more pronounced in *soleus* muscle, which expresses the highest level of PGC1 $\alpha$  in wild-type mice [42]. In contrast, mRNA levels of *Pgc1 $\beta$*  were increased to about 150% in all examined muscles of TSCmKO mice (Figure 3D, E). In support of a direct regulation of *Pgc1 $\beta$*  transcripts by mTORC1, *Pgc1 $\beta$*  expression was diminished in RAMKO mice (*soleus* muscle in RAMKO mice:  $73 \pm 4.6\%$ ; control mice:  $100 \pm 10.3\%$ ; mean  $\pm$  SEM;  $N \geq 5$ ;  $P < 0.05$ ). Hence, unlike expression of the E3 ubiquitin ligases *atrogenin-1/MAFbx* and *MuRF1*, expression of *Pgc1 $\alpha$*  and *Pgc1 $\beta$*  did not differ between TA and *soleus* muscles in TSCmKO mice. Overexpression and knock-down experiments of PGC1 $\beta$  in C2C12 myotubes indicate that expression of *Pgc1 $\alpha$*  is tightly regulated by PGC1 $\beta$  (Figure 3F). Such counter-regulation between PGC1 $\alpha$  and PGC1 $\beta$  has also been reported in other tissues [43]. Thus, the increased levels of *Pgc1 $\beta$*  transcripts in the TSCmKO mice likely suppress expression of *Pgc1 $\alpha$* . Interestingly, TSCmKO mice showed an increase in their capacity for oxidative phosphorylation in TA and *soleus* muscles as shown by stainings for NADH-TR (Figure 3G), succinate dehydrogenase (SDH; Additional file 1: Figure S4A, B) and cytochrome oxidase (COX; Additional file 1: Figure S4A, B). This increase was accompanied by a slight, although not significant, increase in the number of mitochondria as determined by qPCR of mitochondrial DNA (Additional file 1: Figure S4C). Taken together, these data suggest that PGC1 $\beta$  is responsible for the increased oxidative properties of skeletal muscle of TSCmKO mice.

#### mTORC1 is required for muscle fiber hypertrophy

Because acute perturbation of mTORC1 function by knockdown experiments showed a strong effect on muscle

size in experimental paradigms of HOR and denervation-induced atrophy (Figure 1), we next tested muscle plasticity in RAMKO and TSCmKO mice. We first used the synergist ablation/mechanical overload model, in which *gastrocnemius* and *soleus* muscles including their tendons are surgically removed, a procedure that results in the functional overloading (FO) of the remaining *plantaris* muscle [44-46]. Seven or 28 days after surgery, mice were euthanized and the *plantaris* muscle of the overloaded leg was compared with *plantaris* from the contralateral, sham-operated leg. In control mice, FO increased muscle weight after 7 days to 140% and to more than 200% after 28 days (Figure 4A). Muscle weight also increased in RAMKO mice, although the increase was significantly reduced compared to control animals after 28 days of FO (Figure 4A). However, and in contrast to control mice (Figures 4B and S5A), individual muscle fibers did not increase in size in RAMKO mice after 7 days (Additional file 1: Figure S5B) or after 28 days of FO (Figure 4C). H&E staining of the *plantaris* after 28 days of FO did not reveal differences between contralateral and overloaded RAMKO muscles (Figure 4D). In contrast to RAMKO mice, TSCmKO muscle responded to FO like control muscle (Figure 4E-G).

There is evidence that FO also causes some damage and muscle regeneration and that satellite and other cells outside the muscle's basal lamina contribute to the weight increase [47,48]. As *HSA-Cre* is not expressed in non-muscle cells and satellite cells [24], we treated control mice with rapamycin during FO to eliminate mTORC1 function in all cells. This treatment abolished both the increase in weight and the shift in fiber size distribution (Additional file 1: Figure S5C), suggesting that mTORC1 expressed in non-muscle cells or in satellite cells might contribute to the increased weight of *plantaris* muscles in RAMKO mice after FO.

As FO induces a relative increase in the number of oxidative fibers [46], we also stained the overloaded *plantaris* from control and mutant mice by NADH-TR. As shown in Figure 4H, *plantaris* muscles remained largely non-oxidative in RAMKO mice, whereas in the overloaded *plantaris* of TSCmKO mice even the large myofibers remained highly oxidative (Figure 4I).

#### *Soleus* and TA muscles of TSCmKO mice respond differently to denervation-induced atrophy

To determine whether mTORC1 activation is sufficient to prevent atrophy, we next submitted TSCmKO muscle to denervation by cutting the sciatic nerve unilaterally and compared the muscles of the denervated and the contralateral (non-denervated) leg six days later. TA and *soleus* muscles of control mice lost 7% and 14% of their weight, respectively (Figure 5A). Importantly, the weight loss in both muscles was significantly higher in RAMKO mice

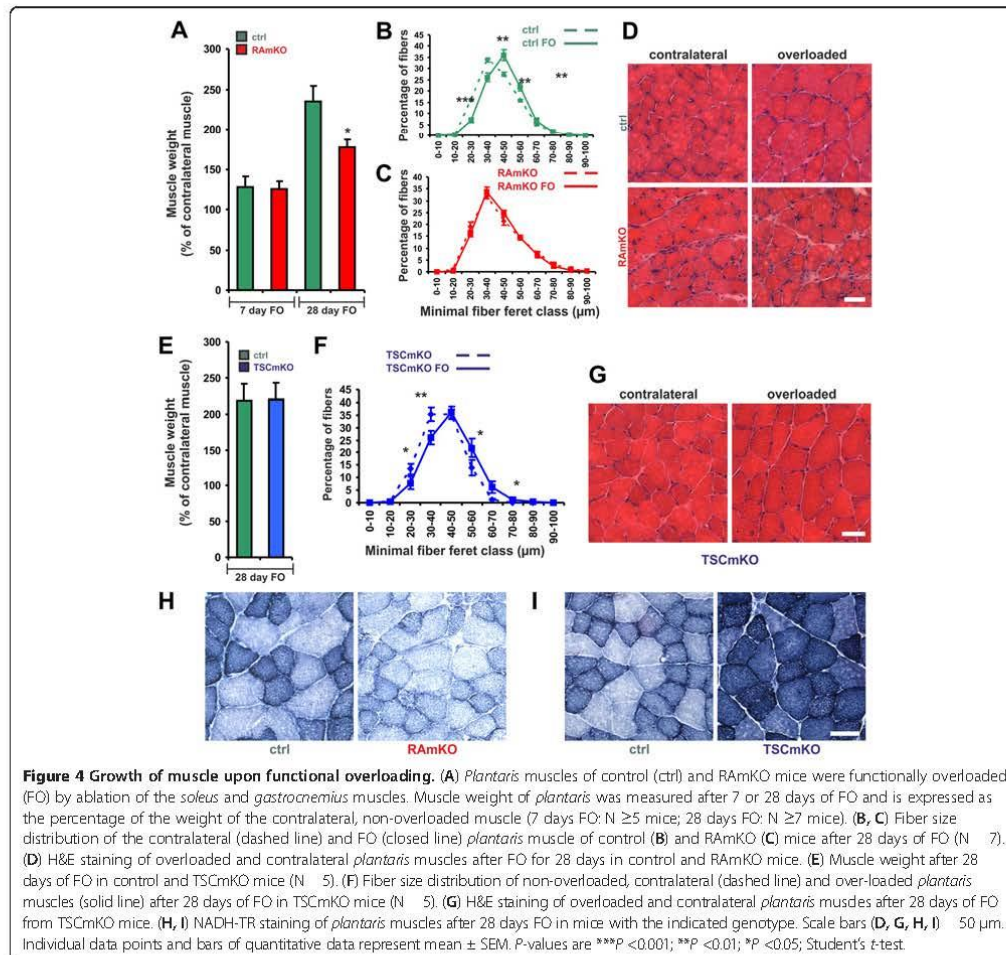
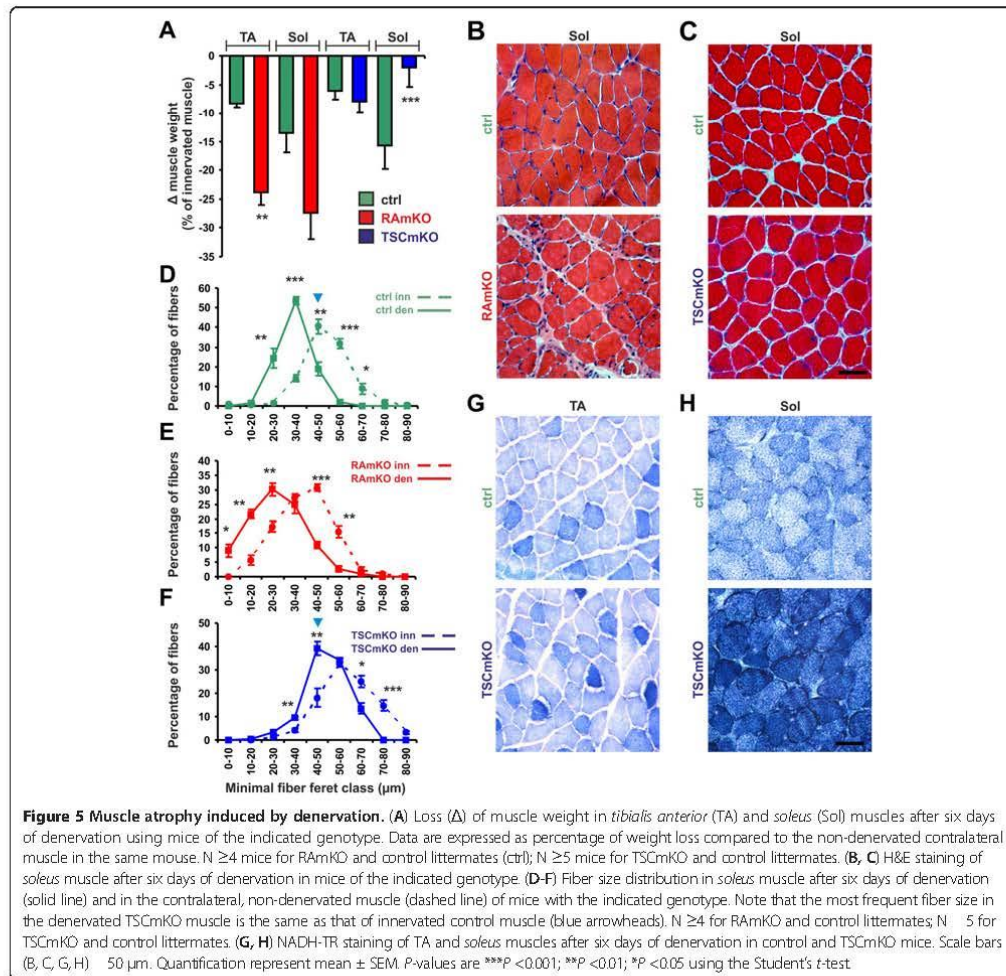


(Figure 5A). In TSCmKO mice, the response to denervation differed between TA and *soleus* muscles. Whereas loss of weight in the TA was the same in TSCmKO and control mice, *soleus* muscles of TSCmKO mice were largely spared (Figure 5A). H&E staining of the denervated muscles and contralateral muscles did not reveal major structural changes in mutant mice (Figure 5B, C). In *soleus* muscles, the substantial weight loss upon denervation in control and RAMKO mice was mirrored by a shift in fiber size distribution. The leftward shift was seen in control mice (Figure 5D) and was even more pronounced in RAMKO mice (Figure 5E). In TSCmKO mice, muscle fiber size distribution also shifted slightly toward smaller size when compared to the hypertrophic, contralateral innervated *soleus* muscles (Figure 5E), but remained similar

to innervated muscle from control mice. These results suggest that TA and *soleus* muscles differ in the response to mTORC1 activation under atrophy conditions and they suggest that the atrophy observed in the TSCmKO mice requires adaptive, long-term processes that are not induced by acute perturbation of mTORC1 signaling (see Figure 1). In both TSCmKO and control mice, the TA muscle showed a loss of oxidative capacity upon denervation (Figure 5G) whereas the *soleus* muscle of TSCmKO mice remained oxidative (Figure 5H).

#### Feedback control of PKB/Akt is active during muscle atrophy

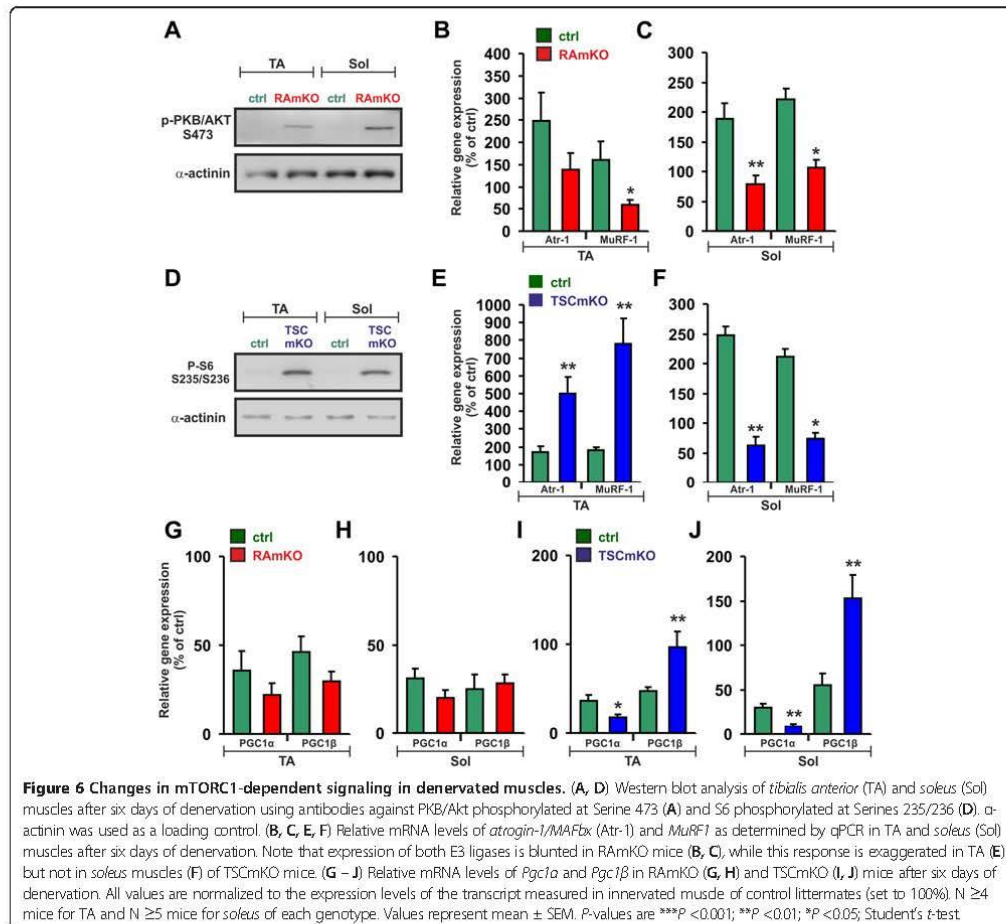
The difference in the atrophy response between TA and *soleus* muscles indicated that the underlying signaling



mechanisms might also differ in the two muscles. To examine this, we analyzed the changes in expression of the E3 ligases *atrogen-1/MAFbx* and *MURF1*, and the coactivators *Pgc1 $\alpha$*  and *Pgc1 $\beta$*  in response to denervation. Denervation has been reported to activate mTORC1, most likely due to the increase in free amino acids [49]. However, in RAmKO mice phosphorylation of S6K, S6 and 4EBP remained low six days after denervation (Table 1 and data not shown) whereas phosphorylation at Serine 473 of PKB/Akt remained high in RAmKO mice (Figure 6A). In parallel to the activation state of PKB/Akt, denervation increased transcript levels of *atrogen-1/MAFbx* and *MuRF-1* in TA and *soleus* muscles of control mice but not of RAmKO mice (Figure 6B, C).

The effect on the expression of the two E3 ubiquitin ligases was particularly striking in *soleus* muscles where their expression did not differ from innervated control muscles (Figure 6C). In TSCmKO mice, phosphorylated PKB/Akt was too low to be detected in denervated muscles (Table 1) but phosphorylation of S6 remained high (Figure 6D). Although phosphorylation of PKB/Akt was low in both TA and *soleus* muscles, transcript levels of *atrogen-1/MAFbx* and *MuRF-1* were increased in TA but were significantly lower in *soleus* compared to the denervated muscles from control mice (Figure 6E, F, Table 1).

The expression of the mTORC1 target *PGC1 $\alpha$*  is also controlled by denervation [39]. In innervated *soleus* muscle of RAmKO mice, *Pgc1 $\alpha$*  mRNA levels are less



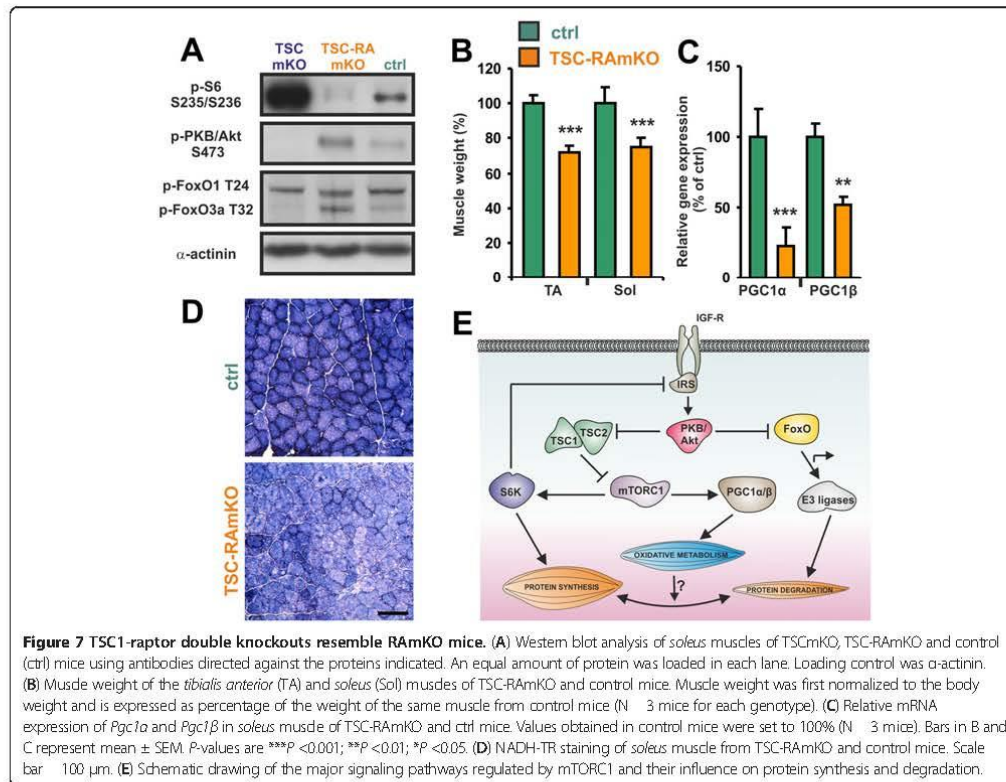
than 40% [16] and *Pgc1 $\beta$*  mRNA levels are approximately 70% of control muscle. In denervated TA and *soleus* muscles of control mice, expression of *Pgc1 $\alpha$*  and *Pgc1 $\beta$*  was lower than in innervated muscle (Figure 6G, H). Similarly, denervation lowered the levels of both transcriptional co-activators in RAmKO mice although the significant difference to control mice was lost (Figure 6G, H). In contrast, expression of *Pgc1 $\alpha$*  and *Pgc1 $\beta$*  was very different in TSCmKO mice. While *Pgc1 $\alpha$*  mRNA levels were decreased upon denervation both in TA and *soleus* muscles, *Pgc1 $\beta$*  was significantly increased in both muscles (Figure 6I, J). Taken together, our results show that atrophy is accelerated in RAmKO mice despite low levels of *atrogenin-1/MAFbx* and *MuRF1*. Conversely, the sparing of *soleus* muscles from denervation-induced atrophy in TSCmKO mice could be based on the low

levels of the two E3 ubiquitin ligases in this particular muscle. In contrast, the relative levels of *Pgc1 $\alpha$*  and *Pgc1 $\beta$*  did not differ between TA and *soleus* muscles upon denervation and are thus unlikely contributors to the differential response.

#### Genetic inactivation of mTORC1 reverses the phenotype of TSCmKO mice

While the inhibitory function of TSC1/2 onto mTORC1 is well established, there is evidence that this protein complex can also regulate mTORC2 [50,51]. To test whether any of the effects observed in TSCmKO mice would be maintained in RAmKO mice, we generated double knockout mice (termed TSC-RAmKO). First, we examined phosphorylation of known mTORC1 and mTORC2 substrates. As shown in Figure 7A, the





mTORC1 substrate S6K and S6 were not phosphorylated in TSC-RAmKO mice and phosphorylation of PKB/Akt at Serine 473 was increased compared to control mice. In addition, similar to RAmKO mice, the PKB/Akt target FoxO3a was hyperphosphorylated. The weight of all muscles including TA and *soleus* was lower in TSC-RAmKO mice than in controls (Figure 7B). Moreover, transcript levels of both *Pgc1α* and *Pgc1β* were lower in *soleus* muscle (Figure 7C) and its oxidative capacity was decreased (Figure 7D). Finally, the TSC-RAmKO mice developed the same pathology as the RAmKO mice and they eventually died at the age of four to six months (data not shown). Thus, all the hallmarks of RAmKO mice are present in the double mutants, indicating that TSC acts mainly via mTORC1 in skeletal muscle.

### Discussion

Here we describe the phenotype of mice in which mTORC1 is constitutively active in skeletal muscle (TSCmKO) and compare it to mice with inactivated mTORC1 signaling (RAmKO). While the oxidative changes in TSCmKO mice were largely the opposite of

those observed in RAmKO mice and affected all examined muscles, the effect of mTORC1 activation on muscle size was unexpected as all muscles except *soleus* muscles were slightly but significantly smaller. Thus, our work highlights the existence of several feed-forward or auto-inhibitory loops that allow fine-tuning of the signaling networks involved in the control of muscle mass (Figure 7E).

Based on the current concepts, mTORC1 activation should result in an increase in muscle mass and muscle fiber size. This view is based on the findings that activation of the mTORC1 upstream components PKB/Akt or IGF-1 receptor causes an increase in muscle mass [5,10,11,52,53] and that this increase is rapamycin-sensitive [11,53]. Moreover, overexpression of Rheb in single muscle fibers by electroporation leads to hypertrophy of the transfected fibers [20] and whole body knockout of the mTORC1 target S6K1 results in smaller muscle fibers [21]. Consistent with these experiments, acute knockdown of TSC1/2 by shRNA resulted in slightly bigger muscle fibers in *soleus* or TA muscles, confirming that transient activation of the mTORC1 pathway is sufficient to induce muscle fiber growth.

However, under conditions of prolonged activation of mTORC1 in TSCmKO mice, all muscles examined, with the exception of *soleus*, were smaller than in control mice. As mTORC1 targets are activated and protein synthesis in EDL muscle of TSCmKO mice is increased, the atrophy induced by chronic mTORC1 activation is likely related to the feedback inhibition of activated S6K onto IRS1, which in turn, decreases activation of PKB/Akt. This tight feedback control of S6K on IRS1-PKB/Akt was also observed in mice deficient for raptor or mTOR in some tissues including skeletal and heart muscle [16,54-56] but not in others [57]. Similarly, deletion of TSC1 strongly decreases activation of PKB/Akt in cultured mouse embryonic fibroblasts [23], whereas it does not at all affect PKB/Akt phosphorylation in some tissues [58,59]. These data indicate that the feedback control of S6K depends on the cellular context and our data now show that this feedback is particularly strong in skeletal muscle.

Consistent with decreased inhibition of FoxO transcription factors by PKB/Akt, TA muscle from TSCmKO mice express high levels of *MuRF1* and *atrogen-1/MAFbx*, involved in protein degradation through the proteasome [7,8]. Hence, the atrophy observed in muscles of the TSCmKO mice is likely caused by the prevalence of the FoxO pathway over mTORC1 activation. This differs from the muscle hypertrophy observed using the transient, partial activation of mTORC1 with shRNA electroporation. Thus, the atrophy response caused by the sustained, saturated mTORC1 activation by genetic *Tsc1* deletion may unveil a long-term adaptation of the FoxO pathway. Consistently, transient overexpression of Rheb does not seem to affect PKB/Akt phosphorylation [20], further supporting the idea that muscle atrophy in TSCmKO mice is related to the indirect PKB/Akt-dependent activation of FoxO pathways.

Importantly, contrasting with the atrophic phenotype of most muscles, sustained activation of mTORC1 leads to increased mass of *soleus* muscle in TSCmKO mice. Although PKB/Akt was similarly inhibited in *soleus* and TA muscles, expression of *MuRF1* and *atrogen-1/MAFbx* was not increased in *soleus* muscle, indicating that an additional regulatory mechanism suppresses their expression, thereby overruling the regulation by PKB/Akt. This differential regulation of *MuRF1* and *atrogen-1/MAFbx* expression did not seem to be mediated by PGC1 $\alpha$ , previously identified as a negative regulator of FoxO [39], because there was no significant difference in PGC1 $\alpha/\beta$  expression between *soleus* and TA muscles from TSCmKO mice.

With different atrophy and hypertrophy paradigms, we also demonstrate that mTORC1 plays a critical and complex role in muscle plasticity. Using shRNA electroporation, we show that transient activation of mTORC1 is sufficient to limit denervation-induced atrophy and to

enhance fiber hypertrophy upon re-innervation. Similarly, TSCmKO mice display atrophy resistance to denervation in *soleus* muscle, which shows only moderate expression of the E3 ubiquitin ligases *MuRF1* and *atrogen-1/MAFbx*. By contrast, long-term activation of mTORC1 did not protect TA muscle from atrophy and did not exacerbate the hypertrophy response to overloading of *plantaris* muscle. These results indicate that the increased protein synthesis by mTORC1 hyperactivation is not sufficient to maintain muscle mass in cases where the FoxO-MuRF1-atrogen-1/MAFbx axis is active due to the absence of PKB/Akt signaling. Importantly, both transient and long-term inactivation of mTORC1 increased denervation-induced atrophy and prevented muscle growth associated with re-innervation or overloading, indicating that increased protein synthesis is required even when the catabolic proteasomal activity is reduced. Thus, our results provide genetic evidence that muscle growth requires mTORC1.

In our previous work, we demonstrated that raptor-deficient skeletal muscles show a strongly decreased oxidative capacity due to changes in mitochondrial function [16]. This loss of oxidative capacity correlated with a substantial decrease in the transcript levels of *Pgc1 $\alpha$* , consistent with the direct regulation of *Pgc1 $\alpha$*  expression by mTOR [38], and could be restored by transgenic expression of PGC1 $\alpha$  [22]. Contrary to the expectations and the effect of mTORC1 activation in embryonic fibroblasts [38], all examined muscles of TSCmKO mice showed a decreased expression of *Pgc1 $\alpha$*  but increased levels of *Pgc1 $\beta$* . Thus, the increase in the oxidative capacity in TSCmKO mice may be mediated by PGC1 $\beta$ . Indeed, PGC1 $\beta$  has also been shown to be sufficient to increase oxidative capacity in skeletal muscle despite the concomitant reduction in PGC1 $\alpha$  expression [60]. Moreover, depletion of both PGC1 $\alpha$  and PGC1 $\beta$  results in much more severe loss of oxidative capacity than depletion of either protein alone [61]. The reason for the unexpected down-regulation of *Pgc1 $\alpha$*  transcripts in TSCmKO mice might be the counter-regulation of PGC1 $\alpha$  and PGC1 $\beta$ . We show here that overexpression of PGC1 $\beta$  in C2C12 myotubes results in a strong suppression of the endogenous *Pgc1 $\alpha$*  expression and, conversely, *Pgc1 $\beta$*  knock-down leads to increased expression of *Pgc1 $\alpha$*  transcripts. These data indicate that the total amount of both PGC1 co-activators is tightly controlled in skeletal muscle.

## Conclusions

Our study provides new functional insights into the molecular mechanism of muscle atrophy and hypertrophy. The data demonstrate that mTORC1 modulation downstream of PKB/Akt is subject to biological robustness. A fine-tuned feedback loop controlled by the anabolic mTORC1 pathway mediates crosstalk to E3 ubiquitin

ligase system that increases protein degradation and thus compensates for imbalance. However, this feedback system fails to fully re-establish muscle homeostasis, leading to prevalence of either an anabolic or a catabolic net response. Our observations emphasize that muscle growth requires both activated PKB/Akt and mTORC1 in parallel, and they provide a new rationale for the development of pharmacologic agents that target this system.

#### Additional file

**Additional file 1: Contains supplemental figures S1 to S5 and supplemental Table S1.** See text and additional file 1 for more details.

#### Abbreviations

4EBP: eIF-4E-binding protein; BSA: Bovine serum albumin; CSA: Cross-section area; FoxO: Forkhead box O; FO: Functional overloading; H&E: Hematoxylin & eosin; HOR: Hypertrophy on recovery; HSA: Human skeletal actin; IGF1: Insulin-like growth factor-1; ip: Intraperitoneal; mTORC1: Mammalian target of rapamycin complex 1; NADH-TR: Nicotinamide adenine dinucleotide hydrogen-tetrazolium reductase; NLS-GFP: Nuclear-localized GFP; PBS: Phosphate-buffered saline; PFA: Paraformaldehyde; PI3K: Phosphatidylinositol 3-kinase; PKB: Protein kinase B (also called Akt); PGC-1: Peroxisome proliferator-activated receptor gamma coactivator 1; Raptor: Regulatory-associated protein of mTOR; RAmKO: Raptor muscle knockout; Rheb: Ras homolog enriched in brain; Rictor: Rapamycin-insensitive companion of mTOR; S6K: p70/S6 kinase; SUNSET: Surface sensing of translation; TA: Tibialis anterior; TBS: Tris-buffered saline with 0.1% Tween 20; TSC: Tuberous sclerosis complex; TSCmKO: TSC muscle knockout.

#### Competing interests

The authors declare they have no competing interests.

#### Authors' contributions

CFB, SL and MAR conceived and designed the study. CFB and SL performed most of the experiments and analyzed the data. KR, PC, MG and SS conducted some of the experiments and CH, LAT and MNH provided scientific input. CFB, SL, PC and MAR wrote the manuscript. All authors read and approved the final manuscript.

#### Acknowledgements

We thank Drs. Xian Chu Kong and Céline Costa for their help with the shRNA constructs. We thank Dr. Philippe Pierre (CIML Parc Scientifique de Luminy, Marseille, France) for providing us with the anti-puromycin antibody. This work was supported by the Cantons of Basel-Stadt and Baselland, grants from the Swiss National Science Foundation, the Swiss Foundation for Research on Muscle Disease, Swiss Life and the Association Française contres les Myopathies (AFM).

#### Author details

<sup>1</sup>Biozentrum, University of Basel, Basel CH-4056, Switzerland. <sup>2</sup>Neuromuscular Research Center, Department of Biomedicine, University of Basel, Basel CH-4056, Switzerland. <sup>3</sup>INRA, UMR866, Université Montpellier 1, Université Montpellier 2, Montpellier, France.

Received: 3 October 2012 Accepted: 15 February 2013

Published: 6 March 2013

#### References

1. Sandri M: Signaling in muscle atrophy and hypertrophy. *Physiology (Bethesda)* 2008, **23**:160–170.
2. Ruegg MA, Glass DJ: Molecular mechanisms and treatment options for muscle wasting diseases. *Annu Rev Pharmacol Toxicol* 2011, **51**:373–395.
3. Wullschlegler S, Loewith R, Hall MN: TOR signaling in growth and metabolism. *Cell* 2006, **124**:471–484.
4. Laplante M, Sabatini DM: mTOR signaling in growth control and disease. *Cell* 2012, **149**:274–293.
5. Bodine SC, Stitt TN, Gonzalez M, Kline WO, Stover GL, Bauerlein R, Zlotchenko E, Scrimgeour A, Lawrence JC, Glass DJ, Yancopoulos GD: Akt/mTOR pathway is a crucial regulator of skeletal muscle hypertrophy and can prevent muscle atrophy *in vivo*. *Nat Cell Biol* 2001, **3**:1014–1019.
6. Zhao J, Brault JJ, Schild A, Cao P, Sandri M, Schiaffino S, Lecker SH, Goldberg AL: FoxO3 coordinately activates protein degradation by the autophagic/lysosomal and proteasomal pathways in atrophying muscle cells. *Cell Metab* 2007, **6**:472–483.
7. Stitt TN, Drujan D, Clarke BA, Panaro F, Timofeyeva Y, Kline WO, Gonzalez M, Yancopoulos GD, Glass DJ: The IGF-1/PI3K/Akt pathway prevents expression of muscle atrophy-induced ubiquitin ligases by inhibiting FOXO transcription factors. *Mol Cell* 2004, **14**:395–403.
8. Sandri M, Sandri C, Gilbert A, Skurk C, Calabria E, Picard A, Walsh K, Schiaffino S, Lecker SH, Goldberg AL: Foxo transcription factors induce the atrophy-related ubiquitin ligase atrogin-1 and cause skeletal muscle atrophy. *Cell* 2004, **117**:399–412.
9. Mammucari C, Milan G, Romanello V, Masiero E, Rudolf R, Del Piccolo P, Burden SJ, Di Lisi R, Sandri C, Zhao J, Goldberg AL, Schiaffino S, Sandri M: FoxO3 controls autophagy in skeletal muscle *in vivo*. *Cell Metab* 2007, **6**:458–471.
10. Lai KM, Gonzalez M, Poueymirou WT, Kline WO, Na E, Zlotchenko E, Stitt TN, Economides AN, Yancopoulos GD, Glass DJ: Conditional activation of akt in adult skeletal muscle induces rapid hypertrophy. *Mol Cell Biol* 2004, **24**:9295–9304.
11. Izumiya Y, Hopkins T, Morris C, Sato K, Zeng L, Viereck J, Hamilton JA, Ouchi N, LeBrasseur NK, Walsh K: Fast/Glycolytic muscle fiber growth reduces fat mass and improves metabolic parameters in obese mice. *Cell Metab* 2008, **7**:159–172.
12. Jacinto E, Loewith R, Schmidt A, Lin S, Ruegg MA, Hall A, Hall MN: Mammalian TOR complex 2 controls the actin cytoskeleton and is rapamycin insensitive. *Nat Cell Biol* 2004, **6**:1122–1128.
13. Sarbassov DD, Ali SM, Kim DH, Guertin DA, Latek RR, Erdjument-Bromage H, Tempst P, Sabatini DM: Rictor, a novel binding partner of mTOR, defines a rapamycin-insensitive and raptor-independent pathway that regulates the cytoskeleton. *Curr Biol* 2004, **14**:1296–1302.
14. Lamming DW, Ye L, Katajisto P, Goncalves MD, Saitoh M, Stevens DM, Davis JS, Salmon AB, Richardson A, Ahima RS, Guertin DA, Sabatini DM, Baur JA: Rapamycin-induced insulin resistance is mediated by mTORC2 loss and uncoupled from longevity. *Science* 2012, **335**:1638–1643.
15. Kumar A, Harris TE, Keller SR, Choi KM, Magnuson MA, Lawrence JC Jr: Muscle-specific deletion of rictor impairs insulin-stimulated glucose transport and enhances basal glycogen synthase activity. *Mol Cell Biol* 2008, **28**:61–70.
16. Bentzinger CF, Romanino K, Cloëtta D, Lin S, Mascarenhas JB, Oliveri F, Xia J, Casanova E, Costa CF, Brink M, Zorzato F, Hall MN, Ruegg MA: Skeletal muscle-specific ablation of raptor, but not of rictor, causes metabolic changes and results in muscle dystrophy. *Cell Metab* 2008, **8**:411–424.
17. Rommel C, Bodine SC, Clarke BA, Rosman R, Nunez L, Stitt TN, Yancopoulos GD, Glass DJ: Mediation of IGF-1-induced skeletal myotube hypertrophy by PI(3)K/Akt/mTOR and PI(3)K/Akt/GSK3 pathways. *Nat Cell Biol* 2001, **3**:1009–1013.
18. Kline WO, Panaro FJ, Yang H, Bodine SC: Rapamycin inhibits the growth and muscle-sparing effects of clenbuterol. *J Appl Physiol* 2007, **102**:740–747.
19. Wan M, Wu X, Guan KL, Han M, Zhuang Y, Xu T: Muscle atrophy in transgenic mice expressing a human TSC1 transgene. *FEBS Lett* 2006, **580**:5621–5627.
20. Goodman CA, Miu MH, Frey JW, Mabrey DM, Lincoln HC, Ge Y, Chen J, Hornberger TA: A phosphatidylinositol 3 kinase/protein kinase B-independent activation of mammalian target of rapamycin signaling is sufficient to induce skeletal muscle hypertrophy. *Mol Biol Cell* 2010, **21**:3258–3268.
21. Ohanna M, Sobering AK, Lapointe T, Lorenzo L, Praud C, Petroulakis E, Sonenberg N, Kelly PA, Sotiropoulos A, Pende M: Atrophy of S6K1(–/–) skeletal muscle cells reveals distinct mTOR effectors for cell cycle and size control. *Nat Cell Biol* 2005, **7**:286–294.
22. Romanino K, Mazelin L, Albert V, Conjard-Duplany A, Lin S, Bentzinger CF, Handschin C, Puigserver P, Zorzato F, Schaeffer L, Gangloff YG, Ruegg MA: Myopathy caused by mammalian target of rapamycin complex 1 (mTORC1) inactivation is not reversed by restoring mitochondrial function. *Proc Natl Acad Sci U S A* 2011, **108**:20808–20813.
23. Kwiatkowski DJ, Zhang H, Bandura JL, Heiberger KM, Glogauer M, el-Hashemite N, Onda H: A mouse model of TSC1 reveals sex-dependent lethality from liver hemangiomas, and up-regulation of p70S6 kinase activity in Tsc1 null cells. *Hum Mol Genet* 2002, **11**:525–534.

24. Schwander M, Leu M, Stumm M, Dorchies OM, Ruegg UT, Schittny J, Muller U: **Beta1 integrins regulate myoblast fusion and sarcomere assembly.** *Dev Cell* 2003, **4**:673–685.
25. Kong XC, Barzaghi P, Ruegg MA: **Inhibition of synapse assembly in mammalian muscle in vivo by RNA interference.** *EMBO Rep* 2004, **5**:183–188.
26. Shavlakadze T, White JD, Davies M, Hoh JF, Grounds MD: **Insulin-like growth factor I slows the rate of denervation induced skeletal muscle atrophy.** *Neuromuscul Disord* 2005, **15**:139–146.
27. Stockholm D, Herasse M, Marchand S, Praud C, Roudaut C, Richard I, Sebille A, Beckmann JS: **Calpain 3 mRNA expression in mice after denervation and during muscle regeneration.** *Am J Physiol Cell Physiol* 2001, **280**:C1561–C1569.
28. Dunn SE, Burns JL, Michel RN: **Calcineurin is required for skeletal muscle hypertrophy.** *J Biol Chem* 1999, **274**:21908–21912.
29. van Slegtenhorst M, Nellist M, Nagelkerken B, Cheadle J, Snell R, van den Ouweland A, Reuser A, Sampson J, Halley D, van der Sluijs P: **Interaction between hamartin and tuberlin, the TSC1 and TSC2 gene products.** *Hum Mol Genet* 1998, **7**:1053–1057.
30. Schmidt EK, Clavarino G, Ceppi M, Pierre P: **SUnSET, a nonradioactive method to monitor protein synthesis.** *Nat Methods* 2009, **6**:275–277.
31. Dunant P, Larochelle N, Thirion C, Stucka R, Ursu D, Petrof BJ, Wolf E, Lochmuller H: **Expression of dystrophin driven by the 1.35-kb MCK promoter ameliorates muscular dystrophy in fast, but not in slow muscles of transgenic mdx mice.** *Mol Ther* 2003, **8**:80–89.
32. Briguet A, Courdiere-Fruh I, Foster M, Meier T, Magyar JP: **Histological parameters for the quantitative assessment of muscular dystrophy in the mdx-mouse.** *Neuromuscul Disord* 2004, **14**:675–682.
33. Tonge DA: **Physiological characteristics of re-innervation of skeletal muscle in the mouse.** *J Physiol* 1974, **241**:141–153.
34. Liu M, Zhang D, Shao C, Liu J, Ding F, Gu X: **Expression pattern of myostatin in gastrocnemius muscle of rats after sciatic nerve crush injury.** *Muscle Nerve* 2007, **35**:649–656.
35. Meikle L, Talos DM, Onda H, Pollizzi K, Rotenberg A, Sahin M, Jensen FE, Kwiatkowski DJ: **A mouse model of tuberous sclerosis: neuronal loss of Tsc1 causes dysplastic and ectopic neurons, reduced myelination, seizure activity, and limited survival.** *J Neurosci* 2007, **27**:5546–5558.
36. Mori H, Inoki K, Munzberg H, Opland D, Faouzi M, Villanueva EC, Ikenoue T, Kwiatkowski DJ, MacDougald OA, Myers MG Jr, Guan KL: **Critical role for hypothalamic mTOR activity in energy balance.** *Cell Metab* 2009, **9**:362–374.
37. Zeng LH, Rensing NR, Zhang B, Gutmann DH, Gambello MJ, Wong M: **Tsc2 gene inactivation causes a more severe epilepsy phenotype than Tsc1 inactivation in a mouse model of tuberous sclerosis complex.** *Hum Mol Genet* 2011, **20**:445–454.
38. Cunningham JT, Rodgers JT, Arlow DH, Vazquez F, Mootha VK, Puigserver P: **mTOR controls mitochondrial oxidative function through a YY1-PGC-1alpha transcriptional complex.** *Nature* 2007, **450**:736–740.
39. Sandri M, Lin J, Handschin C, Yang W, Arany ZP, Lecker SH, Goldberg AL, Spiegelman BM: **PGC-1alpha protects skeletal muscle from atrophy by suppressing FoxO3 action and atrophy-specific gene transcription.** *Proc Natl Acad Sci U S A* 2006, **103**:16260–16265.
40. Braut JJ, Jesspersen JG, Goldberg AL: **Peroxisome proliferator-activated receptor gamma coactivator 1alpha or 1beta overexpression inhibits muscle protein degradation, induction of ubiquitin ligases, and disuse atrophy.** *J Biol Chem* 2010, **285**:19460–19471.
41. Puigserver P, Spiegelman BM: **Peroxisome proliferator-activated receptor-gamma coactivator 1 alpha (PGC-1 alpha): transcriptional coactivator and metabolic regulator.** *Endocr Rev* 2003, **24**:78–90.
42. Lin J, Wu H, Tarr PT, Zhang CY, Wu Z, Boss O, Michael LF, Puigserver P, Isotani E, Olson EN, Lowell BB, Bassel-Duby R, Spiegelman BM: **Transcriptional co-activator PGC-1 alpha drives the formation of slow-twitch muscle fibres.** *Nature* 2002, **418**:797–801.
43. Lelliott CJ, Medina-Gomez G, Petrovic N, Kis A, Feldmann HM, Bjursell M, Parker N, Curtis K, Campbell M, Hu P, Zhang D, Litwin SE, Zaha VG, Fountain KT, Boudina S, Jimenez-Linan M, Blount M, Lopez M, Meirhaeghe A, Bohlooly-Y M, Storlien L, Stromstedt M, Snaith M, Oresic M, Abel ED, Cannon B, Vidal-Puig A: **Ablation of PGC-1beta results in defective mitochondrial activity, thermogenesis, hepatic function, and cardiac performance.** *PLoS Biol* 2006, **4**:e369.
44. Goldberg AL: **Work-induced growth of skeletal muscle in normal and hypophysectomized rats.** *Am J Physiol* 1967, **213**:1193–1198.
45. Baldwin KM, Valdez V, Herrick RE, MacIntosh AM, Roy RR: **Biochemical properties of overloaded fast-twitch skeletal muscle.** *J Appl Physiol* 1982, **52**:467–472.
46. Dunn SE, Michel RN: **Coordinated expression of myosin heavy chain isoforms and metabolic enzymes within overloaded rat muscle fibers.** *Am J Physiol* 1997, **273**:C371–C383.
47. Tamaki T, Uchiyama Y, Okada Y, Tono K, Nitta M, Hoshi A, Akatsuka A: **Multiple stimulations for muscle-nerve-blood vessel unit in compensatory hypertrophied skeletal muscle of rat surgical ablation model.** *Histochem Cell Biol* 2009, **132**:59–70.
48. Tedesco FS, Dellavalle A, Diaz-Manera J, Messina G, Cossu G: **Repairing skeletal muscle: regenerative potential of skeletal muscle stem cells.** *J Clin Invest* 2010, **120**:11–19.
49. Quy PN, Kuma A, Pierre P, Mizushima N: **Proteasome-dependent activation of mammalian target of rapamycin complex 1 (mTORC1) is essential for autophagy suppression and muscle remodeling following denervation.** *J Biol Chem* 2013, **288**:1125–1134.
50. Yang Q, Inoki K, Kim E, Guan KL: **TSC1/TSC2 and Rheb have different effects on TORC1 and TORC2 activity.** *Proc Natl Acad Sci U S A* 2006, **103**:6811–6816.
51. Huang J, Dibble CC, Matsuzaki M, Manning BD: **The TSC1-TSC2 complex is required for proper activation of mTOR complex 2.** *Mol Cell Biol* 2008, **28**:4104–4115.
52. Musaro A, McCullagh K, Paul A, Houghton L, Dobrowolny G, Molinaro M, Barton ER, Sweeney HL, Rosenthal N: **Localized Igf-1 transgene expression sustains hypertrophy and regeneration in senescent skeletal muscle.** *Nat Genet* 2001, **27**:195–200.
53. Pallafacchina G, Calabria E, Serrano AL, Kahlvode JM, Schiaffino S: **A protein kinase B-dependent and rapamycin-sensitive pathway controls skeletal muscle growth but not fiber type specification.** *Proc Natl Acad Sci U S A* 2002, **99**:9213–9218.
54. Polak P, Cybulski N, Feige JN, Auwerx J, Ruegg MA, Hall MN: **Adipose-specific knockout of raptor results in lean mice with enhanced mitochondrial respiration.** *Cell Metab* 2008, **8**:399–410.
55. Shende P, Plaisance I, Morandi C, Pellicoux C, Berthonneche C, Zorzato F, Krishnan J, Lerch R, Hall MN, Ruegg MA, Pedrazzini T, Brink M: **Cardiac raptor ablation impairs adaptive hypertrophy, alters metabolic gene expression, and causes heart failure in mice.** *Circulation* 2011, **123**:1073–1082.
56. Risson V, Mazelin L, Roceri M, Sanchez H, Moncollin V, Corneloup C, Richard-Bulteau H, Vignaud A, Baas D, Defour A, Freyssenet D, Tanti JF, Le-Marchand-Brustel Y, Ferrier B, Conjard-Duplany A, Romanino K, Bauché S, Hantai D, Mueller M, Kozma SC, Thomas G, Ruegg MA, Ferry A, Pende M, Bigard X, Koulmann N, Schaeffer L, Gangloff YG: **Muscle inactivation of mTOR causes metabolic and dystrophin defects leading to severe myopathy.** *J Cell Biol* 2009, **187**:859–874.
57. Gödel M, Hartleben B, Herbach N, Liu S, Zschiedrich S, Lu S, Debreczeni-Mör A, Lindenmeyer MT, Rastaldi MP, Hartleben G, Wiech T, Fomoni A, Nelson RG, Kretzler M, Wanke R, Pavenstädt H, Kerjaschki D, Cohen CD, Hall MN, Ruegg MA, Inoki K, Walz G, Huber TB: **Role of mTOR in podocyte function and diabetic nephropathy in humans and mice.** *J Clin Invest* 2011, **121**:2197–2209.
58. Mori H, Inoki K, Opland D, Munzberg H, Villanueva EC, Faouzi M, Ikenoue T, Kwiatkowski DJ, MacDougald OA, Myers MG Jr, Guan KL: **Critical roles for the TSC-mTOR pathway in beta-cell function.** *Am J Physiol Endocrinol Metab* 2009, **297**:E1013–E1022.
59. Inoki K, Mori H, Wang J, Suzuki T, Hong S, Yoshida S, Blattner SM, Ikenoue T, Ruegg MA, Hall MN, Kwiatkowski DJ, Rastaldi MP, Huber TB, Kretzler M, Holzmann LB, Wiggins RC, Guan KL: **mTORC1 activation in podocytes is a critical step in the development of diabetic nephropathy in mice.** *J Clin Invest* 2011, **121**:2181–2196.
60. Arany Z, Lebrasseur N, Morris C, Smith E, Yang W, Ma Y, Chin S, Spiegelman BM: **The transcriptional coactivator PGC-1beta drives the formation of oxidative type IIX fibers in skeletal muscle.** *Cell Metab* 2007, **5**:35–46.
61. Zechner C, Lai L, Zechner JF, Geng T, Yan Z, Rumsey JW, Collia D, Chen Z, Wozniak DF, Leone TC, Kelly DP: **Total skeletal muscle PGC-1 deficiency uncouples mitochondrial derangements from fiber type determination and insulin sensitivity.** *Cell Metab* 2010, **12**:633–642.

doi:10.1186/2044-5040-3-6

Cite this article as: Bentzinger et al.: Differential response of skeletal muscles to mTORC1 signaling during atrophy and hypertrophy. *Skeletal Muscle* 2013 **3**:6.

## 7. ACKNOWLEDGEMENTS

First and foremost, I must thank Professor Markus Rüegg for giving me the opportunity of working in this project, and accepting me as a member of his lab. He has been a great mentor, always available for my enthusiastic outbursts, and ready to tone down my excessive excitement, which I agree would cloud my rational judgement sometimes (only sometimes). But I still believe I have been able to infect him with a little bit of extra enthusiasm. I really enjoyed the lengthy discussions about science and life in general, and I will definitely miss having someone to run to when I get some new and exciting results. It has been an amazing journey, and it would have not been possible without the constant supervision and support from Markus.

The second person that comes to my mind that I should specially thank is Dr. Lionel Tintignac. He has been my accomplice in this adventure, and the reason that the first two years were as smooth and successful as they were. I was very lucky to be seating next to him, and I will always be thankful to him for having so much patience with my slow technician brain. I really enjoyed our lengthy conversations, and I am convinced we made a great team: he was the brains while I was the hands of our shared research projects. Couldn't have worked better.

Of course, I am in debt with the support I received from all of the past and present lab members, which are too many to name individually (but I hope they all know who they are). From the start, the environment in the Rüegg lab was amazing, welcoming and fun, with a great support system. I could always run to anyone and annoy them with technical, theoretical or even official paperwork related questions, and not once did anyone lose their smile while helping me through all. I am convinced this also helped me navigate through my PhD thesis smoothly, so I am extremely thankful for the great support system that each and every lab member helped build. I specially would like to thank my closest lab member Marco Kaiser, which has been there almost from the beginning and together with Lionel made every day way more exciting. I am also grateful for the latest addition to our lab, Denis Falcetta, which is now in charge of continuing the FGF21 project and whose help has been invaluable for me to advance this fast. And lastly, I would like to make a special mention for Dr. Perrine Castets,

which was intensely involved in the writing of our manuscript, which I am convinced greatly helped for its final publication.

I would also like to thank many members from Christoph Handschin's and Michael Hall's groups, for their continued support on my never ending theoretical and technical questions. Special thanks go to Barbara Kupr, which was involved with me in the lengthy and crazy metabolism project from the beginning, and from whom I learnt almost everything I needed to succeed in this. I also would like to thank Professor Christoph Handschin, not only for being part of my committee and helping me progress every year, but for suggesting I should apply to Markus Rügge's lab over 3 years ago. Perfect choice.

Last but not least, I am extremely grateful for the support I have continuously received from my family. Even though I will not get a Nobel award as she always insisted on, I know my mother will still be proud of me. This would have not been possible without their never-ending belief in me and my potential. From the beginning until the end. And of course, I would not even know how to thank my partner in this crazy adventure, which I know has suffered more than I have during this past three years of my PhD (because he constantly reminded me so). My husband is, and always will be, the best support I could have, the one who makes everything more challenging and exciting, and the one who will always be there no matter what. It was him who helped me decide to pursue a PhD, it was him who stuck with me during all this process, and it is him who will be there to see my next steps, so I am forever grateful for him. I cannot wait to see how life unveils its next challenges now that I have finished this chapter, and I could not be happier knowing I will be able to share it once again with the best companion. Thank you.

## 8. CURRICULUM VITAE

### Maitea Guridi Ormazabal

Salmenweg 14 • 4057 • Basel • SWITZERLAND  
( 076 666 5179 • ✉ [metter\\_potxi@hotmail.com](mailto:metter_potxi@hotmail.com)  
12<sup>th</sup> May 1984, Spain



#### PROFILE

---

A reliable, organized and enthusiastic PhD in Neurobiology with a CAS in Clinical Research and eight years of international professional experience as a research scientist. Proven track record of research and development in cellular and molecular biology, animal sciences, scientific publishing and project management.

#### EDUCATION

---

**PhD in Neurobiology** 07.2012 – 01.2016

**Biozentrum, University of Basel (Basel, Switzerland)**

- Dissertation entitled: Skeletal muscle mTORC1 regulates whole body metabolism through ER stress induced FGF21.
- Specialized in neuromuscular dystrophies, metabolism, animal experiments, biochemistry and molecular biology.

**CAS in Clinical Research** 01.2014 – 12.2014

**Clinical Trial Unit, University Hospital Basel (Basel, Switzerland)**

- Advanced studies in clinical research conducted at the Clinical Trial Unit of the University Hospital Basel.
- Specialized in basics of clinical research, SOPs, PIS, GCP training, ICH guidelines, EC, regulatory authorities, clinical study planning and conduct, risk analysis, monitoring, QC/QA and data management.

**Master in Biotechnology** 09.2008 – 09.2009

**Public University of Navarra (Pamplona, Spain)**

- Conducted in the department of animal sciences, dissertation entitled: Single nucleotide polymorphisms in the Melanocortin 1 Receptor gene are linked with lightness of fiber color in Peruvian Alpaca (*Vicugna pacos*).

**Licentiate in Biology and Biochemistry** 09.2002 – 06.2007

**University of Navarra (Pamplona, Spain)**

- Three years of generalized studies in biology (Bachelor in Science – Biology and Biochemistry) followed by two years specialization in biomedical biology with an internship and thesis in the Dept. of Physiology and Nutrition.

#### PROFESSIONAL EXPERIENCE

---

**Assistant Research Scientist** 10.2009 – 06.2012

**New York Langone Medical Center, Department of Neurology (New York, NY, USA)**

- Animal facility managing, from multiple mice line maintenance to phenotypic characterization of transgenic mouse models for Alzheimer's disease.
- Expertise in an exclusive *in-vivo* intracranial surgery procedure for osmotic pump experiments in mice; molecular laboratory techniques such as ELISA, Western Blotting, qPCR and Immunohistochemistry, as well as drug development and animal behavioral testing.

**Research Scientist** 09.2007 – 09.2009

**Public University of Navarra, Department of Animal Sciences (Pamplona, Spain)**

- Independently conducted a research project on genetics of the fiber color in the Peruvian alpaca, and successful publication of the results.

- In charge of the regulation of quality control and geographical origin trademark for the meat company “Ternera de Navarra”. Expertise in molecular laboratory techniques like cloning, PCR, primary cell culture and sequencing.

**Tutor** 06.2008 – 07.2009

**Academia school (Pamplona, Spain)**

- Worked as a private tutor for high school and university students teaching subjects from science to advanced English.

## INTERNSHIPS

---

**pRED Clinical Operations, Study Management Team (Hoffman-LA Roche, Switzerland)** 12.2014

- Specialized in early phase development- Phase I and II trials. Followed several study managers, study management leaders, clinical scientist and clinical operations leader in their daily job responsibilities.
- Successfully obtained experience and knowledge in: project management, study coordination and timelines, budgeting, CRO outsourcing, vendors, site feasibility assessment, health authorities’ regulations, patient recruitment, eTMF, archiving and database management.

**Cardiovascular research team at CTU (University Hospital Basel, Switzerland)** 11.2014

- Specialized in Investigator Initiated Trials, from Phase I to Phase IV. Followed the study manager and the study nurse during their job assignments.
- Obtained experience and knowledge in: study protocol, IB, PIS, ICF, patient recruitment, compliance, CRF and eCRF, source documents, SOPs, TMF, EC approval, study randomization and blinding methods, PK/PD, drug accountability and database management.

**Visiting Scientist (Universidad de Huancavelica, Peru)** 07.2009 – 08.2009

- Supervisor of an international course on introduction to molecular laboratory techniques.
- In charge of organizing the equipment, protocols, supplies and material for the initialization of a new research laboratory in animal production; as well as the formation of personnel and students on basic laboratory skills.

**Graduate Student position (Washington State University, USA)** 06.2008 – 09.2008

- Three months internship at the Department of Animal Sciences as part of my Master degree.
- Specialized in primary cell culture techniques, from tissue extraction to cell treatment, immunohistochemistry and basic laboratory skills.

**Graduate student position (Oncology Hospital of San Sebastian, Spain)** 07.2005 – 09.2005

- Two months internship at the Institute for prevention, diagnostic and treatment of cancer as part of my bachelor studies. Obtained training and experience in patient diagnostic techniques, biomarkers and genetic analysis.

## LANGUAGES

---

**English:** Proficient    **Spanish:** Native language    **Basque:** Native language    **German:** Intermediate (B1)

## CERTIFICATES

---

**Introduction to Project Management (University of Basel, Switzerland)** 02.2015

- Based on PMI (Project Management Institute) standards, executed by SPOL Training Center.
- Two day workshop about project types, phases, deliverables, project charter, risk management and project closure with case-study exercises.

**Good Clinical Practice (University Hospital Basel, Switzerland)** 04.2014

- As part of the CAS in Clinical Research, in addition to online learning tools for continuing education.



- Five days course about ICH and regulatory bodies, REC, international quality standards, laws and regulations, sponsor and investigator responsibilities, quality assurance, safety and pharmacovigilance.

#### Research Ethics Evaluation (TREE online learning)

04.2014

- Online learning tools for continuing education programs, as part of the CAS in Clinical Research.
- One day course about history of ethical research, REC, patient rights/ patient safety and quality assurance.

#### SELECTED PUBLICATIONS

---

- **Guridi M**, Tintignac L, Lin S, Kupr B, Castets P, Ruegg M. Activation of mTORC1 in skeletal muscle regulates whole-body metabolism through FGF21. Accepted for publication in *Science Signalling*. November **2015**.
- Pankiewicz JE, **Guridi M**, Kim J, Asuni AA, Sanchez S, Sullivan PM, Holtzman DM, Sadowski MJ. Blocking the apoE/A $\beta$  interaction ameliorates A $\beta$ -related pathology in APOE  $\epsilon$ 2 and  $\epsilon$ 4 targeted replacement Alzheimer model mice. *Acta Neuropathol Commun*. **2014** Jun 28; 2(1):75.
- Asuni AA, **Guridi M**, Pankiewicz JE, Sanchez S, Sadowski MJ. Modulation of amyloid precursor protein expression reduces  $\beta$ -amyloid deposition in a mouse model. *Annals of Neurology*, **2014** May; 75(5):684-99.
- Castets P, Lin S, Rion N, Di Fulvio S, Romanino K, **Guridi M**, Frank S, Tintignac LA, Sinnreich M, R $\ddot{u}$ egg MA. Sustained activation of mTORC1 in skeletal muscle inhibits constitutive and starvation-induced autophagy and causes a severe, late-onset myopathy. *Cell Metabolism*, **2013** May 7; 17(5):731-44.
- Bentzinger CF, Lin S, Romanino K, Castets P, **Guridi M**, Summermatter S, Handschin C, Tintignac LA, Hall MN, R $\ddot{u}$ egg MA. Differential response of skeletal muscles to mTORC1 signaling during atrophy and hypertrophy. *Skeletal Muscle*, **2013** Mar 6;3(1):6.
- Kuszczczyk MA, Sanchez S, Pankiewicz J, Kim J, Duszczyk M, **Guridi M**, Asuni AA, Sullivan PM, Holtzman DM, Sadowski MJ. Blocking the interaction between apolipoprotein E and A $\beta$  reduces intraneuronal accumulation of A $\beta$  and inhibits synaptic degeneration. *American Journal of Pathology*, **2013** May; 182(5):1750-68.
- Duszczyk M., Kuszczczyk M.A., **Guridi M.**, Lazarewicz, J.W., Sadowski, M.J. In vivo Hippocampal Microdialysis Reveals Impairment of NMDA Receptor–cGMP Signaling in APP(SW) and APP(SW)/PS1(L166P) Alzheimer’s transgenic Mice. *Neurochemistry International*, **2012** Dec; 61(7):976-80.
- **Guridi M.**, Soret, B., Alfonso, L., Arana, A. Single Nucleotide Polymorphisms in the Melanocortin 1 Receptor gene are linked with lightness of fibre colour in Peruvian alpaca (*Vicugna pacos*). *Animal Genetics*, 10.1111/j.1365-2052. **2011**.
- **Guridi M.**, Soret, B., Alfonso, L., Arana, A. Analysis of Melanocortin 1 receptor (MC1R) gene in alpaca (*Vicugna pacos*) and its association to fibre colour. In: *Aportes del Procasud al conocimiento de la alpaca y vicuna*. **2011**.
- Chen, J., **M. Guridi**, M.E. Fernyhough, Z. Jiang, L.L. Guan, G.J. Hausman and M.V. Dodson. **2009**. Clonal mature adipocyte production of proliferative-competent daughter cells requires lipid export prior to cell division. *International Journal of Stem Cells* 2: 76-79.
- Chen, J., **M. Guridi**, M.E. Fernyhough, Z. Jiang, L.L. Guan, G.J. Hausman and M.V. Dodson. **2009**. Initial differences in lipid processing leading to pig- and beef-derived mature adipocyte dedifferentiation. *Basic and Applied Myology (European Journal of Translational Myology)* 19(5): 243-246.

#### OTHER INTERESTS

---

##### Volunteer work at the Animal shelter (Muttentz, Switzerland)

2013-2015

- Weekly assistance at cleaning, animal rehabilitation and visitors guiding at the local animal shelter in Basel (Katzenheim from Tierschutzbund Basel).

##### Professional Volleyball player (Irunavoley Sports Club, Spain)

2002-2009

- Competed in the Spanish National First League, helping our team win for two consecutive years.
- Currently playing volleyball at the University of Basel.

##### Professional Athlete (Club Atletico de San Sebastian, Spain)

1999-2002

- Competed in the Spanish National First League, winning several medals for high jump, shotput and javelin.